Mechanical Handling Effects on Brewers' Yeast

by

Andrew Robinson

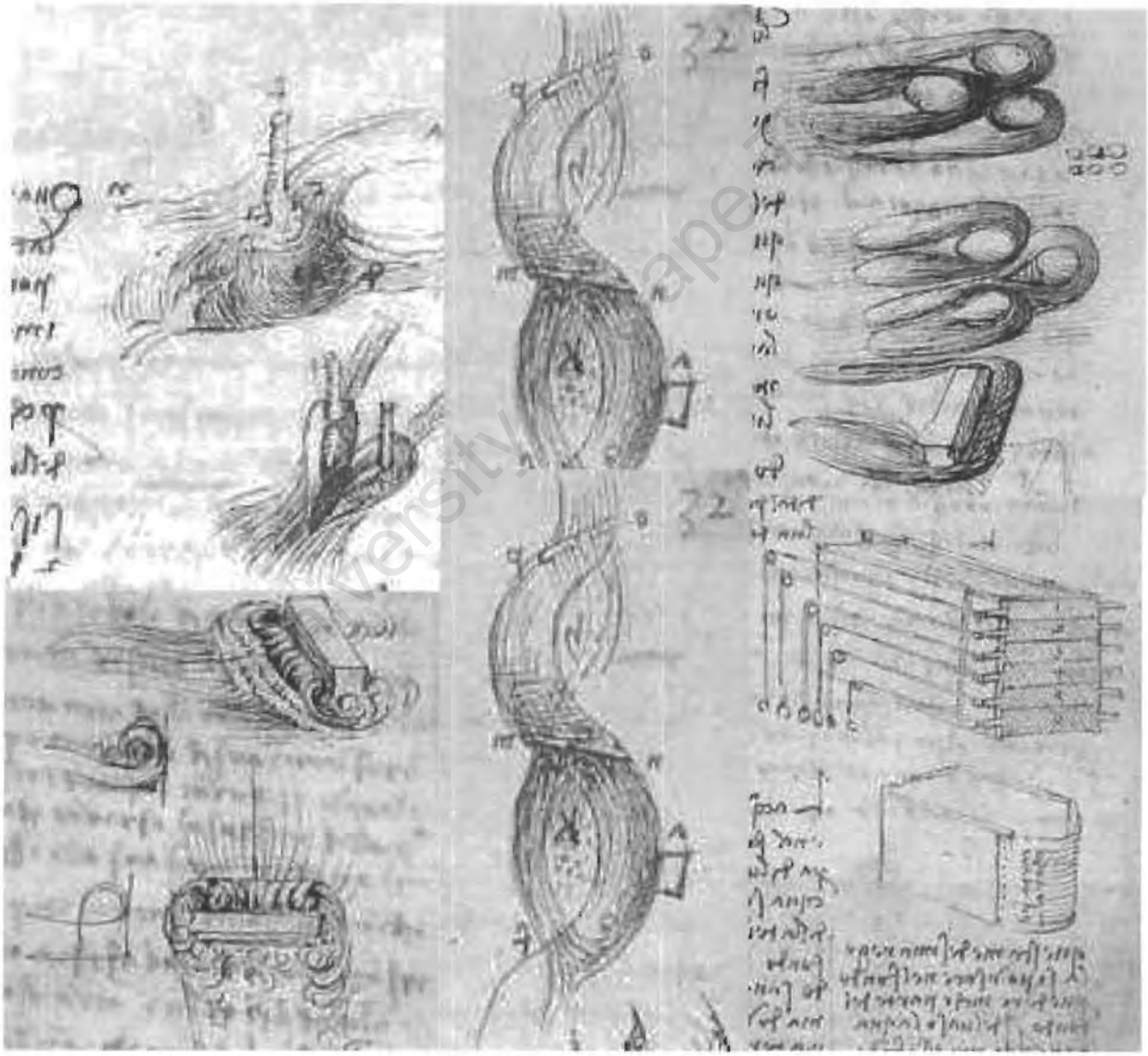

March 2001

Front Cover: *Montage of drawings by Leonardo da Vinci – artist & engineer*
Drawings depict flow of water around various obstacles generating turbulence and a device for measuring liquid velocity and pressure.

Mechanical Handling Effects on Brewers' Yeast

Andrew Robinson

Department of Chemical Engineering, University of Cape Town, Private Bag, Rondebosch, 7701

March 2001

Biological particles are known to be sensitive to hydrodynamic shear. Specifically within the brewing industry, yeast is subjected to mechanical handling which exposes the yeast cells to hydrodynamic shear. This has the potential to result in undesirable beer properties such as haze and low foam stability as well as inefficiencies during fermentation due to poor yeast quality. This leads to increased costs of production.

Mild hydrodynamic stress mediated at the cell surface may cause the loss or rearrangement of surface compounds (polysaccharides, lipids and proteins). These effects could result in changes to the hydrophobicity, surface charge and flocculation potential of the cells. Further, the permeabilisation of the cell or loss of cell membrane integrity may occur leading to the loss of viability and release of intracellular protease. These changes can be associated with the occurrence of particulate haze and foam instability as well as decreased fermentation performance. Severe hydrodynamic stress can cause cell disruption. From this study of flow of yeast slurries through pipework under laminar and turbulent conditions, a laboratory cell disrupter (French Press) and pilot scale disc stack centrifuges, the effect on the cell surface, membrane integrity and fermentation performance have been observed.

At the cell surface the results indicate that shear stress causes a loss of yeast flocculation potential and an increase in surface charge with the occasional loss of hydrophobicity. These observations can be explained in terms of the major constituents of the cell wall. The increase in the number of chargeable groups (N_S) on exposure to hydrodynamic shear can be explained by the loss of phosphomannan from the cell surface. The latter also decreases the ratio of phosphate to carboxyl groups (q) provided there was no loss of protein. The loss of cell flocculation potential observed would result from the damage or loss of either flocculins or receptor sites. Cell membrane integrity loss was indicated by the increased protease release although the viability assay was not sufficiently sensitive to support this finding in all cases. With regard to fermentation performance there were no consistent trends in either the rate or extent of fermentation as well as beer quality with hydrodynamic stress.

It is postulated that a critical stress is required to induce a biological response from the yeast and that the rate of such response occurring is proportional to the overstress above the critical value as well as the exposure time to such a stress.

Mechanical Handling Effects on Brewers' Yeast

Andrew Robinson

Thesis presented for the degree of

Doctor of Philosophy

In the Department of Chemical Engineering

University of Cape Town

March 2001

Summary

Brewery fermentation involves the conversion of sugars to ethanol by yeast with the repeated reuse of the yeast to maximise the overall conversion of sugars to ethanol. Within this environment the yeast is subjected to mechanical handling which exposes the cells to shear stress. It is known that biological particles are sensitive to hydrodynamic stress and the resultant biological response may be observed by a decrease growth rate (Cherry and Papoutsakis, 1988), decreased viability, vitality and fermentation performance (Basson *et al.*, 1996), release of enzymes (Stathopoulos and Hellums, 1985), the release of fine particles from the cell wall (Lewis and Poerwantaro, 1991) and cell disruption (Engler and Robinson, 1981; Zhang et al., 1993). In particular with the handling of yeast, filtration difficulties have been reported as a result of excessive haze production caused by the action of centrifuges (Lim et al., 1992; Siebert et al., 1987). Mannan haze material has also been shown to result from the agitation of yeast slurries in baffled shake flasks (Lewis and Poerwantaro, 1991). The implications of yeast handling in the brewing industry are poor fermentation performance due to decreased yeast viability, foam instabilities caused by the release of protease and the formation of beer haze brought about by abrasion of the cell wall and cell lysis. It is generally accepted brewery practice to minimise the hydrodynamic stress to which the yeast is exposed (Boughton 1983, 1987; Ball, 1994). Few technical reports or rigorous experimental data are however available on the effect of hydrodynamic stress on the yeast in the brewing industry thereby indicating the need for this study.

An analysis of the brewing flowsheet highlighted processes that have the potential to cause hydrodynamic stress damage to the yeast. These major processes include the transfer flow of yeast suspensions between the various stages in the yeast propagation plant as well as the pumping and flow of yeast slurries from a fermentation vessel, through a plate and frame heat exchanger to an agitated storage vessel. The separation of low concentrations of excess yeast between primary and secondary fermentations by centrifuges is a further shear environment to which yeast is exposed. Yeast handling occurs between the stages of a 'multiple batch propagation' and at the end of a fermentation when the yeast is in the late exponential growth or stationary phase respectively.

The primary objective of this study was to assess the effect of hydrodynamic stress on brewers' yeast quality. Towards this aim, stationary phase yeast was exposed to hydrodynamic shear generated within a laboratory French Press following its aerobic and anaerobic growth. Within the brewery, the centrifugal separation of yeast and flow of yeast slurries through the cropping circuit were investigated with the aim of identifying critical operating conditions to minimise cell damage.

The above objective was addressed by:

(i) Identifying yeast quality and beer quality indicators which can be used to inform the study.

(ii) Monitoring the yeast quality (hydrophocity, surface charge and composition, flocculation potential) as a function of growth phase under both aerobic and anaerobic propagation conditions for different flocculent (SAB1, SAB1/96 and SAB5) and non-flocculent (SAB2) yeast strains.

(iii) Studying the yeast quality as a function of hydrodynamic stress generated in a French Press apparatus for both aerobically and anaerobically propagated yeast to expand the scope of stresses beyond that normally encountered in the brewery.

(iv) Investigating the effect of centrifugation on yeast quality.

(v) Investigating the effect of flow of yeast slurries through the yeast handling circuit at SAB-Newland brewery on its quality.

A scheme is proposed whereby damage to the yeast cell can occur either at the cell surface, membrane or cytoskeletal or metabolic level or can cause cell disruption depending on the severity of the hydrodynamic stress. The indicators selected to identify and quantify minor damage at the cell wall are hydrophobicity, charge, flocculation potential and molecular composition along with haze formation in the slurry supernatant and process beer streams. Indicators of cell membrane integrity are cell viability and protease release. The viability assay was found to be less sensitive than the protease assay as an indicator of membrane integrity. Changes at the metabolic level were investigated by the fermentation performance at small scale. Complete cell disruption was quantified microscopically.

Yeast handling occurs between propagation stages and at the end of fermentation when the yeast is in the late exponential or stationary phase respectively. Under these conditions it was found, that the surface properties approached constant values for both aerobically and anaerobically propagated yeast. The cell surface changes observed following hydrodynamic shear action could therefore be attributed to cell damage and not a sensitivity to the growth phase. At the end of propagation of the flocculent yeast strains, the aerobically grown yeasts were more flocculent than the anaerobically grown yeast despite the higher surface charge and lower hydrophobicity of the yeast produced aerobically. This finding supports the specific lectin/receptor site mechanism of flocculation in brewing yeasts. The non-flocculent strain on the other hand showed a slight increase in flocculence when its hydrophobicity increased and surface charge decreased under anaerobic propagation. This is in accordance with the DLVO theory of colloidal flocculation.

The results from the French Press study indicate that a critical pressure differential was required before cell disruption occurred (6-10 MPa for the eight laboratory propagated yeasts; 20 MPa for

production SAB5 yeast). Below this critical disruption pressure, the sub-lytic effects observed at the cell surface included an increased surface charge and decreased flocculation potential. This further supports the scheme for hydrodynamic damage of the cell wall at sub-lytic shear forces.

It was postulated that cell damage in a centrifuge could be attributed to shear stress in the disc stack and/or the solids discharge zone. Shear damage resulting in compromised membrane integrity was attributed to the disc stack zone. The loss in cell flocculation potential was found to be a result of the shear stress in both the disc stack and solids discharge zone. The decrease in cell hydrophobicity and increased surface charge could not be assigned to either zone. It is recommended that the disc stack centrifuge be operated at low feed solids concentration with short solids discharge intervals to minimise the negative effects of shear stress on the yeast quality.

The effect of hydrodynamic shear caused by flow of yeast slurries in the laminar or turbulent regimes on yeast quality was also investigated. The results showed that laminar flow along a fixed pipe length resulted in more cell damage than turbulent flow, as seen by increased protease release and decreased fermentation performance. This was partly explained by noting that the Reynolds shear stress contribution to total shear in the turbulent flow regime could be negated as the Kolmogorov eddy microscale length was approximately 20 times larger than the average cell size. The remaining viscous shear stress in the turbulent regime was, however, still higher in a large portion of the pipe cross-section than the shear stress for the laminar flow. It was therefore postulated that not only the magnitude of the shear stress but also the exposure time are important parameters in determining the extent of cell damage due to hydrodynamic stress.

The recirculation trial investigated this combination of shear stress and exposure time under laminar conditions. It was seen that increased protease release occurred with increasing total energy dissipation. This has implications in the brewery circuit as the yeast is repeatedly exposed to hydrodynamic stress. Investigation of the brewery handling circuit showed no significant change to the yeast quality although there was an increase in protease release along the handling circuit and hydrophobicity decreased slightly after the plate and frame heat exchanger. Within the context of the brewery it is recommended that cell damage can be minimised by either operating in the laminar flow regime with linear velocities such that the wall shear stress is below the critical shear stress as indicated by current practice or operating within the turbulent flow regime with large eddy size to minimise exposure time of the yeast to the stress.

Since both the shear stress and exposure time were found to determine the type and extent of yeast cell damage the following hypothesis was proposed. A critical shear stress exists, below which no biological response is observed despite an infinitely long exposure time. At shear stresses above this

value, cell damage will be seen to occur with increasing stresses reducing the exposure time required to cause cell damage. The rate of cell damage is therefore proposed to be proportional to the magnitude of the 'overstress' and the exposure time. This hypothesis was supported by the absence of loss of yeast quality in the pipe sections of the online trials where the wall shear stress was low (less than 7 Pa despite the long exposure times of more than 1200 seconds in the region close to the pipe wall. At higher shear stresses, as occurred in the recirculation trial where the maximum shear stress was 38 Pa, 9 exposures to the holding tubes each lasting only 33 seconds resulted in significant loss of membrane integrity and protease release. The turbulent flow trial with a maximum exposure time of 3 seconds and shear stress of 149 Pa did not cause cell damage. As seen in the French Press, where shear stresses of between 2.8 and 9.5 x 10^6 Pa were generated and exposure times were in the range 10^{-4} to 10^{-5} seconds, a range of cell damage from mild surface changes to cell disruption were achieved.

Acknowledgements

- My supervisor, Prof. Sue Harrison, who gave me both guidance and free rein to explore and develop the project. Her enthusiasm during the experimental phase and patience during the writing phase were key components in seeing this through.

- For his stimulating discussions and helpful ideas I wish to thank Prof. Geoff Hansford as well as the entire academic staff on whose help I have called upon at various times throughout my time in the department.

- For the many days you gave unselfishly of your time in formatting this manuscript, I thank Jo-Ann and Gillian Moon.

- To the workshop staff, both electrical and mechanical, as well as the laboratory and cleaning staff, thanks for your constant, prompt and efficient service you have offered me.

- Thanks to Lauren Basson, Jenny Lowenadler and Garnet Titus for helping me in the early days with the methods, experimental and operational procedures at the breweries. Likewise to the members, both past and present, of the 'Bio group' who provide a pool of knowledge and experience on which to draw.

- The laboratory staff of SAB – Newlands under the leadership of Abdul Karachi as well as the production staff at Newlands brewery. The staff of SAB – Central Office and Gavin Hulse in particular for your continued support for the project over the years, laboratory assays and intellectually stimulating debate.

- Equipment suppliers, Westphalia centrifuges from GEA Process Technology SA and the Scandi Brew pump from Micro Matic.

- Financial assistance for the project from SAB as well as personal bursaries from the NRF and UCT.

- To my parents for providing the loving, understanding and supportive home as a base from which I could operate I am eternally grateful.

- Last but by no means least a special thanks to Jo-Ann Moon for listening to my ideas, painstakingly reading and helping to refine the arguments in this work. Also for keeping me sane to greater than 95 % confidence and lifting my spirits when the pressure was really on.

Glossary

Attenuation	The conversion of wort sugars to ethanol, CO_2 and other fermentation products leading to a drop in specific gravity of the fermentation medium.
CIP (Cleaning In Place)	The cleaning of equipment and associated process piping without dismantling and reassembling.
Consistency	The concentration of yeast in a slurry, expressed as a weight percent.
Cropping	The transfer of yeast from fermentation vessel to collection vessel for reuse in subsequent fermentations.
Fermentation vessel	Cylindro-conical vessels within which fermentation occurs.
Gravity	A measure of the sugar concentration of wort, based on its specific gravity and expressed as °P.
Green beer	Beer at the end of primary fermentation which has 'grassy' flavours due to elevated concentration of off-flavours produced during fermentation.
Hung fermentation	The incomplete use of fermentable sugars during fermentation.
Lagering	The secondary fermentation conducted at low temperature, used for the removal of off-flavours produced during primary fermentation.
Physiological state	The existence of different phenotypes of a cell as a result of different protein expression in response to stresses and environmental conditions.

Physiological status	The cells' position within the cell cycle, i.e. lag, exponential, stationary or death phase.
Pitch	The addition of yeast cells to the wort to initiate fermentation (inoculate).
°Plato	The measure of sugar concentration in brewers' wort with units of grams of extract per 100 ml.
SAB	South African Breweries plc.
SAB1	Flocculent strain of *Saccharomyces pastiaranus* (formerly *S. cerevisiae*) used within most SAB breweries prior to 1997.
SAB1/96	Re-isolation of strain SAB1 believed to be less flocculent than SAB1.
SAB2	Non-flocculent strain of *Saccharomyces pastiaranus* (formerly *S. cerevisiae*)
SAB5	Flocculent strain of *Saccharomyces pastiaranus* (formerly *S. cerevisiae*) used in most SAB breweries in South Africa from 1997.
Scrapping	The process of pumping spent yeast out of its final fermentation vessel to storage for later disposal.
Wort	The sugar and amino acid media produced from malted barley containing the nutrients required for yeast growth and beer production.
XPS	X-ray Photoelectron Spectroscopy used to examine the chemical composition of surfaces.

Nomenclature

α	volume fraction of cells
β	$1/X_\infty$ (g^{-1})
δ	thickness of laminar sublayer (m)
ε	energy dissipation rate ($J.s^{-1}.kg^{-1}$ or $m^2.s^{-3}$)
ε	extinction coefficient of NADPA at 340nm in Equations B.8, B.9 & B.10 ($mmol^{-1}.cm^{-1}$)
ε	permitivity of solution in Equation C.4 ($C^2J^{-1}m^{-1}$)
γ	shear rate (s^{-1})
κ	Debye-Huckel parameter (m^{-1})
λ	constant in Moser Equation 4.4
μ	viscosity ($N.s.m^{-2}$)
μ	Monod specific growth rate (h^{-1})
μ_{max}	maximum specific growth rate constant (h^{-1})
ν	kinematic viscosity ($m^2.s^{-1}$)
θ	half included disc angle (°)
ρ	fluid density ($kg.m^{-3}$)
ρ_p	particle/cell density ($kg.m^{-3}$)
σ	cavitation number
σ_d	charge density at the shear plane ($Coulombs.m^{-2}$)
σ_0	charge density at the surface ($Coulombs.m^{-2}$), Equations 3.5 and 3.6
σ_0	Constant defined in Equation 2.21
τ	shear stress ($N.m^{-2}$)
τ	solids discharge interval in the disc stack centrifuge (min)
τ_0	wall shear stress ($N.m^{-2}$)
τ_{avg}	average shear stress ($N.m^{-2}$)
τ_{max}	maximum shear stress on cell ($N.m^{-2}$)
τ^R	total shear stress under conditions of Reynolds stress dominance ($N.m^{-2}$)

τ^v	total shear stress under conditions of viscous stress dominance ($N.m^{-2}$)
ω	angular velocity ($rad.s^{-1}$)
ψ	potential (V)
ψ_0	surface potential (V)
ψ_d	potential at shear plane (V)
ξ	zeta potential (V)
Σ	equivalent surface area of a centrifuge (m^2)
c	concentration of electrolyte ($mole.dm^{-3}$)
C_1	constant in Equation 2.27
C_{in}	feed solids concentration
CS_s	collision severity based on shear model ($J.s^{-1}$)
CS_T	collision severity of cell-cell impacts based on eddy velocity
d	light path (cm)
d_c	cell diameter (m)
d_p	particle diameter (m)
D	pipe diameter (m)
dP/dx	pressure gradient ($Pa.m^{-1}$)
dv/dy	velocity gradient (s^{-1})
e	electron charge $1.6x10^{-19}$ (C)
E_L	energy dissipation in laminar sublayer ($J.s^{-1}$)
E_T	total energy dissipation rate ($J.s^{-1}$)
$f(K_a)$	factor including double electric layer thickness and particle diameter
f_{local}	frequency of local maxima experienced by the cell (Hz)
f_{max}	frequency of maximum exposure to peak shear (Hz)
HI	hydrophobicity index (%)
k	rate constant (h^{-1})
k_B	Boltzman's constant ($1.38x10^{-23}$ $J.K^{-1}$)
k_e	death rate constant (h^{-1})
K_p	product saturation constant ($g.l^{-1}$)
K_i	substrate saturation constant ($g.l^{-1}$)
K_S	saturation constant ($g.l^{-1}$)
l	characteristic length (m)

l_c	Kolmogorov microscale (m)
L	length of tube (m)
M_i	molar concentration of species i (moles.dm^{-3})
MW	molecular weight of a substance (g.mol^{-1})
n	number of discs
$n_{i\infty}$	bulk ion concentration (ions.m^{-3})
N	centrifuge speed
$N_{3\text{-bead-cells}}$	number of cells with more than 3 beads attached
N_A	6.02x10^{23} (mol^{-1})
N_{blue}	number of blue cells counted
N_c	frequency of cell-cell collisions in Equation 2.31 (Hz)
N_C	total number of carboxyl groups
N_{final}	cell count after French Press
N_h	holding tube cycle
$N_{initial}$	cell count before French Press
N_N	total number of amine groups
N_P	total number of phosphate groups
N_S	total number of chargeable groups on cell surface
N_{total}	total number of cells
OUR	oxygen utilisation rate (mg.l^{-1}.min^{-1}/10^9 viable cells)
P	Pressure (Pa)
pI	isoelectric point
ΔP	pressure drop (Pa)
P_∞	pressure upstream of an orifice (Pa)
P_v	pressure at the point of maximum fluid velocity (Pa)
q	ratio of phosphate to carboxyl groups on cell surface
Q	volumetric flow rate (m^3.s^{-1})
r	radial position (m)
r	ratio of phosphate to carboxyl groups at the cell surface
r_i	disc inner radius (m)
r_o	disc outer radius (m)
r_x	rate of cell growth (g.l^{-1}.h^{-1})
R	pipe radius (m)
Re	Reynolds number

R_S	radius of the particle (m)
S	substrate concentration ($g.l^{-1}$)
t	time (h)
$t_{95\%}$	residence time at 95% of pipe diameter (s)
t_{avg}	mean residence time (s)
T	Temperature (K)
TE	total energy dissipated (J)
U_E	electrophoretic mobility ($\mu m.s^{-1}.V^{-1}.cm^{-1}$)
v	fluid velocity ($m.s^{-1}$)
v^+	dimensionless velocity
v_{avg}	average velocity ($m.s^{-1}$)
$\tilde{v}_{(d_c)}$	velocity difference between points separated by distance d_c ($m.s^{-1}$)
v_{max}	maximum linear velocity ($m.s^{-1}$)
v_{stokes}	Stokes terminal settling velocity ($m.s^{-1}$)
v_∞	velocity upstream of the orifice ($m.s^{-1}$)
V_L	volume in the laminar sublayer (m^3)
V	volume (m^3)
W	flow rate ($kg.\ min^{-1}$)
x	distance away from the particle surface (m)
X	cell mass concentration ($g.l^{-1}$)
X_o	initial cell concentration ($g.l^{-1}$)
X_∞	maximum biomass concentration ($g.l^{-1}$)
y	distance from the wall (m)
y^+	dimensionless position
$Y_{X/(S+E)}$	biomass yield coefficient (10^6 cells.ml^{-1} / °P)
$Y_{X/S}$	wet weight yield
z_i	charge on the ion

Table of Contents

List of Figures

List of Tables

Chapter 1: Introduction

The mechanical handling of yeast in a brewery involves the physical processes of transfer, separation and agitation of yeast slurries. The handling of these yeast slurries produces hydrodynamic shear stresses which have the potential to harm the living yeast cells and in so doing, reduce the beer quality. The potential for a loss of yeast quality under harsh handling conditions was highlighted by Boughton (1987) while Lewis and Poerwantaro (1991) observed the formation of haze material in agitated yeast slurries and attributed the yeast cell wall to be the source of the haze material. This study investigates the effect of shear stress on yeast and the biological consequences of hydrodynamic action.

1.1 The Brewery Yeast Handling Circuit

The handling of yeast within the brewery begins during its propagation phase. The propagation of yeast entails a series of sequential aerobic batch growth stages of increasing volume to produce the final quantity of yeast to serve as inoculum to the fermentation stage. Between each step in the process, the yeast is transferred by pump to the next, larger propagation vessel or transferred by air top pressure to avoid use of pumps. On completion of the propagation stage, the yeast is pumped into a stream of aerated wort leading to a fermentation vessel where fermentation commences. Each of these transfers takes place when the yeast is in the late exponential to early stationary phase following aerobic growth.

Fermentation is the anaerobic process by which sugars in the wort medium are converted into ethanol and carbon dioxide as major products, with a small increase in biomass. On depletion of the sugars, the lager yeast flocculates and settles to the bottom of the fermentation vessel from where it is pumped, cooled and stored as inoculum for a subsequent fermentation. Once propagated, a batch of yeast is reused as many as 8 to 20 times depending on the specific requirements of each brewery

and the type of beer produced. The yeast is pumped using positive displacement pumps through large diameter pipes to minimise shear rates and associated risk of cell damage due to shear. The cooling of the slurry is achieved by passing it through a plate and frame heat exchanger. The constrictions and expansions in the flow path, including those found in the plate and frame chiller, increase the shear stress and risk of damage to the yeast. Once within the storage vessel, the slurry is agitated to maintain its homogeneity and prevent compaction of yeast. Yeast exposed to this handling circuit between fermentations is produced mainly as the result of anaerobic growth and is in the stationary phase.

Consequently, both aerobically and anaerobically produced yeast are exposed to hydrodynamic stresses at different positions within the brewery, thus requiring the study of the potential of yeast exposed to these different oxygen availabilities during growth to be damaged.

1.2 The Effect of Hydrodynamic Shear

The effect of hydrodynamic stress on yeast may result in changes to the cells' integrity and viability or metabolic activity (Prokop and Bajpai, 1992). Shear, being a force acting at the interface between the cell and its fluid environment, has its first impact on the cells' outer surface. Here it may cause the rearrangement or loss of surface molecules from the cell wall. The components most likely affected by shear at the cell surface are phosphomannan, lipids and protein. Rearrangement or loss of these molecules from the cell wall can affect the surface properties of the yeast cell and the quality of beer produced. For instance, the release of phosphomannan from the surface may be detected by increased haze in the beer (Lewis and Poerwantaro, 1991; Siebert *et al.*, 1987) while at the yeast surface, the charge may be affected. Surface hydrophobicity, generated predominantly by the presence of surface lipids, may be affected by the loss of lipid. Flocculation of brewers' yeast is governed by the presence and availability of 'lectin-like' surface proteins and mannan receptor sites which may also be susceptible to shear damage (Miki *et al.*, 1982a, b). Such damage may result in a loss of flocculation potential of the yeast.

In addition to these cell surface effects, the effect of shear could be propagated through the cell surface and affect the cell membrane. At this level, the energy dissipated may result in a loss of membrane integrity causing the release of intracellular molecules including protease (Basson, 1996) which affects the foam stability of the beer. Further, a loss of cell viability may result. Part of the energy associated with shear stress may be dissipated to the cells' cytoskeleton and here result in the loss of metabolic activity or vitality. Such changes may be detectable as changes to the oxygen uptake rate and fermentation rate of the yeast. Fermentations also provide additional information on the yeasts' performance as well as resultant beer quality under the specific conditions unique to

brewing. Only the most severe form of shear would result in complete cell disruption. Under conditions prevalent within the brewery, however, the milder forms of damage specific to the cell wall and membrane may be postulated to occur.

The objective of this study was to investigate the effect of hydrodynamic shear stress, that may occur in the brewery, on yeast cells. This was investigated for flow of yeast slurry in a pipe and in centrifuges. Here the effect of hydrodynamic shear stress for flow in a pipe was investigated at both conditions occurring within the brewery and those exceeding typical brewery practice. In addition, a French Press was used at a laboratory scale to extend the range of shear stress studied as well as a tool to study the effect of oxygen availability during cell growth on hydrodynamic shear stress resilience.

1.3 Structure of Thesis

The literature review detailing yeast cell wall composition, structure and function is presented in **Chapter 2**, together with the detailed yeast handling procedures within breweries. Together, they inform the study of the potential for mechanical handling to damage yeast cells. The mechanism by which hydrodynamic shear affects yeast cells through surface, membrane and cytoskeletal damage is postulated and relevant biological responses at each cell state identified to enable the process to be assessed. The calculation procedures required to quantify the shear stress and energy dissipation within pipe flow are also presented.

Chapter 3 contains the methods used for laboratory propagation and trial fermentations as well as the yeast quality and cell surface assays used to identify cell damage. Since the variables used to monitor yeast quality vary during the growth phase of yeast culture, they need to be monitored during cell growth and their stability in the stationary phase determined before the handling studies could be conducted. The progression of surface properties during cell propagation is reported in **Chapter 4**. The parameters associated with cell propagation, yield and growth rate are also compared for three flocculent strains (SAB1, SAB1/96, SAB5) and a non-flocculent strain (SAB2) under both aerobic and near anaerobic propagation conditions.

To investigate the effect of oxygen availability during cell growth on the resilience of cells to shear, laboratory studies were conducted using a French Press, a type of high pressure homogeniser. This allowed for the testing and validation of the methods in a well defined energy dissipation apparatus as well as for the extension of hydrodynamic stress beyond those obtainable within the brewery. Different yeast strains were studied to assess whether strain characteristics, specifically the presence

or absence of flocculation potential, alter the biological response of mechanically handled yeast. These trials are presented in **Chapter 5**.

In **Chapter 6**, the biological response to shear in two pilot scale disc stack centrifuges was analysed in terms of two identified 'zones' within the centrifuge in which the cells are exposed to hydrodynamic shear. The first zone is within the disc stack itself where the feed is introduced, accelerated and separation is achieved. The centrifuge operation results in the discharge of accumulated solids through the intermittent opening of nozzles around the periphery of the bowl and this was considered as the second shear zone. Through the experimental design, the observed damage to the cells was attributed to the relevant zone within the centrifuge.

A series of brewery system trials were performed within a commercial brewery to determine the effect of shear and energy dissipation within a test pipe-work section. Variations in shear and energy dissipation were achieved by the variation of flow rate and circulation time. These 'offline' trials were followed by 'online' trials to determine the effect of standard brewery flow conditions on yeast as it passes along a length of pipe, through a plate and frame heat exchanger as well as during storage and preparation of yeast for its eventual reuse. These brewery system trials are reported on in **Chapter 7**.

In **Chapter 8**, conclusions from the study are drawn and given an overall perspective. Recommendations are put forward with respect to process modifications to minimise damage. Furthermore, recommendations are made of areas in which further work is anticipated.

Chapter 2: Literature Review

2.1 Shear Sensitivity of Biocatalysts

A key parameter in the design and operation of bioprocesses is the sensitivity of the biological particle to hydrodynamic shear stress. The biological particles can vary in size, shape, structure and complexity from enzymes to bacteria, fungi, plant, insect and animal cells. Fungi, yeast and to a lesser extent bacteria have been known to be relatively shear resilient while plant, insect and animal cells are more sensitive in so far as cell disruption is concerned (Prokop and Bajpai, 1992). Due to their structure, filamentous fungi are known to be affected by hydrodynamic stress resulting in damage and changes to their morphology. In Table 2.1, a review of the biological response of various biological cell types to hydrodynamic stress environments observed in the recent literature is provided. While most of these investigations have concentrated on the more far reaching effects of disruption kinetics and decreased growth rates, biological cells including yeast may demonstrate more subtle responses to hydrodynamic shear. This thesis further investigates the hypothesis that brewers' yeast experiences changes to the cell envelope in response to hydrodynamic shear stress. Damage to the cell wall may result in changes to the molecular cell wall composition, the cell surface properties (hydrophobicity and charge) and the bulk slurry behaviour (flocculence) while the loss of cell membrane integrity may result in a loss of viability and the release of intracellular enzymes (including protease). A review of yeast handling in breweries will now be presented to assess the potential for a loss of yeast quality.

Table 2.1. Summary of biological response of various cells to hydrodynamic shear.

Cell Type	Shear Generation Device	Biological Effect	Investigators
Bovine kidney cells	Microcarrier bioreactor	Decreased growth rate	Cherry & Papoutsakis (1988)
Brewing trub	Pipe bends & process equipment	Disruption of trub floccules	Denk (1995)
Candida utilis	High pressure homogeniser	Disruption	Engler & Robinson (1981)
Carrot cells	Stirred bioreactor and couette viscometer	Viability, activity & membrane integrity	Dunlop *et al.* (1994)
Corynebacterium glutamicum	Stirred bioreactor & capillary flow loop	Cell aggregate breakup	Illing & Harrison (1999)
Escherichia coli	Bead mill & high pressure homogeniser	Disruption	Agerkvist & Enfors (1990)
	High pressure homogeniser	Disruption	Middelberg *et al.* (1991) Middelberg *et al.* (1992a, b) Middelberg (1993)
	High pressure homogeniser	Preferential disruption of septated cells	Hull & Middelberg (1993)
Human kidney cells	Laminar flow channel	Altered cell morphology, enzyme release & decreased viability.	Stathopoulos and Hellums (1985)
Human diploid fibroblasts	Microcarrier bioreactor	Increased death rate & decreased growth rate	Croughan *et al.* (1987)
Hybridoma cells	Turbulent capillary flow	Disruption	Zhang *et al.* (1993)
Mouse myeloma cells	Turbulent capillary flow	Cell lysis	Mc Queen *et al.* (1987)
Mucor rouxi	Stirred bioreactor	Altered morphology, increased liberation of intracellular product	Dabee (1997)

Table 2.1 cont.

Cell Type	Shear Generation Device	Biological Effect	Investigators
Saccharomyces cerevisiae	Homogeniser	Disruption	Doulah *et al.* (1975)
	Agitation of yeast slurry	Haze release from cell walls	Lewis & Poerwantaro (1991)
	Homogeniser and bead mill	Disruption	Milburn & Dunnill (1994)
	Cavitation through constriction, blender and ultrasonication	Disruption and reduced activity of liberated macromolecules	Save *et al.* (1994, 1997)
	Centrifugation, disc stack type	Fine particle release from cell wall	Siebert *et al.* (1987)
	Pump design, centrifugation and flow through pipes	Yeast viability, vitality and fermentation performance	Basson *et al.* (1997)
	High pressure homogeniser	Disruption	Shirgaonkar *et al.* (1998)
S. cerevisiae, protein precipitates and poly vinyl chloride	Centrifuge, disc stack	Decreased recovery of shear sensitive particles relative to PVC beads	Maybury *et al.* (2000)
Skeletonema costatum & *Haslea ostrearia*	Circulation of microalgae through pumps & valves	Fracture and disruption	Vandanjon *et al.* (1999)
Spodoptera frugiperda	Airlift column	Reduced viability	Trinh *et al.* (1994)

2.2 The Potential Loss of Yeast Quality in a Brewery

Yeast is used in the brewery to convert the sugar rich media (wort) into ethanol, carbon dioxide and flavour compounds in a process known as fermentation. During fermentation the yeast quantity increases, flocculates at the end of fermentation and settles to the base of the fermentation vessel (FV). The brewer takes advantage of the increase in biomass by removing the yeast for reuse to

inoculate (pitch) further fermentations. During this removal and reuse operation, the yeast is exposed to mechanical handling and shear. In order to maintain a high quality of yeast, it has to be removed from the fermenter as soon as the required degree of substrate usage (attenuation) has been obtained. The settled yeast in the fermenter prior to removal (cropping) is in a deleterious environment with high ethanol concentration, depleted substrate and nearly stagnant slurry which results in poor heat transfer causing the yeast to be exposed to cold shock and/or 'hot spots'. If maintained in this environment for too long, the yeast loses quality, viability and starts to lyse. Yeast of poor quality when leaving the fermenter may present lower stress resilience and altered handling characteristics. Yeast quality indicators need to be identified to detect and quantify the quality of the yeast. These indicators can then be used to monitor the progress of good quality yeast through possible physiological and/or mechanical routes which result in the damage of yeast cells. This section of the literature review is structured to first present the yeast quality indicators(Section 2.2.1), the possible routes leading to the loss of yeast quality (Section 2.2.2) and finally the handling procedures to which the yeast is exposed in the brewery (Section 2.2.3).

2.2.1 Yeast Quality Indicators

Yeast quality can be defined in terms of its fermentation capacity and the quality of the produced beer. Factors which determine these aspects of yeast quality have been defined by Basson (1996) to be the following:

- the ability of the yeast to reproduce
- the rate and extent of biomass growth
- the overall metabolic rate of the yeast
- the rate of various metabolic pathways, influencing the flavour compounds formed
- the flocculation and sedimentation characteristics of the yeast
- the integrity of the cell envelope
- the ability of the yeast to withstand stress

Attempts have been made to determine indicators based on the above interpretations of yeast quality which accurately predict the fermentation performance of the yeast. Indicators which can be used as a measure of the above points are introduced here and the chosen methods described in more detail in Chapter 3.

2.2.1.1 Ability to reproduce

During the initial stages of the fermentation, the rate of attenuation is related to the ability of the yeast to reproduce. While oxygen is present in the first 6-12 hours of fermentation the cells reproduce and produce lipids and sterols required for further cell reproduction (Rose, 1977) which

continues for the first 2-3 days of fermentation. Once cell replication ceases, the remaining attenuation is achieved by the fermentative metabolism of the biomass present. Ability of the yeast to reproduce is termed its viability and is dependent on an intact functional cell membrane. A limit to the number of times a single yeast cell can reproduce has been observed (Barker and Smart, 1996) and this is linked to problematic brewery fermentation performance when full attenuation does not occur resulting in a 'hung' fermentation. The methods used to determine the cells' viability are based on either regrowth studies or vital stain techniques. Staining techniques are based on sustained metabolic activity such that the dye is either excluded from the cell by a fully functional cell membrane or is reduced to a colourless compound inside the cell (Smart *et al.*, 1999). Cell phenotypes which are unable to reproduce but are nevertheless metabolically active are not always distinguishable from non-viable cells using viability stains. Of the staining techniques, methylene blue is the most frequently used in breweries despite its known shortcomings. Of these are the stains overprediction of true regrowth ability of the yeast when viability is below 90% (King *et al.*, 1981) and the lack of purity of the dye compound resulting in variable staining intensities (Smart *et al.*, 1999). The second problem has been partially overcome by using methylene violet as an alternative to methylene blue.

2.2.1.2 Rate and extent of biomass growth

Sterols and unsaturated fatty acids are integral compounds which determine the extent of yeast growth and membrane integrity (Pickerell *et al.*, 1991). During the initial stages of fermentation, these products are produced by the consumption of available oxygen as well as by the conversion of the internal glycogen reserve of the cell. These two factors may be the most important in limiting the extent of biomass growth and, together with the yeasts' activity, form the predominant factors governing the rate of biomass growth. To determine the extent of biomass growth, the ratio of final to initial biomass concentrations has been used (Basson, 1996). Under conditions of identical initial oxygenation, differences in the biomass growth factor can be related to differences in the initial glycogen content of the cells as glycogen is the predominant source of carbohydrate during the first 4 hours of fermentation when oxygen is consumed and the sterols and fatty acids which are required for cell growth, are produced (Quain *et al.*, 1981).

2.2.1.3 Metabolic rates and pathways

The overall metabolic rate of the cells determines the sugar utilisation rate and hence the rate of attenuation. During fermentation, the metabolic rate varies according to oxygen and other nutrient availability, product inhibition (predominantly ethanol) and growth phase (physiological status) of the yeast. To predict overall metabolic activity of yeast, oxygen utilisation rates can be used. For more detailed analysis of metabolic rates, fermentations may be performed. From such fermentations, the

rate of attenuation is a useful parameter of overall fermentative rate while certain beer quality indicators can be used to track individual metabolic pathways.

The fermentative metabolism of yeast converts sugars into energy, carbon dioxide and ethanol via the Embden-Meyerhof-Parnas (EMP) pathway. Apart from these major products, a number of other compounds including higher alcohols, aldehydes, esters, acids and sulphur containing compounds are produced by yeast which contribute to the flavour of beer (Masschelein, 1986). When present at elevated concentrations, these compounds can result in off flavours in the beer or reduce its shelf life hence reducing the beer quality. The pathways which are responsible for their production can be affected by the yeast quality at the beginning of fermentation as well as the fermentation conditions of temperature, nutrient concentration and pH (Stanley and Pamment, 1993). Due to the complex network of metabolic pathways which produce these flavour compounds, the interpretation of beer quality in terms of the initial yeast quality and fermentation process is convoluted. The major indicators of beer quality which are routinely used are ethanol, sulphur dioxide, diacetyl and acetaldehyde.

Following the period of aerobic growth when yeast is first inoculated into wort, anaerobic fermentation commences. The equation which can be used to describe anaerobic fermentation is given as follows (Hough, 1985):

$$\text{maltose} + \text{amino acids} \Rightarrow \text{biomass} + \text{ethanol} + CO_2 + \text{heat}$$
$$100\,g + 0.5\,g \Rightarrow 5\,g + 48.8\,g + 46.8\,g + 209\,kJ$$

This equation therefore predicts that pure anaerobic metabolism would result in an ethanol yield of nearly 49% of converted maltose. The true yield of ethanol is generally lower than this because of the initial aerobic growth of yeast on sugars as well as inefficiencies in yeast metabolism which results in the accumulation of storage products (glycogen and trehalose) in the later stages of fermentation. The flavour compounds, produced at low concentrations, provide more subtle indicators of sub-optimum fermentations.

Acetaldehyde and CO_2 are produced by the decarboxylation of pyruvate in the EMP pathway. This acetaldehyde is reduced to ethanol and is a reversible reaction. Acetaldehyde can also be produced by the decarboxylation of oxo-acids during the formation of higher alcohols (Rose, 1977). At low concentrations, acetaldehyde imparts smoothness to beer but at higher levels it results in an unpleasant characteristic grassy 'green' flavour.

Sulphur dioxide (SO_2) is produced by yeast from sulphur containing amino acids and free sulphate in the wort. The compound acts as a natural anti-oxidant at low concentrations but has an unpleasant flavour at higher concentrations.

Diacetyl in beer is another flavour compound which should be present at low levels (less than 100 ppm) in the final beer but at higher levels results in the beer having a 'butterscotch' off taste. It is produced by the decarboxylation and oxidation of acetolactate which is excreted by the yeast cells. This process can lead to diacetyl concentrations in excess of 500 ppm during the early stages of fermentation. As fermentation proceeds, the diacetyl can be reabsorbed by the yeast and converted to 2,3-butanediol. Fermentation conditions are usually controlled so that higher diacetyl levels are reduced at the end of fermentation by using elevated temperature storage, longer storage times and higher concentrations of freely suspended yeast in the lagering stage.

The interpretation of these beer quality indicators are not always conclusive since wort composition, fermentation time, temperature and initial oxygenation rate influence the concentration of these compounds. Hence beer quality analysis cannot be compared across different fermentation batches. However, under the identical fermentation conditions used within each set of experiments, beer quality indicators are valid indicators of initial yeast quality at the start of fermentation.

2.2.1.4 Flocculation characteristics of yeast

The timing of the onset of flocculation towards the end of fermentation plays an important role in good brewing practice. Due to mass transfer effects, freely suspended cells have higher fermentation rates than cells in flocs and so it is advantageous to keep the yeast cells separate for as long as possible during the fermentation of the sugars. Since the recovery of yeast for reuse is a vital part of brewing, flocculation and the resultant sedimentation of these cells aids in their removal from the fermentation vessel. Flocculation associated problems that can occur during fermentation include 'hanging fermentations' which occur when the yeast flocculates before the completion of fermentation. This effectively stops the attenuation process, leaving a high residual sugar content in the beer. In the opposite condition if the yeast does not flocculate adequately after fermentation has ceased, high separation loads and associated costs are incurred to remove the yeast from the beer. Yeast with incorrect flocculation characteristics is not suitable for reuse and as such represents an additional loss to the brewer since it needs to be disposed and replaced with newly propagated yeast. Because of the importance of yeast flocculation potential to good yeast quality, an in-depth overview of yeast flocculation is provided in Section 2.4.

2.2.1.5 Cell envelope integrity

The loss of cell envelope integrity occurs when either the cell membrane or cell wall or both are ruptured. This represents the most extreme form of yeast cell damage and loss of yeast quality since the structural integrity of the cell is compromised, rendering the cell more susceptible to stresses. The rupture of the cell envelope results in the release of intracellular compounds into the beer,

reducing beer quality and shortens its shelf life. Despite the cell retaining its viability, uncontrolled protease release can occur when the cell membrane is permeabilised, the presence of which reduces foam stability of beer (Ormrod *et al.*, 1991). The release of other intracellular compounds result in off flavour production (McCaig and Bendiak, 1985) and haze formation (O'Connor-Cox, 1994), all of which result in reducing beer quality and shortening its shelf life. The partial disruption of the cell wall, although not lethal to the cell can also result in release of wall compounds including mannan, glucan, protein and lipid. The release of these compounds have been observed to cause haze formation (Lewis and Poerwantaro, 1991) and result in filtration difficulties due to the increased fine particle concentration (Siebert *et al.*, 1987).

2.2.1.6 Ability to withstand stress

Various compounds have been reported to be stress protectants. Under conditions of reduced water availability, cells accumulate polyols like glycerol, amino acids like proline and the disaccharide trehalose. These solutes protect cell components from freezing, heating, high pressure and dehydration which all cause the disruption of hydrogen bonding. The mode of action of these stress protectants has been reviewed by Hallsworth (1998). Trehalose, a disaccharide which accumulates within the cell during times of environmental stress (Quain, 1991), has been shown to be important in fermentation as yeast cells with depleted trehalose content do not perform as well during fermentation (O'Connor-Cox, 1995). Glycogen is another such compound which aids fermentation when present intracellularly at higher concentrations and as such has been linked to improved yeast quality (Quain *et al.*, 1981). Since glycogen has been shown to be consumed during adverse storage conditions (Murray *et al.*, 1984), it may be regarded as a yeast stress protectant. Heat shock proteins (HSPs) are another class of compounds which provide protection to a cell under physiological stress conditions. HSPs are found in all organisms including yeast cells. Under conditions such as elevated temperature or oxygen limitation, the cells proteins may be denatured as a result of the loss of protein tertiary structure. HSPs help to repair these damaged proteins by binding to them and causing them to refold correctly (www.antigenics.com, 2000). One of these proteins, HSP12 is found to be incorporated into the cell wall of yeast where it acts as a protectant against desiccation and high ethanol concentrations (Sales *et al.*, 2000).

2.2.2 Possible Routes Leading to the Loss of Yeast Quality

The terms usually used in the brewing industry to describe yeast quality are 'viability' and 'vitality'. Basson (1996) demonstrated the inability of these two terms alone to fully describe yeast quality and instead proposed a scheme for the progression of yeast between the various physiological states (Figure 2.1). Cells in each of these physiological states can be identified by the appropriate yeast quality indicators as follows:

- **Physiologically stressed cells:** Their metabolic rates are reduced, resulting in lower oxygen utilisation rates. Fermentation is slower and the flavour profile may be different. The yeast may also have altered levels of intracellular stress resistance compounds, such as trehalose, glycogen and heat shock proteins.
- **Replicatively deactivated cells:** These yeast do not have the ability to reproduce due to impaired membrane integrity. This is detectable by viability assays such as methylene blue staining and regrowth ability. The cells do, however, retain complete or at least partial metabolic activity.
- **Cells with minor envelope damage:** Cells with envelope damage are not necessarily of poorer quality in terms of fermentation performance but the presence of these cells may negatively affect beer quality because of haze release (Lewis and Poerwantaro, 1991). These cells may have altered surface charge and hydrophobicity as well as impaired flocculation ability.
- **Dead cells:** These cells are unable to reproduce and also show no metabolic activity. Given time these cells will go through autolysis, releasing cytoplasmic components into the bulk phase.
- **Disrupted cells:** These cells can be either partially (visible as cellular entities) or completely (visible only as cell fragments) disrupted. Both forms are the terminal result of extreme hydrodynamic shear forces or autolytic processes of dead cells.

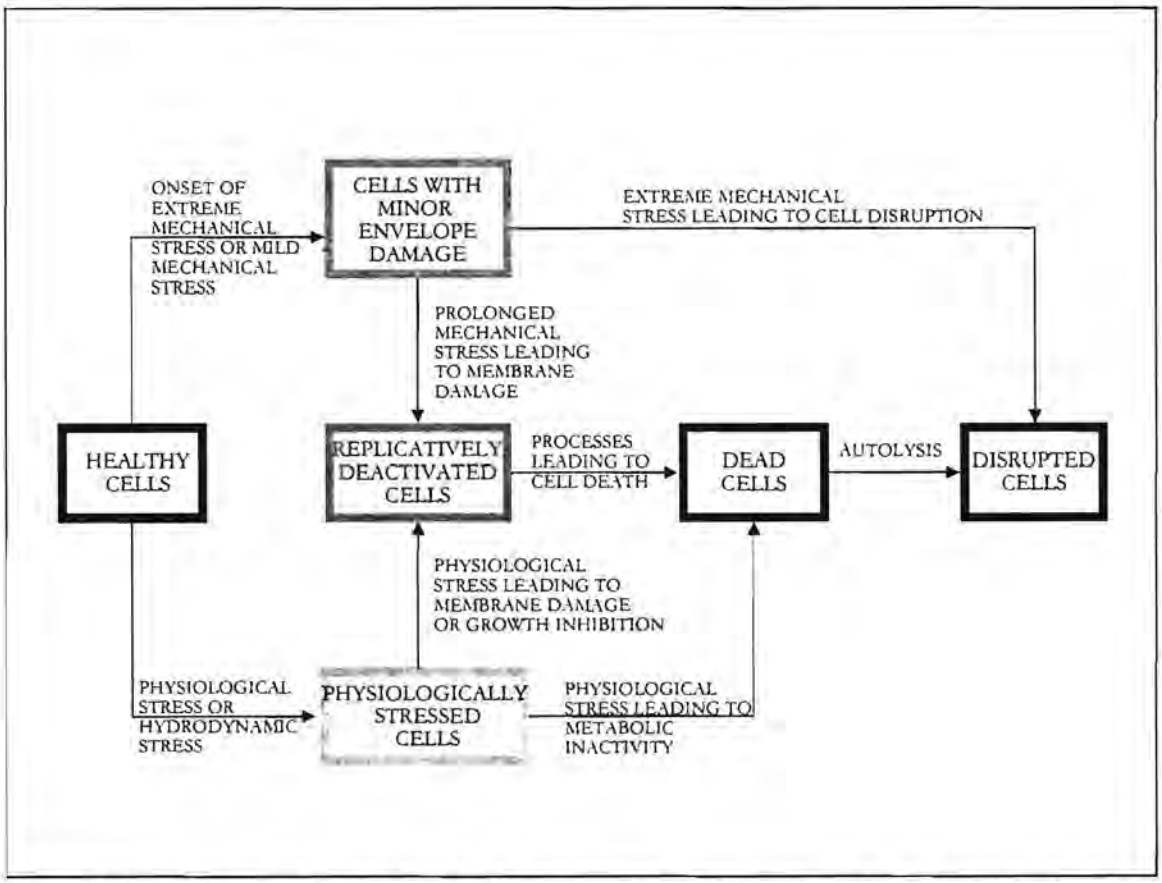

Figure 2.1. Scheme for the loss of yeast quality due to applied physiological and hydrodynamic stresses (Basson, 1996).

This approach is useful as it illustrates how different physiological and hydrodynamic stress can result in similar physiological states of yeast. In this thesis, the focus is placed on loss of yeast quality following exposure to hydrodynamic stress imposed by mechanical handling. Hence, the upper branch of the proposed scheme for loss of yeast quality presented in Figure 2.1 is expanded in Figure 2.2. This scheme investigates the understanding that the effect of shear stress is propagated through the outer layers of the cell towards the centre of the cell. Slight hydrodynamic shear would then only be 'felt' at the outer cell wall and damage to the membrane and cytoskeleton would not be possible. As the severity of the forces is increased, damage is observed at the membrane and cytoskeleton levels successively and only the most extreme of forces would be able to disrupt the cell. It has been shown that physiological stress can also affect the surface properties of brewers' yeast by reducing its surface charge (Smart *et al.*, 1995) and causing the yeast to be less flocculent (Rhymes and Smart, 1996). Should similar biological effects be observed when the yeast is exposed to hydrodynamic stress, it would support the dual mechanism leading to the physiological states depicted in Figure 2.1.

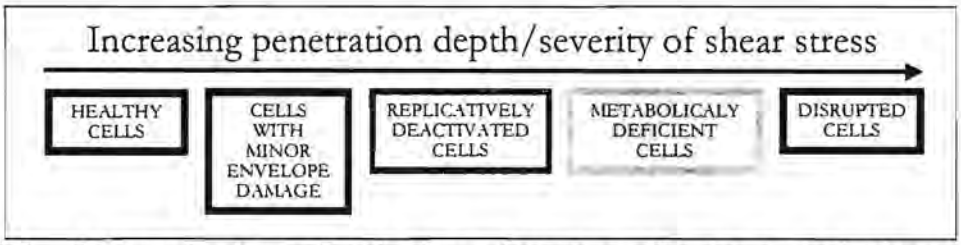

Figure 2.2. Proposed scheme for the loss of yeast quality due to hydrodynamic shear stress.

2.2.3 Yeast Handling Procedures

In the yeast handling circuit at SAB-Newlands brewery, as depicted in Figure 2.3, yeast is pumped from the base of a fermentation cone with a positive displacement pump through 65 mm diameter piping for distances of up to 150 meters to a plate and frame heat exchanger (chiller) where it is cooled from 14 to 2 °C before passing into a storage vessel. This process is termed cropping and occurs at the end of each fermentation. Once the yeast is in the storage vessel, agitation is started and the yeast concentration (consistency) and viability are measured to determine the quantity to be used in the next series of fermentations. The process of inoculating a fermentation with yeast is termed pitching. Since the quantity of yeast increases three fold during fermentation, each yeast crop can be reused to pitch up to three new fermenters. The required quantity of yeast for a subsequent fermentation is pumped from the storage vessel to a separate pitching vessel (also agitated) where it is stored until needed for fermentation (generally not longer than 8 hours). For strain SAB1, the yeast is washed with acid for 30 minutes before pitching. This process involves the addition of a volume of food grade phosphoric acid equal to the yeast volume while agitation is maintained. This

reduces the slurry viscosity and yeast flocculence as well as reducing bacterial contamination since few common brewery contaminants are able to withstand the low pH (2.7) of the slurry. After acid washing, the yeast slurry is pumped out and injected into the main wort line with the feed to the next fermenter.

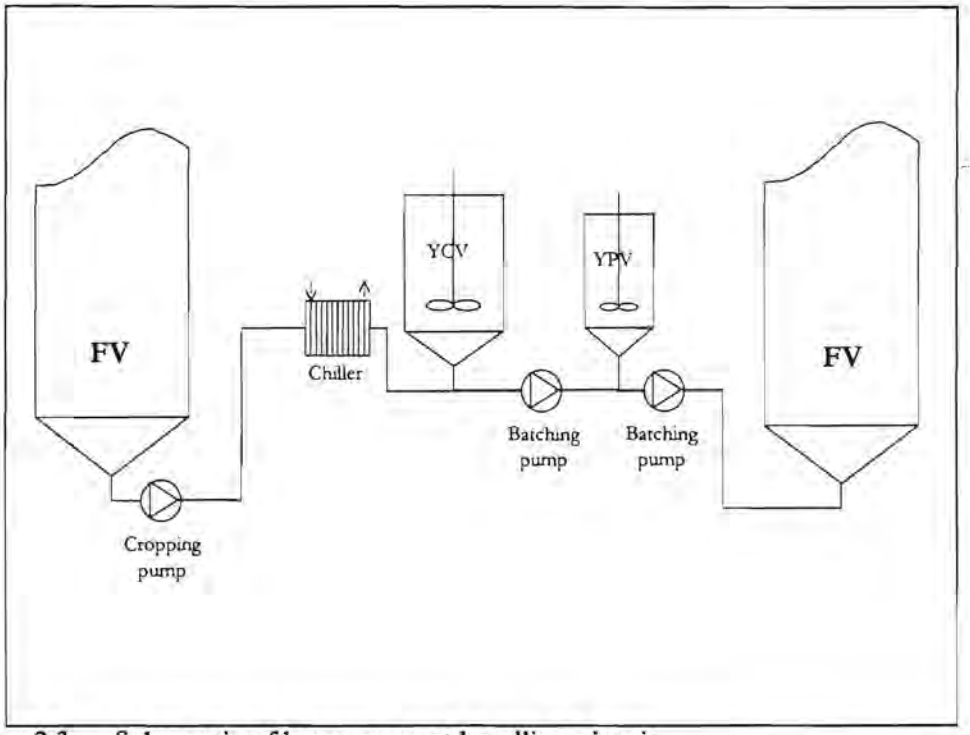

Figure 2.3. Schematic of brewery yeast handling circuit.

Apart from the yeast handling circuit at the brewery, the green beer circuit also contains yeast which is exposed to shear and therefore susceptible to damage thus affecting beer quality (Figure 2.4). Once the settled yeast has been removed from the fermentation vessel the beer still contains significant quantities of suspended yeast. Before the beer can be transferred to lagering vessels, the yeast concentration has to be lowered to between 1 and 3 x 10^6 cells/ml to achieve the desired secondary fermentation where flavour maturation occurs. This may be achieved by adding a flocculating agent to the beer en route to the lagering vessels which causes the yeast to flocculate and settle in the lagering vessel, from where it is removed. This method of achieving the required yeast concentration is imprecise and leads to variations in secondary fermentation performance and beer quality. Another method of removing the excess yeast is by centrifugation of the beer as it is transferred to the lagering vessel. The centrifuge can be operated to ensure the desired average cell concentration in the lagering vessel. This is the current preferred method employed at SAB. After secondary fermentation in the lagering vessels, the process beer is filtered to remove the final traces of yeast before pasteurisation and packaging.

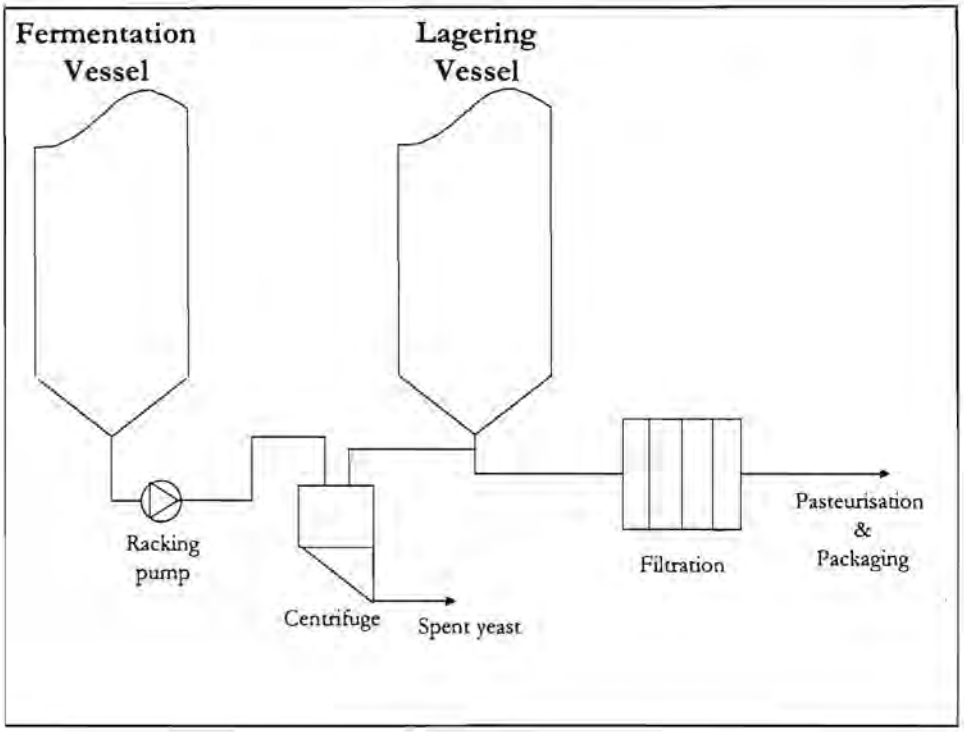

Figure 2.4. Schematic of the brewery beer fermentation circuit.

Thus in a brewery, the yeast is subjected to shear generated due to pumping, flow through pipework and constrictions, changing flow patterns in the chiller, agitation of yeast slurries and separation of yeast in centrifuges. Of these operations, pumps and flow conditions, agitation and centrifuges have been studied in some detail with respect to their effect on yeast quality.

2.2.3.1 Pumps

Positive displacement pumps with low flow pulsation characteristics (< 15 kPa) are required in the brewing industry to transport yeast slurries because of the high differential pressures which are required to be produced, the high viscosity of concentrated yeast suspensions and concern surrounding the damage of cells by hydrodynamic stress. Cleanability is also of paramount importance since aseptic transfer conditions are required at all times and CIP needs to be performed before and after each transfer (Boughton, 1983; Boughton, 1987; Ball, 1994; Basson, 1996). Based on the investigation of Basson (1996) into the effect of various pump types on yeast quality and fermentation performance, none of the pumps tested (peristaltic, lobe, sine, gear, diaphragm and centrifugal) showed any significant differences in their effect on yeast quality. Due to the cleanability and almost absence of flow pulsation, she recommended the use of the sine or gear type pump in addition to the lobe pumps currently in use.

2.2.3.2 Flow conditions

The rheology of the yeast slurry is a function of yeast solids concentration and flocculation characteristics. Jin and Speers (1998) show the effect of temperature, cell size, shape, age and nutritional status as well as pH and ionic species and concentration present in suspension on floc structure and shape. These parameters influence the apparent viscosity of brewers yeast slurries. Although noted that shear history may play a role in floc structure and hence viscosity, no report was given on the effect of shear damage of yeast flocculins affecting flocculation potential and apparent viscosity. The apparent viscosity together with pumping rate and pipe diameter, determines the magnitude of the hydrodynamic forces experienced on yeast handling. The magnitude of shear and the time of exposure determine the nature and extent of cell damage. Pumping rates have been reported to be maintained below 50 – 55 $kg.min^{-1}$ to avoid yeast damage (Boughton, 1983; Boughton, 1987) while pipe diameter should be chosen to limit the linear velocity to 0.5 $m.s^{-1}$ (Ball, 1994). More recently the effects of higher linear velocities (0.1 – 3.7 $m.s^{-1}$) and Reynolds numbers ranging from 86 to 1114 were investigated (Basson, 1996). Basson reported no adverse effect on either yeast quality or fermentation performance under these operating conditions. The study was performed at pilot scale with yeast analysed in terms of viability, vitality, storage product concentration as well as fermentation performance.

Pipe fittings, constrictions and expansions as well as other pieces of process equipment which cause changes in the flow pattern of yeast slurries result in increased shear forces and the associated increased possibility of cell damage. To minimise the risk of cell damage, yeast handling should be minimised (Ball, 1994) but individual studies on the effects of shear generated in these pieces of process equipment and fittings on brewers' yeast have not been reported. Recently a report on the effects of shear as a result of flow through pumps, valves and tangential flow filtration systems on microalgae species used a pressure drop coefficient to correlate damage to shear (Vandanjon *et al.*, 1999). The flow of fluid past a constriction has the potential to cause cavitation which is known to disrupt yeast cells (Save *et al.*, 1994). Save *et al.* (1997) report that cavitating flow of yeast slurries through an orifice were an order of magnitude more energy efficient than other standard disruption techniques (ultrasonication and blender) at causing cell disruption. Should cavitation occur in the brewery yeast handling circuit, the possibility of it causing cell disruption is significant.

2.2.3.3 Agitation of yeast slurries

It has been found that the agitation of yeast slurries may result in the formation of fine particulate haze material (Lewis and Poerwantaro, 1991). This material was traced back to the cell wall and identified as being carbohydrate. It was also observed that cells in the stationary phase are more susceptible to haze release than growing cells. This has implications in the brewing environment since cropped yeast is in the stationary phase and as such is susceptible to cell wall damage.

Damaged cell walls would have the dual result of increased concentrations of haze material in the beer as well as a decreased yeast quality.

2.2.3.4 Centrifugation of green beer

Siebert *et al.* (1987) reported sporadic haze production in a brewery which was traced back to the centrifugation of process beer prior to filtration. The haze was predominantly water soluble (85 – 99 %). The water soluble fraction contained some 14 % protein while the water insoluble fraction averaged 53 % protein. The carbohydrate content of the water soluble and water insoluble fractions averaged 25 and 92 % mannan respectively. Staining procedures illustrated the presence of fungal cell walls and mannan residues from the yeast cell surface. The haze particulate size was between 0.5 and 1.0 μm. No evidence of ghost cells was observed although thiamine was found to increase in the clarified stream indicating cell autolysis.

2.3 Influence of Cell Structure on Hydrodynamic Shear Stress Resilience

The four key aspects of cellular anatomy which influence the response of cells to a shear environment as proposed by Prokop and Bajpai (1992) are:

1) The cell wall and/or membrane which acts as the first barrier of defence against shear.
2) The viscous cytoplast containing the cytoskeleton which can absorb and dissipate a large proportion of the total kinetic energy acting upon the cell.
3) The cell size which determines the extent to which the cell will absorb kinetic energy in the fluid environment.
4) The existence of receptors which receive and amplify fluid mechanical stimuli.

The different responses of cells to hydrodynamic shear can be related to differences in one or more of the above mentioned aspects of the cell anatomy. All cells are surrounded by a membrane arranged in the form of a lipid bilayer. The membrane contains various structural and enzymic proteins which facilitate communication between the cell interior and the environment. Bacteria, plant, fungi and yeast cells also have a cell wall which plays a role in the metabolism, information processing and immunological identification of the cell. All cell walls are relatively thick polysaccharide gels containing carbohydrate, protein or carbohydrate/protein fibres for structural reinforcement. Despite the apparent strength offered to a cell by such tough walls, plant cells are known to be highly shear sensitive. Dunlop *et al.* (1994) reported that carrot cells lost their regrowth ability at energy dissipation values four orders of magnitude below that at which the cells were lysed (Figure 2.5). They also observed the loss of mitochondrial activity and membrane integrity at lower energy dissipation values than required for cell lysis. It is therefore apparent that cells can loose viability and activity under hydrodynamic shear conditions well below the mechanical strength of

cells. The cell wall nevertheless remains a physical barrier between the cell and the environment. The detailed function, composition and structure of the yeast cell wall is discussed below to enable hydrodynamic effects to be better understood and predicted in the brewing industry.

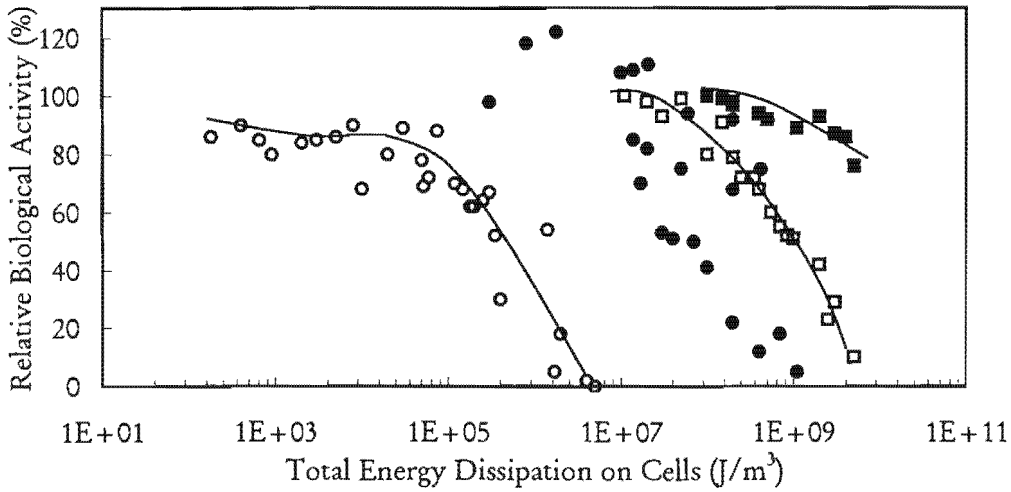

Figure 2.5. Relative biological activities of carrot cells under laminar conditions, adapted from Dunlop *et al.* (1994).

(○ regrowth activity, □ membrane integrity, ■ non-lysed cells, ● mitochondrial activity)

2.3.1 Yeast Cell Wall

The cell wall is regarded as an assemblage of mostly polysaccharide polymers, the rigidity of which imparts form and strength to the cell. The properties and functions of the cell wall change constantly during the life cycle of the cell. The function, structure and composition of the yeast cell wall are detailed in this section.

2.3.1.1 Cell wall function

The wall is a multifunctional organelle of the cell providing the following:

- structural strength, protection and shape
- enzymic activity to hydrolyse extracellular nutrients (Arnold, 1981) and wall compounds (Fleet, 1984) during morphogenisis and re-utilisation
- cellular recognition, interaction and attachment by specific macromolecules, receptors and wall polymers (Calleja, 1987).

Since it is the cell wall of *Saccharomyces cerevisiae* which contacts its environment, it is the cell wall properties, most notably the hydrophobicity and surface charge, of this surface which determine its interaction with the environment.

2.3.1.2 Cell wall macromolecular composition

In studying the cell wall components and structure, harsh mechanical methods to disrupt the cell are often employed. These include bead milling, pressure homogenisation and ultrasonication to cause cell rupture. The harsh conditions needed to purify yeast cell walls may cause some rearrangement and degradation of its constituents thus making the analysis of the composition of the wall more complicated. The loss of proteinaceous material (Straver *et al.*, 1994) and of mannan (Lewis and Poerwantaro, 1991) from cell walls has also been found to occur in their studies under milder conditions of prolonged agitation. Because of these difficulties, only the bulk cell wall composition can be determined accurately by these mechanical disruption methods and more gentle disruption methods involving sequential partial enzymatic digestion of the cell wall are used to examine finer structural details.

The yeast cell wall consists predominantly of 3 macromolecular components; lipids, proteins and polysaccharides (mannan, glucan and chitin) as detailed in Section 2.3.1.3. These constituents, together with phosphate groups are combined to form a complex heterogeneous polymer (Wessels and Sietsma, 1981; Matile *et al.*, 1969; Klis, 1994). The cell wall accounts for between 15 and 25 % of the dry cell weight of the cell. Polysaccharides are the most abundant constituents in the wall, accounting for 80 - 90 % of the wall by mass. Glucan and mannan are the predominant polysaccharides with only a small amount of chitin present.

2.3.1.3 Structure of the cell wall constituents

Glucan is a polymer of glucose, accounting for approximately 60 wt% of the cell wall. Different types of glucan have been classified by Manners *et al.* (1973a, b) and Fleet and Manners (1975), according to the relative abundance of β(1,3) and β(1,6) linkages between the glucose residues. The alkali insoluble/acid insoluble fraction has a fibrillar appearance and confers rigidity to the wall. The predominantly β(1-6) fraction is thought to be the anchorage point for chitin while the alkali soluble portion is amorphous and confers flexibility to the wall. Glucan is also the anchorage point for mannan and provides an extracellular metabolic store of glucose. The composition and amount of each type of glucan, as a percentage of the total glucan present, is given in Table 2.2.

Table 2.2. Types and abundances of glucan present in yeast cell walls according to Manners *et al.* (1973a, b) and Fleet and Manners (1975).

Classification	β(1-3)	β(1-6)	wt% of wall
Alkali insoluble, acid insoluble	95	-	35
Predominantly β(1-6)	5	65	5
Alkali soluble	80-85	8-12	20

The compositions do not sum up to 100%. Since these are the only types of glucan present, this represents the accuracy of the methods used in extraction.

Mannan is a polysaccharide with a highly branched polymeric structure of mannose with an α(1-6) linked backbone and side chains of ($M^{2-1}M$), ($M^{2-1}M^{2-1}M$), ($M^{2-1}M^{3-1}M$) and ($M^{2-1}M^{2-1}M^{3-1}M$) (Ballou *et al.*, 1980). A schematic representation of the outer chain mannan structure typical of wild strains of *S. cerevisiae*, based on strain X2180 (Ballou and Raschke, 1974 and Ballou, 1982 cited in Stratford 1992a), is shown in Figure 2.6. The chain consists of between 10 and 15 mannan units with the number and position of the different side branches varying between strains. Mannan is known to be the antigenic receptor of yeast cells (Suzuki, 1981), with some strains showing the tetrasaccharide to be the most inhibitory, thus indicating the dominance of the α(1-3) link. Raschke and Ballou (1971) found other strains which showed α-D-mannophosphate to be the dominant antigen site. Because of the similarities between antigen and flocculation interactions between cells, the antigen sites could also play a role in flocculation interactions between cells.

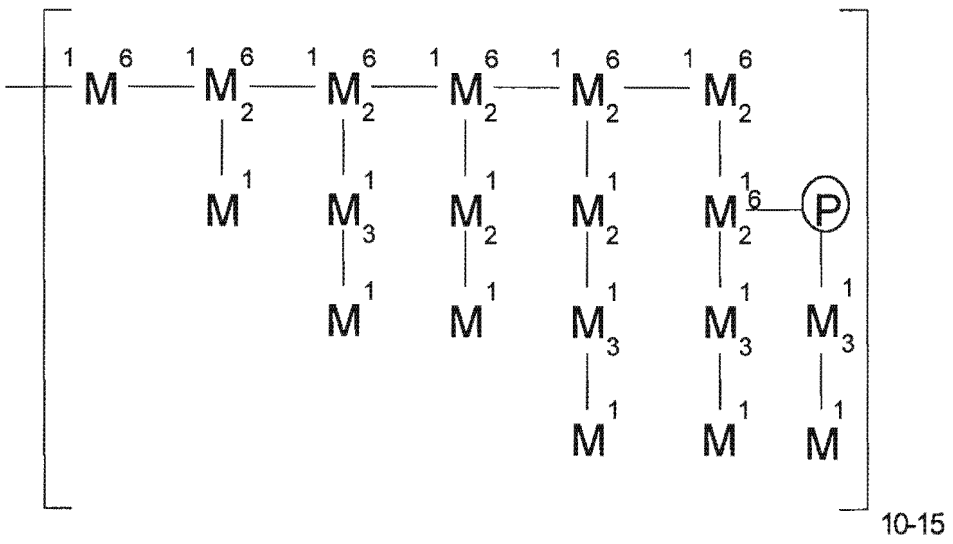

Figure 2.6. Schematic representation of the outer chain mannan structure of *S. cerevisiae* X2180 (Ballou and Raschke, 1974; Ballou, 1982).

In the yeast cell wall, mannan is always found to be covalently linked to protein and so **mannoprotein** is a better representation for this macromolecule. The mannan portions of

mannoprotein structures are linked to the protein as short oligosaccharides at serine and threonine (Fleet, 1991). Four classes of mannoproteins exist:

1) Intracellular mannoproteins with enzymic properties.
2) Structural mannoproteins lying on top of the glucan layer which are not strong by themselves but act synergistically with glucan to provide wall structure and rigidity.
3) Sexual and/or flocculating agglutination factors which are involved in specific cell/cell interactions.
4) Mannoproteins occurring extracellularly and showing enzymatic activity e.g. invertase.

The mannoproteins represent 25-50 % of the cell wall of *S. cerevisiae* (Jayatissa and Rose, 1976) with the protein content amounting to 5 - 10 %. These complexes also contain small amounts of glucosamine and phosphorus (0.1 - 1 %). The mannoproteins are linked by phosphorus bonds as well as a combination of sulphur-sulphur, thioester bonds and hydrophobic interactions.

The **protein** content of the walls is between 13 and 15 % (Ramsay and Douglas, 1979). Some of the protein serves to attach mannan to the cell wall thus indicating its structural role while other protein compounds serve enzymatic roles by cleaving nutritional substrates or as turnover enzymes during cell morphogenesis (Arnold, 1981). Enzymes found in the cell wall include invertase, acid phosphatase, aminopeptidases and other hydrolases. The enzymes are complexed to the glucan and mannan constituents in the wall forming glycoproteins and glyco-mannoproteins, often referred to as mannoproteins. Other proteins function as receptor molecules during cell mating and as agglutination factors during flocculation (Hodgson *et al.*, 1985; Hussain *et al.*, 1986; Bony *et al.*, 1998).

Chitin is an unbranched and highly rigid polymer of N-acetyl-D-glucosamine, joined through β(1-4) linkages. Less than 10 % of the cell wall consists of glucosamine polymers. Of this, only 1-2 %, depending on the extent to which budding has occurred, is in the form of chitin. Most of the chitin is found in the bud scar zone of mother cells. This suggests that chitin has a specific involvement with cell division but its precise role remains unclear (Bacon *et al.*, 1966; Cabib *et al.*, 1982 cited by Fleet, 1991). Because of the rigidity of the chitin molecules, older yeast cells with more bud scars are more rigid and inelastic which may cause them to respond differently to hydrodynamic stress.

McMurrough and Rose (1967) have reported a **lipid** content of the cell wall of 2 to 14 % of the dry weight of the wall. Lipids are thought to be bound to mannan but its role is not well understood. The major lipids in *S. cerevisiae* are unsaturated palmitoyl (C_{16}) and oleyl (C_{18}) residues (Breezer *et al.*, 1986 cited by Fleet, 1991). Breezer *et al.* (1986) also suggest that lipids are formed in response to antibiotics as a protectant.

2.3.1.4 Macromolecular organisation of the cell wall

An outer layer of mannoprotein is intimately associated with an amorphous matrix of alkali soluble glucan. This layer overlays the rigid fibrillar component of alkali insoluble β(1-3) glucan. β(1-6) glucosidic linkages anchor the high mannan layer to the alkali insoluble glucan layer. The lipids and protein are dispersed through both the glucan and mannan rich layers. Although it is useful to think of the wall as consisting of two layers, they are not distinct because the mannoprotein layer penetrates the glucan layer, forming pores. It is therefore the mannoproteins which determine the cell wall porosity (Gerhardt and Judge 1964; De Nobel *et al.* 1989).

The structure of the yeast cell wall, proposed by Lampen (1968), is shown schematically in Figure 2.7. This remains a good approximation of the actual structure, except that the two layers are less distinct with lipids interspersed throughout and mannan lined pores extending through the glucan rich layer.

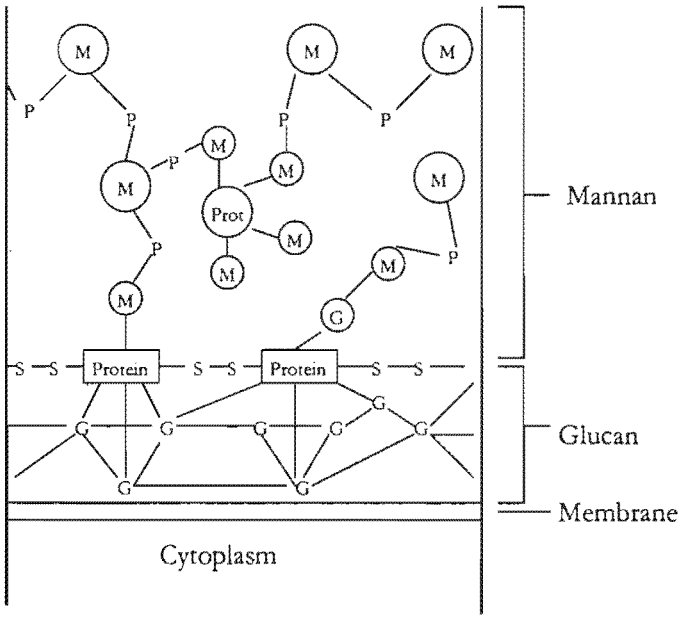

Figure 2.7. Structure of the cell wall of yeast (Lampen, 1968).

2.3.1.5 Factors affecting the cell wall composition and structure

The composition of the cell wall is not static but dynamic and is affected by nutritional supply in the culture media and the age of the cell.

Nutritional Variation

Yeast grown in a medium containing a high glucose concentration develops a cell wall with a higher glucan content. Similarly, when mannose is used as the carbon source, the cell walls contain a higher mannan to glucan ratio. Under conditions of nitrogen limitation, the cells incorporate more lipids

into the cell wall and have a lower protein content while phosphate limitation causes a decrease in the mannan content of the walls. Inisotol starvation results in more mannan with a concomitant decrease in glucan polysaccharide content, altered protein composition and double the chitin content (Amri *et al.*, 1982). The cells' ability to excrete macromolecules (amylase and cellobiohydrolase) has been shown to be dependent on the growth medium with complex media resulting in more efficient excretion than minimal media. This effect was shown to be a result of increased cell wall porosity of yeast grown in complex media relative to its growth in minimal media (De Nobel *et al.*, 1989). No difference to the mannan, protein or β-glucan content of the outer cell wall of a strain of lager yeast occurred upon starvation of the cells in a nutrient depleted medium (Rhymes and Smart, 1996). A decreased density of the cell wall was observed which allowed bulky dye molecules to penetrate deeper into the cell wall. The phosphate composition of the cell surface was found to decrease by both XPS and surface charge analysis. Both the less dense cell wall and lower phosphate content are consistent with the expectation that the cell wall can be used as a carbon and phosphate source under starvation conditions to maintain cell viability.

Culture age

It is generally observed that older microbial cells are more refractile to mechanical and enzymic disruption than younger cells which suggests differences in the cell walls' composition and structure (Felix, 1982; Golovinn *et al.*, 1973; Fish and Lilly, 1984; Harrison *et al.*, 1991). Lyons and Hough (1970) found an increase in mannan to glucan ratio as both flocculent (NCYC1005 and NCYC1026) and non-flocculent (NCYC1004 and NCYC1040) yeast cultures move from exponential growth to stationary phase. Amri *et al.* (1982) also showed that as the cells of two flocculent strains (SU0006 and SU0019) progressed from exponential to stationary phase their mannan to glucan ratio increased, protein content decreased and mineral ratio of Ca^{2+}/K^{+} decreased. The cells were also found to become flocculent when stationary phase was reached while remaining non-flocculent during the exponential growth phase. Using an ale yeast (M2 from Morrells Brewery, Oxford, U.K.), Smart and Whisker (1996) reported changes in the cell surface properties as a result of the serial repitching of brewers yeast which imparted changes in the flocculation characteristics of the successive generations of yeast. Although the wall composition was not determined, they postulated that the altered hydrophobicity, charge and flocculence of the yeast was due to altered cell wall composition.

2.3.1.6 Class of yeast

Although differences in wall composition have been observed between flocculent and non-flocculent strains (Mill, 1966) as well as between top and bottom fermenting strains (Amory and Rouxhet, 1988), there does not appear to be any systematic method of classifying a strain from its wall composition alone.

2.3.1.7 Elemental composition

The major elements present in the cell wall of yeast are C, N, O, H, S and P with Na, K, Ca and Zn appearing in trace amounts. In studying the physicochemical properties of the yeast surface (charge and hydrophobicity), the elemental composition at the surface is more informative than the bulk cell wall compositions. X-ray photoelectron spectroscopy provides a detailed elemental composition of the outermost 2-5 nm of the surface of solids. The technique is used increasingly to determine the surface composition of biological samples including yeast, fungi and bacteria (Amory *et al.*, 1988; Dengis *et al.*, 1995b). Initially it was postulated that the surface of a dehydrated sample used in this analysis may not be representative of the natural surface in a hydrated environment but there is increasing evidence to support its validity (Amory *et al.*, 1988; Amory and Rouxhet, 1988; Dengis *et al.*, 1995a, b; Dengis and Rouxhet, 1996; Dufrêne and Rouxhet, 1996; Rouxhet *et al.*, 1994). Typical elemental compositions, with 95 % confidence intervals, for two strains of *S. cerevisiae*, MUCL38475 (a top fermenting strain) and MUCL28285 (bottom fermenting), in the exponential and stationary phases are provided in Table 2.3. The elemental composition indicates that although there are differences depending on the growth phase of the yeast, these are not significant. There are, however, significant differences between the top and bottom fermenting strains at the stationary phase. Relative to the bottom fermenting strain (MUCL28285), the top fermenting strain (MUCL38475) has more total carbon and nitrogen with a corresponding lower total oxygen content. Of the total carbon, the ratio C-(C,H)/C-(O,N) is higher while for the oxygen the ratio C-O/C=O is lower.

Table 2.3. Typical elemental composition of yeast cells in the exponential and stationary phases. (Dengis *et al.*, 1995b).

	MUCL38475		MUCL28285	
	Exponential	Stationary	Exponential	Stationary
Total C	70.5±3.0	70.4±1.2	67.8±1.8	67.6±2.4
C-(C,H)	38.7±1.2	36.3±3.2	30.7±2.1	29.2±5.0
C-(O,N)	24.1±5.6	25.9±1.8	28.9±1.0	30.0±2.6
C=O	6.5±1.4	6.6±0.5	7.1±0.7	7.2±0.7
O-C=O	1.2±0.2	1.5±0.2	1.1±0.3	1.2±0.3
Total O	26.3±3.7	27.4±1.4	30.3±1.5	30.9±2.5
O-(C,H)	21.6±6.0	24.3±2.0	27.7±1.0	28.9±2.8
O=C	4.7±3.2	3.1±1.0	2.6±1.0	1.9±0.7
Total N	2.6±1.1	2.0±0.3	1.2±0.3	1.2±0.3
N	2.4±0.8	1.8±0.2	1.1±0.2	1.1±0.3
N^+	0.3±0.2	0.2±0.1	0.1±0.1	0.1±0.1
P	0.28±0.22	0.15±0.09	0.28±0.06	0.17±0.05
K	0.33±0.15	0.15±0.07	0.45±0.31	0.16±0.08

The elemental composition of the surface can be used to calculate the molecular composition of the surface. Based on elemental composition and bond ratios of the three model compounds believed to be present on the surface (protein, lipid and polysaccharide), Dengis *et al.* (1995b) determined the surface concentrations of these compounds in *Saccharomyces cerevisiae.* The macromolecular compositions of the two strains described above were calculated for the exponential and stationary phases of growth and are provided in Table 2.4. As with the elemental composition data presented in Table 2.3, no statistically significant difference between the exponential and stationary growth phases can be seen. The inter strain variation is, however, evident. In this case strain MUCL38475 has a higher surface protein and hydrocarbon content than MUCL28285 while the polysaccharide content is lower. The hydrocarbon like compound was representative of a molecule with high carbon to carbon bond content and this molecule is similar to lipid which is known to occur in yeast cell walls.

Table 2.4. Macromolecular composition of strains MUCL38475 and MUCL28285 during exponential and stationary phases (Dengis *et al.*, 1995b).

Compound	MUCL38475		MUCL28285	
	Exponential	Stationary	Exponential	Stationary
Protein	14.3±5.1	10.5±1.3	6.7±1.1	6.7±1.5
Polysaccharide	52.9±6.0	56.9±3.2	65.2±3.2	66.1±5.9
Hydrocarbon	32.8±6.5	32.7±2.7	28.1±3.8	27.2±5.0

2.3.1.8 The origin of cell surface charge and hydrophobicity

Phosphate groups bound to mannan in the outer layers of the cell wall (Figure 2.5) are the most important charge determining group on the yeast cell surface (Amory and Rouxhet, 1988; Bowen *et al.*, 1992; Jayatissa and Rose, 1976). Mozes *et al.* (1988) reported that phosphate is the major charge determining element at the cell surface with a correlation between the ratio of nitrogen to phosphate content and electrostatic charge. The same ratio was found to be inversely proportional to yeast hydrophobicity. It is generally believed that the charge carried by yeast causes the stability of the suspension. Carboxyl groups on surface proteins also impart negative charge to the cells while the amino groups of proteins are positively charged. To determine the relative importance of the two negatively charged groups on overall surface charge, the pH dependence of electrophoretic measurements (Bowen and Cooke, 1989; Beavan *et al.*, 1979; Jayatissa and Rose, 1976; Eddy and Rudin, 1958) and direct titrations (Bowen *et al.*, 1992) have been used. In general the charge attributed to phosphate groups was proportional to the electrokinetic mobility of the cells at pH 4.0 while that attributed to carboxylic groups was proportional to the difference in mobility between pH 7.0 and pH 4.0. Bowen and Cooke (1989), however, used the mobility at pH 3.5 to represent phosphate and the difference between pH 5.5 and pH 3.5 to represent carboxyl contributions.

Bowen *et al.* (1992) made further refinements based on the expected pK values of groups in the yeast wall environment to approximate the phosphate contribution at pH 3.25 and the carboxyl groups as the difference between pH 5.5 and pH 3.5. These are based on the following equilibrium reactions for the various charged groups in the cell wall.

$$RR'HPO_3 \xleftrightarrow{K_1} RR'PO_3^- + H^+$$
$$COOH \xleftrightarrow{K_2} COO^- + H^+$$
$$R''NH_3^+ \xleftrightarrow{K_3} R''NH_2 + H^+$$

The equilibrium constants are as follows: pK_1 of 6.2 for phosphomannan extracted from yeast cell walls; pK_2 of 4.1 based on aspartic acid and glutamic acid; pK_3 of 11.5 from the basic amino acids lysine and arginine.

Differences have been reported between the surface charge and hydrophobicity of top and bottom fermenting yeast strains, lager and ale strains as well as changes in the surface properties during storage and serial repitching. The hydrophobicity of top fermenting strains is greater than that of bottom fermenting strains (Amory and Rouxhet, 1988) and is correlated to the nitrogen to phosphate ratio measured by XPS. The measured contact angles of strains MUCL38485 (top fermenting) and MUCL28285 (bottom fermenting) are 77 ± 12 and 31 ± 15 degrees in the stationary phase (Dengis *et al.*, 1995b), confirming that top fermenting strains are generally more hydrophobic. The surface charge at pH 4 was found to be proportional to the phosphate content of the yeast with bottom fermenting strains having more negative zeta potentials than top fermenting strains: - 35 ± 5 and - 12 ± 9 mV respectively. Dengis *et al.* (1995b) found the isoelectric point of the bottom fermenting strain to be pH 2 while that of the top fermenting strain was pH 4. At higher pH values found during fermentation (pH 5.3) the zeta potentials were similar.

Smart *et al.*(1995) observed changes in the surface properties of yeast as a result of physiological stress induced by starvation. The negative charge of cells on starvation, (BB5, Bass Brewers Ltd.) measured by zeta potential in 10 mM KCl at pH 4.0 was found to decrease from - 42.6 ± 7.1 to - 32.5 ± 2.5 mV. Since phosphate is the predominant charged species at pH 4, this represents a loss of phosphomannan at the cell surface. Rhymes and Smart (1996) studied the effect of starvation on the surface properties of two strains of yeast, the lager yeast BB5 and the ale yeast NCYC1168. They found a reduced surface charge on the lager yeast as a result of starvation and an increase in charge for the ale yeast. There was also a small decrease in hydrophobicity of the lager yeast and a more substantial decrease for the ale yeast. Rhymes and Smart (1996) also observed the preferential attachment of hydrophobic latex beads to the polar regions of individual cells and when cells were budding there was a distinct lack of attachment to the mother/daughter region. This indicates that the mature regions of the cells, particularly old bud scars might be more hydrophobic than younger

cell wall material. Recalling the discussion on cell wall composition, chitin is the major component of bud scars, hence it is probable that chitin content of cells is a major determinant in its level of hydrophobicity.

The surface properties of yeast which was repitched extensively in a brewery was also found to change (Smart and Whisker, 1996). An ale strain from Morrells Brewery Ltd. (M2) was found to lose charge during the first five serial repitchings measured by decreasing alcian blue dye retention from 8.0 to 0.2 μg/mg, and then maintain this level until the 23'rd reuse of the yeast. This strain did not show any appreciable change in the hydrophobic nature irrespective of the number of times it was reused.

2.4 Flocculation

Flocculation is the process whereby particles in a colloidal suspension come together to form unstable particles which can grow into agglomerates and settle out of suspension. A colloidal suspension is one in which the individual particles remain as separate particles in a dispersed state. Although yeast cells are too large to form a true colloidal solution, they may act in a semi-colloidal manner (appearing as a stable suspension) as their individual sedimentation rates are small in aqueous solutions. Using the Stokes law of terminal settling velocity (Equation 2.1) the settling velocity of a unicellular yeast and a floc of cells were calculated. This was based upon the average cell size (6.65 μm diameter) and density (1150 $kg.m^{-3}$) calculated for the yeast strains used in this study (presented in Appendix A.2), the average free terminal settling velocity of a unicellular yeast in water is 13 mm/hr. Yeast may flocculate into aggregates of up to several millimetres in diameter and settle at velocities some 10^4 times the single cell settling velocity owing to the dependence of settling velocity on the square of particle diameter. For example, a cubic close packed yeast aggregate of 2 mm diameter, has a settling velocity of $7x10^5$ mm/hr.

$$v_{stokes} = \frac{d_p^2 g}{18\mu}(\rho_p - \rho) \qquad (2.1)$$

where: v_{stokes} = Stokes terminal settling velocity ($m.s^{-1}$)

d_p = diameter of particle (m)

g = gravitational acceleration ($m.s^{-2}$)

ρ = density of solution ($kg.m^3$)

ρ_p = density of particle ($kg.m^3$)

In the brewing process, lager yeast flocculates at the end of the primary fermentation and collects at the bottom of the fermenter while ale yeast either floats to the top of the fermenter or settles to the bottom like lager yeast. Besides these differences in yeast types, the extent of flocculation may also

vary and some strains do not flocculate at all. Since flocculation is of such importance in the brewing industry, the mechanisms by which flocculation can occur needs further examination. Firstly classical flocculation of a colloidal suspension is discussed in terms of the forces of attraction enhanced by hydrophobicity of particles, and repulsion caused by the charge carried on the particles. The classical mechanism of flocculation, as described by hydrophobic destabilisation, can be dominated by another mechanism involving bridge formation. In bridging flocculation the adsorption of polymeric substances onto the surfaces of particles alters the surface of the particles thereby changing their flocculation character. A third and more specific mechanism of flocculation can occur, known as the antigen/antibody reaction. This enhances flocculation and cell adhesion in living systems. These mechanisms are discussed in greater detail in Sections 2.4.1, 2.4.2 and 2.4.3.

2.4.1 'Classical' flocculation

Flocculation commences from a suspension of discrete particles or a colloidal solution. The stability of such discrete particles is brought about by surface charge and layers of hydration. The extent of such water layering around a particle is commonly referred to as the extent of hydrophobicity or hydrophilicity. A hydrophilic particle has an affinity for water molecules. This can result in a significant amount of water being bound to the particle, as much as 10 times the dry mass of the particle itself (Bratby, 1980). A hydrophobic particle, however, also has a layer of adsorbed water but typically only one molecular layer thick. This is bound strongly enough to move with the particle as a single unit, such that the plane of shear lies between the bound water and the free water.

Because of the polar nature of water, the water molecules will orientate themselves around a charged particle and this orientation extends into the bulk liquid. The extent of orientation, however, diminishes with increasing distance from the surface. A hydrophobic particle can be destabilised because the influence of the surface charge is reduced due to a decrease in the extent to which the ordered structure extends into the water. This allows hydrophobic particles to approach each other such that van der Waal forces of attraction become significant. These forces of attraction, if strong enough, enable the particles to stick together and particle growth is initiated which will culminate in the agglomerate settling.

Colloidal stability is brought about by repulsion between particles of high surface charge. Conversely, the attractive London forces between hydrophobic particles in aqueous environments augment flocculation. Thus, the balance of forces between charge and hydrophobicity determine colloidal stability.

The surface charge of particles is generated by one or a combination of the following processes (Bratby, 1980).

- By chemical reaction at the surface, functional groups can be ionised. In biological samples amine (NH_2), carboxyl (COOH) and phosphate (PO_4^{3-}) are the major charge forming groups, having varying degrees of ionisation depending on the pH of the environment.
- Specific adsorption of ions onto the surface may occur as a result of van der Waals forces or hydrogen bonding.
- Owing to lattice imperfections in a crystal structure, the substitution of one ion for another of different valency will result in a charged matrix.

All charged surfaces attract counter-ions (ions of opposite charge) and repel co-ions. In addition there is a natural mixing of the ions due to thermal diffusion. These two processes result in the formation of the electrical double layer, the charged surface surrounded by a diffuse cloud of counter- and co-ions which neutralises the charge away from the surface. This approach of using the DLVO (Derjaguin, Landau, Verwey and Overbeek) theory to explain flocculation of yeast has been attempted by various authors (Speers *et al.* 1993 and van Hammersveld *et al.* 1994) as detailed in Section 2.4.3.2. Their conclusion is however that the forces responsible for yeast flocculation are larger than those predicted by DLVO. These forces are detailed in Section 2.4.3.

2.4.2 Bridging Flocculation

During bridging flocculation, polymers can adsorb onto particles and thereby allow polymer bridges to be established between adjacent particles to form a floccule (Koopal, 1978). The adsorbed polymer may be more hydrophobic than the particle and thereby exclude more water from the surfaces enabling the particles to have closer contact with each other and flocculate. Alternatively, the polymers can form bridges that span the electrostatic potential barrier causing the particles to flocculate without having to come into as close contact, as illustrated in Figure 2.8. The polymer forms a series of attached train segments, floating loops, bridge sections and tails. Interactions between particles and polymers may be enhanced if the polymer is a polyelectrolyte or it could involve specific electrochemical interactions with functional groups on the particle surfaces. Such enhanced bonding of the polymer to the particle stabilises flocculation.

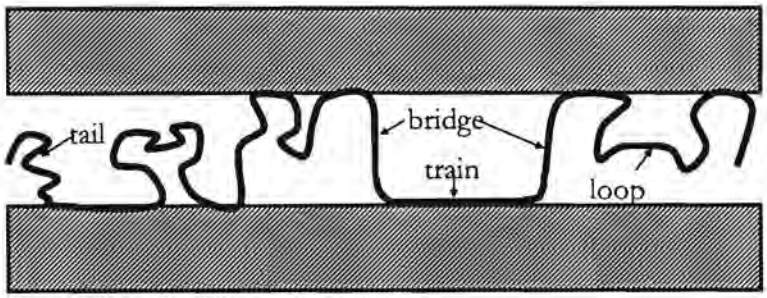

Figure 2.8. Illustration of bridging flocculation.

2.4.3 Yeast Flocculation

Yeast flocculation is described to be an intercellular process requiring calcium or magnesium ions whereby cells aggregate to form clumps which then separate from the medium. Flocculation by this definition is a reversible process in which cell clumps can be broken up and resuspended in the presence of ethylenediamine tetra-acetic acid (EDTA). Following much debate in the literature, brewers' yeast is now accepted to flocculate generally by a mechanism different to classical and bridging flocculation. The theory of yeast flocculation is now based on ligand-receptor or antibody/antigen type reactions.

Early studies concentrated on the visual differences of the cell surface between flocculent and non-flocculent yeasts and these findings are discussed in Section 2.4.3.1. This is followed by a review of the initial thinking of the mechanism, based largely on classical theory to describe non-specific repulsion between yeast due to electrostatic interaction. Evidence for the specific interactions between the carbohydrate receptor site and proteinaceous lectin is then provided. The structure and identification of each is also discussed together with the genetic requirement for lectin manufacture in the cell. Since flocculation was found to be inducible and growth phase specific, the availability and activation of both the mannan receptor sites and flocculins are considered in an effort to explain the flocculation trigger.

2.4.3.1 Visual appearance

Visual studies by Johnson *et al.* (1989) on the differences between flocculating and non-flocculating fission-yeast cells indicate that the flocculent strains have fuzzy fission scars while the scars on non-flocculent strains are sharp. The obscured definition on the flocculent yeast was caused by a heavy coating of hairy appendages. They were not able to discern similar differences between non-flocculent and flocculent budding yeast strains using similar methods of visualisation by a scanning electron microscope. The hairy appendages on the surface of flocculent strains of *Saccharomyces cerevisiae*, called fimbriae by Poon and Day (1975) and Day *et al.* (1975) play a vital role in conjugation, protein excretion/uptake and flocculation. By preparing shadow casts with tungsten oxide and negative stains with phosphotungstate of yeast cells, they were able to visualise short, unbranched cylindrical fimbriae, 0.5 μm in length and 60-70 Å in diameter under the electron microscope. The fimbriae were digested with pronase but not by α-amylase or cellulase, though the latter caused the fimbriae to contract into tight coils, indicating a predominantly protein composition with some polysaccharide content. Day *et al.* (1975) found that non-flocculent *Saccharomyces cerevisiae* yeast had fewer fimbriae than flocculent strains. Flocculent strains lost their ability to flocculate after treatment with pronase to remove the fimbriae. The cells treated with α-amylase retained fimbriae but lost their ability to flocculate. In addition, flocculent strains often only developed this ability at the end of

exponential growth, coincident with the appearance of the fibres. This provided an indication that the presence of these hair-like fimbriae is necessary for these yeast strains to flocculate.

2.4.3.2 Opposing forces in flocculation

Flocculation was described by Kihn *et al.* (1988a) as being governed by the two competing forces: **non-specific repulsion** due to electrostatic charges caused predominantly by phosphodiester linkages of the cell wall phosphomannan, and **specific polysaccharide-protein bonds** which penetrate the potential barrier surrounding the cells. They postulated that, irrespective of the presence of the polysaccharide protein bonds, all strains of yeast would flocculate, due to the hydrophobic nature of cells in the absence of the potential barrier caused by the charged surface. As a result of the high surface charge of some yeast strains, hydrophobicity alone is unable to account for the flocculating nature of the cells and the formation of specific protein-polysaccharide bonds are required for flocculation. In a study conducted by van Hamersveld *et al.* (1994), the net attractive force between cells of a flocculent strain of yeast was calculated using the DLVO theory of flocculation and compared to the measured force of attraction. The experimentally measured force was 2000 times greater than that predicted by DLVO theory. From this they were able to conclude that DLVO theory of classical colloidal flocculation was insufficient to account for the level of flocculation observed.

2.4.3.3 Evidence for protein-polysaccharide interactions

Miki *et al.* (1982a, b) proposed a model for yeast flocculation consisting of a proteinaceous recognition factor which attaches to α-mannan receptor sites on other cells. Concanavalin A-ferritin was found to bind to branched α-mannan polysaccharide chains on the yeast surface and inhibit flocculation. This inhibition was reversible. This confirms the importance of polysaccharides in flocculation.

As proteolysis and reduction of disulphide bonds caused irreversible inhibition of flocculation, the role of proteins as recognition factors was implicated. This supports the visual evidence of Day *et al.* (1975) that the proteinaceous fibrils are active flocculation components. It was suggested that the fibrils have a manno-protein composition owing to the inhibition of synthesis of fimbriae, glucan and mannan by cycloheximide (Farkas *et a.*, 1970; Baker and Kirsop, 1972; Stewart *et al.*, 1973).

Inorganic cations play a vital role in flocculation (Jansen and Mendlik, 1951; Stratford, 1989a). The washing of yeast suspensions with water or EDTA to remove cations was found to render yeast cells non-flocculent. Ca^{2+} was found to be a prerequisite for flocculation while a number of other divalent

and monovalent ions including strontium, barium and sodium have an inhibitory effect on flocculation with the strongest inhibitors being those with atomic radii similar to that of calcium (Kihn *et al.*, 1988a). These other cations are proposed to fit into the calcium binding site thus preventing calcium from binding. The presence of calcium conforms the protein to allow for a phosphomannan binding site such that cell-cell adhesion occurs with a bond energy of 500 kJ/mole. A single hydrogen bond normally formed between a sugar and protein would yield a bond energy of 25 kJ/mole (Huheey, 1983). Magnesium, manganese and other dipositive ions of transition metals have been reported to induce flocculation (Jansen and Mendlik, 1951; Miki *et al.*, 1982a). This is proposed to be an indirect effect as these salts cause the excretion of calcium by the cell (Stratford, 1992b). The role calcium ions play in flocculation is clearly not a charge balancing function between phosphate groups on adjacent cells.

Lectins are glycoproteins that bind sugars with as high a specificity as antibody/antigen interactions (Kabat, 1978), require metal ions for activation, are inhibited by simple sugars with similar structures to their receptors (Sharon and Lis, 1972) and play an important role in cell/cell interactions and recognition (Feizi, 1985). The proteinaceous fimbriae, described earlier, possess a lectin-like structure (Miki *et al.*, 1982a) which requires Ca^{2+} as a cofactor to activate the formation of binding sites. Einspahr *et al.* (1988) reported that divalent ions were required to maintain a *cis* peptide bond between Ala 81 and Asp 82 near but not proximal to the sugar binding sites of pea lectins. Miki *et al.* (1982a) also proposes a specific adhesion model similar to those of other organisms like bacteria and slime moulds. The proteins on the surface bind to specific sugar residues of adjoining cells thereby achieving attachment. It therefore appears that the flocculation fibrils are lectins. In summary, the three key compounds required for flocculation are the proteinaceous flocculins (lectins), α-mannan receptor sites and calcium ions.

2.4.3.4 Inhibition of flocculation by sugars

Some sugars are able to inhibit flocculation while others do not affect flocculation as shown in Figure 2.9 which indicates the inhibitory effect of mannopyranose and the non-inhibitory effect of glucose (Stratford, 1989b; Stratford and Assinder, 1991; Masy *et al.*, 1991, 1992). Inhibition by free sugars results from the mimicking of α-mannan receptors used for flocculation, resulting in the free sugar occupying the sugar binding sites of lectins.

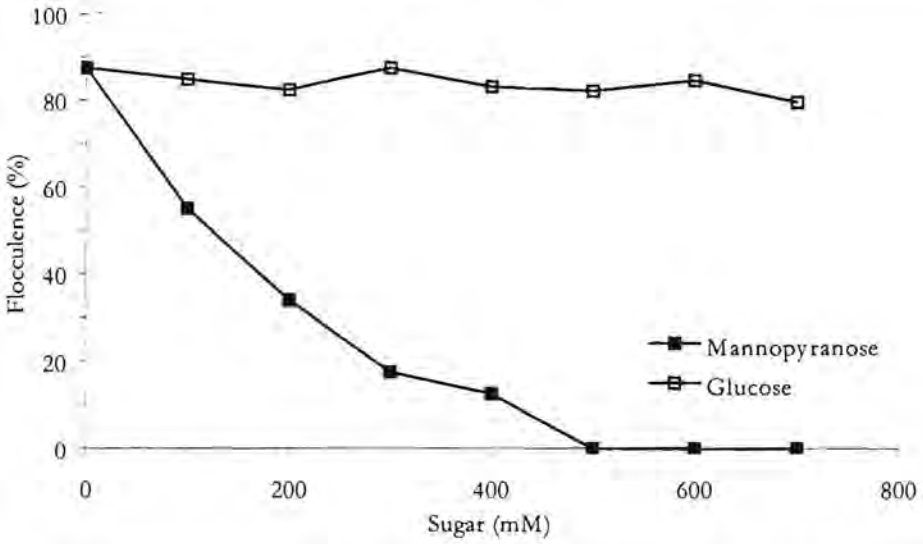

Figure 2.9. Inhibition of yeast flocculation by sugars, strain NCYC 870. Adapted from Masy *et al.* (1992).

Based upon the ability of different sugars to inhibit flocculation, Masy *et al.* (1992) grouped yeasts into three categories according to the sugars inhibiting flocculation: mannose sensitive (MS), glucose-mannose sensitive (GMS) and mannose insensitive (MI). When an inhibitory effect is observed, the concentration of sugar required to cause complete inhibition is sometimes used to classify the inhibitory power of the sugar. Table 2.5 is an abridged version of the sugars used to classify the inhibitory patterns for two yeast strains. Yeast strains belonging to the GMS classification were totally inhibited by a broad spectrum of sugars including mannose and glucose while MS were partially inhibited by a smaller group of sugars including mannose but not glucose. Strains belonging to the MI group were not inhibited by any sugars. The data provides confirmatory evidence that MS and GMS yeast strains flocculate as a result of specific interactions between mannans and proteic factors. The mannose insensitive (MI) strains are postulated to flocculate by hydrophobic interactions or specific interactions not involving mannans.

Table 2.5. Classification of sugars according to their degree of inhibition for NCYC 1195 (GMS group) and NCYC 869 (MS group) (Masy *et al.*, 1992).

Sugar concentration (mM)	NCYC 1195 (GMS group)	NCYC 869 (MS group)
0.5 – 10	p-Aminophynyl-α-D-mannopyranose	3-O-α-D-Mannopyranosyl-α-D-mannopyranose Methyl-2-O-α-D-mannopyranosyl-α-D-mannopyranose
10 – 50	Methyl-α-D-mannopyranose Maltose Maltotriose	p-Aminophenyl-α-D-mannopyranose
50 – 100	D-Mannopyranose Methyl-α-D-glucopyranose Methyl-β-D-glucopyranose Sucrose	
100 – 500	N-Acetyl-α-D-glucosamine D-Glucose D-Mannosamine	D-Mannopyranose D-Mannose-6-phosphate
No inhibition	D-Cellobiose D-Fructose D-Galactose D-Lactose D-Mannitol L-Mannopyranose	N-Acetyl-α-D-glucosamine D-Cellobiose D-Fructose D-Galactose D-Glucose D-Lactose Maltose Maltotriose D-Mannitol L-Mannopyranose D-Mannosamine Methyl-α-D-glucopyranose Sucrose

2.4.3.5 Genetic control of flocculation

Genes present in flocculent strains

Gilliland (1951) showed flocculation to be an inheritable characteristic indicating its genetic basis. The first gene found to be associated with flocculation was *FLO1* which encodes a flocculin (Stewart and Russell, 1977) and was later shown to encode a cell surface protein (Bidard *et al.*, 1995). This gene was found to be allelic to subsequent genes discovered: *FLO2* and *FLO4*. *flo3* was also identified but found to be recessive. *FLO5* was described by Johnston and Reader (1982 cited by Stratford, 1992b) to be non-allelic to *FLO1* and found on chromosome VIII while *flo6* and *flo7* are said to be semidominant genes subject to suppression and may be alleles to *FLO1*. *FLO5* shows a 96 % similarity to *FLO1*. *FLO8*, mapped onto chromosome I by Teunissen *et al.* (1995), is allelic to *FLO1*. *FLO9* (96% similar to *FLO1*) and *FLO10* (58% similar to *FLO1*) were also identified as being dominant structural genes occurring on chromosomes IX and XI. *FLO11* was identified and mapped onto chromosome IX by Lo and Dranginis (1996). It was found to produce a surface lectin able to cause flocculation in yeast despite only a 37 % similarity to *FLO1*. *FLO11* is currently the only structural flocculation gene known to be regulated by mating type. Carstens *et al.* (1998) identified the *FLO11* gene as *MUC1* which encodes a mucin-like protein which plays a key role in pseudohyphal development and invasive growth but did not confer the phenotype of flocculation as previously reported.

Suppression and regulation of *FLO* genes

In a continuous culture lasting 300 days the maximum petite mutation frequency reached 87% on the 27th day, indicating the high incidence of mutation rate that can occur (Gasent-Ramirez *et al.* 1999). The *fsu1* gene is a suppresser gene, suppressing flocculation in *FLO4* strains. It was proposed by Stratford (1992b) that suppression of flocculation could be caused by modifications to the protein secretory system limiting the secretion of glycoproteins like glucoamylases (Yamashita and Fukui, 1984) and flucculins. Mutations at other gene sites have been shown to induce flocculation in previously non-flocculent strains (*TUP1* and *CYC8*). Since this gene mutation is unable to produce genes encoding for flocculation proteins, mutations in the regulatory genes allow other structural *FLO* genes to be expressed causing yeast flocculation. Miki *et al.* (1982b) found that flocculation of yeast could be repressed under anaerobic conditions but was restored under aerobic growth. They found changes in flocculence were accompanied by changes in 16 proteins separated by electrophoresis.

Phenotypes of yeast flocculation

Two phenotypes have been distinguished according to the inhibitory effect of different sugars on flocculation. The phenotype Flo1 is partially inhibited by mannopyranoses while the other phenotype NewFlo is completely inhibited by manno- and glucopyranoses including the specific

sugars mannose, glucose, maltose and sucrose (Masy *et al.*, 1992). The method by which sugars inhibit flocculation can be attributed to two distinctly different lectins on the surface of the yeast cell. These lectins appear as fibrils which facilitate binding between cells. Evidence for the presence of one of two distinct lectins at the surface of flocculating cells depending on the yeast phenotype is presented by Stratford and Assinder (1991). The Flo1 phenotype is proposed to have only mannospecific lectins while NewFlo has gluco- and mannospecificity. Strains containing *FLO1*, *FLO4*, *FLO5* and *FLO8* as well as *tup1* and *cyc8* mutants all show Flo1 phenotype behaviour with mannose specific inhibition of flocculation. According to Stratford (1992c) the dominant *FLO* genes are positive regulators of flocculation and not only structural genes. The genetics of NewFlo phenotype flocculation, its suppression and regulation remain poorly understood.

The flocculation in the two phenotypes are affected differently by cultural and nutritional conditions (Soares *et al.*, 1994). The NewFlo phenotype strain is more sensitive to growth temperature and flocculation was repressed when grown in defined media. This was attributed to the poorer pH buffering capacity of the media. The Flo1 phenotype strains were flocculent in both defined and complex media. High concentrations of cations were also found to inhibit flocculation with NewFlo being more susceptible to such inhibition. Stratford and Brundish (1990) found that the inhibition was caused by protein dehydration, thus NewFlo type surface lectins are more susceptible to dehydration. Extreme values of pH can cause protein distortion which decreases the ability of the flocculins to form bridges, leading to inhibition of flocculation. Stratford (1996) reported that many flocculent brewing strains do not flocculate in laboratory media due to the low level of pH buffering which allows the pH to drop below that reached in industrial media by the end of fermentation. NewFlo strains were found to flocculate across a narrow pH range while Flo1 phenotype are less sensitive to flocculation inhibition by pH. The surface proteins are also affected by the presence of proteases. Pronase E, a non-specific protease, removes the surface proteins on both phenotypes rendering them non-flocculent. Trypsin and Proteinase K, both specific in their scission sites, were more effective against the NewFlo strains. The Flo1 phenotype showed flocculence throughout its growth cycle while NewFlo strains only developed flocculence at the end of exponential growth phase (Soares and Mota, 1996). The differences in surface protein instability caused by pH, salt, protease digestion, media and growth phase dependence of flocculation indicates that flocculation in *S. cerevisiae* is caused by two distinctly separate lectins.

2.4.4 Identification of Carbohydrate Receptor

Having determined that brewers' yeast flocculates by the lectin/receptor mechanism, the structural determination and availability of the receptor molecule requires identification to determine its possible susceptibility to hydrodynamic shear damage.

2.4.4.1 Structure of the receptor

Ballou *et al.* (1980) used *mnn* mutants which produce yeasts with truncated mannan cell walls to investigate cell morphology and these mutant strains formed the basis for the later investigations into flocculation receptor structure. The inhibition caused by specific sugars (Kihn *et al.*, 1988a; Stratford and Assinder, 1991; Masy *et al.*, 1992) led to the postulation that a flocculin binds to the Manα→3Manα→R_2PO4^-→6Manα→2Manα of phosphomannan. Based upon the extent that different sugars inhibit flocculation, Stratford and Assinder (1991) identified the receptor site as the non-reducing termini of α-(1-3)-linked mannan side branches, two or three residues in length in both Flo1 and NewFlo phenotypes.

In order to determine the nature of the receptor structure, Stratford (1992a) used *mnn* mutants with different outer mannan structures to the wild type (illustrated in Figure 2.6) and which lacked flocculins. Concanavalin A, a lectin with known gluco and mannospecific interactions, was used to agglutinate the mutants and examine similarities between Concanavalin A and the NewFlo phenotype lectin. Concanavalin A is able to attach to mannan residues at each of its termini, thus allowing cells deficient in lectins to form bridges and flocculate. This study confirmed that the flocculation receptors for both Flo1 and NewFlo phenotypes are the α-mannan outer chain side branches of two or three mannose residues in length. Concanavalin A was found to only attach to the terminal mannose residues. Using strains containing no phosphomannan, Stratford confirmed the results of Jayatissa and Rose (1976) that phosphate does not take part in flocculation. As non-flocculent but fully saturated Concanavalin A cells flocculated to the same extent as wild type yeast, the yeast has receptor sites well in excess of that required for flocculation. Thus the limiting component dictating the extent of flocculation is the type and number of lectins present in the cell wall.

2.4.4.2 Receptor availability

Studies by Herrera and Axcell (1991a, b) showed premature flocculation to be caused by the binding of yeast to a polysaccharide fraction of malt husk. This premature flocculation is considered to result from large polysaccharides, to which lectins have higher affinity than simple sugars, forming bridges between lectins on adjacent cells. This indicates that receptor availability is developed during the growth cycle of the yeast and flocculation is initiated by such sites becoming available. Stratford (1993) used *mnn* mutants and Concanavalin A to investigate this hypothesis. He found that receptor availability was present early in a fermentation, while flocculation was only evident towards the end of fermentation. He concluded that receptor availability, therefore, did not determine the onset of flocculation.

2.4.5 Identification of the Flocculation Factor (Flocculin)

As with the identification of the structure and availability of the receptor molecule, the same needs to be done for the flocculin.

2.4.5.1 Structure of the flocculin

Since no discernible differences could be found between the receptor structures of the phenotypes Flo1 and NewFlo, the difference in flocculation behaviour must originate from flocculin structure. The flocculins have both a carbohydrate and a protein nature and are encoded by various genes (*FLO1*, *FLO5*, *FLO9*, *FLO10* and *FLO11*). The surface protein (flocculin) binds to mannan by multiple hydrogen bonds based on the high bond energy reported by van Hamersveld *et al.* (1994). Evidence from the inhibitory effect of high temperatures and urea on protein aggregation (Shankar and Umesh-Kumar, 1994) also supports the binding of flocculins to mannan by multiple hydrogen bonds. A number of the proteins expressed by these genes have great similarity to the protein Flo1p. The protein lengths and similarities to Flo1p summarised in Table 2.6 indicate the high degree of homology to the dominant gene *FLO1*. Detailed amino acid structures of these flocculins can be obtained from the yeast proteome data base (http://quest7.proteome.com/YPDhome.html).

Table2.6. Similarities between the flocculin Flo1p (gene product of *FLO1*) and the lesser flocculins.

Gene	Protein length	Similarity to other flocculins
FLO1	1513 (amino acids)	
FLO5	1051	96% homology to Flo1p
FLO8	729	
FLO9	1298	near identity to Flo1p over 850 amino acids
		74% identity to Flo5p over 970 amino acids
FLO10	1145	58% similarity to Flo1p
FLO11	1367	37% identity to Flo1p

Straver *et al.* (1994) isolated a protein from the surface of flocculent *Saccharomyces cerevisiae* cells which showed a high degree of similarity to the proposed protein encoded by the gene *FLO1* and concluded that it was the flocculin Flo1p. The isolated flocculins were found to agglutinate non-flocculent cells. The flocculin appeared only at cell division arrest which coincided with an increase in surface hydrophobicity and cell flocculence. The Flo1 protein (Flo1p), encoded by the gene *FLO1*, has several distinctive structural features (Bony *et al.*, 1997). The N-terminal region is highly N and O glycosylated while the C-terminal end is highly hydrophobic. The amino acid sequence predicted by the *FLO1* gene encodes a protein of mass 160 kDa but because of the high degree of

glycosylation it has a molecular mass in excess of 200 kDa. This corresponds to the reported sugar content of a Flo1p homologue of 63% (Straver *et al.*, 1994). By using plasmids containing the *FLO1* gene with truncated regions, they were able to show that the hydrophobic C-terminal end anchors the protein noncovalently to the cell wall. Without the C terminal end, the protein is excreted into the media. Similarly the N-terminal domain of the protein was found to be essential for cellular aggregation and this region is postulated to be the site of attachment to the mannan chains of adjoining cells.

By using immunoelectron microscopy, Bony *et al.* (1997) observed the Flo protein in the lumenal space of the nuclear envelope and in the endoplasmic reticulum tubules, indicating that it was synthesised and then secreted. The proteins also showed high concentrations in the plasma membrane and the outer electron dense mannoprotein layer of the cell wall. From the localisation of the protein it is postulated that the protein is transiently anchored to the plasma membrane before it is excreted and incorporated into the cell wall in a similar way to the α-agglutinin studied by Lu *et al.* (1994).

2.4.5.2 Flocculin availability

The majority of brewing strains exhibit the phenotype NewFlo, showing inhibition of flocculation with both mannose and glucose (Stratford and Assinder, 1991). These strains are unicellular in the growth phase and only flocculate in the stationary phase. Since lectin receptors are available throughout the life cycle of yeast (Stratford, 1993), lectin availability appears to determine the onset of flocculation. This was confirmed by Stratford and Carter (1993). The addition of cycloheximide to terminate cytoplasmic production of proteins was used to confirm the continual synthesis of lectins and their incorporation into the cell wall during growth. The lectins lie dormant in the cell wall for up to 14 hours prior to activation and the commencement of flocculation. Heating of flocculent cells prior to development of flocculence (pre flocculent) was found to activate the lectins into flocculence while flocculence was not induced in non flocculent strains by heat treatment. Growth arrested cells (treated with cycloheximide) treated with the protease, pronase E, were found not to develop preflocculence while cells treated with pronase E only regained flocculence after a recovery period.

By using immunological approaches, Bony *et al.* (1998) confirmed that the Flo proteins increased in number at the cell wall during growth. Flocculation was correlated to the abundance of Flo protein at the cell surface indicating that the onset of flocculation is determined by the availability of the protein at the cell surface. In the *FLO1* and *FLO5* genotypes, the flocculins are incorporated into the cell wall at the bud, with the highest concentration being at the bud tip and the mother-daughter

neck. This polarisation of proteins in the cell wall persists into maturity for the *FLO1* type. The *FLO5* type gradually showed a more homogenous distribution of the protein across the whole cell surface. In strains with slower protein fluxes, the incorporation of the protein into the cell wall occurred when the bud cell wall was nearly fully extended. This late incorporation of Flo protein into the wall corresponds to the finding of Stratford and Carter (1993) that cells can replace lectins damaged by proteolysis to recover their flocculence.

2.4.6 Effect of Surface Charge on Flocculation

Phosphates were previously postulated as the attachment sites between yeast cells with calcium ions forming charge neutralising bridges. This was supported by Lyons and Hough (1970) who found flocculent strains to have higher levels of phosphorus in the cell walls than non-flocculent strains. In addition they reported flocculent yeast binds twice as much calcium. This type of cation bridging was disproved by Jayatissa and Rose (1976) who showed that non-flocculent yeast may become flocculent after excision of the wall phosphates by hydrofluoric acid treatment and other flocculent strains, undergoing the same treatment, retained their flocculence but lost its inhibition by sugars.

It is important to recall that yeast flocculation is a competition between non-specific repulsion and specific bonding. Without electrostatic repulsion (caused predominantly by the presence of negatively charged phosphate groups), cells would agglomerate naturally due to hydrophobic interactions. The role of phosphate is therefore to provide the surface charge that maintains the stability of the suspended cells until flocculins are formed to induce flocculation.

Carboxyl groups of surface proteins also contribute to the negative charge on yeast cells. Their effect on flocculation in yeast has been noted by chemical modification by esterification of carboxyl groups (Jayatissa and Rose, 1976; Lyons and Hough, 1970, 1971). This treatment decreased the surface charge, lowered the calcium binding ability and decreased flocculence. While lowered surface charge is expected to improve flocculation, epoxyfication of the carboxyl groups on the flocculins caused lower calcium binding and decreased flocculation.

2.4.7 Effect of Hydrophobicity on Flocculation

Yeast hydrophobicity has been correlated to flocculence by Smit *et al.* (1992), Kamada and Murata (1984) and Amory *et al.* (1988). Straver *et al.* (1993) observed a sharp increase in hydrophobicity towards the end of cell growth as a result of oxygen limitation. This coincided with increased flocculence. In *Corynebacterium glutamicum*, cells saturated with phosphate have been shown to be more hydrophobic and more flocculent (Büchs *et al.*, 1988). Hydrophobicity has also been identified

as an important parameter in the attachment and immobilisation of bacteria (van Loosdrecht *et al.*, 1987a, b). The appearance of a cell surface protein (flocculin) as the cells reached stationary phase (Smit *et al.*, 1992) increased both hydrophobicity and flocculation. This was observed shortly before the onset of flocculation. Treatment with polycations to increase hydrophobicity increased flocculation. Smit *et al.* (1992) postulated the involvement of flocculins in both cell surface hydrophobicity and flocculation.

2.4.8 Flocculation Physics

Yeast cells are physically too large to form a true colloidal suspension but, due to relatively slow terminal settling velocity, they are still subject to the same forces of electrostatic repulsion and van der Waals forces of attraction. Colloids remain in suspension because of the Brownian motion of the particles. When such colloids do coagulate, the rate of this aggregation is limited by the collision frequency. For cells to aggregate they need to come into contact with each other and since they do not move under Brownian motion (because of their physical size) they require agitation to initiate flocculation.

Due to charge, the cells repel each other, forming an energy barrier. The agitation required to initiate flocculation provides the cells with sufficient potential energy to overcome this energy barrier allowing cells to collide. Collision is essential to form the necessary lectin-receptor bonds required for cell flocculation. At the iso-electric point of the cell (neutral cell surface), charged groups on the surface attract an orientated water layer around themselves causing water cushion layers which add to the repulsion between cells. Steric hindrance from large protruding glycoproteins at the surface may also prevent surface to surface contact. In addition many biological components of the cell wall are hydrophilic, resisting the displacement of water molecules caused by cell contact. Hence, despite bulk charge repulsion being negligible at the iso-electric point, considerable repulsive forces remain. It is these forces which enable the prediction to be made that it is collision intensity and not merely collision frequency which would determine the rate of flocculation. Stratford (1992b) presented data of initial rate of flocculation in an agitated system indicating a minimum threshold agitation frequency for an orbital shaker required to initiate flocculation thus strengthening the proposition of a minimum collision energy for flocculation. This collision energy needed to initiate flocculation is analogous to the activation energy required for chemical reactions.

Under conditions of continuous agitation the rate of floccule growth declines from its initial high value to a net zero growth rate with an eventual steady state concentration of free cells. The time taken to reach this equilibrium is dependent on the degree of agitation with the equilibrium position between free cell and floccule concentration also being determined by agitation rate. At this

equilibrium, free cells form flocs at the same rate as cells are lost from flocs by abrasion, resulting in a dynamic equilibrium.

2.5 Quantification of Forces Causing Damage to Cells

Hydrodynamic forces which cause damage to micro-organisms are a result of the dissipation of kinetic energy on the surface of the cell. The magnitude of these forces (the shear stress) is proportional to the viscosity of the suspending fluid and the velocity gradient in the boundary layer around the cell. This relationship is formalised in Equation 2.2, the Newtonian viscosity relationship.

$$\tau = \mu\gamma = -\mu\left(\frac{dv}{dy}\right) \tag{2.2}$$

where τ = shear stress ($N.m^{-2}$)

μ = viscosity ($N.s.m^{-2}$)

γ = shear rate (s^{-1})

(dv/dy) = velocity gradient (s^{-1})

Two distinctly different flow types are identified according to the motion of a fluid. **Laminar** flow is a smooth flow of layers of fluid across each other with the energy dissipation between adjacent layers being dominated by viscous interactions. **Turbulent** flow describes the situation whereby packets of fluid (eddies) are randomly interchanged between adjacent fluid layers which causes a fluctuating velocity vector at each point in the flow. The type of flow is characterised by the Reynolds number (Re) of the system as defined by Equation 2.3.

$$\mathrm{Re} = \frac{\rho l v}{\mu} \tag{2.3}$$

where ρ = fluid density ($kg.m^{-3}$)

l = characteristic length (m)

v = fluid velocity ($m.s^{-1}$)

High Reynolds numbers, above a critical number indicate that the flow is turbulent. These critical transition numbers are system specific and are summarised in Table 2.7 (Perry *et al.*, 1984). It is generally accepted that for pipe flow with Reynolds numbers greater than 3000, the flow is always turbulent while Reynolds numbers less than 2100 are associated with laminar flow. Pipe flow with

Reynolds numbers between these limits are laminar but unstable with sufficient surface roughness being able to cause the formation of a turbulent flow pattern.

Table 2.7. Critical Reynolds numbers for laminar – turbulence transitions.

System	Characteristic Length	Reynolds Number
Pipe flow	Pipe diameter	3000
Stirred tanks	Impeller diameter	1000
Particle / Cell	Particle diameter	1

2.5.1 Shear Stress and Velocity Distribution in Pipe Flow

The velocity profile for the case of steady laminar flow of a Newtonian fluid in a pipe can be described by Equation 2.4 (Welty *et al.*, 1984).

$$v = -\frac{\Delta P}{4L\mu}\left(R^2 - r^2\right) \tag{2.4}$$

where L = length of tube (m)

ΔP = pressure drop (Pa)

r = radial position (m)

R = pipe radius (m)

v = velocity ($m.s^{-1}$)

For the case of turbulent flow the velocity at any point is the sum of the time averaged velocity and the randomly fluctuating velocity caused by the eddies present in the flow. The velocity distribution of turbulent flow in a pipe can be approximated by the empirically derived one-seventh power law of Equation 2.5 while the ratio of average to maximum time averaged velocity is given as a function of Reynolds number in Figure 2.10 (Perry *et al.*, 1984). The universal velocity distribution for turbulent flow in smooth pipes has been determined by defining three zones across the pipe radius: the laminar sublayer against the pipe wall, the buffer layer and the turbulent layer situated in the core of the pipe. The universal velocity distribution makes use of a dimensionless velocity (v^+) and dimensionless position (y^+) given in Equation 2.6 to describe the velocity profile under turbulent conditions. The equations for the three layers are provided in Table 2.8.

$$\frac{v}{v_{max}} = \left(1 - \frac{r}{R}\right)^{1/7} \tag{2.5}$$

where v_{max} = maximum velocity in the pipe ($m.s^{-1}$)

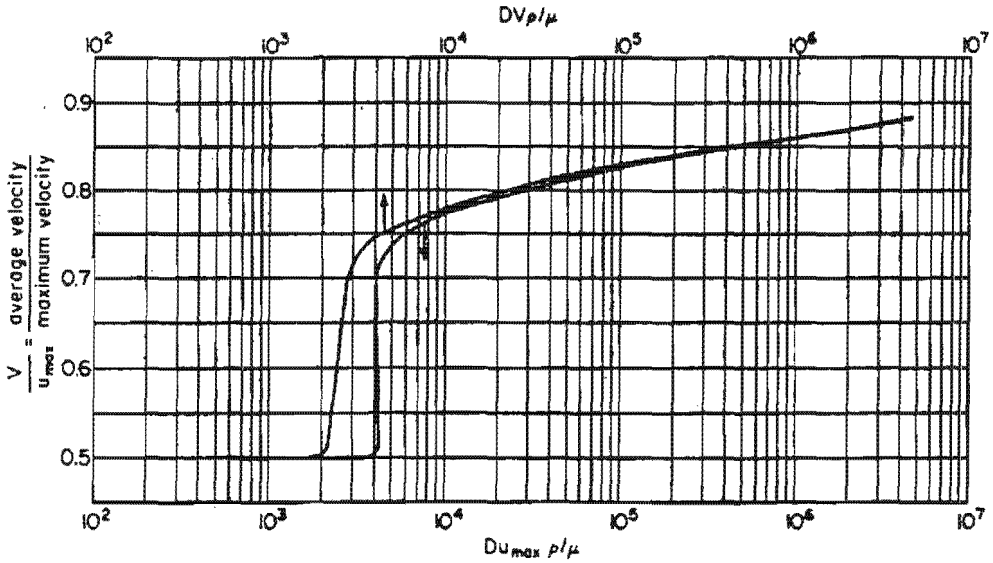

Figure 2.10. Ratio of average to maximum time average velocity as a function of Reynolds number (Perry *et al.*, 1984).

$$v^+ = \frac{v}{\sqrt{\tau_0/\rho}} \quad and \quad y^+ = \frac{y\rho\sqrt{\tau_0/\rho}}{\mu} \tag{2.6}$$

where τ_0 = wall shear stress (Pa)

y = distance from pipe wall (m)

Table 2.8. Universal velocity profile correlations for turbulent flow in a pipe.

Expression	Region of applicability
$v^+ = 2.5 \ln y^+ + 5.5$	Turbulent core: $y^+ \geq 30$
$v^+ = 5 \ln y^+ - 3.05$	Buffer layer: $30 \geq y^+ \geq 5$
$v^+ = y^+$	Laminar layer: $5 \geq y^+ \geq 0$

For the case of flow in a pipe, the shear stress is related to the pressure gradient and radial position within a pipe by Equation 2.7 from which it is seen that the shear stress profile is linearly dependent on radial position.

$$\tau = \left(\frac{dP}{dx}\right)\frac{r}{2} \tag{2.7}$$

where dP/dx = pressure gradient ($Pa.m^{-1}$)

The maximum shear stress can also be obtained by noting that the shear stress is greatest at the pipe wall (i.e. at r = R). The wall shear stress (τ_0) is given by Equation 2.8 which is valid for both laminar and turbulent flow and requires only that the pressure drop per unit length be known. The average shear stress in the pipe can be obtained by integrating of Equation 2.7 across the cross-sectional area of the pipe and dividing by the total area as indicated in Equation 2.8 to give the final integrated form, Equation 2.10. The wall shear stress is therefore 50% greater than the average shear stress.

$$\tau_0 = \frac{R}{2}\left(\frac{dP}{dx}\right) \tag{2.8}$$

$$\tau_{avg} = \frac{\int_0^R \left(\frac{dP}{dx}\right)\frac{r}{2}\,dr}{\pi R^2} \tag{2.9}$$

$$\tau_{avg} = \frac{R}{3}\left(\frac{dP}{dx}\right) \tag{2.10}$$

where τ_{avg} = average shear stress ($N.m^{-2}$)

For turbulent flow in a pipe, the Blasius' correlation (Equation 2.11) can be used to calculate the wall shear stress for Reynolds numbers less than 10^7 (Welty *et al.*, 1984) without the constraint of having to know the pressure drop per unit length.

$$\tau_0 = 0.0225\rho v_{max}^{\,2}\left(\frac{\nu}{v_{max}R}\right)^{1/4} \tag{2.11}$$

where ν = kinematic viscosity = μ/ρ ($m^2.s^{-1}$)

The total time-averaged shear stress for turbulent flow (equal to the shear stress calculated in Equation 2.7) is the sum of the viscous (τ^V) and turbulent or Reynolds stress (τ^R) components (Equation 2.12). The Reynolds stress arises from the random motion of eddies while the viscous stress is a result of molecular motion. Since the ratio of turbulent to viscous shear is given by Equation 2.13, the total shear stress in turbulent flow can be divided into portions attributable to both viscous and eddy action (Bird *et al.*, 1960).

$$\tau = \tau^V + \tau^R \tag{2.12}$$

$$\frac{\tau^R}{\tau^V} = \frac{1-\left(y/R\right)}{dv^+/dy^+} - 1 \tag{2.13}$$

where τ^R = Reynolds shear stress (Pa)

τ^v = viscous shear stress (Pa)

dv^+/dy^+ = dimensionless velocity gradient

2.5.2 Energy Dissipation in Pipe Flow

Both laminar and turbulent flow of fluids in a pipe occur with the concomitant loss of pressure along the pipe length. This loss of pressure is due to the energy dissipated due to viscous interactions in laminar flow and viscous and eddy interactions in turbulent flow. Equation 2.14 relates the total energy dissipation rate to the pressure drop, pipe cross-sectional area and mean velocity for both types of flow. Since the total energy dissipation rate is essentially a power term, the total energy dissipation is calculated by multiplying by the mean residence time (Equation 2.15).

$$E_T = \Delta P \frac{\pi}{4} D^2 v_{avg} \tag{2.14}$$

$$TE = E_T * t_{avg} \tag{2.15}$$

where: D = pipe diameter (m)

E_T = total energy dissipation rate ($J.s^{-1}$)

TE = total energy dissipated (J)

t_{avg} = mean residence time (s)

v_{avg} = average linear velocity ($m.s^{-1}$)

During yeast handling in the brewery situation, turbulent energy dissipation also can be found to occur downstream of flow restricting valves and other pipe fittings which results in the rapid change of the flow patterns. For example, the generation of turbulence may occur downstream of an orifice in a pipe. In these situations the energy dissipation rate can be calculated using Equation 2.16.

$$\varepsilon = \frac{\Delta P Q}{\rho V} \tag{2.16}$$

where: ε = specific energy dissipation rate ($m^2.s^{-3}$)

Q = volumetric flow rate ($m^3.s^{-1}$)

V = volume in which energy dissipation occurs (m^3)

The specific energy dissipation rate per unit mass (ε) requires that the volume in which the energy is being dissipated be known. For the orifice in a pipe, the volume of fluid absorbing the energy can be calculated by recognising that the pressure loss is greatest at some distance downstream of the orifice. Further downstream, the pressure recovers to a value which provides the permanent

pressure loss across the constriction. The distance downstream of the orifice at which this pressure recovery is complete is generally taken to be 8 pipe diameters. Thus, the volume in which energy dissipation occurs downstream of an orifice is therefore given by Equation 2.17.

$$V = 16\pi R^3 \tag{2.17}$$

As in the case with shear stress, the total energy dissipation rate under turbulent flow conditions is the sum of the energy dissipation rate in the laminar and turbulent regions. The analysis of Zhang *et al.* (1993) for turbulent flow in a capillary assumed that cells are only found in the turbulent region of the flow and not in the laminar sublayer close to the pipe wall. For this reason they subtracted the energy dissipation rate attributable to the laminar layer, given by Equation 2.18, from the total energy dissipation rate to correlate with cell disruption.

$$E_L = \mu\gamma^2 V_L \tag{2.18}$$

where: E_L = energy dissipation rate in the laminar sublayer ($J.s^{-1}$)

γ = shear rate in the laminar sublayer (s^{-1})

V_L = volume in the laminar sublayer (m^3)

The laminar sublayer shear rate can be calculated (Equation 2.19) assuming that there is a linear velocity profile in the layer, while the volume in the laminar sublayer can be calculated from Equations 2.20, 2.21 and 2.22 (Zhang *et al.*, 1993).

$$\gamma = \frac{\Delta P}{4\mu L/D} \tag{2.19}$$

$$V_L = \frac{\pi}{4}\left[D^2 - (D-2\delta)^2\right]L \tag{2.20}$$

where: $\delta = \dfrac{5\nu}{\left(\sigma_0/\rho\right)^{0.5}}$ = laminar sublayer thickness (m) (2.21)

$$\sigma_0 = \frac{\Delta P}{4L/D} = \text{wall shear stress (Pa)} \tag{2.22}$$

In the turbulent region of fully developed flow in a pipe where energy dissipation occurs by eddy interaction, the scale of the energy transfer between eddies and between eddies and cells becomes significant since the energy dissipation occurs by the breakdown of large eddies into progressively smaller ones until the smallest eddies disintegrate by viscous action. For isotropic turbulence, the size of these smallest eddies, known as the Kolmogorov microscale length, are calculated by

Equation 2.23 with the eddy velocity given in Equation 2.24 (Kolmogorov, 1941a, b; Bird *et al.*, 1960; Cherry and Papoutsakis, 1988). Isotropic turbulence is defined as the complete randomness of motion of eddies with no bias for their motion in any direction.

$$l_c = \left(\frac{\nu^3}{\varepsilon}\right)^{1/4} \tag{2.23}$$

$$v = (\varepsilon\nu)^{1/4} \tag{2.24}$$

where l_c = Kolmogorov microscale length (m)

v = velocity of Kolmogorov sized eddy ($m.s^{-1}$)

The specific energy dissipation rate (ε) can be estimated by determining the volume in which the energy is dissipated and the time scale of the event. Depending on the system and the position within the system, various dissipation rates can exist within a non-homogenous system. For example, within a stirred tank bioreactor, the energy is applied to the system through the impellers which act on the relatively small volume swept by the blades. Here the dissipation rate will be high and Kolmogorov length scale small. Within the rest of the vessel lower dissipation rates occur because of the larger volume resulting in larger Kolmogorov lengths in the bulk of the reactor.

The extent to which turbulent kinetic energy is transferred to micro-organisms depends on the relative size of the Kolmogorov eddies and the cell. Eddies larger than the cell size will not dissipate energy at the cell surface and the cell is described as moving with the eddy in a pocket of stagnant fluid. Eddies of the same size or smaller than the cell are, however, able to transfer their energy to the cell surface. A number of researchers have investigated the microscale length on cell viability in stirred and bubble column bioreactors on plant cells, animal cells and microcarrier systems (Prokop and Bajpai, 1992; Dunlop *et al.*, 1994; Cherry and Papoutsakis, 1988; Croughan *et al.*, 1987; McQueen *et al.*, 1987; Papoutsakis, 1991; Illing and Harrison, 1999). In general, significant shear damage to cells in a turbulent flow environment is only observed when the cells, cell aggregates or microcarriers are of the same size or smaller than the Kolmogorov eddies. For example, the size of the micro-eddies calculated to exist in highly turbulent small scale stirred tank fermenters are in the range of 25 to 200 μm in the bulk while in the impeller zone they range from 5 to 16 μm (Prokop and Bajpai, 1992; Illing and Harrison, 1999). Individual yeast cells with diameters between 3 and 8 μm are an order of magnitude smaller than these smallest eddies in the bulk, which would indicate that turbulent shear stresses in such small scale fermenters would have negligible effects on the cells except in the impeller zone where cells are similarly sized to typical Kolmogorov lengths. Brewers' yeast, however, forms flocs with sizes between 30 and 600 μm as seen in Figure 3.7 which may fall within the Kolmogorov microscale of less intense turbulent events. Turbulent energy may be

dissipated on these flocs and the cells on the floc surface resulting in damage to the floc structure and the cells at the floc surface.

Based on the analysis of the energy dissipation in turbulent eddies of similar or smaller size than the cell or floc, Croughan *et al.*(1987) approximated the Reynolds shear stress on a particle in turbulent flow (Equation 2.25).

$$\tau^R = 0.37\rho\left(\frac{\varepsilon}{\nu}\right)d_p^2 \tag{2.25}$$

where: d_p = particle diameter (m)

Under conditions of laminar flow or within regions of the flow where viscous shear would dominate, Equation 2.26 can be used as an approximation of the total shear stress.

$$\tau^V = 2\left(\frac{2}{15}\right)^{1/2}\left(\frac{\varepsilon}{\nu}\right)^{1/2}\mu \tag{2.26}$$

Dunlop *et al.*(1994) used Equation 2.27 to estimate the total shear stress acting on plant cells in a turbulent flow since under highly turbulent conditions the viscous shear stress is negligible. Here the stress is proportional to the square of the velocity difference between two points separated by a distance equal to the cell diameter. The velocity difference is calculated by Equation 2.28.

$$\tau^R = \rho\,\tilde{v}_{(dp)}^2 \tag{2.27}$$

where: $\tilde{v}_{(dp)}$ = velocity difference between two points a distance d_p apart ($m.s^{-1}$)

$$\tilde{v}_{(dp)} = C_1(\varepsilon d_c)^{1/3} \tag{2.28}$$

where: C_1 = constant between 1.57 (Dunlop *et al.*, 1994) and 1.0 (Zhang *et al.*, 1993)

For the carrot cell system studied by Dunlop *et al.* (1994), the calculated Reynolds shear stresses were between 0.2 and 1.5 $N.m^{-2}$ in the bulk phase of a bioreactor (based on total energy dissipation rates within the total volume of the reactor) and between 3.6 to 32.4 $N.m^{-2}$ in the impeller region of the bioreactor, while the Reynolds shear stress was between 0.1 and 21.6 $N.m^{-2}$ in a turbulent flow viscometer. Zhang *et al.* (1993) obtained energy dissipation rates of between 800 and 19 780 ($m^2.s^{-3}$) in flow through capillaries.

Using a mathematical model to describe the motion of a single turbulent eddy, Cherry and Kwon (1990) calculated the shear stress on a neutrally buoyant cell as it crossed through the eddy. They found that the shear stress on the cell surface oscillated as the cell rotated within the eddy and reached a maximum in the centre of the swirling eddy. The expression for the maximum shear rate they developed as a function of the energy dissipation rate and kinematic viscosity is given in Equation 2.29. Typical values of shear stress calculated with this formula are in the range of 0.05 to 0.5 $N.m^{-2}$. The frequency with which the cell experienced this maximum is equal to the frequency with which the cell encounters these turbulent eddies and can be approximated by the time taken for a cell to move a distance equal to the Kolmogorov length. Based on the assumption that the cell is moving with a velocity similar to that of the eddy itself, this frequency of maximum exposure to peak shear stress is given by Equation 2.30 with typical values of between 1 and 4 Hz. They also observed a higher frequency of the order of 20 to 80 Hz, with which the cell experienced smaller local maxima which make up the near sinusoidal manner in which the absolute maxima are generated. This frequency can be determined from Equation 2.31 using knowledge of the energy dissipation rate and kinematic viscosity of the fluid.

$$\tau_{max} = 5.33\rho(\varepsilon\nu)^{1/2} \tag{2.29}$$

$$f_{max} = \left(\frac{\varepsilon}{\nu}\right)^{1/2} \tag{2.30}$$

$$f_{local} = 0.678\left(\frac{\varepsilon}{\nu}\right)^{1/2} \tag{2.31}$$

where: τ_{max} = maximum shear stress on cell in turbulent flow ($N.m^{-2}$)

f_{max} = frequency of maximum exposure to peak shear (Hz)

f_{local} = frequency of local maxima experienced by cell (Hz)

2.5.3 Cell-Cell and Cell-Obstacle Interactions

Another mechanism of cell damage is by physical cell-cell or cell-obstacle collision. Such damage is a function of both the frequency and intensity of the collisions. A collision of a cell requires the force driving the objects together to exceed the force required to remove the liquid layer between them. The energy transferred during a collision depends on the extent to which the objects/cells are able to deform. The frequency of cell-cell collisions where the Kolmogorov microscale is of a similar size to the cells can be estimated by Equation 2.32 derived by Cherry and Papoutsakis (1988):

$$N_c = \left(v\alpha^2 / d_p^4 \right) \left(\pi d_p^3 / 6\alpha \right) \tag{2.32}$$

where α = volume fraction of cells

v = relative cell velocity ($m.s^{-1}$)

N_c = frequency of cell-cell collisions (Hz)

The relative cell velocity can be equated to the eddy velocity in isotropic turbulence (Equation 2.24). The collision severity is then defined as the product of the frequency and kinetic energy of collisions per cell (Equation 2.33). Alternatively the relative velocity can be based on a shear model which leads to a shear based collision severity expression given in Equation 2.34. Similar expressions for the severity of interactions can be derived based upon knowledge of the expected collision frequency and kinetic energy transferred.

$$CS_T = \frac{(\nu\varepsilon)^{3/4} \pi^2 \rho_p \alpha d_p^2}{72} \tag{2.33}$$

$$CS_s = \left(\frac{\varepsilon}{\nu} \right)^{3/2} \left(\frac{\pi^2 \rho_p \alpha d_p^5}{72} \right) \tag{2.34}$$

where: ρ_p = particle/cell density ($kg.m^{-3}$)

CS_T = collision severity based on eddy velocity ($J.s^{-1}$)

CS_s = collision severity based on shear model ($J.s^{-1}$)

2.5.4 Cavitation as a Mechanism of Cell Damage

In regions of low pressure within the flow, cavities of vapour can be spontaneously formed which then collapse in regions of higher pressure in a process called cavitation. It is this oscillating behaviour and rapid collapse of the bubbles which exerts large forces on particles suspended in the fluid (Save *et al.* 1994, 1997; Shirgaonkar *et al.* 1998). The vapour of the cavity can originate from either dissolved gasses in the fluid (causing the more ready onset of cavitation but decreasing its intensity) or from the fluid itself. The likelihood of cavitation occurring can be determined from the cavitation number (σ) defined in Equation 2.35 which is the ratio of forces collapsing cavities to those causing their formation. Cavitation will therefore occur at cavitation numbers below a critical inception number σ_i. Cavities will therefore be formed when the pressure is less than the vapour pressure of the fluid with the pressure within the cavity being equal to the vapour pressure. This method of using hydrodynamic cavitation to intentionally cause yeast disruption and protein release is reported to be an order of magnitude more energy efficient than other disruption techniques such

as ultrasonication and as such is a possible candidate for industrial scale application(Save *et al.*, 1994, 1997).

$$\sigma = \frac{P_\infty - P_v}{\left(\rho v_\infty^2\right)/2} \tag{2.35}$$

where P_∞ = pressure upstream of an orifice (Pa)

P_v = pressure at the point of maximum fluid velocity (Pa)

v_∞ = velocity upstream of the orifice ($m.s^{-1}$)

2.5.5 Correlating Cell Damage to an Engineering Variable

Correlating the biological response of a cell to an engineering variable will assist in the understanding of the conditions which result in cell damage across flow regimes. All cell damage caused by hydrodynamic effects must be mediated by a force acting on the cell surface. Forces which can act are either shear stress or normal (pressure) forces. It is intuitively correct that the higher the force, the greater the damage while a certain critical force event must be exceeded to overcome the cells' natural strength.

McQueen *et al.* (1987) studied mammalian cell lysis as a result of turbulent flow and found that the probability of cell lysis increased with increasing wall shear stress as expected. They also found that the time period for which the cells were subjected to the shear influenced cell lysis. Increasing the residence time from 0.33 to 0.99 ms in a capillary resulted in an increase in the specific cell lysis rate. This suggests that cell fatigue may weaken the cell, allowing lysis to occur at a reduced force event. This hypothesis was contradicted by Zhang *et al.* (1993) who measured similar specific cell lysis rates with different residence times in capillary flow and found that the specific cell lysis rate was independent of the residence time for residence times in the range 2.2 to 4.3 ms. These residence times are significantly longer that those used by McQueen *et al.* (1987), hence the constant lysis rate may result if these times exceed the time required to weaken the cell.

The time period to which the cells are exposed, and possibly frequency with which the stress acts on the cell plays an important role in determining the response of the cell. A small force may not have an effect on a cell if applied once but upon repeated exposure to this force, the cell may be weakened and damaged. Hence, total energy dissipated on the cells is a useful parameter against which damage can be correlated, where the energy is supplied with a force exceeding the minimum required to effect damage on the cells. Dunlop *et al.* (1994) used the total energy dissipation approach to correlate cell death rates of carrot cells across the various experimental conditions. They observed

the extent of damage to cells exposed to laminar flow conditions was less than the damage under turbulent flow, with Kolmogorov microscale eddies smaller than the cells, at the same total energy dissipation. Thus, from their work it appeared that the cells were more susceptible to damage in turbulent than in laminar flow under the conditions studied.

2.6 Summary

Based upon the cell wall structure, an effect of hydrodynamic shear mediated at the level of the cell wall can result in changes and/or the loss of polysaccharide, proteinaceous or lipid material. The loss of any of these compounds may not be detected by its increased concentration in the liquid environment around the cell due to the high dilution effects. Instead, the loss of cellular material can be detected by changes to the elemental composition of the outermost cell surface and changes to the molecular composition (protein, carbohydrate or lipid) at the surface. Such changes at the outer wall surface may result in changes to the observed hydrophobicity and surface charge of the yeast. Another indicator of damage at the cell surface is given by the cells' ability to interact with the environment e.g. the ligand/receptor mechanism of flocculence. The loss of (or damage of) such receptor or ligand molecules could result in reduced flocculation. Hence a decrease in the cells' ability to flocculate may occur when cells are subjected to shear environments. Shear forces mediated at the membrane level may also result in a change in cell viability and integrity, causing a release of intracellular protease. More severe damage of the cytoskeleton may alter the cells' growth and fermentation ability. Total cell disruption can occur under the most extreme handling conditions.

Within a typical brewery operation, yeast cells are mechanically handled which exposes them to hydrodynamic stress. Engineering variables used in literature to quantify the hydrodynamic stress include maximum shear stress and exposure time to this shear stress, energy dissipation rate and total energy dissipation. Quantification of the hydrodynamic stresses which result in cell damage would enable a better design of yeast handling circuits which would minimise cell damage.

Chapter 3: Materials and Methods

This chapter is subdivided into 4 sections, each dealing with an aspect of the materials or methods used in this investigative study on yeast handling. Section 3.1 introduces the yeast strains used, their propagation and the fermentation protocol used to evaluate fermentation performance. Section 3.2 details the complete set of analyses used to identify and quantify yeast and beer quality. Section 3.3 covers the range of mechanical handling and flow conditions to which the yeast was subjected in both the brewery and laboratory situations. Section 3.4 details analysis of zeta potential and XPS results to provide information on the surface composition of the yeast.

3.1 Yeast Growth and Fermentation Methods

3.1.1 Yeast Strains

The four strains of commercial brewers' yeast, supplied by South African Breweries (SAB) for trial purposes in this study are detailed in Table 3.1. They were all classed as *Saccharomyces cerevisiae* according to the classification system used by Hammond (1986). Strains SAB1 and SAB5 were used in brewery system testing, conducted at SAB Newlands Brewery as well as at the laboratory scale. The other two strains were studied at the laboratory scale only to provide useful insight into yeast handling effects across a broader sample of yeast strains.

Table 3.1. The strains of *Saccharomyces cerevisiae* studied.

Strain No.	Characteristics
SAB1	Highly flocculent, bottom fermenting at fermentation temperatures.
SAB1/96	A re-isolation of strain SAB1, isolation for reduced flocculence.
SAB2	Non-flocculent yeast strain.
SAB5	An internationally used bottom fermenting strain, less flocculent than SAB1 and SAB1/96.

3.1.2 Yeast Propagation Procedure

Reactor system and conditions: The yeast was propagated under full aerobic and near anaerobic conditions at the laboratory scale. Propagation was conducted in 2 litre, autoclaveable glass vessels, with 16°P brewery wort (Castle brand unless stated otherwise in the results) at 18°C. Agitation was provided with a 6 bladed Rushton impeller operated at 400 rpm equating to a tip speed of 1.7 $m.s^{-1}$. Temperature control of the bioreactor was achieved by circulating water at the desired temperature through a cooling coil. The propagation system is shown schematically in Figure 3.1. For near anaerobic propagation, the wort was saturated with oxygen at a partial pressure of 0.21 atm prior to inoculation, thereafter no further aeration occurred. The aerobic propagations were sparged continually at 2.2 $l.min^{-1}$ (1.5 vvm) with air. No pH control was used which caused an increase in the acidity of the medium with a starting pH of approximately 5.5 to a final pH of 4.0.

Pre-inoculum: A scraping of yeast cells was removed from a slant, inoculated into 50 ml of MYPG and grown in a 30°C shaker incubator (120 rpm) for 24 hours. MYPG media consists of malt extract (3 g/l), yeast extract (3 g/l), bacteriological peptone (5 g/l) and glucose (10 g/l).

Inoculum: 10 ml of 24 hour pre-inoculum was transferred aseptically into 100 ml of MYPG media and incubated at 30°C for 12 hours with shaking at 120 rpm.

Wort media: 16°P cold brewers wort was collected from the brewery and filtered to remove any residual trub. A 1.5 l aliquot of clear wort was added to the bioreactor. This was steamed inside an open autoclave for 40 minutes to sterilise the media.

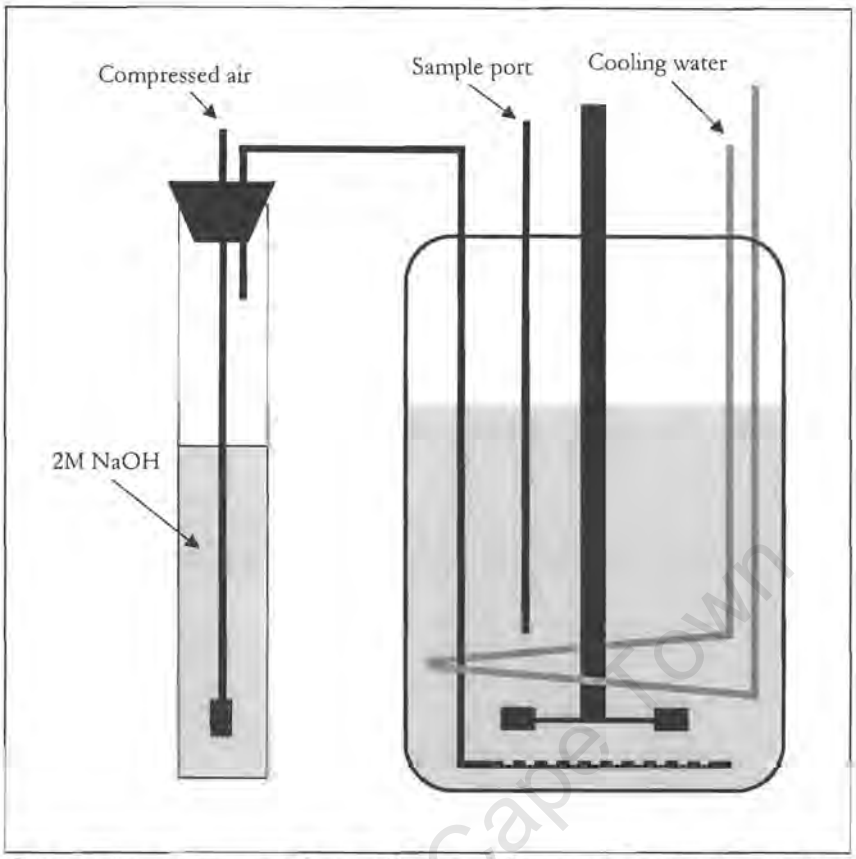

Figure 3.1. Schematic representation of the bioreactor system used for aerobic propagation the yeast.

Inoculation procedure: The steamed vessel was removed from the autoclave. Water at 17°C was circulated through the cooling coil to cool the media to 30°C. Yeast food containing a mixture of essential nutrients and vitamins (Nutromix supplied by Brent Chemical Technologies (Pty) Ltd) was added at the rate of 0.08 g/l wort by dissolving 0.12 g in 5 ml of water and steam sterilised prior to addition to the inoculum. The media was aerated for 5 minutes at 30°C to achieve saturation. The aeration ceased at the point of inoculation with the Nutromix/yeast mixture. For anaerobic propagation, no further air was supplied and agitation commenced. For aerobic propagation, sterile air at 1.5 vvm was supplied by first bubbling it through a 2M NaOH solution to humidify the air and provide pre-sterilisation. After inoculation with 115 ml yeast culture, the cooling was resumed to cool the vessel from 30°C to 17°C within approximately 20 minutes. This slow cooling of the yeast/wort mixture was implemented to avoid temperature shock of the yeast (Hottiger *et al.*, 1987; Lewis *et al.*, 1995; Piper, 1995). Samples were removed aseptically through the sample port at 4 – 8 hour intervals. The total volume sampled did not exceed 15 % of the total initial volume.

3.1.3 Small Scale Fermentation Method

To assess the overall fermentation performance of the yeast, small scale fermentations were conducted under conditions which mimicked brewery conditions closely, allowing investigation of aspects of yeast quality during fermentation. These include the fermentation rate, extent of attenuation, beer quality indicators, cell growth and sedimentation. Small scale fermentations were performed on two scales using either 2 l EBC tubes (EBC Analytica Microbiologica, 1977) or 500 ml measuring cylinders. Apart from the differing volumes in the two systems, identical set-up procedures were followed.

Wort media: Cold wort collected from the brewery was filtered to remove residual trub. A 2 l aliquot of wort was placed inside a 5 l round bottom flask (EBC system) or 500 ml into a 1 l Schott bottle (measuring cylinder system) and steam sterilised for 30 minutes in an open autoclave.

Inoculation procedure: For the 2 l EBC system, 0.16 g of pre-sterilised Nutromix (yeast food) was added to the cooled wort (room temperature) in the round bottom flask (5 l). The yeast was added at the desired pitching rate. The standard pitching rate of yeast in the brewery is 14 g of 100 % viable wet yeast per litre of wort, Equation 3.1. In order to detect more subtle changes in yeast performance, lower pitching rates were used in this work. Yeast slurries with lower viabilities were pitched so as to give an inoculation rate of 3.5 g of 100 % viable wet yeast per litre wort (1/4 the standard rate), unless stated otherwise in the results. The flasks were sealed with rubber stoppers and shaken through a 2 foot arc, 30 times after which the rubber stopper was removed and replaced with a sterile cotton wool bung to allow for the escape of produced CO_2. The flasks were allowed to stand at room temperature for 4 hours before the bung was again replaced with the rubber stopper and shaken a further 30 times. The evolved gas was released and the flasks shaken another 30 times before pitching of the wort/yeast mixture into the tall EBC tubes where fermentation took place at 11°C for 10 – 12 days. (Kruger *et al.*, 1982)

$$pitching\ rate\left(kg.hl^{-1}\right) = \frac{14*60}{consistency} * \frac{viability}{100} \qquad (3.1)$$

In the 500 ml measuring cylinder system, 0.04 g of pre-sterilised Nutromix was added to 500 ml of wort in 1 l Schott bottles. These bottles were inoculated at the same pitching rate used for the tubes and aerated as described above, prior to transfer into the 500 ml measuring cylinders where fermentation took place at 11°C for 10 days.

Data on cell counts, density and beer quality from the reproducibility study of 5 replicate fermentations are provided in Appendix B.8.

3.2 Yeast Quality Assay Methods

As outlined in Section 2.2.1, various assays can be used to identify the nature of change of yeast quality as well as to quantify the biological response induced. The assays chosen as indicators of yeast quality of each physiological state illustrated in Figure 2.2 are summarised in Table 3.2. The principle of each assay is discussed while the detailed methods are provided in Appendix B.

Table 3.2. Summary of yeast quality assays for the different physiological states of damaged yeast.

Physiological State	Yeast Quality Indicator
Minor envelope damage (wall)	Hydrophobicity - latex microbead attachment - solvent partitioning Surface Charge - dye adsorption - zeta potential Surface composition - X-ray photoelectron spectroscopy Flocculation - rate & extent of sedimentation Haze - particle size - dye staining - mannan release
Minor envelope damage (membrane)	Protease release
Replicative ability	Methylene blue viability stain
Metabolic activity	Fermentation

3.2.1 Hydrophobicity

Several methods exist to measure the hydrophobicity of micro-organisms. These include contact angle measurement (Gerson *et al.*, 1980a, b, c), partitioning between aqueous and hydrocarbon phases (Rosenberg *et al.*, 1980), hydrophobic affinity chromatography (Smart *et al.*, 1995) and polystyrene bead attachment (Hazen and Hazen, 1987). The two methods evaluated here are the solvent partitioning and bead attachment methods.

Contact angle measurements are made by coating a surface (usually filter paper) with cells. Drops of a hydrocarbon or water are placed on the dried surface and the angle between the edge of the drop and cell layer is measured using a microscope. The more hydrophobic the cells, the greater is the contact angle of water on the cells while the angle made using a hydrocarbon will be less. The method has the advantage of providing the surface free energy of the cells based on the surface tensions of the liquids used. Factors which affect the measured contact angle include the dryness of the surface and length of time the droplet is in contact with the surface. These issues result in questionable meaning being placed on results obtained from this method without rigorous testing of experimental conditions.

Hydrophobic interaction chromatography can be used to measure the hydrophobicity of cells based on hydrophobic interactions between ligands and cells. The chromatography column is packed with a material to which hydrophobic ligands are attached. The cells are loaded into the column where, dependent on their hydrophobicity, they attach to the ligands by hydrophobic interactions. Sterile medium is passed through the column to transport non-hydrophobic cells out of the column. The more hydrophobic the sample is, the more medium is required to remove the particles. The eluent is monitored for cell concentration. This is compared against the cell concentration emanating from a control column containing no hydrophobic ligands. The results are reported as a hydrophobic retention index, quantified as the percentage of loaded cells that exit the column as a function of time.

In an aqueous suspension, hydrophobic particles will attract one another. On introducing hydrophobic particles into a microbial suspension, micro-organisms with hydrophobic surface properties adhere to these particles. By using hydrophobic microbeads, a hydrophobicity index can be measured by enumerating the number of beads attached to individual cells and defining a cut off number of beads by which cells with more beads are termed hydrophobic and those with less, hydrophilic. The suspension can be observed under magnification to determine its relative hydrophobic and hydrophilic content. An advantage of using bead attachment to study hydrophobic interactions is that the sites of greatest hydrophobicity can be identified on the yeast cells. Hazen and Hazen (1987) used polystyrene microbeads to study hydrophobicity variations within populations of *Candida albicans* populations. The method used in this study is based on a modification of that of Wilcocks and Smart (1995). The method is described in Appendix B.1.1.

Aqueous hydrocarbon partitioning requires the use of two immiscible liquids with different hydrophobicity. Hydrophobic particles tend to redistribute themselves out of a hydrophilic aqueous environment into a hydrophobic or organic environment, where possible. By preparing a suspension of yeast cells in an aqueous solution and adding a hydrocarbon solvent, the hydrophobic cells will be

removed from the aqueous phase. The more hydrophobic the cells, the greater their concentration in the hydrophobic phase. Results obtained are reported as a hydrophobicity index, i.e. the percentage of the total cells that partition into the hydrophobic phase. The method of Smart *et al.* (1995) is used in this study is detailed in Appendix B.1.2.

It should be noted that the aqueous environment may affect the apparent hydrophobicity of the cells. In the brewing situation, yeast is in an environment of fermented wort containing variable concentrations of compounds including ethanol, sugars, amino acids and inorganic salts. It is especially important that a defined medium be used when measuring the cells' hydrophobicity to enable comparison between different treatments or different yeast. Hence, hydrophobicity is measured in buffer solutions.

The reproducibility study conducted to determine the cells' hydrophobicity (Appendix B.1.3) indicates that the solvent partitioning method is the most reproducible with a coefficient of variance of 3.9%.

3.2.2 Surface Charge

The surface charge on a cell can be investigated by either measuring the zeta potential through electrophoretic mobility studies or measuring the affinity of a charged molecule for the cell surface by detecting its adsorbed concentration. The adsorption of a charged dye is particularly easy to perform, requiring only a spectrophotometer. Zeta potential measurement requires specialist equipment (not currently available for routine use in the brewery) but provides more quantifiable results. For these reasons both methods have been examined: the dye adsorption for a routine brewery assay and the zeta potential measurement for more detailed analysis of the cell surface.

In the dye adsorption technique, Alcian blue 8GX (Sigma, Cat no. A 3157), a dye containing four positively charged isothiuron groups (Figure 3.2), is used. The dye adsorbs preferentially onto the negatively charged sites on the yeast surface. The initial and residual dye concentrations are measured spectrophotometrically and the cell concentration determined by either dry weight or microscopic cell counts, allowing the concentration of dye adsorbed per unit cell surface area to be determined. The detailed procedure of performing the dye retention technique is found in Appendix B.2.1.

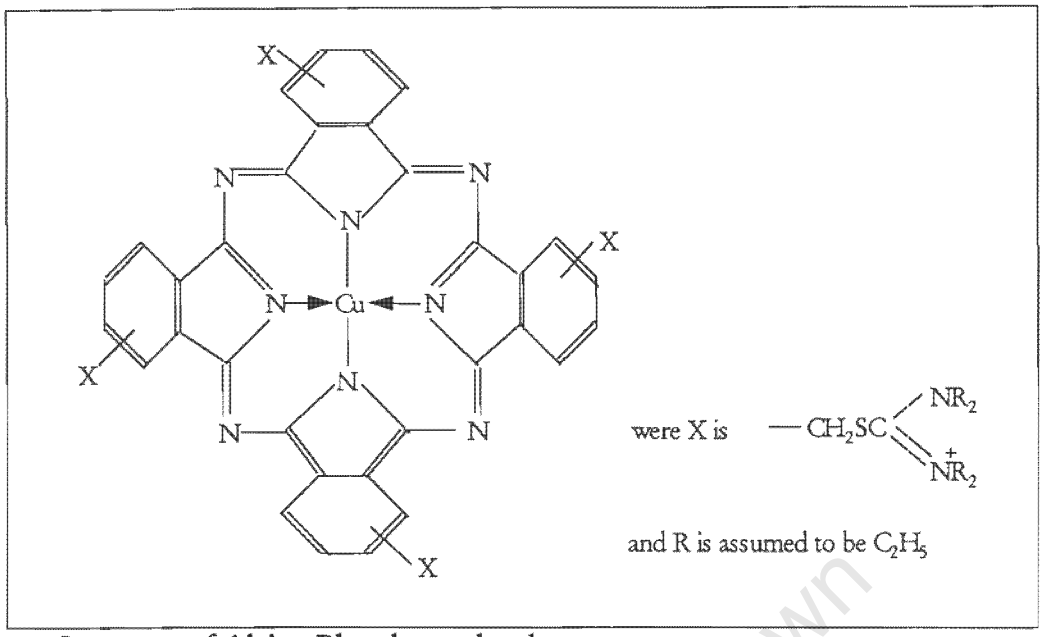

Figure 3.2. Structure of Alcian Blue dye molecule.

Zeta potential is determined from the measured electrophoretic mobility of a charged particle in an electric field. When a charged particle is placed in an electric field, it accelerates to its terminal velocity which is limited by the opposing viscous drag on the particle. A charged particle gathers ions of opposite charge (counter-ions). Close to the particle the ions will be strongly adsorbed making them immobile. Further away from the particle, hydrated counter-ions form a diffuse layer. These two layers are called the electrical double layer. The plane of shear is where these two layers meet. The potential caused by the ionic distribution increases from zero in the bulk fluid to the surface potential (ψ_o) at the surface. The zeta potential (ξ) is the potential at the plane of shear and is therefore not the true surface potential. It is dependent on the nature of the adsorbed ions as well as the ionic strength of the electrolyte. The ionic strength determines the thickness of the ionic cloud surrounding the particle, thereby shielding the surface charge from the applied electric field and lowering the particle's mobility. The solution pH is also important when measuring electrophoretic mobility. The pH determines the extent of ionisation of surface groups responsible for surface charge. In the case of yeast cells the most important groups are the weak acid (carboxyl and phosphate) and weak base (amine) groups. The pH at which the surface of the particle is neutral is called the point of zero charge (pI) or isoelectric point.

The surface charge of yeast cells can influence the flocculation potential in strains of yeast which do not flocculate by the lectin mechanism as described in Section 2.4.3. (i.e. strains belonging to the MI group according to sugar classification). Higher surface charge results in increased repulsion between cells and hence decreases the likelihood of van der Waals forces causing flocculation. In this study, use was made of a Malvern Zetasizer 4 to measure electrophoretic mobility. Particles are accelerated by an applied potential difference, pass through the intersection point of two, in phase, laser beams.

Young's fringes are set up by the intersecting beams. When the particles pass through these fringes they scatter light to a receiver which detects the light intensity. The intensity of the light is related to the particle's velocity and so can be correlated to mobility and zeta potential. The yeast was prepared for zeta potential measurement according to a modification of the method used by Smart *et al.* (1995) to study the surface properties of brewers yeast under physiological stress. A 20 mM sodium acetate / acetic acid buffer was used for cell suspension as the pH could be adjusted within the range of interest (pH 2.2 – 7.5). This buffer was also used to measure the flocculation potential of the yeast. The method for zeta potential determination is provided in Appendix B.2.2.

The reproducibility study conducted (Appendix B.2.3) indicates a coefficient of variance for the dye retention assay of 7.0 % while the standard deviation of zeta potential measurements across the pH range is less than 0.3 mV.

3.2.3 X-ray Photoelectron Spectroscopy (XPS)

Classical methods of determining the chemical composition of yeast cell walls require cell fractionation, hence depend on its efficacy. In addition, this approach provides information on the bulk composition of the wall only. Through use of X-ray photoelectron spectroscopy (XPS), the composition of the surface can be determined. A Physical Electronics, Quantum 2000 scanning ESCA Microscope was used to analyse the samples in this study. Due to the analysis chamber of the spectrometer operating under vacuum, the biological sample were first freeze dried with care taken to preserve the natural state of the cell to represent the hydrated environment. The method of sample preparation was adapted from Rouxhet *et al.* (1994) and Dengis *et al.* (1995a). In XPS, the whole freeze dried cells are irradiated with a beam of X-rays to induce the ejection of electrons. Because inelastic scattering of the electrons occurs, only the outermost molecular layer is analysed, typically only the outer 2 – 5 nm of the surface. A more detailed description of the principles by which these spectrometers work can be found in Rouxhet and Genet (1991).

The kinetic energy of these emitted electrons is analysed to give their binding energy which is unique to the various elements. A detailed examination of the binding energy spectrum of each observed element to determine the shape and position of the peaks provides insight into atomic bond structure. This is done by deconvoluting the spectrum into individual peaks produced by the bonds by which each element is attached. The peaks were broken down according to the model compounds used by Rouxhet *et al.* (1994) and Dengis *et al.* (1995a). The position of the peaks found by the above authors as well as the bonds attributed to the peaks are summarised in Table 3.3. Sample preparation for XPS analysis and operation of the spectrometer is detailed in Appendix B.3. Section 3.4.2 details analysis of XPS results to provide information on surface composition of yeast.

Since cells interact with their environment at their outer cell surface, XPS can be used to investigate the links between such surface phenomena as hydrophobicity, charge, flocculation and surface mediated damage and the chemical composition of the outermost layers of the yeast cell.

Table 3.3. XPS - Bond types and energies representing peak decomposition positions.

	Binding Energy (eV)	
Atomic Bond	Rouxhet *et al.*, (1994)	Dengis *et al.*, (1995a)
Carbon (C_{1s})		
C-(C,H)	284.8	284.8
C-(O,N)	286.3	286.3
C=O	288.0	287.8
O=C-OH	289.0	289.0
Oxygen (O_{1s})		
O=C	531.3	531.3
C-OH	532.6	532.6
Nitrogen (N_{1s})		
N-C	399.6	399.9
N^+	401.3	401.3

3.2.4 Flocculation Assay

The assay is based on a modification of the spectrophotometric method described by Miki *et al.* (1982a) and modified by Smit *et al.* (1992). The two variations on the method measure the initial settling rate of yeast flocs and the equilibrium position between single cells and yeast flocs. Washed and deflocculated yeast is resuspended in a flocculation buffer and allowed to acclimatise. In these methods, the yeast is agitated to initiate flocculation and placed in a cuvette in the spectrophotometer to measure the time course of settling flocs. The measurements provide an indication of the flocculation potential of the yeast using environmental and measurement conditions optimal for flocculation. The disadvantage of these methods is the low degree of reproducibility between the various laboratories due to variation in the degree of agitation. Agitation ranged from 15 seconds of inversions of the cuvette used for measurement (Miki *et al.*, 1982a), through 15 seconds of mixing with a Vortex generator (Kihn *et al.*, 1988b), 30 seconds of vortex mixing (Kuriyama *et al.*, 1990), vigorous stirring of cell suspension test tubes for 15 seconds followed by rotary shaking at 60 rpm until equilibrium was reached between free and floc concentrations (Masy *et al.*, 1992) to 20 seconds of vortex mixing followed by 5 inversions of the cuvette, (Smit *et al.*, 1992). To eliminate operator variability a system was chosen whereby the cell suspension could be agitated by bubbling air at a

standard flow rate with bubbles of constant and uniform size through a glass U tube directly inside the spectrophotometer for a fixed length of time. After agitation ceased, the absorbance was measured as a function of time. From this, the extent of flocculation as well as the maximum rate of sedimentation was determined by converting the absorbance data to cell concentration data. The detailed method and an analysis of its reproducibility is provided in Appendix B.4. The coefficient of variance for the flocculation assay is 0.5%. A typical result of suspended cell concentration as a function of time is provided in Figure 3.3 indicating the extent of flocculation.

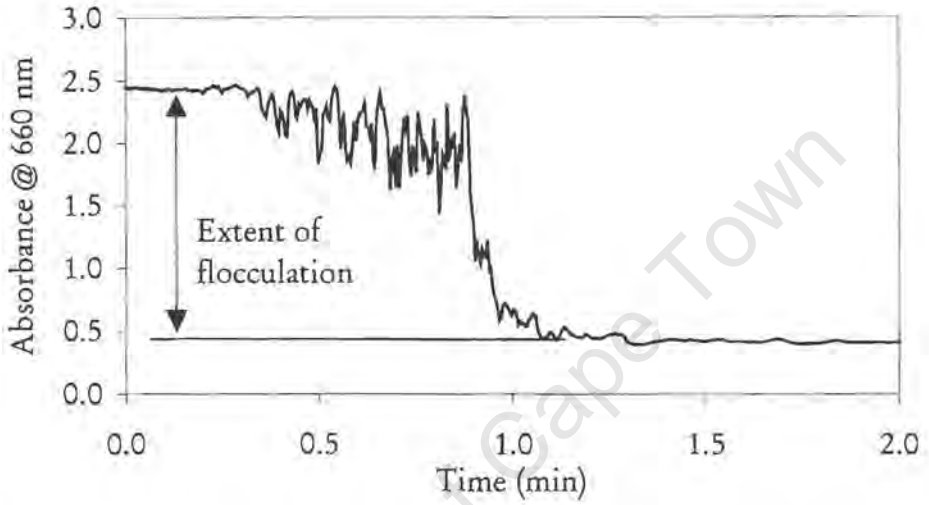

Figure 3.3. Absorbance profile during flocculation test of production yeast, SAB1.

The recommended concentration of Ca^{2+} needed to achieve flocculation in strains of bottom fermentation brewing yeast's was reported to be between 1 mM and 10 mM (Kihn *et al.*, 1988b). Tests were performed on SAB1 to determine the optimal calcium concentration (Figure 3.4) and flocculation pH (Figure 3.5) required for flocculation. As seen from this data, the maximum extent of flocculation is reached at an approximate calcium ion concentration of 1 mM with no significant benefit being obtained at higher concentrations. The maximum rate of sedimentation was reached at 100 mM. Higher concentrations were found to reduce the rate dramatically. Because of these findings the extent of flocculation was measured at a calcium ion concentration of 10 mM.

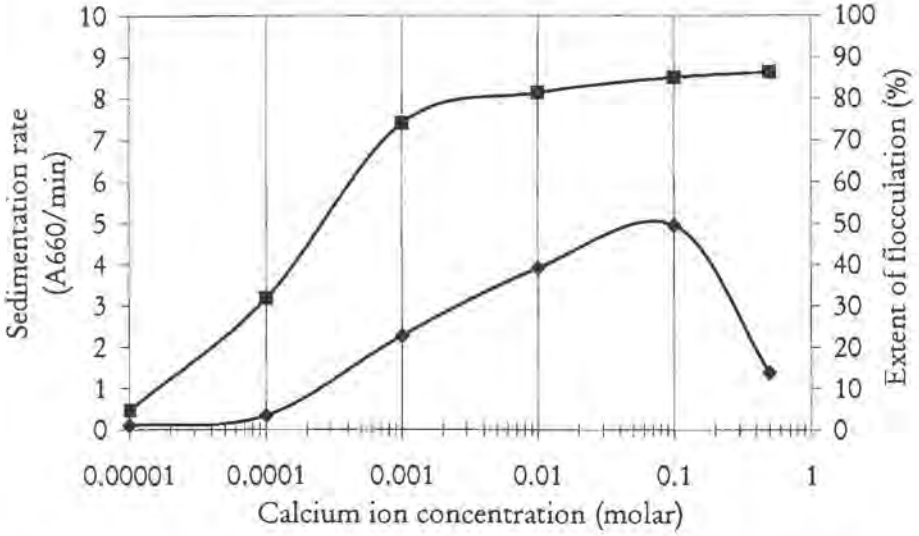

Figure 3.4. Dependence of flocculation on calcium concentration, pH4.5.
(♦ sedimentation rate, ■ extent of flocculation)

It was reported by Smit *et al.* (1992) that the rate of flocculation was dependent on pH with an optimum rate of sedimentation being found at pH 4.5 when using a calcium concentration of 9 mM. The pH dependence of flocculation observed for SAB1 is compared with the results of Smit *et al.* (1992) in Figure 3.5. The optimum sedimentation rate of this strain was found to occur at pH 5.5 while the maximum extent of sedimentation was between pH 4.5 and 5.0. A pH of 4.5 was chosen as being optimal for the measurement of extent of flocculation.

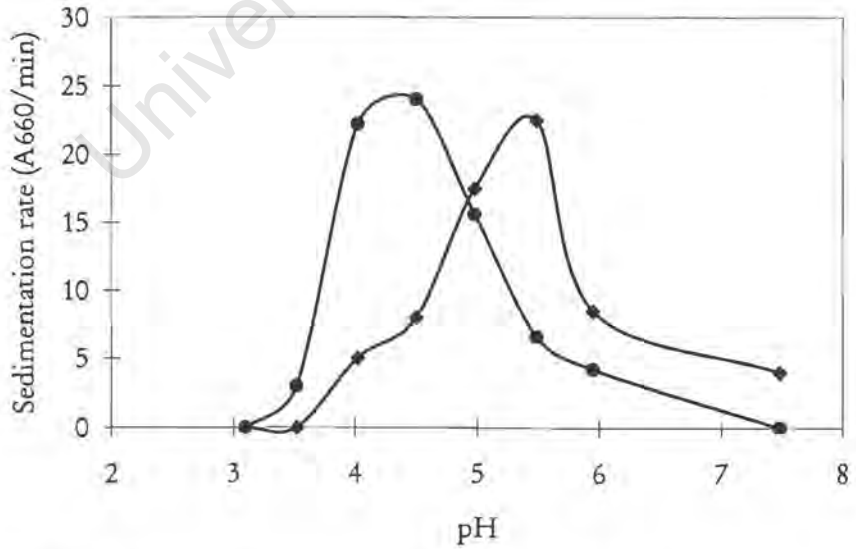

Figure 3.5. Dependence of flocculation on pH at 9 mM Ca^{2+}.
(● Smit *et al.* (1992), ♦ SAB1)

3.2.5 Haze Analysis

The presence of sub-micron particles in the yeast slurry or beer can contribute to the occurrence of haze in beer, resulting in compromised beer quality. Lewis and Poerwantaro (1991) demonstrated the release of haze material from the cell walls of yeast on agitation. Siebert *et al.* (1987) found reduced filtration performance follows yeast removal by centrifugation. It is therefore reasonable to hypothesise the release of sub-micron particles from the yeast surface when it is handled mechanically. To investigate this, the size distribution of particles over a broad range as well as the origin of the particles must be determined. It is particularly important to determine whether the haze material originates from the cell wall of yeast, indicating damage to the yeast.

As mannan forms the outer layer on the surface of the yeast, it is reasonable to expect a high proportion of mannan in haze originating from yeast damage. Glucan is associated with the mannan, in the cell wall material and may arise in haze. However, the husks of barley also contain glucan, hence its presence does not necessarily confirm yeast damage. Mannan is not found in the wort, hence its presence is attributed solely to the presence of cell wall material in the haze. Three approaches to the determination and analysis of beer haze have been taken. Firstly, the particle size distribution can be measured to confirm its presence. The nature of the haze, proteinaceous or carbohydrate can be determined using dye staining techniques and finally the carbohydrate can be identified and quantified using enzyme assay procedures.

The size of yeast and haze particles was determined using a Malvern Mastersizer (long bed version 2), based on laser light scattering. Smaller particles scatter the light at greater angles while larger particles allow the light to pass through almost undeflected. By detecting the angle and intensity of the scattered light the size and concentration of particles in a given size range can be calculated. Equipped with a 300 mm lens, the particle sizer is able to detect particles in the size range from 0.05 to 850μm. This range is suitable for detection of yeast as well as smaller haze particles. Data is collected as volume percent of particles falling within defined size ranges. This can be converted to either surface area or number of particles based on the assumption that the particles are spherical.

Before haze samples can be analysed, the proportion of yeast particles must be decreased so that the larger yeast particles do not obscure the smaller haze particles. Care must be taken when removing the yeast not to generate haze. Yeast was removed by centrifuging the sample for 3 minutes at 200 g in a Beckman TJ-6 refrigerated centrifuge. The supernatant was recovered and a portion analysed for haze (termed Haze 1 in Figure 3.6). The process was repeated a second time on the remainder of the supernatant with the resultant supernatant labelled Haze 2 in Figure 3.6. The resultant supernatant consists mainly of the smaller haze particles with a small amount of yeast still present. A size analysis of these suspended haze particles was conducted following dilution in physiologically buffered saline

(0.9% NaCl) to avoid size change owing to osmosis of water into the particles. The samples were deflocculated in the ultrasound bath for 2 minutes at 50 % power. The suspension was pumped continually at 50 % of the maximum flow rate through the measuring chamber and the size measurement taken.

A resultant particle size distribution is presented in Figure 3.6, from which it is evident that not all of the yeast particles (3 – 13 μm) were removed when preparing the haze concentrate and that the centrifugation caused some aggregation of the yeast (13 – 500 μm). The depicted data of % volume as a function of size results in the smaller haze particles being overshadowed by the yeast cells. Since the haze is present in the size range from 0.08 to 2μm, distinct from the size of the yeast (average of 8.2μm, with 20 and 80% passing bounds of 7.1 and 17.6 μm respectively), valuable data can be extracted by conversion of the data to a surface area basis or a particle number basis as shown in Figure 3.7. The percent surface area and particle number clearly show the large proportion of haze in the sample.

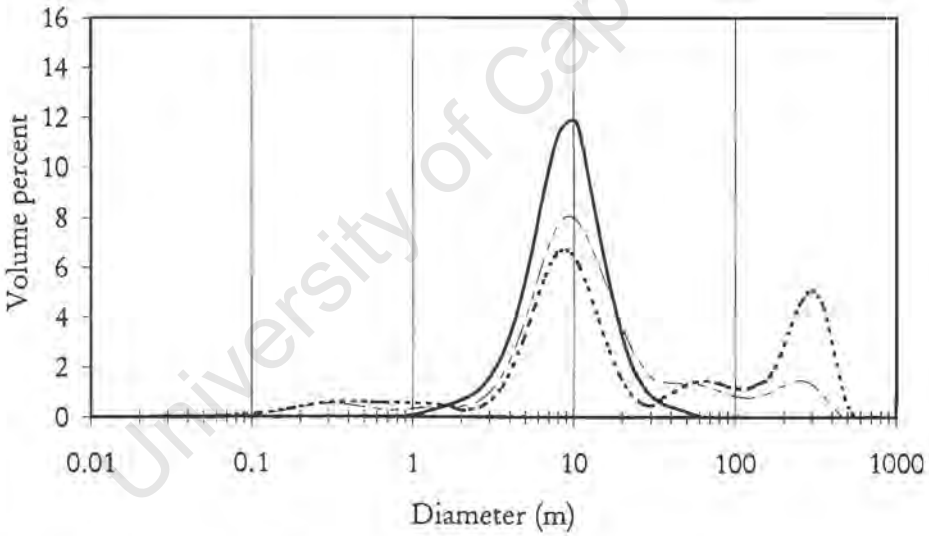

Figure 3.6. Size distribution of yeast and haze suspensions.
(— SAB1, —– Haze sample 1, — Haze sample 2)

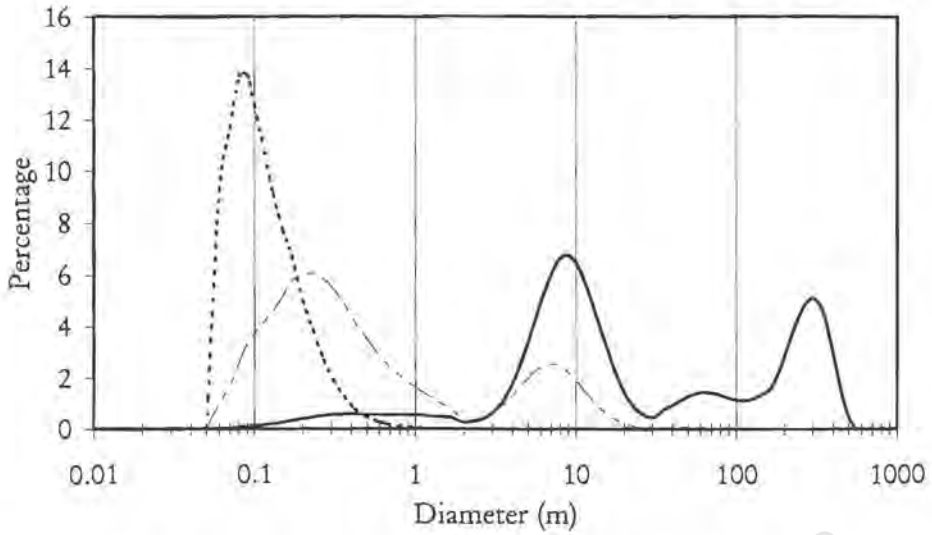

Figure 3.7. Size distribution of haze concentrate (Sample Haze 2).
(— volume %, ----- area %, ···· particle number %)

The presence of proteinaceous and carbohydrate compounds can be detected by staining the haze material before viewing by bright field microscopy. Eosin yellow is an anionic dye which combines with acidic proteinaceous matter. The stain lactophenol blue is specific for the cell walls of yeast and mold by staining polysaccharide components (Siebert *et al.*, 1981; Lillie, 1977). Eosin Y (Sigma, Cat no. E 4382) is prepared by dissolving in water to a concentration of 1 g/l while lactophenol blue (Fluka, Cat no. 61335) is diluted to 1 ml/l. Both stains are used in a 1:1 volume ratio with haze. Using these stains, the haze can be found to be either protein-based (indicating the presence of excess protein from the mashing process or from the lysis of yeast) or yeast cell wall-based (indicating the formation of particulates as a result of damage to the yeast walls).

The carbohydrate content of the haze can be hydrolysed to release its primary sugar monomers. These monomers (glucose, fructose and mannose) can be measured enzymatically and thus reveal information about the origin of the haze. Both water soluble and water insoluble haze fractions can be measured. The method as well as the limits of detection and maximum sugar content which can be determined without dilution of the sample are provided in Appendix B.5.

3.2.6 Methylene Blue Viability

Methylene blue staining is the most commonly used indicator of viability in the brewing industry, despite inaccuracies resulting from populations of low viability (< 50%) or when yeast has been rendered non-replicative by prolonged storage (Parkkinen *et al.*, 1976). There are two possible mechanisms for the action of this viability stain. The first is the exclusion of the dye molecule from the cell by the cell membrane of a viable cell. The other possible mechanism based on dye entering

the cell being reduced enzymically to a colourless compound in viable cells. Viable cells appear unstained while dead cells are stained blue. Errors in the overestimation of viability in cell populations of low replicative ability have been linked to impurities in commercial dyes which result in blue stains with variable intensities (Smart *et al.*, 1999). From this study the use of a purer and more stable vitality dye (methylene violet 3 RAX) is proposed to counter the problems associated with methylene blue. The methylene blue stain developed by Lee *et al.* (1981) was, however, chosen as the viability indicator in this work because of the expected high viabilities of yeast. The detailed method of methylene blue viability is provided in Appendix B.6. The standard deviation for replicate samples was calculated to be 0.95%.

3.2.7 The Protease Assay

Proteases are a class of intracellular enzymes used by the cell to degrade proteins to amino acids available for the formation of new proteins. Protease is released from yeast cells if the membrane is damaged. The release of protease has also been observed under conditions of nitrogen limitation (Slaughter and Nomura, 1992), where the released protease aids the extracellular breakdown of proteins to alleviate the limitation. With the use of appropriate blank samples which are not subjected to hydrodynamic stress but processed after the same length of time, the protease release can be divided into that released as a result of nitrogen limitation and that as a result of hydrodynamic damage to the cell membrane.

The method is based on the work of Mochaba *et al.* (1993) to determine quality of cropped yeast. A resorufin labelled casein substrate is incubated in the presence of sample to allow any protease present to cleave the dye marker from the casein. Following precipitation of undigested protein, the dye concentration is determined spectrophotometrically. The indicated incubation times suitable to effect an absorbance change for the detection of protease range from 15 minutes to 18 hours. To enable comparison between samples with different levels of protease, a linear response between absorbance and protease concentration is required. With samples of low protease concentration, longer incubation times are favourable to increase the sensitivity of the assay. When high protease concentrations are present, these long incubation times cause the casein substrate to become limiting, hence absorbance as a function of protease activity deviates from linearity. Under these conditions, shorter incubation times are required. The loss of linearity as a result of substrate limitation is illustrated in Figure 3.8. The range of absorbance over which a linear response is observed is between 0.0 and 0.6. Using an incubation time of 1 hour, the range of protease concentrations corresponding to a linear increase in absorbance was found to be successfully increased over an 18 hour incubation time as illustrated in Figure 3.9. The absorbance range where linearity was observed remained approximately the same as in the 18 hour incubation study with the maximum absorbance

giving a linear response in the 1 hour incubation study being 0.8. In this work both 18 hour and 1 hour incubation times were used to quantify low and high levels of protease release respectively. The method as well as the reproducibility study are presented in Appendix B.7. The coefficient of variance for samples with an absorbance of 0.6 is 4.1 %.

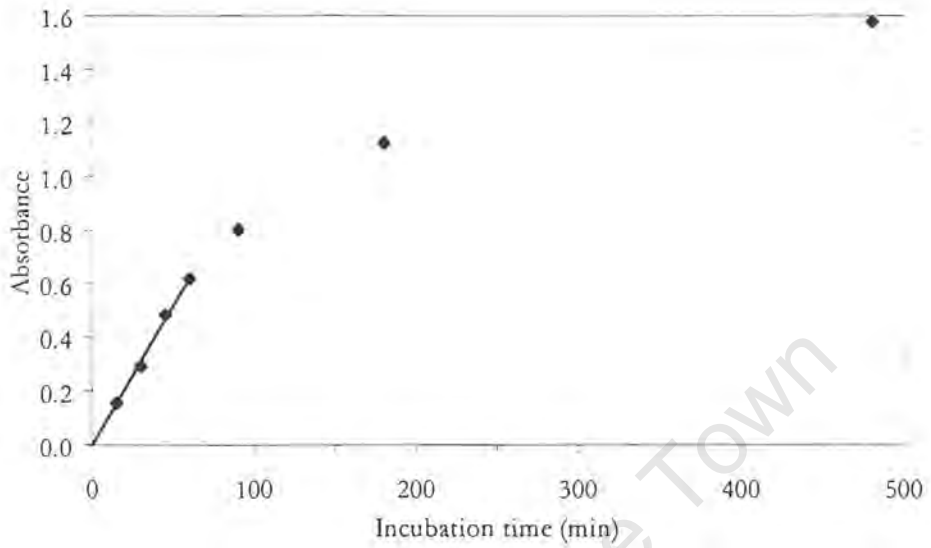

Figure 3.8. Protease absorbance as a function of incubation time.

(♦ absorbance data, — linear response region)

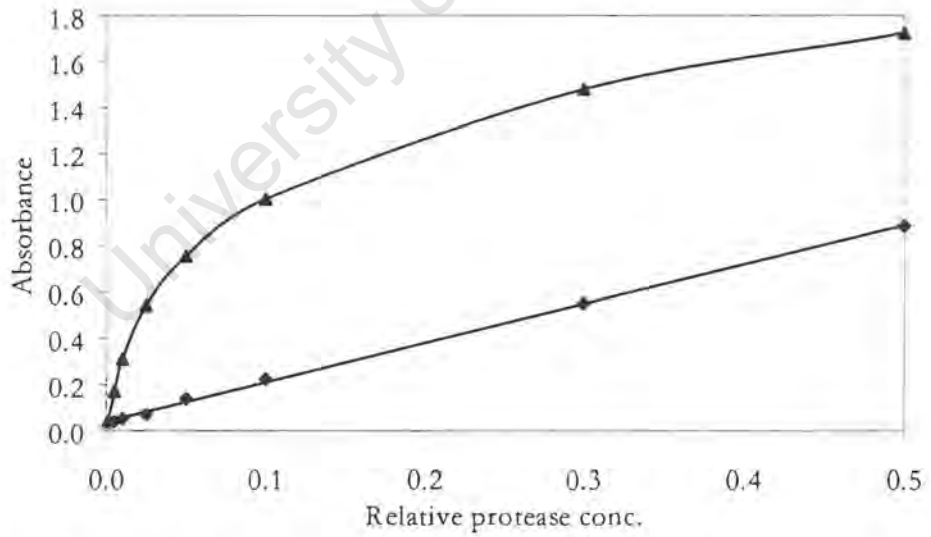

Figure 3.9. Protease absorbance as a function of protease concentration for different incubation times

(▲ 18 hour incubation, ♦ 1 hour incubation)

3.2.8 Fermentation Performance

Good fermentation performance is characterised by a rapid rate of attenuation with a low residual sugar concentration. This is best achieved by yeast cells which remain freely suspended throughout fermentation and flocculate rapidly upon sugar exhaustion. Towards the end of fermentation, the temperature is generally increased by 3 to 4 degrees firstly to improve yeast metabolic rate and so speed up the consumption of the remaining sugars and secondly to aide the cells reabsorption of excess aromatic compounds such as diacetyl. The temperature increase at the end of fermentation did not form part of the experimental methodology for this study. Once the yeast has settled it is removed so that cell lysis does not occur to any great degree. The unflocculated yeast remains in suspension at such a concentration that its presence will satisfactorily reabsorb the remaining diacetyl but low enough to minimise cell lysis which would harm the beer flavour. During this time the temperature is usually reduced so that lysis is minimised and the green beer is matured at sub-zero temperatures until the bouquet of flavour compounds have reached the required concentrations.

The pH of the final beer is an indicator of both yeast quality and beer quality. To within reasonable limits the lower the pH of the final product the better since it would have a preservative effect on the beer as fewer organisms are able to grow at the lower pH values. The pH of the green beer is also an indicator of yeast quality and fermentation performance as lysed yeast causes an increase in the pH of the beer. A good fermentation is one in which the sugars are converted rapidly and to completion followed by flocculation and removal of the yeast before cell lysis sets in. A poor fermentation is characterised by a slow rate of attenuation with the yeast starting to settle out before the sugars are consumed. The settled yeast in the cone of the fermenter remains metabolically active in this case and generates heat. Poor heat transfer in the stagnant zone at the base of the vessel accelerates cell metabolism with the rapid depletion of nutrients and accumulation of ethanol. This unfavourable environment results in significant cell lysis before the required degree of attenuation has been reached. Slow attenuation is often accompanied by high yeast slurry pH values and indicates the unsuitability of the yeast for reuse.

Small quantities of sulphur dioxide in the green beer are advantageous as it has a role as a preservative. The required concentration to achieve this effect is lower than that normally produced in fermentation with high SO_2 concentrations resulting in beer with a sulphurous taste. For this reason, lower SO_2 concentrations are generally accepted as being indicators of good beer quality.

Diacetyl is a flavour compound that is produced by the yeast as a by-product of ethanol formation. In the metabolic pathway, ethanol is produced from acetaldehyde. When this pathway is inhibited, the accumulated acetaldehyde can be converted into diacetyl. During normal cell growth the diacetyl produced is excreted from the cells. Towards the end of fermentation, however, diacetyl is

reabsorbed by the cells and converted via acetaldehyde to produce further ethanol. For this reason a maximum diacetyl concentration is reached during active fermentation and the concentration gradually decreases towards the end of fermentation. Diacetyl as a flavour compound imparts a buttery aroma to the beer, reducing its quality. A good fermentation is characterised by low diacetyl production and the reabsorption of diacetyl produced by the yeast leaving a low residual diacetyl concentration. High diacetyl concentrations are also reported to be an indicator of infection by certain organisms. Elevated temperatures during fermentation also cause more diacetyl to be produced by the yeast.

Data on cell counts, density, biomass growth factor and the beer quality indicators SO_2, diacetyl, acetaldehyde and pH from the reproducibility study of 5 replicate fermentations are provided in Appendix B.8.

3.3 Yeast Handling Methods

Various yeast handling processes occur within the brewery environment which pose hazards to the yeast quality (viability and vitality). These include equipment where the flow is constricted (e.g. plate and frame heat exchangers and partially throttled valves), high shear equipment (e.g. rotating disc centrifuges) and equipment generating large pressure fluctuations (e.g. pumps). All these equipment units exert high fluid shear rates on the suspended cells. To investigate the general phenomena of high shear rates on yeast slurries, a laboratory yeast handling unit was chosen to produce high shear rates (high pressure homogeniser, the French Press) as well as shear rates typical within brewery equipment (online brewery yeast handling circuit and disc stack centrifuge). Hence, mechanical yeast handling was investigated across a range of conditions at laboratory scale as well as within the brewery yeast handling circuit.

3.3.1 French Press Apparatus

The French Press (SLM Instruments Inc., Urbana Illinois) is a small scale high pressure homogeniser with a working volume of 40 ml (exploded view depicted in Figure 3.10), conventionally used to cause microbial disruption. The pressure is produced by a manually operated hydraulic pump mounted above the pressure cell. Once the desired operating pressure has been obtained, the flow valve is opened and the pressure allowed to decrease by 2 Mpa before the valve is closed and the cell repressurised. This operation is repeated until the complete sample volume has been processed. The flow rate is estimated from the time during which the valve is opened to process the sample. The pressurised yeast suspension is allowed to escape through a narrow orifice. This rapid release of pressure causes the formation of high shear environments through the orifice resulting in damage to

the cells. By varying the operating pressure, it is possible to operate in the range of cell disruption or under milder cell damage conditions. The yeast used was grown either aerobically or anaerobically in wort until the cells had reached the stationary phase, or the yeast was collected from the yeast collection vessels (YCV) at SAB – Newlands brewery. The cells were concentrated by centrifugation at 700 g for 5 minutes at 4 °C, washed once with 2 volumes of distilled water and collected by centrifugation. The recovered cells were diluted to 180 x 10^6 cells/ml with distilled water and placed on ice to maintain the temperature below 4 °C. A sample volume of 20 ml of the yeast suspension was required in the compression cell of the French Press. The pressure in the compression cell was varied between 3 and 40 MPa and generally maintained at either 3, 6, 10, 20, 30 or 40 MPa. To minimise the effect of heating on the yeast, the sample exiting the French press was collected into a Mc Cartney bottle placed in an ice bath. The pressure cell was rinsed and dried between samples. After the samples had passed through the French Press, total cell count, viability and protease determination were conducted. Fermentation performance of selected samples was carried out. Yeast in a portion of the sample was collected by centrifugation at 700 g for 5 minutes at 4 °C and washed twice. The hydrophobicity, zeta potential and flocculence of the washed yeast were also determined.

Figure 3.10. Exploded view of French Press model no. FA-073, 40 ml cell.

3.3.2 Brewery Yeast Handling Systems

Four 'offline' flow trials were conducted on spent yeast or yeast being removed from fermentation duty at SAB – Newlands Brewery using strain SAB1. The first of these trials involved extending the flow rate from the standard brewery cropping rate for SAB1 (60 – 70 $kg.min^{-1}$) to approach 190 $kg.min^{-1}$ to test the response of the yeast to increased shear stress. Thereafter, the effect of repeated exposure of yeast to a pump and pipe-work section was studied to determine the effect of total

energy dissipation on yeast quality over periods of 2 and 6 hours. A trial was conducted on the total yeast crop being pumped out of a fermentation vessel en route to a spent yeast storage vessel to monitor the condition of yeast as a function of time and position in the fermentation vessel during cropping. Two online trials were conducted on yeast during the cropping procedure under the standard pumping conditions used in the brewery for strains SAB1 and SAB5. The trial with SAB1 included the effect of storage and acid washing procedure while the trial with SAB5 includes only the effect of mechanical handling. A schematic representation of the yeast pumping circuit used for the scrapping, high flow rate and recirculation trials is presented in Figure 3.11. The flow/pump rig consists of three parts: A – recirculation tank, B – pump trolley and C – holding tubes. There are three sampling points on the rig: before the pump, between the pump and holding tubes, after the holding tubes. The yeast can be routed to either leave the test rig before or after the holding tubes, or the recirculation tank can be filled for later reuse. The holding tubes (13.5 m in length) could be interchanged to provide piping with diameters of 25, 50 or 65 mm.

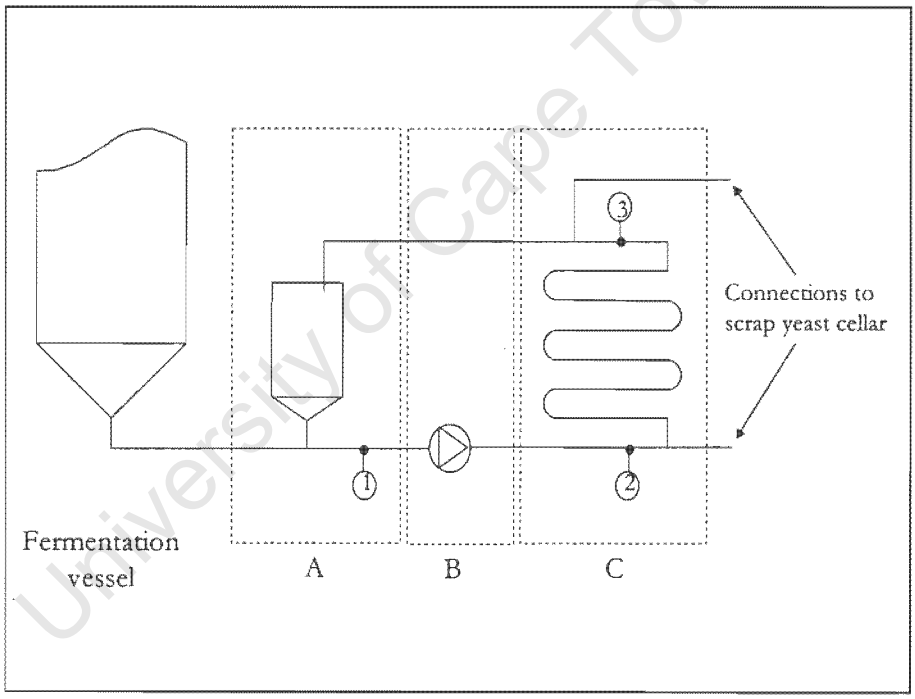

Figure 3.11. Schematic of the pump test rig.

The effect of high flow rates was investigated using the Scandi Brew gear pump because of its high pumping capacity and low pulsation fluid delivery. In a study on the effect of pump design on brewers' yeast quality, Basson (1996) observed no adverse effects in terms of cell viability, protease release, oxygen utilisation rate or fermentation performance when using the Scandi Brew gear pump at flow rates of 99 and 193 $l.min^{-1}$. The 25 mm diameter holding tubes were used since higher velocities and shear stress could be obtained. Fifth generation yeast was used. Samples were taken at

positions two (after pump) and three (after holding tubes). The flow conditions of the trial are summarised in Table 3.4.

Table 3.4. Operating conditions for brewery high flow rate trials.

Yeast/Gen. Number	Flow Rate ($kg.min^{-1}$)	Reynolds Number[1]	Tube Diam. (mm)	Linear Velocity ($m.s^{-1}$)
SAB1 5th Gen	187.1	3568	25	6.0
SAB1 5th Gen	178.1	3396	25	5.7
SAB1 5th Gen	67.5	1287	25	2.2

3.3.2.1 Recirculation

Two recirculation trials (one lasting 2 hours and the second lasting 6 hours) were conducted by first filling the holding tank with yeast slurry from the bottom of the fermentation vessel. The yeast was then circulated through the 25 mm holding tubes at a flow rate of 70 $l.min^{-1}$ using a NDE lobe pump with sampling taken at position 2 (after the pump) as indicated in Figure 3.11. The flow conditions and sampling times are summarised in Table 3.5. After the six hour trial, one of the butterfly valves on the rig was throttled to the 45° position and recirculation continued for another 30 minutes to quantify the effect of a flow constriction. In the first trial 500 litres of a second generation yeast was used while 400 litres of a seventh generation yeast was used in the second trial.

Table 3.5. Recirculation trials.

Yeast/Gen. Number	Recirculation Time (h)	Flow Rate ($kg.min^{-1}$)	Temp. (°C)	Sampling Times (min)	Tube diameter (mm)
SAB1 2nd Gen	2	74.4	16 – 20	15, 45, 75, 90, 110, 130	25
SAB1 7th Gen	6	74.3	15 – 23	0, 50, 110, 170, 230, 330	25

3.3.2.2 Removal of spent yeast from a fermentation vessel

The aim of this trial was to determine the variability of yeast quality in the fermentation cone. This information was used to identify suitable sampling times for the online trials. The Bredal SP/40 hose pump was operated at a flow rate of 60 $kg.min^{-1}$ with flow through the 65 mm diameter piping to the

[1] Reynolds numbers calculated according to method described in Section 7.2.1

spent yeast cellar. Samples were taken every hour at sampling point 2 (after the pump) for the six hours that it took to remove the entire yeast batch.

3.3.2.3 Brewery online trials

The online sampling trials were conducted at SAB – Newlands brewery during the normal cropping procedures on yeast batches which were destined for reuse. The first online trial was performed on 4th generation SAB1 yeast. A flow rate of 65 kg.min^{-1} was used. Sampling commenced one hour after the start of cropping and lasted 45 minutes. During this time a total of 2950 kg of yeast was cropped. The starting time of sampling was chosen such that 3900 kg had already been cropped and sampling continued until 6850 kg had been cropped. Figure 3.12 illustrates the yeast handling circuit at the brewery and the sampling points available. Sequential samples were taken at points 1 (before the pump), 3 (before the chiller, approximately 90 m after the pump), 4 (after the chiller), 5 (a mixed sample from the yeast cropping vessel, 30 minutes after the end of cropping 10790 kg), 6 (from the yeast pitching vessel, 19 hours after the end of cropping and before acid washing) and 6 (30 minutes after the start of acid washing) in the first trial. The second trial was conducted on an 8th generation SAB5 yeast which was cropped at a rate of 26 kg.min^{-1}. Three sets of samples were collected at the sampling points along the pipework corresponding to the cropping of 800 to 1200 kg, 3500 to 3900 kg, and 4000 to 4400 kg yeast. The total amount cropped was 4650 kg. Samples were drawn at positions 1 (before the pump), 3 (before the chiller) and 4 (after the chiller). Two samples were taken from the yeast storage vessel, the first 30 minutes after the end of cropping and the second 90 minutes later.

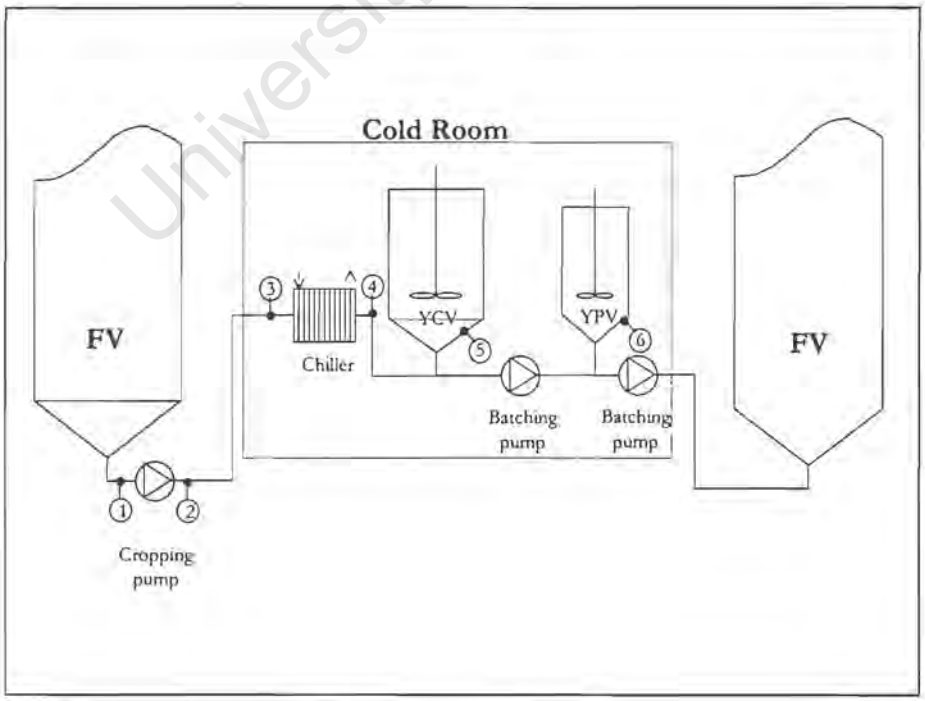

Figure 3.12. Schematic of brewery yeast handling circuit.

3.3.3 Pilot Plant Centrifugation

In this study two models of the Westphalia disc stack centrifuge were used, both supplied by GEA Process Technology SA (Pty) Ltd: Model SA 1-02-175 and model OSC 4-91-006. Their technical specifications are summarised in Table 3.6. The conditions under which the centrifuges were tested are summarised in Table 3.7 for the SA1 and Table 3.8 for the OSC4. As indicated in Table 3.7, a number of trials were conducted by using a gravity feed scheme whereby the feed hold-up vessel was placed above the centrifuge and the feed rate controlled by limiting the flow through a valve. The trials on model SA1 where a pump was used were conducted using a Watson Marlow 501S peristaltic pump. The trials with the OSC4 model centrifuge were all performed using a feed pump set-up as illustrated in Figure 3.13 with positive displacement type pumps.

Table 3.6 Technical specifications of the Westphalia disc stack centrifuges.

Details	SA 1-02-175 (SA 1)	OSC 4-91-006 (OSC 4)
Bowl volume (l)	0.9	1.5
Solids hold-up volume (l)	0.25	0.9
Rotational Speed (rpm)	4 000, 6875 & 9 800	9 000
Number of discs [n]	23	69
Disc inner radius (m)	0.0374	0.06
Disc outer radius (m)	0.0861	0.124
Disc spacing (mm)	0.5	0.5
Half included disc angle [θ]	38 °	38 °
Σ (m^2)	618, 1 826 & 3 862	28 315

Table 3.7. Experimental conditions used in centrifuge trial using SA 1-02-175 and strain SAB1.

Trial	Yeast Used	Yeast Gen. #	Feed Conc. (vol. %)	Mode and Rate of Feed ($l.h^{-1}$)	Rotation Speed (rpm)
1	Cropped	1	7.4 – 29.3	Pumped @ 7.2	10 000
2	Cropped	4	2.2-7.3	Gravity @ 25.2-30.0	10 000
3	Deflocculated	3	2.4-6.7	Gravity @ 25.2-30.0	10 000
4	Cropped	4	20	Gravity @ 21.6	4 000, 6 875, 10 000
5	Budding (6 h)	7	2.0	Gravity @ 24.0	10 000
6	Growing (40 h)	5	2.2	Gravity @ 32.4	10 000
7	Cropped	5	29.6	Pumped @ 9.6	10 000

Table 3.8. Experimental conditions used in centrifuge trial using OSC 4-91-006 and strain SAB5.

Trial	Yeast Used	Yeast Gen. #	Feed Conc. (vol. %)	Feed Rate ($l.h^{-1}$)	Residence Time (min)
1	Cropped	1	1.1 – 3.2	570	1.5 – 12
2	Cropped	7	0.6 – 1.7	950	1.5 – 9
3	Cropped	5	0.5 – 1.6	570, 950 & 1470	1.5 – 3
4	Cropped	5	0.8 – 2.5	570, 950 & 1470	1.5 – 3
5	Cropped	5	1.8 – 4.8	570 & 1050	1.5 – 5
6	Cropped	5	1.0 – 2.2	570	1.5 – 6

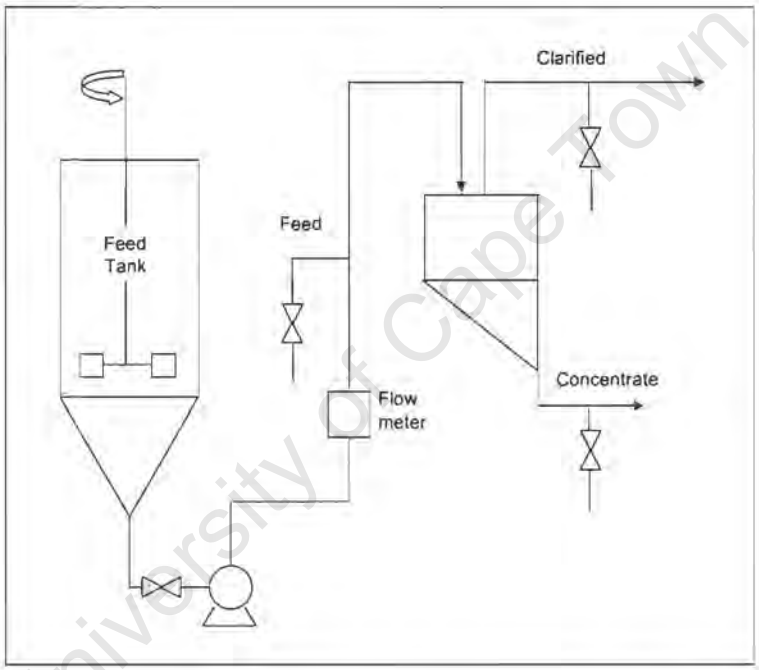

Figure 3.13. Schematic of pilot scale centrifuge rig for centrifuge model OSC4.

3.4 Data Analysis Methods

The data obtained from the zeta potential and XPS measurements needs to be analysed to assist with their interpretation.

3.4.1 Charge Group Analysis From Zeta Potentials

Using a two dimensional site dissociation model of the electrical double layer at the outer cell wall-solution interface, one can develop an analysis of the number and proportion of chargeable surface groups from the electrokinetic data. This method was first used by Bowen *et al.* (1992) who studied

the electrokinetic properties of *S. cerevisiae* during fermentation. The number and ratio of carboxyl to phosphate groups as well as the number of amine groups were determined by this method. Bowen *et al.* (1992) interpreted their data according to the second ionisation of phosphate at pH 6.2. Due to the structure of phosphomannan reviewed in the literature, the first ionisation of phosphate at pH 2.2 is a better estimate of phosphate content at the surface. Bowen *et al.* (1992) were not able to detect this first ionisation as they only made measurements above pH 3.25. The analysis used in this study assigns the jump in charge occurring at pH 2.2 to phosphate and that at pH 4.5 to carboxyl.

The major charge forming groups at the surface of yeast cells are phosphate arising from the mannan component, and carboxyl and amine groups occurring in the protein fraction of the cell wall. Based on the assumption that these are the chargeable groups the following equilibria can be used to explain the charge – pH profile of the cells:

$$pK_1 = 2.2 \qquad H_3PO_4 \overset{K1}{\longleftrightarrow} H_2PO_4^- + H^+$$

$$pK_2 = 7.2 \qquad H_2PO_4^- \overset{K2}{\longleftrightarrow} HPO_4^{2-} + H^+$$

$$pK_3 = 12.4 \qquad HPO_4^{2-} \overset{K3}{\longleftrightarrow} PO_4^{3-} + H^+$$

$$pK_4 = 4.4 \qquad RCOOH \overset{K4}{\longleftrightarrow} RCOO^- + H^+$$

$$pK_5 = 11.0 \qquad RNH_3^+ \overset{K5}{\longleftrightarrow} RNH_2 + H^+$$

The three ionisation pHs for phosphate are the experimentally determined values for phosphoric acid (Ebbing and Wrighton, 1990). The ionisation pH for carboxyl and amine are the mean values for the acidic (aspartic and glutamic acid) and basic (lysine and arginine) amino acids (Stryer, 1988). Due to the local environment in which the groups are found within the cell wall, these ionisation pH values can vary. Since the zeta potential measurements were all made at values below pH 8, all the amine groups can be assumed to be in the positive (+) charge state.

The two dimensional site dissociation model couples the Gouy – Chapman model of the electrical double layer with the assumed point charges occurring at the solid surface. Equating the surface charge density to the space charge in the diffuse part of the double layer (using the Poisson – Boltzmann distribution), one derives for an aqueous buffer at 25 °C in a 1:1 electrolyte, the expression for surface charge density in Equation 3.2.(See Appendix C.1 for its derivation):

$$\sigma_d = 0.117\, c^{1/2} \sinh(19.45\,\Psi_d) \qquad (3.2)$$

where c = electrolyte concentration (mole.dm^{-3})

Ψ_d = potential at plane of shear (V)

σ_d = charge density at shear plane (Coulombs.m^{-2})

Between pH 2 and 8, the charge forming and charged groups are then taken as R_2HPO_4, $R_2PO_4^-$, RCOOH, $RCOO^-$ and RNH_3^+ with the equilibrium equations governing the charge profile given in Table 3.9.

Table 3.9. Equilibrium relations governing surface charge – pH profile of yeast.

$R_2HPO_4 \leftrightarrow R_2PO_4^- + H^+$	$pK_1 \approx 2$
$RCOOH \leftrightarrow RCOO^- + H^+$	$pK_2 \approx 4$
$RNH_3^+ \leftrightarrow RNH_2 + H^+$	$pK_3 \approx 11$

The total number of chargeable groups (N_S) is then equal to the sum of the total number of phosphate (N_P), carboxyl (N_C) and amine (N_N) groups (Equation 3.3).

$$N_S = N_C + N_P + N_N \tag{3.3}$$

In each case the total number of ionisable groups of each type is equal to the sum of the charged and neutral groups of that type as indicated in Equation set 3.4.

$$\begin{aligned} N_C &= N_{RCOOH} + N_{RCOO^-} \\ N_P &= N_{R_2HPO_4} + N_{R_2PO_4^-} \\ N_N &= N_{RNH^+} \end{aligned} \tag{3.4}$$

Based upon a surface containing the above groups, the surface charge density is given by Equation 3.5 which can be expressed as Equation 3.6 by incorporating the equilibrium ionisation expressions as derived in Appendix C.2.

$$-\sigma_0 = e\left[R_2PO_4^-\right] + e\left[RCOO^-\right] - e\left[RNH_3^+\right] \tag{3.5}$$

$$-\sigma_0 = eN_S\left[\left(\frac{1}{1+1/q+r/q}\right)\left(\frac{1}{1+[H_S^+]/K_1}\right)+\left(\frac{1}{1+q+r}\right)\left(\frac{1}{1+[H_S^+]/K_2}\right)-\left(\frac{r}{1+q+r}\right)\right] \quad (3.6)$$

where e = charge on an electron = 1.6028×10^{-19} C

$r = N_N/N_C$

$q = N_P/N_C$

$[H_S^+]$ = surface hydrogen ion concentration = $[H_b^+]\exp(\varepsilon\psi_0/k_BT)$

$[H_b^+]$ = bulk hydrogen ion concentration

k_B = Boltzmann constant ($J.K^{-1}$)

The two expressions (Equations 3.2 and 3.6) for the surface charge density can be equated if one assumes that the charge density at the plane of shear equals that on the cell surface and solves for the unknowns (N_S and q) with a knowledge of the values of K_1, K_2 and r. r is taken to be 0.63 based on the amino acid composition of the typical surface proteins found in *S. cerevisiae* by Amri *et al.* (1982).

The solution method to determine N_s and q used Statistica for Windows, version 5.1 distributed by StatSoft, Inc. Using the package, first estimates were obtained for the two pK values at approximately 2.2 and 4.5 as well as estimates for N_s and q for each different yeast strain and experimental data set. Obtaining values for pK_1 and pK_2 were needed because slight differences in the local environments occurring at the surfaces of the yeast cause differences in the two values of pK. With the estimated values, their weighted average was calculated and used to resolve each individual set of zeta potential series and obtain values and confidences of N_s and q. The procedure is described in more detail in Appendix C.3.

3.4.2 Major Compound Analysis From XPS

X-Ray Photoelectron Spectroscopy provides a tool for analysing the outer surface of an object. It provides both the bulk chemical composition as well as bonding information of the elements by detecting small shifts in binding energies about the mean for the pure element. Because bond shifts are dependent on the type of bond and the nature of the sample (roughness, chargeability, etc.), the position of the peaks produced by the true bonds first need to be identified. Thereafter various sensibility tests can be conducted to determine the reliability of the data obtained from the various peak decompositions. With the verified bond concentration data the compounds present can be calculated by knowing their bond composition.

3.4.2.1 Peak position and bond attributions

Rouxhet *et al.*(1994), using a SSI X-probe SSX-100/206 spectrophotometer, analysed peptides and glucose to determine the peak positions and assign the bonds attributable for the peak decompositions components. From their data bonds have been assigned to the peak decompositions observed in this study. Figure 3.14 is the wide scan of the surface of a yeast sample showing the major elements, carbon (C_{1s}), nitrogen (N_{1s}) and oxygen (O_{1s}) located at 286, 400 and 544 eV respectively.

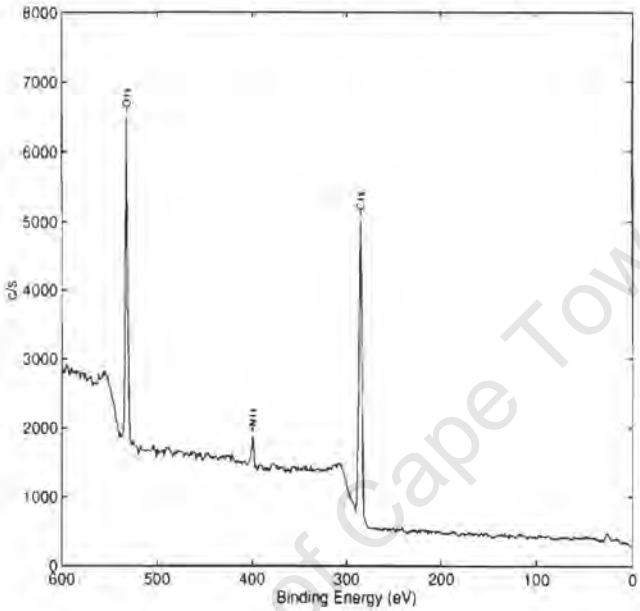

Figure 3.14. XPS wide scan of yeast surface indicating elemental composition (aerobically propagated SAB1).

Zooming in on these peaks of interest the narrow scans were performed. Figure 3.15 depicts the narrow scan on C_{1s} peak in which the peak decompositions are indicated. The decomposition indicates that it is composed of three peaks. The first at 284.8 eV (C-(C,H)) results from carbon making only bonds to carbon and hydrogen and is hydrocarbon in nature. The contribution at 286.3 eV is due to carbon bound either to oxygen or to nitrogen (C-(O,N)) including alcohol, ether, amine and amide groups. At 288.0 eV there is another contribution from carbon making either a double bond to oxygen or two single bonds to oxygen atoms (C=O), found in hemiacetal, acetal, amide carboxylate or carbonyl groups. An additional weak contribution which Rouxhet found at 289.0 eV was attributed to carboxyl (O=C-OH) was not resolved in this study as a separate peak but was included as a broadening of the contribution at 288.0 eV.

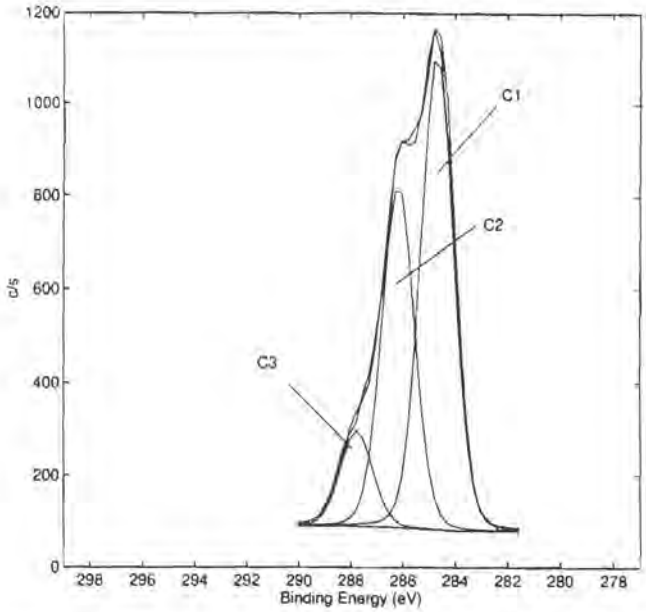

Figure 3.15. XPS narrow scan of carbon (C_{1s}) peak with decomposition shown (aerobically propagated SAB1).

The narrow scan on O_{1s} is presented in Figure 3.16 showing that two sub-peaks are responsible for the peak. The first component at 531.3 eV is indicated as oxygen making either a double bond to oxygen or two single bonds to oxygen (O=C) and attributed to carboxylic acid, carboxylate, ester, carboxyl or amide groups. The second component at 532.6 eV is attributed to alcohol (C-OH) which occurs in hemiacetal, acetal and a contribution from the hydroxyl group of carboxylic acid expected near 533.4 eV.

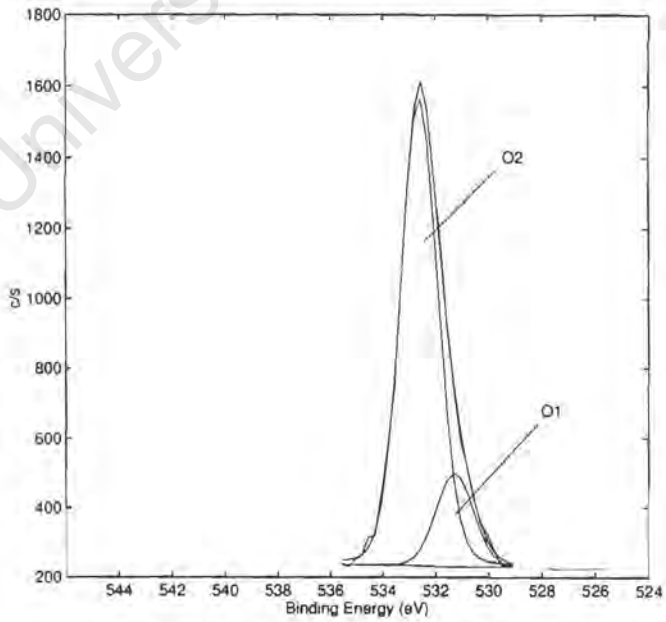

Figure 3.16. XPS narrow scan of oxygen (O_{1s}) peak with decomposition shown (aerobically propagated SAB1).

3.4.2.2 Reliability of peak decomposition

In addition to assigning functionality to the peak decompositions, Rouxhet *et al.* (1994) also recorded the full width half maximum (FWHM) statistic for each of the contributing peaks forming the composite peaks. This was done for model compounds of amide and glucose. For these they observed that the sub-peaks forming the carbon C_{1s} peak had FWHM values of 1.39 with standard deviation of 0.07 and for the oxygen O_{1s} peaks a value of 1.66 with standard deviation of 0.11. The FWHM statistic is an indication of peak broadening due to surface heterogeneity on the chemical bond level, as well as a broadening due to surface charging and surface roughness. The closer the measured FWHM values for the micro organism is to those of the model compounds, the better the attributed bonds are to the real bonds found in the micro-organisms. They found FWHM values for C_{1s} and O_{1s} for a range of micro organisms of 1.35 – 1.60 eV and 1.70 eV respectively. These were treated as being similar to the model compounds and as such were regarded as an indicator of the reliability of the bonds assigned to the various decomposed sub peaks. In this study the values obtained are 1.4 - 1.5 and 1.7 eV. This too is within the ranges reported and thus the peak decompositions obtained can be treated as reliable and reflecting the true bond structures on the yeast surface.

The standard deviations found by Rouxhet *et al.* (1995) for the bond concentrations of a bottom fermenting yeast strain analysed by independent operators for three identical cultures each analysed independently showed low variability (Table 3.10). Due to the similarity of the yeast strains and the data of this study to that of Rouxhet *et al.* (1995), their standard deviations have been used as indicators for the variability of the bond data to determine confidence intervals for atomic, functional group and molecular concentrations.

Table 3.10. Surface composition of yeast strain MUCL 28285, Rouxhet *et al.* (1995).

Element Component	Average	Standard Deviation
Total C	**67.1**	**2.1**
C-(C,H)	25.6	1.8
C-(O,N)	32.4	1.2
C=O	7.9	0.5
O=C-OH	1.3	0.2
Total O	**31.5**	**2.1**
C-OH	29.2	1.4
O=C	2.3	1.0
Total N	**1.2**	**0.1**
N-C	1.2	0.1

To further test the reliability and consistency of the data a balance based on independently measured bond concentrations can be used as a comparison. The first is that the sum of the total atomic concentration ratios of oxygen and nitrogen with respect to carbon (O/C + N/C) should correspond to the fraction of carbon bound to oxygen or nitrogen ((C-(O,N))/C) obtained from the carbon peak decomposition data. If there is more ((C-(O,N))/C) then it would indicate appreciable concentrations of ether and acetal functions. Conversely if the amount of (O/C + N/C) is higher then this would indicate higher concentrations of carboxyl groups at the surface. The data for this test is presented in Figure 3.17 which indicates the close similarity of the data to the parity line. The scatter of the data about the line is an indicator of the variability of the analysis technique.

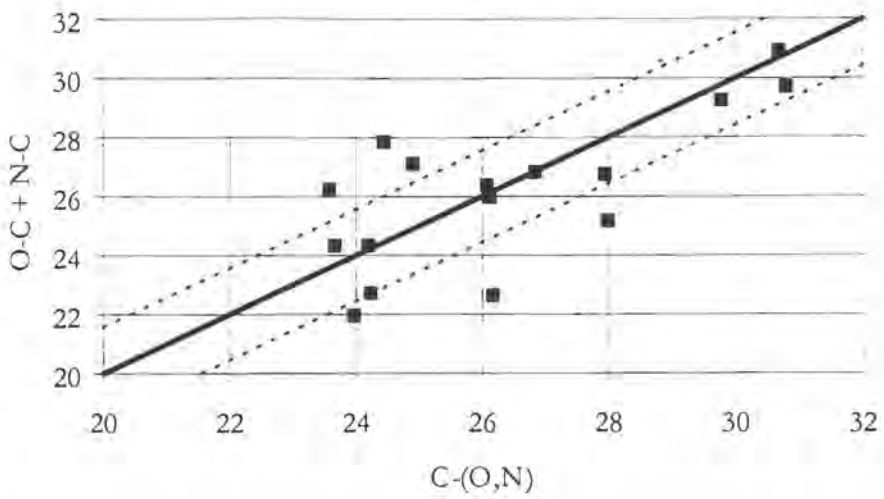

Figure 3.17. XPS data consistency test: total atomic concentrations vs. carbon peak decomposition with lines of standard deviation from Table 3.10.

Taking the chemical and bond composition from XPS results, the molecular composition can be determined if some hypotheses are made about which compounds make up the surface. Using this approach as outlined by Rouxhet *et al.* (1994), the yeast surface can be thought of as consisting of a protein(Pr), polysaccharide(PS) and lipid(Li) component. The composition of each constituent being made up of the atomic and bond fractions indicated in Table 3.11.

Table 3.11. Chemical composition of model constituents at yeast surface.

Model constituent	Atomic Concentration Ratio					Carbon concentration (mmol.g^{-1})
	O/C	N/C	(C-(C,H))/C	(C-(O,N))/C	(C=O)/C	
Protein[a]	0.325	0.279	0.428	0.293	0.279	43.5
Protein[b]	0.330	0.270	0.400	0.320	0.280	42.4
Protein[c†]	0.320	0.272	0.400	0.320	0.280	42.1
Hydrocarbon	0.000	0.000	1.000	0.000	0.000	71.4
Glucan	0.833	0.000	0.000	0.833	0.167	37.0
Lipid†	0.111	0.000	0.889	0.055	0.056	63.7
Mannan†	0.833	0.000	0.000	0.833	0.167	37.0

a Data computed from the amino acid analysis of the major outer membrane protein of a *Pseudomonal fluorescens* strain, Rouxhet *et al.* (1994).

b Data computed from the amino acid composition of different fungal wall proteins, Rouxhet *et al.* (1994).

c Values calculated from the typical wall protein composition of *Saccharomyces cerevisiae*, Amri *et al.* (1982).

† Data used in this study to calculate the molecular composition of yeast cell wall surface.

Using the total atomic concentration ratios, a set of equations (3.7) can be written to describe the surface compound concentrations. This is done by recognising that the total oxygen to carbon and oxygen to nitrogen ratio observed is equal to the sum of the oxygen to carbon or oxygen to nitrogen ratio of each model compound multiplied by the fraction of total carbon appearing in the form of each compound. The balance equation makes up the third equation.

$$\begin{aligned}\left(O/C\right)_{obs} &= \left(O/C\right)_{Pr}\left(C_{Pr}/C_t\right) + \left(O/C\right)_{PS}\left(C_{PS}/C_t\right) \\ \left(N/C\right)_{obs} &= \left(N/C\right)_{Pr}\left(N_{Pr}/C\right) \\ 1 &= \left(C_{Pr}/C_t\right) + \left(C_{PS}/C_t\right) + \left(C_{Li}/C_t\right)\end{aligned} \tag{3.7}$$

This equation set can be solved to provide the carbon ratio associated with each model compound (C_X/C_t). The weight ratio of the model compound to the total carbon weight can then be calculated by dividing the carbon ratio by the carbon concentration of the compound. Finally the weight fraction of each component can be obtained by dividing each carbon weight ratio by the sum of the ratios.

Another set of equations (3.8) can be used to find the concentration of model compounds by using the decomposition bond concentrations of the carbon peak. In a similar method as equation set one above the following equations can be written and solved to obtain the molecular composition:

$$\begin{aligned}\left(\underline{C}=O/C\right) &= \left(\underline{C}=O/C\right)\left(C_{Pr}/C_t\right) + \left(\underline{C}=O/C\right)\left(C_{PS}/C_t\right) \\ \left(\underline{C}-(O,N)/C\right) &= \left(\underline{C}-(O,N)/C\right)\left(C_{Pr}/C_t\right) + \left(\underline{C}-(O,N)/C\right)\left(C_{PS}/C_t\right) \\ \left(\underline{C}-(C,H)/C\right) &= \left(\underline{C}-(C,H)/C\right)\left(C_{Pr}/C_t\right) + \left(\underline{C}-(C,H)/C\right)\left(C_{PS}/C_t\right)\end{aligned} \tag{3.8}$$

The two sets of equations give slightly different results due to inaccuracies in peak attributions, peak decompositions and model compound compositions but they do provide similar trends in the data and so either equation set can be used to approximate surface molecule compositions for the yeast cells.

3.4.3 Fermentation Rate From Attenuation Profile

The rate of attenuation of a fermentation can be used as an indicator of the general yeast quality in terms of metabolic activity. To quantify differences in this rate, an appropriate equation is required to describe the substrate utilisation profile to obtain a rate constant. Basson (1996) used an exponential decay function (Equation 3.9) to model the gravity profile across the steepest portion of the density profile. This was found to be a suitable model but it failed to predict the extended time period of the fermentation. The exponential model overpredicts the density decrease as can be seen from Figure 3.18.

$$\text{Density} = A \exp^{-\beta(t-t_0)} \tag{3.9}$$

where A = preexponential constant

β = exponential constant (h^{-1})

t = time (h)

t_0 = time at start of exponential phase (h)

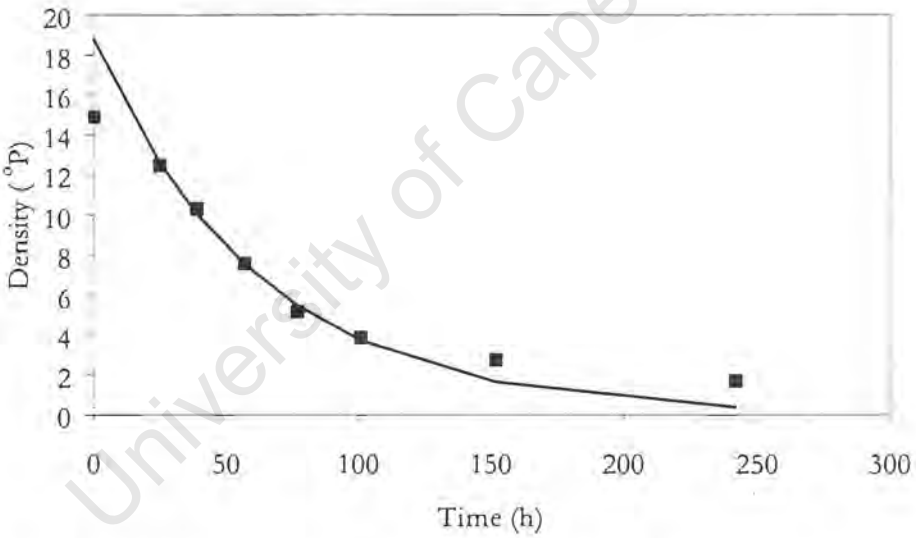

Figure 3.18. Fit of exponential model to typical attenuation profile.

The logistic equation predicts the exponential and stationary phases of biomass growth for batch fermentation systems. In integrated form the logistic equation can be written as:

$$X = \frac{X_o e^{kt}}{1 - \beta X_o \left(1 - e^{kt}\right)} \tag{3.10}$$

where: X = cell mass concentration ($g.l^{-1}$)

X_o = initial cell concentration ($g.l^{-1}$)

$\beta = 1/X_\infty$ (g^{-1})

k = rate constant (h^{-1})

The logistic equation (Equation 3.10) is routinely used to describe the sigmoidal shape of the biomass profile in batch microbial processes. It is based on the decreasing growth rate as the biomass concentration approaches a maximum value (X_∞). The substrate utilisation curve can be viewed as an inverted biomass growth curve and as such is amenable to fitting to the logistic equation.

To do this the gravity profile must be converted into a biomass concentration by use of the apparent yield coefficient i.e. aerobic growth of biomass produced to substrate consumed. In this study, the wet weight yield values provided in Appendix A.2 were used to predict biomass during fermentation as the initial biomass concentration used to pitch the fermentations is always known. The assumptions used here is that the water content of the yeast remains constant throughout the fermentation and that the yield coefficient remains the same throughout fermentation. While the yield coefficient decreases from an initial high value during aerobic growth to a lower value corresponding to anaerobic growth, the use of the overall yield coefficient is justified in this application as the logistic equation is not being used to predict the biomass concentration directly but rather as an intermediate to predict the attenuation profile. The attenuation profile are made up of a substrate utilisation component and an ethanol production component, both serve to decrease the overall wort density. In brewing situations, it is this combined attenuation profile which is used as in indicator of fermentation performance.

Using this approach, the theoretical biomass production can be calculated from the known decrease in wort density. The logistic equation can be fitted to the biomass curve. The only unknown parameter is the rate constant (k) as the value of beta is the inverse of the final theoretical biomass concentration. A typical table of data describing the fit of the logistic equation to the attenuation profile is provided in Table 3.11. As the logistic equation does not account for a lag phase, the data can only be used to predict the data after the end of lag phase, usually after the first 24 hour period. In the example provided in the table, the initial biomass concentration was 0.706 $g.l^{-1}$. Since the lag phase is not predicted by the modelling equation, the start of fermentation was taken to be at 25

hours which corresponds to a higher initial biomass concentration (X_o) of 1.706 $g.l^{-1}$. This is used together with a wet weight biomass yield coefficient of 0.041 $g.g^{-1}$ and the theoretical final biomass concentration of 6.12 $g.l^{-1}$ corresponding to a β value of 0.1747 $l.g^{-1}$. Using these values of the known parameters, the rate constant (k) was obtained by minimising the least square error between the attenuation data and that predicted by the logistic equation.

Table 3.12. Typical table used to calculate the logistic rate constant.

k =	0.0456
β =	0.1747
$Y_{x/s}$=	0.0410
X_o=	1.706

TIME	1	S ($g.l^{-1}$)	X ($g.l^{-1}$)	FIT	curve	ERROR
0	14.91	149.1	0.706	0.685	14.96	
25	12.47	124.7	1.706	1.706	12.47	0.000
39	10.34	103.4	2.579	2.550	10.41	0.071
57	7.59	75.9	3.707	3.698	7.61	0.022
77	5.19	51.9	4.691	4.691	5.19	0.000
101	3.88	38.8	5.228	5.331	3.63	0.251
152	2.77	27.7	5.683	5.683	2.77	0.000
242	1.70	17.0	6.122	5.723	2.67	0.972
					Total error:	1.315

The accuracy with which the above procedure is used to describe the attenuation profile of a fermentation can be assessed by comparing the logistic fit to the data (Figure 3.19) to that of the exponential fit previously presented in Figure 3.18. As can be seen, the logistic equation better represents the entire fermentation profile.

In order to test the reproducibility of fermentations, five identical fermentations were conducted and the attenuation rate constant (k) and β value, as well as the final gravity and pH of fermentation calculated. This data is presented in Appendix B.8 with the coefficient of variance of the rate and beer quality indicators summarised in Table 3.12.

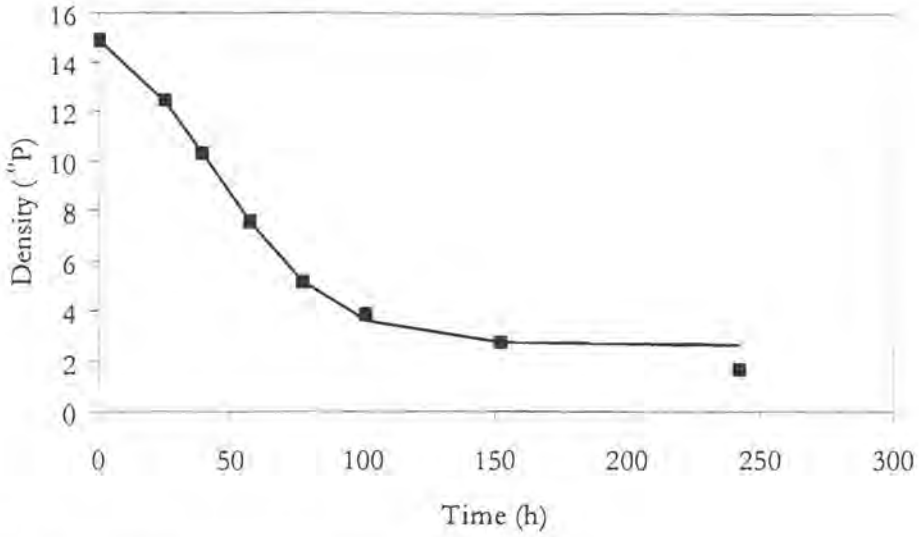

Figure 3.19. Fit of logistic model to typical fermentation data.

Table 3.13. Reproducibility of 500 ml fermentations.

Parameter	Coefficient of Variance (%)
Logistic rate (h^{-1})	4.7
Final density (°P)	5.5
pH	0.9
SO_2 (ppm)	15.2
Diacetyl (ppb)	15.2

Chapter 4: Brewers' Yeast Propagation

4.1 Introduction

The yeast cycle in breweries involves its propagation from laboratory size shake flasks to fermentation sized quantities (1 – 3 tons) via a predominantly aerobic route. Although this is an aerobic process, ethanol is also produced which during the propagation process represents an unwanted product and lowers the biomass production efficiency. The efficiency of sugar utilisation is therefore an important parameter during propagation. The aerobically propagated yeast is then added to aerated wort and transferred to vessels where fermentation begins. During fermentation an approximate three fold increase in biomass occurs during which time the oxygen is rapidly consumed and the cells produce ethanol in the resultant anaerobic environment. At the end of fermentation the yeast is removed, stored for reuse in subsequent fermentations up to between 8 and 20 times depending on the specific brewery, wort gravity and beer type. Each transfer of the yeast during its propagation and also between fermentations involves the mechanical pumping and handling of the yeast which exposes it to potentially damaging hydrodynamic stress. Since the handling of yeast occurs after periods of both aerobic and anaerobic conditions, the extent to which oxygen availability affects yeast has to be determined. The possibility exists that the two variants of yeast (aerobic and anaerobic) will have different handling resiliences which necessitates a better understanding of 'healthy' yeast in each of these forms.

In this chapter, the propagation of the four strains of yeast (SAB1, SAB1/96, SAB2 & SAB5) under conditions of aerobic and near anaerobic growth are compared in terms of the biomass production kinetics and biomass yield coefficient. During propagation, the surface properties of the cells (charge and hydrophobicity) were also monitored. Different strains of yeast have been shown to have different surface properties, chemical compositions and flocculence (Amory and Rouxhet, 1988;

Dengis *et al.*, 1995b). These parameters have also been shown to vary depending on the physiological state of the yeast (Bony *et al.*, 1998; Bowen & Cooke, 1989; Bowen *et al.*, 1992). On completion of propagation, indicated by the levelling off of cell concentration and stabilisation of the yeast surface, the yeast was analysed for flocculation potential, surface composition, surface charge and hydrophobicity. The links between measured yeast flocculation and surface charge and hydrophobicity are also investigated in terms of classical colloidal theory. Using the information obtained from XPS analysis, the fundamental links between charge, hydrophobicity and the chemical and molecular composition are further investigated.

4.2 Cell Growth Kinetics

Cell growth can be modelled by various structured and unstructured (e.g. Monod and logistic) kinetic expressions as well as being either segregated or unsegregated. When a cell population is heterogeneous in terms of cells having different physiological states (i.e. some cells in exponential phase while others in stationary phase), then a segregated model is required. If, however, the average cell approximation can be made where it is assumed that all the cells in a population are at the same physiological state, then an unsegregated model can be used to model the system. A structured model is one in which the cell is represented by multiple components and usually involves an analysis of the cell at the metabolic pathway level. Unstructured models are based on the assumption of balanced growth, where the cell can be represented by a single component. Using these classification systems, the true and complete description of a biological system is a segregated/structured one. Due to the high informational requirement needed to define such a system, simpler models are often used. The simplest models are unstructured/unsegregated models, often used to describe cell population growth, while other more complex models are used for unsteady growth kinetics and metabolic pathway analysis (Bailey & Ollis, 1986). Each of the different models have particular levels of usefulness in terms of the accuracy with which they predict the growth curve and the amount of data required to obtain acceptable model fits. The Monod equation (Equation 4.1) is an example of an unstructured model that describes balanced growth (unsegregated) as is usually observed in chemostats and other continuous type bioreactors. It has also been used successfully to model yeast growth in a fed-batch type environment (Reynders *et al.*, 1996; Pham *et al.*, 1998). The basic Monod model can also be adapted to include a maintenance energy or endogenous respiration term to account for substrate utilisation not resulting in biomass production (Equation 4.2). Other forms of unstructured/unsegregated models include the Tessier (Equation 4.3), Moser (Equation 4.4) and Contois (Equation 4.5) models.

$$\mu = \frac{\mu_{max} S}{K_s + S} \tag{4.1}$$

$$r_x = \frac{\mu_{max} SX}{K_s + S} - k_e X \tag{4.2}$$

$$\mu = \mu_{max}\left(1 - e^{-S/K_s}\right) \tag{4.3}$$

$$\mu = \mu_{max}\left(1 - K_s S^{-\lambda}\right)^{-1} \tag{4.4}$$

$$\mu = \mu_{max} \frac{S}{K_s X + S} \tag{4.5}$$

where: μ = Monod growth rate (h^{-1})

μ_{max} = maximum growth rate constant (h^{-1})

λ = constant in Moser Equation 4.4

k_e = death rate constant (h^{-1})

K_S = saturation constant ($g.l^{-1}$)

K_S = saturation constant proportional to cell concentration ($g_{substrate}$ / $g_{biomass}$) in Eqn. 4.5

r_x = specific biomass growth rate ($g.l^{-1}.h^{-1}$)

S = substrate concentration ($g.l^{-1}$)

X = biomass concentration ($g.l^{-1}$)

Balanced growth as described by the models above can be inhibited by medium constituents such as either substrate or product. Alcoholic fermentation is one such example which can be modelled using the specific growth rate model used by Aiba *et al.* (1968) (Equation 4.6).

$$\mu = \mu_{max} \frac{S}{K_i + S} \frac{K_p}{K_p + P} \tag{4.6}$$

where K_i = substrate saturation constant ($g.l^{-1}$)

K_p = product saturation constant ($g.l^{-1}$)

The models above are, however, unable to predict the maximum biomass population that is observed in real systems. For the situation of unbalanced growth, as is found in batch growth conditions, a segregated model is required. The most common of this type is the logistic equation which is an unstructured/segregated model, based on the exponential growth of cells and includes an inhibitory term to cell growth which is proportional to the square of the biomass concentration. Equation 4.7 is the logistic equation which is the integrated form of the Riccati equation (Equation 4.8). One interpretation of the inhibition term being proportional to the square of the biomass concentration is that a toxin is produced by the cell during normal growth. The rate of production of the toxin is proportional to the population growth rate and so based on the assumption that the initial cell

concentration is insignificant relative to the final cell concentration then the Riccati equation can be derived.

$$X = \frac{X_0 e^{kt}}{1 - \beta X_0 \left(1 - e^{kt}\right)} \tag{4.7}$$

$$\frac{dX}{dt} = kX(1 - \beta X) \tag{4.8}$$

where: $\beta = \frac{1}{X_\infty}$

k = logistic rate constant (h^{-1})

Although the logistic equation does predict the decline in growth rate usually observed towards the end of batch growth, it is unable to predict either the lag or death phases of the cell cycle. The logistic equation was chosen to model batch growth and fermentation progression because of its ability to model unbalanced growth. To minimise the possible lag phase, the following three general rules were applied (Bailey and Ollis, 1986):

1) An active inoculum of cells in the exponential growth phase was used.
2) The inoculation media was similar in composition to the full scale media.
3) An inoculation volume of 5 - 10 % of the total volume was used to avoid diffusional loss of compounds from within the cells.

The cell concentration profiles of the four strains are presented in Figure 4.1 for both aerobic and near anaerobic propagation. The data points illustrate experimental data while the lines are the logistic equation fit to the data. For all strains, the cell concentrations reach their plateau values at approximately the same time for both aerobic and anaerobic experiments.

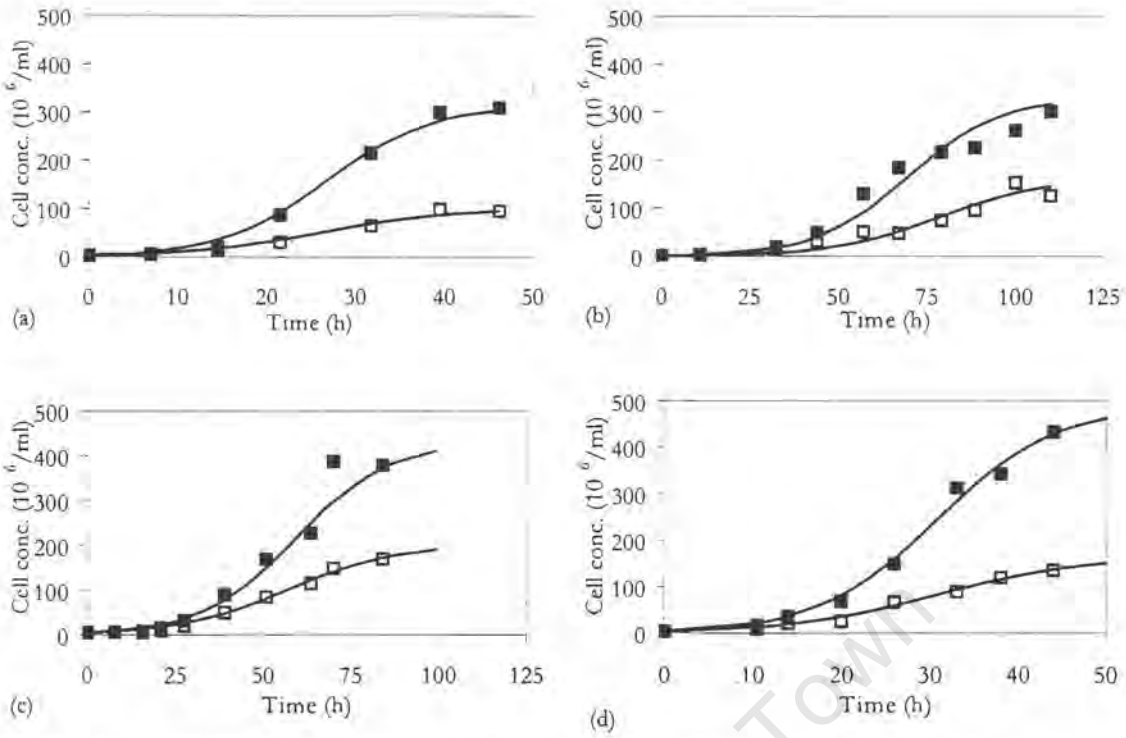

Figure 4.1. Cell growth profiles during aerobic and near anaerobic propagation.
(■ aerobic cell concentration, □ anaerobic cell concentration, — logistic fit, (a) SAB1, (b) SAB1/96, (c) SAB2, (d) SAB5)

The logistic rate constants determined (k value in Equation 4.7) are summarised in Table 4.1 as are the initial (X_o) and final ($1/\beta$) cell concentrations. The ratio of the rate constants ($k_{aerobic}/k_{anaerobic}$) given in Table 4.1 indicate that the aerobic biomass production rates are between 15 and 25 % higher than anaerobic growth rates while there is a two to three fold increase in final cell concentration under aerobic conditions. Krzystek and Ledakowicz (1998) calculated the theoretical biomass yield coefficient of *S. cerevisiae* under aerobic conditions to be three times higher than under anaerobic conditions at 0.913 and 0.305 C-mole(C-mole)$^{-1}$ respectively.

Table 4.1. Logistic constants for cell growth during propagation of yeast strains.

	X_o (10^6cells.ml^{-1})		k (h^{-1})			$1/\beta$ (10^6cells.ml^{-1})		
Strain	aerobic	anaerobic	aerobic	anaerobic	ratio	aerobic	anaerobic	ratio
SAB1	3.4	2.7	0.169	0.138	1.22	309	99	3.1
SAB1/96	1.6	0.9	0.076	0.066	1.15	331	164	2.0
SAB2	5.0	5.0	0.078	0.064	1.22	388	170	2.3
SAB5	4.9	4.1	0.149	0.119	1.25	440	150	2.9

4.3 Yield Coefficients

The growth kinetics of yeast during aerobic propagation can be quantified in one of two ways, either by the rate of biomass increase or by the rate of substrate utilisation, both of which are related through a biomass yield coefficient. Under anaerobic growth conditions, substrate is consumed by yeast cells to produce ethanol with minimal biomass growth. The effect of this is that the observable yield of biomass produced to substrate utilised is lowered. In the brewing industry, density reduction is commonly used as an indicator of substrate utilisation. The unit of density is °P which has basic units of $g_{extract}/100$ g of solution, where extract refers to the total sugars (fermentable and non-fermentable) which are extracted from the malt in the brewing process (SAB Analytical Methods Manual, 1995). These units are adequate for comparing and monitoring wort production as all of the fermentable sugars of glucose, maltose, maltotriose, fructose and the unfermentable sugars contribute nearly equally to the density of the media. However, during both fermentation and propagation, ethanol is produced. Both the ethanol production (with an SG of 0.792) and sugar consumption contribute to the reduction of the density during fermentation and propagation. Owing to the various factors affecting density change, in this study the biomass production was used in Section 4.2 to determine the propagation kinetics while the rate of fermentation in the later chapters was calculated using the rate of density decrease.

By defining the biomass yield coefficient ($Y_{X/(S+E)}$) in an appropriate manner, it can be used for comparing different propagation conditions and strains. The yield coefficient ($Y_{X/(S+E)}$) is defined as the ratio of biomass produced to the combined density reduction effects of sugar utilisation and ethanol production. This is therefore a 'lumped' parameter with contributions from the biomass produced, ethanol produced and sugars consumed.

The density profiles for the strain propagations under aerobic and near anaerobic conditions are presented in Figure 4.2. Noticeable is that in the anaerobic propagation condition of all strains, the density was still decreasing despite the tapering off of biomass production. This is due to the cells continuing to consume sugars to produce ethanol. In the cases of the three flocculent strains (SAB1, SAB1/96 and SAB5) depicted in Figure 4.2 (a, b & d), the aerobic propagation condition resulted in a more rapid decrease in wort density. The non-flocculent strain (SAB2), illustrated in Figure 4.2 (c), performs differently in that the anaerobic density decreases faster than the aerobic. This observation is combined with the observed biomass production curves in the yield coefficient analysis.

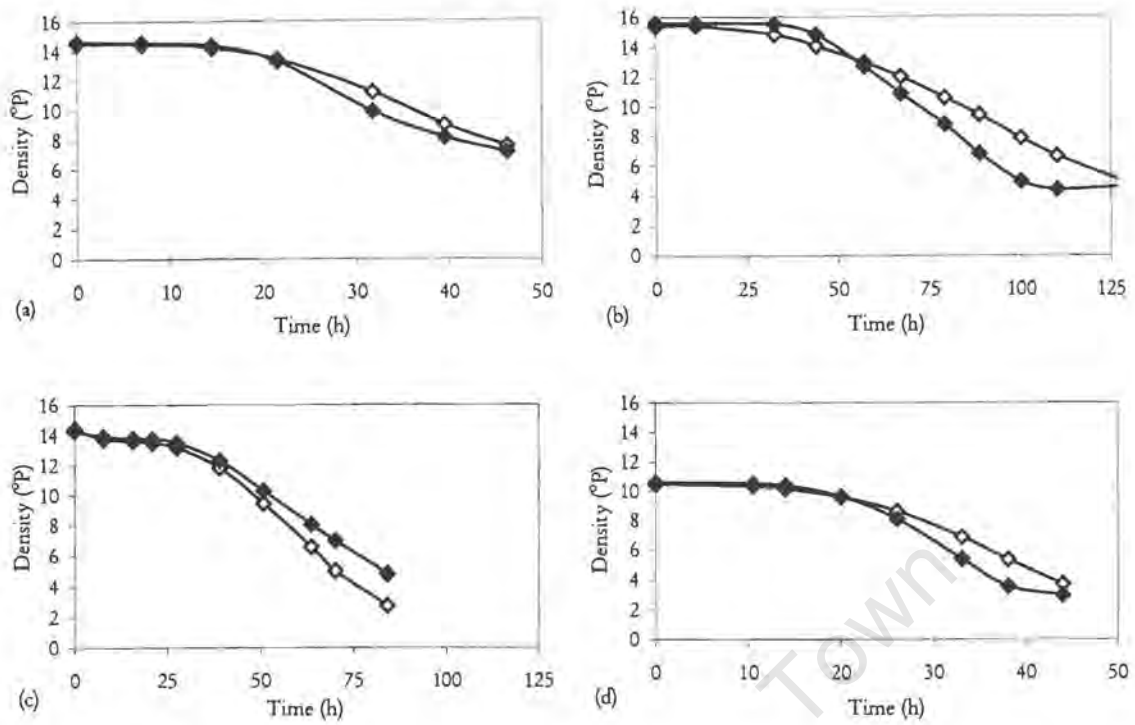

Figure 4.2. Density profiles for propagations under aerobic and near anaerobic conditions.
(♦ aerobic density, ◊ anaerobic density, (a) SA B1, (b) SA B1/96, (c) SA B2, (d)SA B5)

The instantaneous biomass yield coefficient, $Y_{X/(S+E)}$, can be calculated at any time during a propagation by finding the ratio of biomass produced to the decrease in density during a time interval. In the case of yeast propagation from a high sugar medium (wort), large quantities of ethanol are also produced because of the Crabtree effect which decreases the biomass yield. The Crabtree effect is observed when both aerobic and anaerobic metabolic pathways are active under conditions where oxygen is not limiting. This effect is triggered by high substrate concentration and is common among yeasts. Under aerobic conditions the yeast consumes sugars and produces both ethanol and biomass. Under anaerobic conditions, the yeast continues to consume sugars and produce ethanol but produces little or no biomass. When measuring the medium density, both sugar usage to produce biomass and ethanol, and the produced ethanol contribute to the drop in density, thus the need for defining the yield coefficient in this way. By calculating the instantaneous yield coefficient and cumulative coefficient, the overall yield coefficient can be seen to be smoothly approached. Figure 4.3 illustrates the manner in which the instantaneous and cumulative yield coefficients vary during propagation.

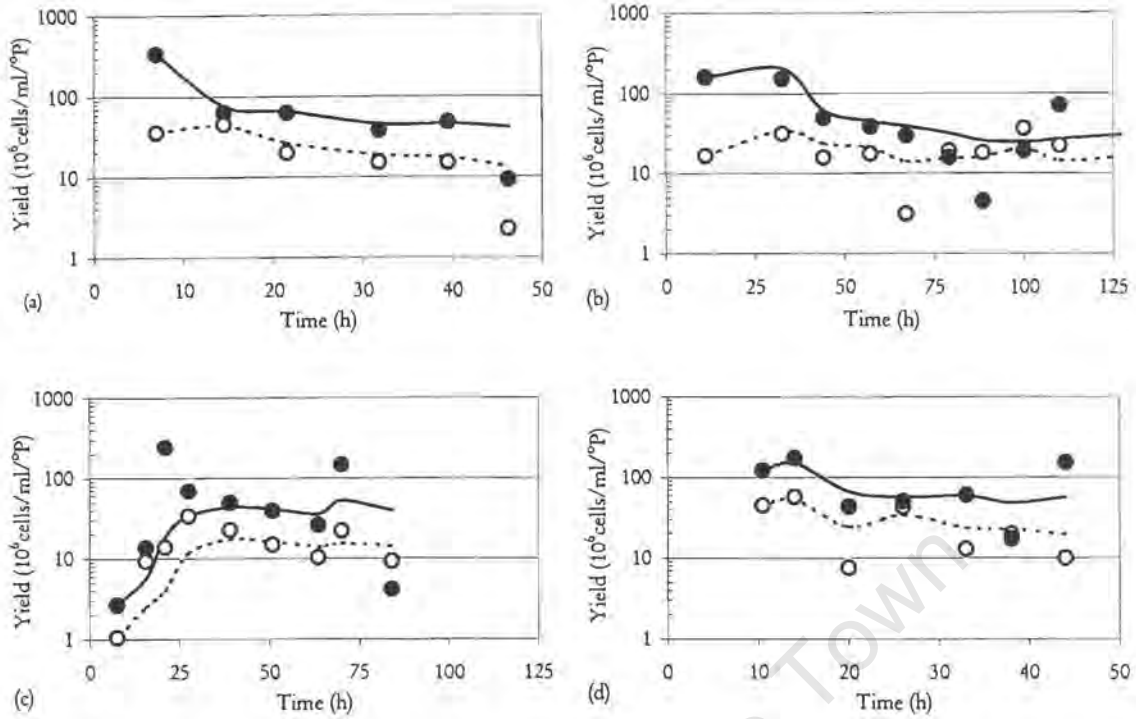

Figure 4.3. Biomass yield coefficients during propagation.

(● instantaneous aerobic yield, ○ instantaneous anaerobic yield, — cumulative aerobic yield, ---- cumulative anaerobic yield, (a)SAB1, (b)SAB1/96, (c)SAB2, (d)SAB5)

The three flocculent strains (Figure 4.3a, b, d) each have a similar shaped yield curve which is distinctly different to that of SAB2, the non-flocculent strain (Figure 4.3c). The biomass yield coefficient of the flocculent strains is initially high, decreasing with time to approach a final 'overall' yield coefficient. SAB2 in comparison has a low initial biomass yield which increases as the cells reach the mid-logarithmic phase of growth. The yield coefficient stabilises at this higher value. The overall yield coefficients calculated at the onset of stationary phase under aerobic and near anaerobic conditions are summarised in Table 4.2. For comparative purposes the ratio of final cell concentrations after aerobic and anaerobic propagation conditions are also included in Table 4.2.

Table 4.2. Biomass yield coefficients for yeast propagation under aerobic and anaerobic conditions.

Strain	Biomass yield coefficient, $Y_{X/(S+E)}$ (10^6 cells.ml^{-1} / °P)		Ratio of yields (aerobic/anaerobic)	Ratio of (1/β) (aerobic/anaerobic)
	Aerobic	Anaerobic		
SAB1	41	13	3.2	3.1
SAB1/96	30	16	1.9	2.0
SAB2	39	14	2.8	2.3
SAB5	56	20	2.8	2.9

Strains SAB1 and SAB5 have high (1/β) ratios on comparing aerobic to anaerobic growth (approx. 3) as a result of the cells having a poor ability to reproduce under anaerobic conditions. Strains SAB1/96 and SAB2 are more able to produce biomass under anaerobic conditions illustrated by lower (1/β) ratios (approx. 2). The aerobic to anaerobic yield ratio is numerically similar to the aerobic to anaerobic (1/β) ratio for strains SAB1, SAB1/96 and SAB5. The implication of this is that under both aerobic and anaerobic conditions, ethanol is produced from the consumed substrate with the same efficiency as can be seen from the numerical derivation below.

$$\frac{\left(Y_{X/(S+E)}\right)_{aerobic}}{\left(Y_{X/(S+E)}\right)_{anaerobic}} \approx \frac{\left(1/\beta\right)_{aerobic}}{\left(1/\beta\right)_{anaerobic}}$$

$$\frac{\left(\frac{X}{(S+E)}\right)_{aerobic}}{\left(\frac{X}{(S+E)}\right)_{anaerobic}} \frac{\left(1/\beta\right)_{anaerobic}}{\left(1/\beta\right)_{aerobic}} \approx 1$$

$$X_{aerobic} \approx \left(1/\beta\right)_{aerobic} \quad and \quad X_{anaerobic} \approx \left(1/\beta\right)_{anaerobic}$$

$$\therefore \frac{(S+E)_{anaerobic}}{(S+E)_{aerobic}} \approx 1$$

This result is supported by the results of (Schatzmann, 1975) who observed the ethanol yield during aerobic growth to be 85% of that under anaerobic growth. Krzystek and Ledakowicz (1998) measured similar ethanol yields under aerobic and anaerobic conditions for continuous fermentations at a value of 0.58 C-mole(C-mole)$^{-1}$. This further supports the observation in this study that ethanol is produced with approximately the same efficiency under both aerobic and anaerobic growth conditions. The non-flocculent strain, SAB2, has a high yield ratio and low (1/β) ratio which implies a preferred production of biomass to ethanol under aerobic conditions. This indicates an improved suitability to the brewing environment. A drawback with this strain is the longer propagation time compared to the other strains under similar temperature conditions.

4.4 Surface Properties during Propagation

Propagation is a batch process which means that the yeast population goes through five phases (lag, exponential, diauxic shift, post diauxic shift and stationary phase) although in practice only lag, exponential and stationary phases are observed in the production of yeast grown on high maltose wort. The yeast experiences different environmental conditions of substrate and product concentrations throughout the batch growth cycle. In addition, near anaerobic propagation has the added influence of a limited oxygen supply causing a switch from respiro-fermentative metabolism to complete fermentative metabolism. Observable changes that have been found to occur during the

life cycle of cells include morphological appearance (Carstens *et al.*, 1998), cell wall composition (Dufrêne and Rouxhet, 1996), metabolic activity (Bailey and Ollis, 1986) and degree of flocculation (Soares and Mota, 1996; Stratford and Carter, 1993). Changes to the cell surface properties (hydrophobicity, charge and composition) have been investigated in this study as a function of growth phase, oxygen availability and yeast strain.

4.4.1 Hydrophobicity

In Figure 4.4, the hydrophobicity index and cell concentration profile are given as a function of time for the batch propagation of strains SAB1, SAB1/96, SAB2 and SAB5. Both propagation conditions have similar levels of hydrophobicity in the early stages of the propagation owing to inoculation with yeast grown aerobically in MYPG. The hydrophobicity of aerobically grown yeast was observed to remain low (HI $\leq$ 5%) while the anaerobic growth condition showed an increase in hydrophobic index (2 $\leq$ HI $\leq$ 30) across the growth cycle.

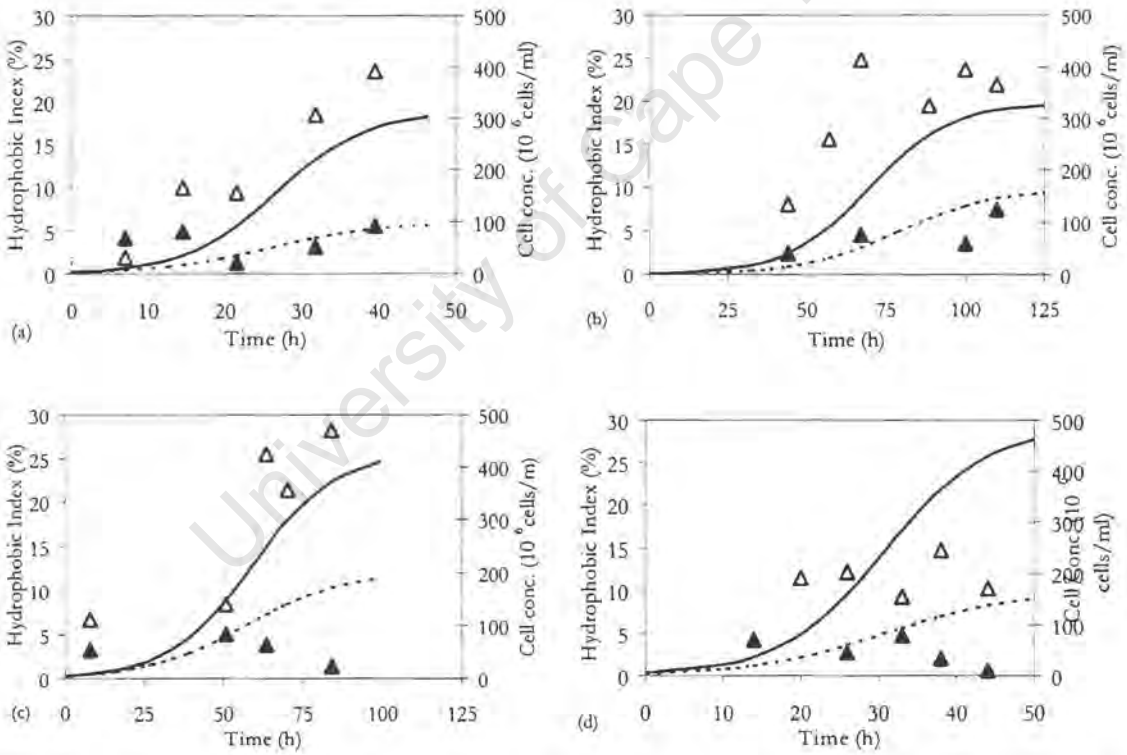

Figure 4.4. Generation of cell hydrophobicity during batch propagation under aerobic and anaerobic conditions.

(▲ aerobic hydrophobicity, Δ anaerobic hydrophobicity, — aerobic cell concentration, --- anaerobic cell concentration, (a) SAB1, (b) SAB1/96, (c) SAB2, (d) SAB5)

The consistency in hydrophobicity index throughout the cell cycle under aerobic conditions indicates little effect of growth media (MYPG vs. wort) on cell hydrophobicity. The extent to which oxygen is available appears to determine the hydrophobic nature of the cells. The SAB2 yeast propagation was used to inoculate a fermentation and the hydrophobicity index monitored to determine the effect of propagation conditions on yeast hydrophobicity in an anaerobic fermentation environment. These results are presented graphically in Figure 4.5. The hydrophobicity index at the start of fermentation is equivalent to the hydrophobicities at the end of their respective propagations. During the early part of the fermentations, the oxygen initially added was consumed by the cells. At the 31 hour point the anaerobically propagated yeast was less hydrophobic (HI = 13.8 %) than at the start of fermentation (HI = 28.2%). The aerobically propagated yeast showed no hydrophobic tendencies at this point. After this point in time, both fermentations were fully anaerobic and the yeast from both aerobic and anaerobic propagations showed an increase in hydrophobicity reaching similar final values at the end of fermentation (HI = 38.2 and 42.8 % respectively). This is further evidence that oxygen availability appears dominant in determining the extent of hydrophobicity of the cells.

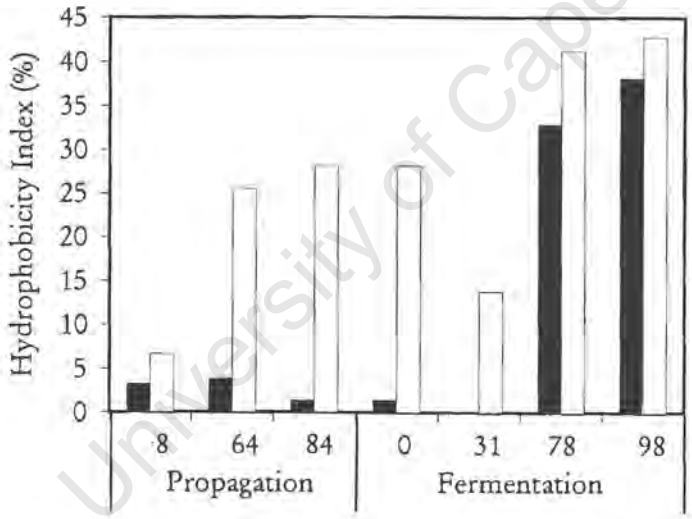

Figure 4.5. Hydrophobicity of SAB2 during aerobic and anaerobic propagation and subsequent fermentation.
(■ aerobic,□ anaerobic)

4.4.2 Surface Charge

The surface charge of many surfaces varies with the pH of the surrounding environment due to the presence of charge forming groups which ionise at distinct pH values. As detailed in Section 3.4.1, the zeta potential of yeast cells can be used to calculate actual surface charge based on knowledge of the ionic strength of the buffer in which the cells are suspended during zeta potential measurement.

Although the pH at the end of typical brewery fermentations is between 4 and 5, trends in zeta potential over a wider range of pH values from 2.1 to 6.7 were measured. This provides additional information on the chemical composition of the surfaces in terms of the concentration of the different charge forming groups present (Bowen *et al.*, 1992). Trends in the zeta potentials of yeast during batch propagation will first be discussed and then the conversion to surface composition will be presented.

4.4.2.1 Zeta Potential

The zeta potential of the aerobic and anaerobically grown yeasts in the stationary phase was found to differ by between 2 and 6 mV across the pH range 2.1 to 6.7. The aerobic cells were more negatively charged. This phenomenon, illustrated in Figure 4.6, was shown for all strains studied throughout the duration of the propagation cycle.

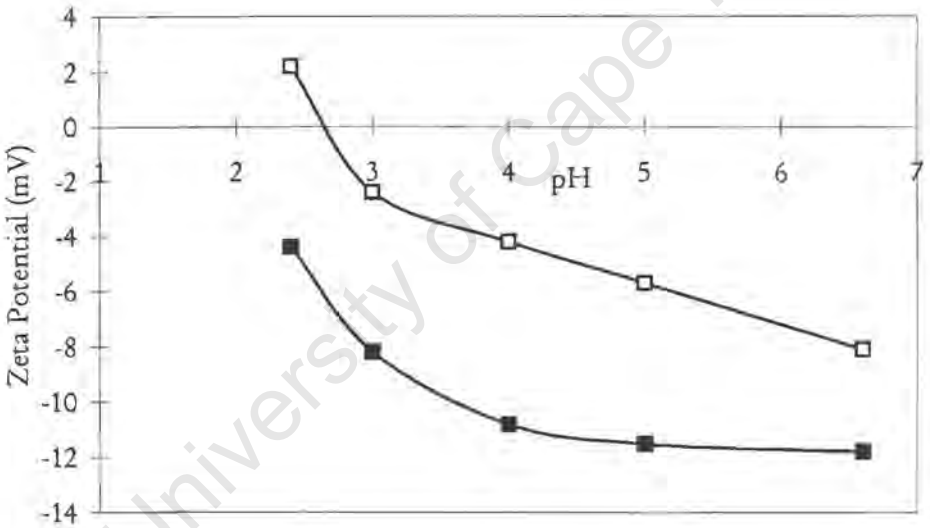

Figure 4.6. Comparison of aerobic and anaerobic zeta potential vs. pH profile for SAB2 at mid-exponential phase.

(■ aerobic cells, □ anaerobic cells)

During propagation, the zeta potential profiles changed according to the phase of growth of the cells. Figures 4.7, 4.8, 4.9 and 4.10 show this progression of zeta potential change for each of the four strains propagated under both aerobic and near anaerobic conditions. The profile changed most with time during the early stages of growth until the late exponential phase is reached. After this the zeta profile changes more slowly and settles into a fixed profile by the onset of stationary phase. The flocculent strains (Figures 4.7, 4.8 & 4.10) showed the greatest changes in zeta potential at the higher pH values around 5 – 7 while the non-flocculent strain, SAB2 (Figure 4.9), showed the greatest variability during growth at the lower pH range (pH 2). All cultures had iso-electric points (pI) below

pH 4.5 although they were generally only quantifiable during the early phase of growth with pI in stationary phase lying below pH 2. Where pI values for both growth conditions lay within the pH range studied, the anaerobic conditions yielded higher pI values. The non-flocculent strain, SAB2 showed the most change in zeta potential during propagation. Its pI shifted from 4.5 at the start of propagation to 2.5 in the stationary phase under anaerobic conditions and from 4.0 to less than 2.5 under aerobic conditions.

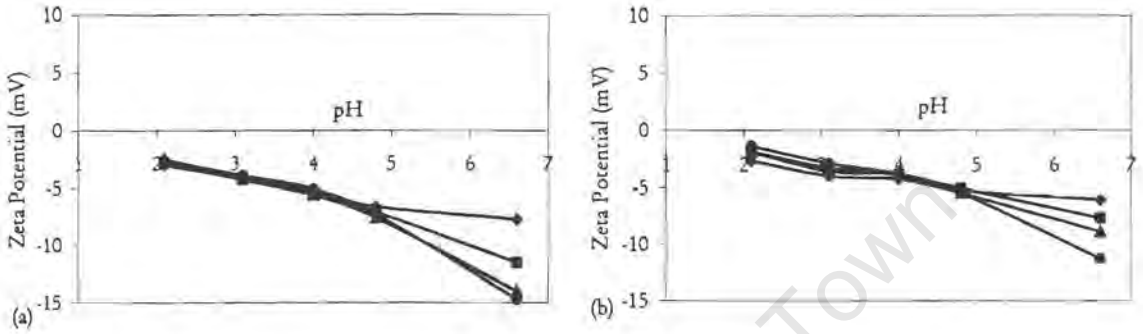

Figure 4.7. The zeta potential of SAB1 as a function of pH and time of propagation.
(♦ early exponential, ■ mid exponential, ▲ late exponential, ● stationary phase, (a) aerobic, (b) anaerobic)

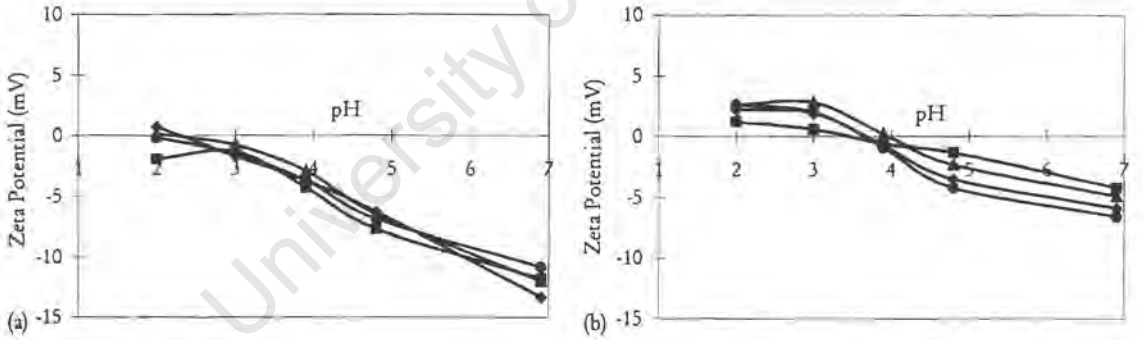

Figure 4.8. The zeta potential of SAB1/96 as a function of pH and time of propagation.
(♦ early exponential, ■ mid exponential, ▲ late exponential, ● stationary phase, (a) aerobic, (b) anaerobic)

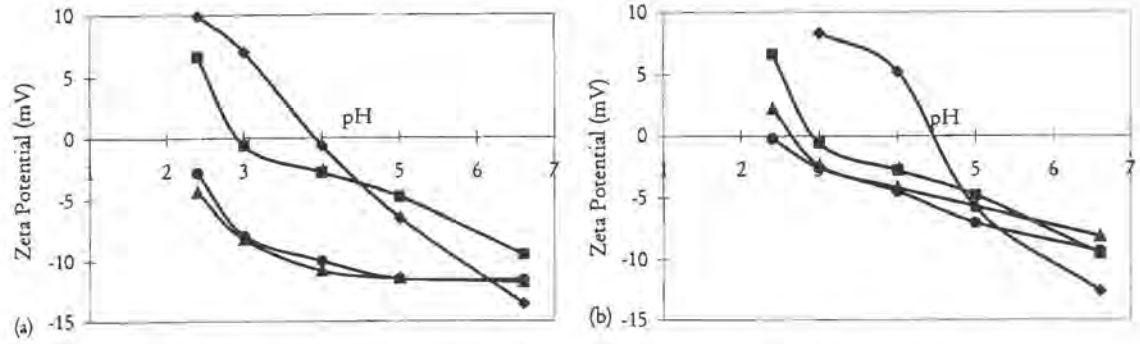

Figure 4.9. The zeta potential of SAB2 as a function of pH and time of propagation.
(♦ early exponential, ■ mid exponential, ▲ late exponential, ● stationary phase, (a) aerobic, (b) anaerobic)

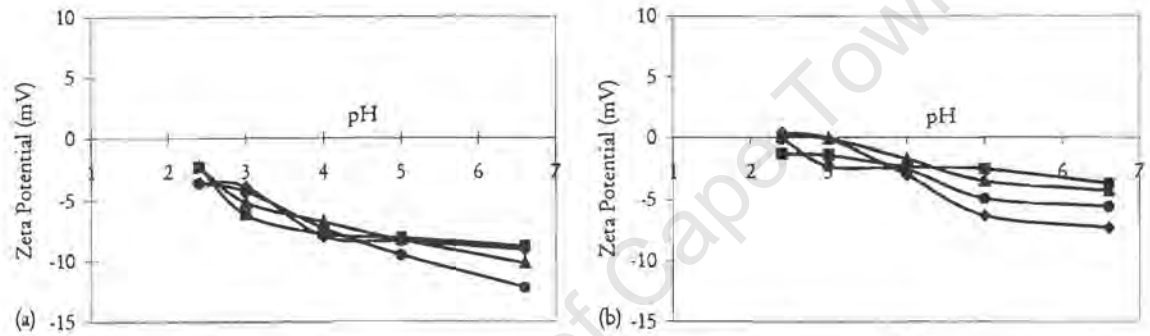

Figure 4.10. The zeta potential of SAB5 as a function of pH and time of propagation.
(♦ early exponential, ■ mid exponential, ▲ late exponential, ● stationary phase, (a) aerobic, (b)anaerobic)

4.4.2.2 Charge Group Composition Analysis

Using the methods discussed in Section 3.4.1, the zeta potential profiles obtained during the propagation of the four strains were converted into charge group compositions. These results including the total number of chargeable groups (N_s) and the ratio of phosphate to carboxyl groups (q), are plotted as a function of propagation time in Figures 4.11 – 4.14 for the four strains under aerobic and near anaerobic conditions. Based on the surface molecular composition of yeast walls, the ratio of phosphate to carboxyl groups (q) is similar to the ratio of phosphomannan to protein. The total number of chargeable groups (N_s) represents the combined concentration of charge groups viz. phosphate from phosphomannan, carboxyl and amine from protein.

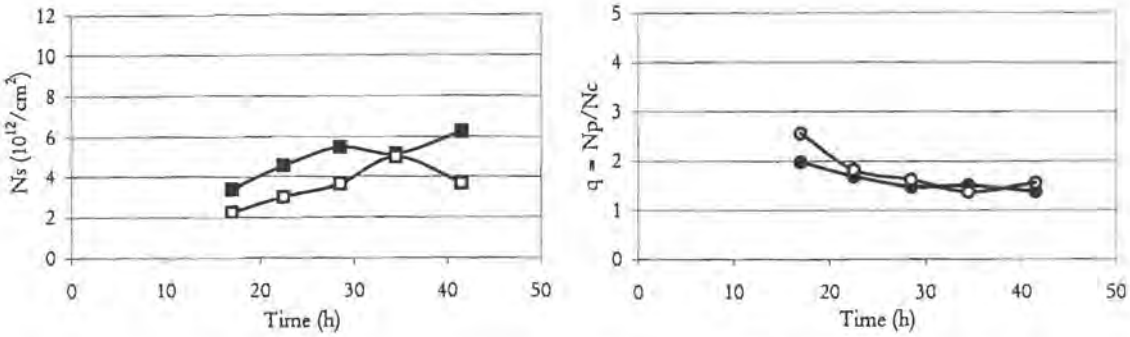

Figure 4.11. Charge group concentration profiles for SAB1 during propagation.
(■ N_s aerobic, □ N_s anaerobic, ● q aerobic, ○ q anaerobic)

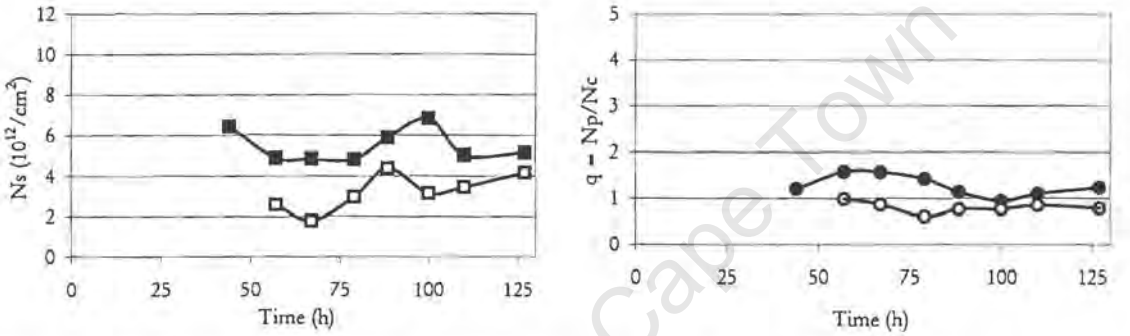

Figure 4.12. Charge group concentration profiles for SAB1/96 during propagation.
(■ N_s aerobic, □ N_s anaerobic, ● q aerobic, ○ q anaerobic)

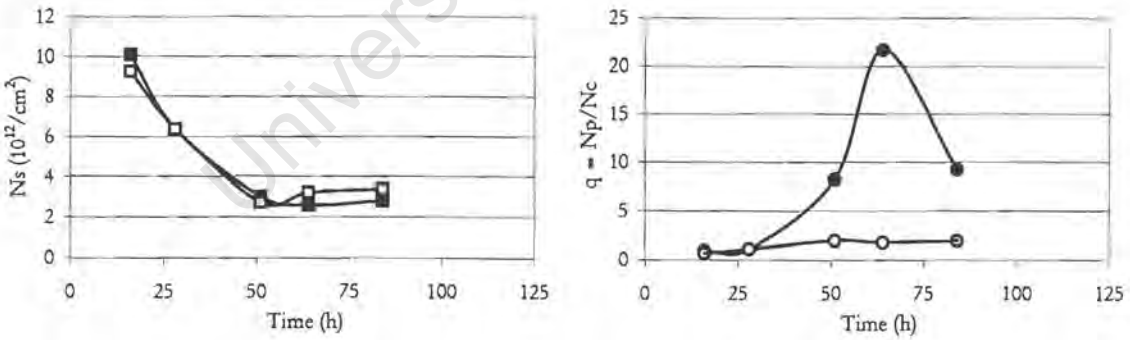

Figure 4.13. Charge group concentration profiles for SAB2 during propagation.
(■ N_s aerobic, □ N_s anaerobic, ● q aerobic, ○ q anaerobic)

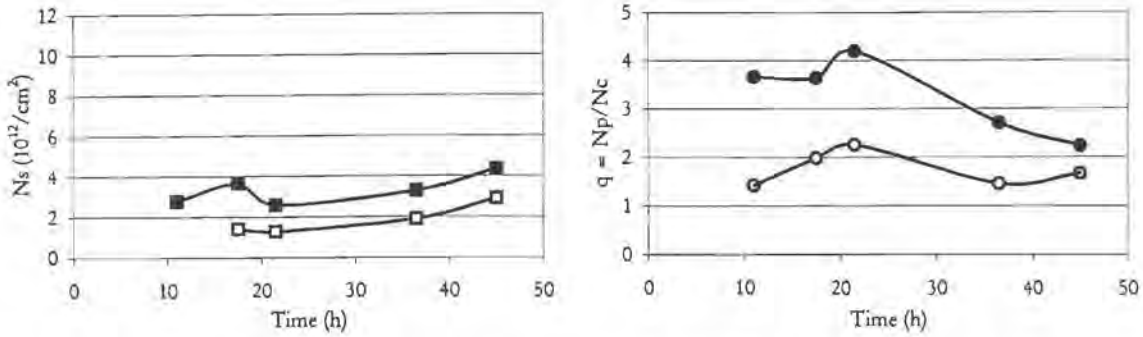

Figure 4.14. Charge group concentration profiles for SAB5 during propagation.
(■ N_s aerobic, □ N_s anaerobic, ● q aerobic, ○ q anaerobic)

Since the inoculum for the propagations are all grown aerobically in MYPG media, the initial surface properties and compositions are expected to be similar. Due to the low initial cell concentration, samples for cell surface property measurement could not be made until a sufficiently high cell concentration had been produced. By this time, the similarity had already been lost. The net change observed in the surface potential and composition of the aerobic propagation is due to the different media used for the inoculum (MYPG) and propagation (wort) substrate since the inoculum was produced aerobically.

Comparing the aerobic and anaerobic propagations, it is seen that the aerobic yeast of the flocculent strains have more chargeable groups than the anaerobic yeast throughout the cell growth cycle. Throughout these propagations the N_s values of the aerobically propagated yeast are 1 to 3 x 10^{12} groups.cm^{-2} higher than the anaerobic equivalent at the same time. This trend is not seen for SAB2, the non-flocculent strain, where the number of chargeable groups on the surface is unaffected by oxygen availability, despite the visual differences in the zeta potential profiles of this strain during aerobic and anaerobic growth. The difference in zeta potential profiles is due to the large difference in q for the strain as a function of oxygen availability. The magnitude of N_s for strain SAB2 differs from the flocculent strains. Significantly more chargeable groups are present in the early stages of the propagation (~ 12 x 10^{12}) than at the end of the cell cycle (~ 2 x 10^{12}). Chargeable group concentration in flocculent strains lay in the range 2 – 6 x 10^{12} groups.cm^{-2}. Hence the growth media has a greater effect on the surface charge group composition of SAB2 than on the other strains studied. While the total number of chargeable groups on the SAB2 yeast surface decreases during propagation the flocculent strains all show no change or a slight increase towards the onset of stationary phase. Bowen *et al.* (1992) showed a decrease in N_s values during fermentations for ale (3.6 decreasing to 2.7 x10^{12}/cm^2) and lager yeast strains (2.7 decreasing to 1.7 x10^{12}/cm^2), corresponding to the lower N_s values observed during anaerobic growth.

The ratio of phosphate to carboxyl groups (q) of all four strains studied was found to be higher for the yeast propagated aerobically. SAB1, SAB2 and SAB5 had q ratios greater than 1 under both aeration conditions throughout the propagation cycle. SAB1/96 had q values closer to unity (between 0.61 and 1.57) during the growth cycle although the aerobic yeast still had the higher values. The general trend for the flocculent strains was for a decreasing q ratio from the mid logarithmic to stationary phase with the early growth phase showing fluctuating values possibly as a result of non representative sampling of cells at too low a concentration. Since all aerobically propagated yeast showed decreasing q values, it is likely that this trend is a result of the change of media causing different yeast surface compositions. The aerobically propagated yeast of the non-flocculent strain, SAB2, had higher q ratios than the flocculent strains. The anaerobic growth condition showed an increasing trend in q during the latter stages in the cell growth cycle although not as great a trend as in the aerobic propagation. Bowen *et al.* (1992) reported an initial decrease in q value early in the aerobic fermentation of yeast followed by its increase during the latter stages. They found q values to range between 0.91 (at start of fermentation) to 0.70 (midway through fermentation) to 0.94 (at the end of fermentation) for lager yeast and q values between 1.26 and 0.56 for ale yeasts.

4.5 Pitching Yeast Properties

Yeast biomass generated during propagation is used to inoculate brewery fermentations i.e. as pitching yeast. Propagation is typically an aerobic batch process with late exponential or stationary phase yeast being used for pitching. Between fermentations the yeast is exposed to an initial oxygenated environment which becomes anaerobic during the later part of fermentation where the yeast goes into stationary phase before being pumped out of the vessel. The mechanical handling of yeast can therefore occur following aerobic and anaerobic acclimatisation by the cells. The resilience of these two yeast cultures to hydrodynamic stress can be different. The surfaces of 'healthy' undamaged yeast needs to be well characterised first before studying the surfaces of damaged yeast. This section summarises the yeast properties viz. hydrophobicity, charge and composition, surface chemical and molecular composition, and flocculation at the end of aerobic and near anaerobic propagation.

4.5.1 Hydrophobicity

A summary of the final hydrophobicity indices of the different strains after propagation under both aerobic and near anaerobic conditions is provided in Table 4.3. Amory and Rouxhet (1988) observed a difference in hydrophobicity between top and bottom fermenting brewing yeasts with bottom strains being less hydrophobic than top strains. This could, however, not be generalised to non-brewing strains of *Saccharomyces cerevisiae*. In this study the difference in hydrophobicity between the

strains is less than the difference between aerobic and anaerobically propagated yeast in the stationary phase. The hydrophobicity index of SAB5 under anaerobic conditions was approximately 50 % that of the other strains. The anaerobic variant of SAB2 showed the greatest hydrophobicity, yet was not flocculent. Despite the differences in hydrophobicity between the strains, no significant difference is seen between the flocculent strains and the non-flocculent strain.

Table 4.3. Final hydrophobicity index (%) values of yeast strains after aerobic and anaerobic propagation.

Strain	Aerobic	Anaerobic
SAB1	5.5	22.8
SAB1/96	4.5	21.0
SAB2	1.8	25.0
SAB5	2.5	12.4

4.5.2 Surface Charge

4.5.2.1 Zeta Potential

The zeta potential for the aerobic and anaerobic yeast at the end of propagation, as a function of pH are represented in Figure 4.15. It was generally found that for both aerobic and anaerobically propagated yeast, SAB2 was the most negatively charged while SAB1/96 was the least negatively charged across the pH range tested. The pI of SAB1/96, propagated anaerobically was determined as 3.8 at the end of the cell growth cycle. The pI of all other strains lay below pH 2.5.

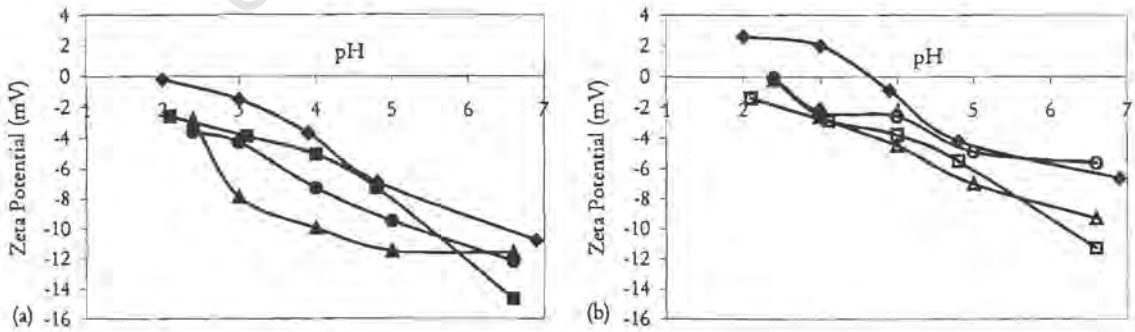

Figure 4.15. Zeta potential profiles of the strains in the stationary phase of aerobic (a) and anaerobic (b) propagation.

(■ aerobic SAB1, ♦ aerobic SAB1/96, ▲ aerobic SAB2, ● aerobic SAB5, □ anaerobic SAB1, ◊ anaerobic SAB1/96, Δ anaerobic SAB2, ○ anaerobic SAB5)

4.5.2.2 Charge Group Composition

The final N_s and q values obtained for the yeast in the stationary phase were calculated from the zeta potential profiles provided in Figure 4.15 and are summarised in Table 4.4. The N_s values show that under aerobic growth conditions, the flocculent strains are more chargeable than under anaerobic conditions (aerobic to anaerobic N_s ratios greater than 1) while the non-flocculent strain is less chargeable under aerobic than anaerobic conditions with its ratio being less than unity. All strains, except SAB1 have a higher phosphate to carboxyl ratio (q) after aerobic growth. Of these strains, SAB2 has the highest q values irrespective of the oxygen availability during propagation.

Table 4.4. Chargeable group composition of yeast in its stationary phase after aerobic or anaerobic propagation.

Strain	Ns (10^{12}.cm^{-2})			$q = N_p/N_c$		
	Aerobic	Anaerobic	Ratio	Aerobic	Anaerobic	Ratio
SAB1	6.23	3.68	1.7	1.38	1.55	0.9
SAB1/96	5.14	4.16	1.2	1.24	0.79	1.6
SAB2	2.81	3.38	0.8	9.24	1.98	4.7
SAB5	4.34	2.90	1.5	2.23	1.66	1.3

4.5.3 Flocculation

Based on visual observation, flocculation in the propagation vessel occurred towards the end of exponential phase only. The flocculation may be attributed to either classical colloidal interactions brought about by low surface charge, hydrophobicity and van der Waal forces, or by specific lectin – receptor site interactions. In the event of lectin-mediated flocculation, the delayed onset may result from the delayed expression of FLO genes with lectins only being incorporated into the cell wall and activated at this time as proposed by Stratford and Carter (1993). Also, should active lectins be present earlier on, flocculation would be inhibited by the high concentration of sugars causing blocking of the site. At the end of propagation, the flocculation potential was determined by the method described in Section 3.2.4. These results are presented in Table 4.5, together with the hydrophobicity index and zeta potential values at pH 4.5, i.e. the pH of the flocculation buffer.

Table 4.5. Flocculation ability, hydrophobicity and zeta potential at pH 4.5, of pitching yeast.

	Extent of Flocculation (% of cells)		Hydrophobicity (%)		Zeta Potential @ pH 4.5 (mV)	
Strain	Aerobic	Anaerobic	Aerobic	Anaerobic	Aerobic	Anaerobic
SAB1	98.6	94.8	4.5	21.0	-7.3	-3.9
SAB1/96	99.1	95.9	5.5	22.8	-5.8	-3.1
SAB2	0.4	4.8	1.8	25.0	-10.8	-5.8
SAB5	96.3	82.4	2.5	12.4	-8.4	-3.8

The results indicate that the three strains designated as being flocculent all show flocculation levels in excess of 80% and generally above 95% while SAB2 showed less than 5% flocculation. For the flocculent strains, the aerobic propagation produced yeast which was more flocculent than near anaerobic growth. SAB2 was found to be slightly flocculent under anaerobic propagation conditions although this level of flocculation does not classify it as flocculent in comparison with the other strains which are highly flocculent.

Derjaguin-Landau-Verwey-Overbeek (DLVO) theory predicts that flocculation for colloids is a result of the attractive forces between the individual particles exceeding the repulsive forces. Like surface charges cause the repulsive force while, in aqueous environments, the hydrophobicity of particles stabilises floc formation. From the results presented above, it is observed that the aerobic flocculent strains were more charged but also more flocculent than the anaerobically grown strains. This contradicts the DLVO prediction that a higher charge would cause a decrease in flocculation. In addition, the aerobic variants were less hydrophobic but more flocculent than the anaerobically produced yeasts of the same strain, again contradicting DLVO theory. These findings are supported by the calculation of the orthokinetic capture coefficient of flocculent yeast strains presented by Speers *et al.* (1993). The calculated coefficient based on DLVO were at least two orders of magnitude smaller than those measured experimentally, supporting the fact that flocculation in brewers' yeast cannot be explained by DLVO theory and that a lectin mechanism is more appropriate.

For the non-flocculent strain (SAB2), anaerobic propagation produced yeast which was less charged but more hydrophobic than the aerobically grown yeast. Although this strain is classified as non-flocculent, low levels of flocculation were found (< 5%). Unlike the flocculent strains, the trends in flocculation were consistent with the predictions of DLVO theory. Hence it may be postulated that in the absence of a genetically encoded lectin based flocculation system, a low level of flocculation occurs as a result of the classical colloidal interactions.

4.5.4 Chemical Surface Composition

The pitching yeast generated by aerobic and anaerobic growth of the four strains was analysed by X-ray photoelectron spectroscopy (Section 3.2.3). This produces an elemental composition of the outer 2 to 5 nm of yeast surface, corresponding predominantly to the mannan layer of the cell wall which is estimated to be approximately 150 nm thick (Rhymes and Smart, 1996). The elemental composition and bond concentrations (mass percent) obtained from the elemental peak decompositions for each strain are summarised in Tables 4.6, 4.7, 4.8 and 4.9.

Table 4.6. **Elemental and bond composition of outer cell wall surface of aerobic and near anaerobic pitching yeast for SAB1.**

Element	Bond	Aerobic	Anaerobic
Carbon		67.61	69.76
	C-(C, H)	42.5	52.1
	C-O	45.5	37.4
	C=O	12.0	10.5
Oxygen		29.67	26.53
	O-(C, H)	91.0	83.9
	O=C	9.0	16.1
Nitrogen		2.72	3.71

Table 4.7. **Elemental and bond composition of outer cell wall surface of aerobic and near anaerobic pitching yeast for SAB1/96.**

Element	Bond	Aerobic	Anaerobic
Carbon		71.25	76.06
	C-(C, H)	57.5	62.5
	C-O	36.6	31.5
	C=O	5.9	6.0
Oxygen		27.31	22.84
	O-(C, H)	91.2	91.4
	O=C	8.7	8.6
Nitrogen		1.45	1.10

Table 4.8. Elemental and bond composition of outer cell wall surface of aerobic and near anaerobic pitching yeast for SAB2.

Element	Bond	Aerobic	Anaerobic
Carbon		70.71	72.98
	C-(C, H)	51.7	56.0
	C-O	39.6	35.9
	C=O	8.7	8.1
Oxygen		28.23	24.64
	O-(C, H)	85.5	82.2
	O=C	14.5	17.8
Nitrogen		1.06	2.38

Table 4.9. Elemental and bond composition of outer cell wall surface of aerobic and near anaerobic pitching yeast for SAB5.

Element	Bond	Aerobic	Anaerobic
Carbon		69.73	72.68
	C-(C, H)	50.7	56.2
	C-(O, N)	40.1	33.3
	C=O	9.2	10.5
Oxygen		28.12	24.4
	O-(C, H)	87.5	81.1
	O=C	12.5	18.9
Nitrogen		2.15	2.92

As discussed in Section 3.4.2.2, the reliability of peak decomposition for this study is within the limits found in previous studies by Dengis *et al.* (1995a). Differences in element and bond composition are seen both between the strains and between aerobic and anaerobic propagation of the same strain. The interstrain differences in surface chemical composition can provide some insight into the surface charge and hydrophobicity of the strains.

The significance of differences measured between the final surface compositions of aerobic and near anaerobic growth conditions of all four strains were evaluated according to the statistical t-test. These findings are summarised in Table 4.10. As seen from the t-test, significant differences are observed in the surface chemical composition of yeast following aerobic and near anaerobic growth. Generally aerobic growth results in surfaces with a greater quantity of elemental oxygen and less carbon. Of both carbon and oxygen forming single bonds with oxygen and carbon respectively (C-(O,N) and C-OH), the concentration of these bonds is greater following aerobic growth while the amount of homogenous carbon bonds (C-(C,H) decreased. The number of carbon double bonded to oxygen groups as seen by C=O and O=C are similar for both aerobic and anaerobic growth.

Using the information on elemental composition, the surface molecular composition was calculated as discussed in Appendix C.2. This analysis determines the concentration of protein, lipid and mannan at the cell surface of the yeast in its stationary phase and is summarised in Table 4.11. The statistical differences observed in molecular composition between the two growth conditions and summary of the differences seen at confidences greater than 95 % are summarised in Table 4.12.

Table 4.10. Differences in outer surface chemical composition between aerobic and anaerobic growth for all yeast strains studied.

Element	Bond	Probability that Aerobic ≠ Anaerobic	@ 95 % confidence Aerobic vs. Anaerobic
Carbon		0.992	<
	C-(C,H)	0.998	<
	C-(O,N)	0.990	>
	C=O	0.626	=
Oxygen		0.999	>
	C-OH	0.999	>
	O=C	0.880	=
Nitrogen		0.922	=

Table 4.11. Comparison of the molecular composition of the outer cell wall surface of the four strains following aerobic and near anaerobic propagation.

	Protein		Lipid		Mannan	
Strain	Aerobic	Anaerobic	Aerobic	Anaerobic	Aerobic	Anaerobic
SAB1	16.3	22.3	32.3	37.0	51.4	40.7
SAB1/96	8.8	6.7	44.1	58.2	47.2	35.2
SAB2	6.4	14.4	43.1	47.7	50.5	37.9
SAB5	13.0	17.6	38.9	46.2	48.1	36.2

Table 4-12. Differences in molecular composition resulting from oxygen supply during propagation.

Compound	Probability of aerobic ≠ anaerobic	@ 95 % confidence Aerobic vs. Anaerobic
Protein	0.922	=
Lipid	0.979	<
Mannan	1.000	>

Since the surface properties of yeast are determined by the molecular composition of its surface, trends in surface properties should correspond with changes in surface composition. The evidence for a lectin-mediated mechanism for flocculation presented in this chapter suggests that there should not be any direct correlation between the extent of flocculation and any of the overall surface molecular compositions. This, because the proteinaceous lectin responsible for flocculation would only be one of many types of protein present at the wall surface and is likely not to contribute significantly to the total surface protein concentration. Indeed no correlation between flocculation and lipid, mannan or protein concentrations were found.

A correlation does, however, exist between the level of hydrophobicity and lipid content. As indicated in Table 4.12, the lipid content of anaerobic cultures (which are found to have hydrophobicity indices in the range 12.4 – 25.0 %) is higher than that of the aerobic ones ($1.8 < HI\% < 5.5$). Of the three model compounds present, lipid is the most hydrophobic and hence its increased presence at the surface accounts for the increased hydrophobicity.

The mannan to protein ratio can be considered to be similar to the q ratio (phosphate to carboxyl groups) obtained from the surface charge composition analysis. The ratios would be expected to correspond since the phosphate groups present at the surface is attached to mannan as phosphomannan. All the carboxyl groups are presumed to be acidic amino acids in proteins. The protein therefore determines the carboxyl group concentration while mannan content determines that of phosphate. The aerobic to anaerobic ratio of mannan to protein ratios provided in Table 4.13 are all greater than one. This is in agreement with the finding that the ratio of aerobic to anaerobic q values which are mostly greater than one.

Since the charged groups are all contained in the protein and mannan fractions according to the analysis performed here, the total number of chargeable groups (N_s) should correspond to the sum of the mannan and protein fractions.

Table 4.13. Correlations of aerobic/anaerobic ratios between surface charge composition and molecular composition.

Strain	$q_{aerobic}/q_{anaerobic}$	$(Mannan/Protein)_{aerobic}/(Mannan/Protein)_{anaerobic}$	$N_{s\,aerobic}/N_{s\,anaerobic}$	$(Mannan + Protein)_{aerobic}/(Mannan + Protein)_{anaerobic}$
SAB1	0.9	1.8	1.7	1.1
SAB1/96	1.6	1.8	1.2	1.1
SAB2	4.7	1.0	0.8	1.3
SAB5	1.3	3.0	1.5	1.1

4.6 Summary

The propagation of yeast strains can be successfully modelled using the logistic growth equation for biomass growth. Using this equation, aerobic growth results in a rate which is 15 – 25 % higher than anaerobic propagation. In addition to the increased growth rate, the final biomass concentration is 2 to 3 times higher. This higher biomass concentration has the effect of increasing the yield coefficient to the same extent. The implication of this is that the efficiency with which yeast produces biomass and ethanol is similar under both aerobic and anaerobic conditions. The significance of the Crabtree effect in yeast production from high sugar substrates is therefore indicated.

Since the mechanical handling of yeast in a brewery occurs when the yeast is in late exponential to stationary phase, it is important to ensure that when studying the resilience of yeast to such handling, that the yeast quality indicators are stable. It is shown that the surface hydrophobicity and surface charge had stabilised towards the end of exponential growth. Changes which are observed in surface properties following exposure to hydrodynamic shear dealt with in the forthcoming chapters are as a result of hydrodynamic damage to the cell surface and not a sensitivity of the yeast surface to slight differences in growth phase.

The availability of oxygen to the yeast during propagation does affect its surface properties in terms of hydrophobicity and charge. Aerobic propagation results in yeast which is less hydrophobic than when grown anaerobically. At the pH typically encountered during brewery propagation and fermentation (pH 4 – 5), the zeta potential of aerobic cultures is more negative than anaerobic equivalents. By deconvoluting its zeta potential vs. pH profile, aerobic propagation is seen to produce a surface which has up to 70 % more charge forming groups (N_s) as well as an increase in the ratio of phosphate to carboxyl groups (q) of up to 4.7 fold.

The extent of flocculation observed by the aerobic and anaerobic cultures of the flocculent strains shows that aerobic propagation produced the more flocculent yeast. This increased flocculation does not correspond to reduced surface charge or increased hydrophobicity which is what would be expected if DLVO theory held as the mechanism of flocculation. This provides additional evidence that a specific lectin mechanism dominates among flocculent strains of brewers' yeast. For the strain of non-flocculent yeast, the small amount of flocculation observed at the end of anaerobic growth decreased still further for aerobic growth which is in agreement with the prediction of DLVO theory. The flocculation observed in the non-flocculent strain can therefore be attributed to the classical colloidal flocculation mechanism and a lack of lectin type flocculation.

The elemental and molecular composition indicated by XPS shows that aerobic propagation results in a cell surface composed of more oxygen, mostly in the form of C-OH and a concomitant decrease

in total carbon content of the homogenously bonded form (C-(C,H). The molecular composition of these surfaces are also found to be different in that the aerobic cultures with a higher mannan and lower lipid concentration. Correlations are seen to exist between the observed surface properties and surface composition in the form of higher lipid content of anaerobic yeast matching its increased hydrophobicity. The differences in charge group concentrations between aerobic and anaerobically propagated yeast also match the differences in molecular composition. The higher total number of chargeable groups (N_s) observed following aerobic growth corresponds to an increased amount of surface mannan and protein which are the compounds responsible for the charge. The higher q value (ratio of phosphate to carboxyl groups) for aerobic over anaerobic cultures supports the higher mannan to protein ratio found in the aerobic cultures.

Chapter 5: Mechanical Damage of Brewers' Yeast in the French Press Apparatus

5.1 Introduction

To investigate the effect of hydrodynamic shear on yeast cells in the laboratory, a French pressure cell was used. The French Press is a type of high pressure homogeniser, typically used to effect cell disruption in the laboratory. A pressure difference of the order of 3 to 300 MPa across the discharge valve causes the fluid to accelerate through the valve, cavitate and generate a high shear turbulent environment (Doulah *et al.*, 1975; Engler and Robinson, 1981; Engler, 1985). This shear is able to cause damage to the cells ranging from mild rearrangement of the cell wall surface, to more extreme permeabilisation of the cell membrane and a loss of viability while at sufficiently high operating pressures cell disruption could occur. The disruption of cells is linked primarily to the magnitude of the pressure drop as well as the rate at which the pressure release occurs (Brookman, 1975). This mechanism is interpreted on the basis of shear stress (Engler, 1979, cited in Engler, 1985) as well as the formation of turbulent eddies of similar size to suspended cells causing cell disruption (Doulah *et al.* 1975). Unlike other high pressure homogenisers which have an impingement plate to enhance disruption, the French Press only has a valve. In the presence of such impingement plates, the velocity of the liquid jet as well as the existence of turbulence in the jet are important factors governing the disruption process (Engler and Robinson, 1981). The French Press enables the laboratory simulation of hydrodynamic shear under a variety of lytic and sublytic conditions on yeast. This permits the study of mechanical damage under more extreme conditions than are possible in the brewery.

In this chapter the effects of the French Press on the viability, membrane integrity and extent of disruption of the yeast under a range of operating pressures as well as changes to the cell surface charge and hydrophobicity are discussed. These effects were determined on the four strains of yeast propagated to stationary phase under aerobic and near anaerobic conditions as reported in Chapter 4. The effect of shear on aerobic and anaerobically produced yeast was compared to provide insight on the status of yeast during different stages of its cycle within a brewery after which it has been exposed to different oxygen availabilities.

A hydrodynamic analysis of the French Press is also presented to enable the biological effects observed to be correlated to the shear stress and energy dissipation experienced by the cells. This is used to compare the damage observed at the laboratory scale to damage observed at a larger scale in centrifuges, pumps and flow conditions present within the brewery.

Strain SAB5 was chosen for further study of the relationship between energy dissipation rates at pressures in the sub-lytic range and changes to the outer wall chemical composition, flocculation and fermentation performance. Yeast propagated under aerobic and anaerobic laboratory conditions were compared against a 'typical' 6'th generation production yeast from SAB-Newlands brewery in terms of its resilience to disruption and changes in its flocculation potential following exposure to the French Press.

5.2 Hydrodynamic Analysis of French Press Operation

The French Press operates by discharging a cell suspension under high pressure through a constriction valve to atmospheric pressure. On accelerating the fluid past the constriction, a loss of pressure to below the final discharge pressure (atmospheric) results. An approximation of the hydrodynamics occurring within the French Press is obtained by likening it to the flow of fluid through an orifice with pressure recovery taking place downstream of the constriction valve. By analogy with flow through an orifice placed in a pipe, the pressure is lowest at a point downstream from the orifice and the pressure recovers to the final pressure loss across the orifice at a distance of approximately 8 pipe diameters after the constriction (Coulson and Richardson, 1990). Using this interpretation energy dissipation rates and shear stresses have been calculated. The parameters applicable to the cell suspension and French Press design are summarised in Table 5.1. The cell density used in the analysis was calculated from the data presented in Appendix A2 which was the average density of strains SAB1, SAB1/96, SAB2 and SAB5.

Table 5.1. Parameters used in the hydrodynamic analysis of the French Press.

Parameter	Value	Units
Pipe diameter	0.0015	m
Cell concentration	9	g/l
Cell density	1150	kg/m^3
Cell suspension density	1001	kg/m^3
Suspension viscosity	0.0016	Pa.s
Kinematic viscosity	1.60×10^{-6}	m^2/s
Volumetric flow rate	0.00154	m^3/s
Cell diameter	$6.1 - 6.8 \times 10^{-6}$	m

By assuming that the energy is dissipated within the volume where the pressure decreases across an orifice and finally recovers at a distance of eight pipe diameters downstream, the specific energy dissipation rate (ε) given in Equation 2.15 can be rewritten as Equation 5.1.

$$\varepsilon = \frac{\Delta P Q}{2\pi\rho D^3} \tag{5.1}$$

where: ΔP = pressure drop across the valve (Pa)

D = diameter of pipe (m)

Q = volumetric flow rate ($m^3.s^{-1}$)

ε = energy dissipation rate per unit mass($m^2.s^{-3}$)

ρ = fluid density ($kg.m^{-3}$)

The Kolmogorov length (l_c) and velocity (v) of the smallest turbulent eddies were calculated using Equations 2.22 and 2.23. Because the eddie size is smaller than the cell size and the energy dissipation rates are high, isotropic turbulence can be assumed and the Reynolds shear stress (τ^R) can be calculated using Equation 2.24 (Croughan *et al*, 1987). The likelihood of cavitation occurring inside the French Press can be predicted by the calculated cavitation number (σ) from Equation 2.34. As can be seen by the low cavitation numbers in Table 5.2, cavitation is likely to be present. The total energy dissipated (TE), specific energy dissipation rate (ε), Reynolds shear stress and cavitation number calculated using the above mentioned equations are presented in Table 5.2. The volumetric energy dissipated on the cells can be calculated by dividing the total energy dissipated (TE) by the volume of cells in the zone downstream of the valve where the turbulent energy is postulated to dissipated. As can be seen by the very low cavitation numbers in Table 5.2, cavitation is likely to be present in the form of large vapour jets (supercavitation) and hence the oscillating collapse of tiny cavities associated with cavitation damage is unlikely to have a dominant effect on cell damage. The size of the smallest eddies generated within the French Press are an order of magnitude smaller than

the yeast cells. Since the eddies are smaller than the cells, it can be assumed that the energy is dissipated at the cell wall.

Table 5.2. Energy dissipation, rate of energy dissipation and Reynolds shear stress calculated for operating pressures within the French press.

Parameter	Units			
ΔP	MPa	3	6	10
σ	–	0.008	0.016	0.026
ε	$M^2.s^{-3}$	2.17×10^8	4.35×10^8	7.25×10^8
TE	J	0.064	0.127	0.212
TE per cell volume	$J.m^{-3}$	3.33×10^7	6.67×10^7	1.11×10^8
l_c	µm	0.37	0.31	0.27
V	$m.s^{-1}$	4.3	5.1	5.8
τ^R	$N.m^{-2}$	2.83×10^6	5.67×10^6	9.45×10^6

5.3 Effect of Discharge Pressure on Yeast Cells

The discharge pressure in a French Press is the controlled variable which can be altered to effect a varying degree of shear and associated damage to the cells. The equipment is usually operated at pressures high enough to disrupt a significant fraction of cells. Numerous studies on the disruption kinetics of Bakers yeast (Doulah *et al.*, 1975; Milburn and Dunnill, 1994) and *E. coli* (Middelberg, 1993; Middelberg *et al.*, 1992a, b; Hull and Middelberg, 1993) have been conducted to determine the mechanisms of cell disruption in high pressure homogenisers. The dominant operating parameter in the disruption of cells was identified as being the pressure. This study does not attempt to present disruption kinetics of yeast but looks at the turbulence disruption model for brewers' yeast. Its objective is to illustrate differences in resilience to mechanical damage between aerobic and anaerobically propagated yeast. The effect of discharge pressure on damage in the French Press was investigated using strains SAB1, SAB1/96, SAB2 and SAB5 propagated in the laboratory under aerobic and near anaerobic conditions at pressures between 3 and 20 MPa. These effects were compared to a 6th generation production yeast from SAB – Newlands Brewery across a pressure range of 5 and 40 MPa. The effect of operating pressure was monitored in terms of the loss of cell viability (methylene blue stain), loss in membrane integrity (release of intracellular protease) and cell disruption (cell counts).

5.3.1 Cell Disruption

Cell disruption was measured by a total cell count microscopically after the French Press treatment. The fraction of cells not disrupted was quantified in terms of percentage intactness (Equation 5.2). The total cell count was performed in conjunction with the methylene blue viability assay. In this analysis, cells which were stained blue were termed intact but non-viable.

$$\%Intact = \frac{N_{final}}{N_{initial}} * 100\% \qquad (5.2)$$

where: N_{final} = cell count after French Press

$N_{initial}$ = cell count before French Press

In Figure 5.1 the percentage intact cells remaining following exposure to the French Press is given for the four strains following aerobic and anaerobic propagation in the laboratory. The comparative study with the 6th generation production yeast is illustrated in Figure 5.2. Little cell disruption is observed at pressures below 6 MPa for the laboratory propagated yeast. As pressures are increased to 20 MPa, 40 – 60 % cell lysis occurs. No significant difference is observed in cell disruption of aerobic and anaerobically grown yeasts. Under both propagation conditions of non-flocculent SAB2, cell disruption was limited to 40%. The extent of disruption at 20 MPa shows that SAB2 is 50% more resilient than the three flocculent strains which showed more than 60% disruption. The 6th generation yeast was found to be resilient to cell disruption up to a much higher pressure (20 MPa) compared to the laboratory propagated yeast (6 MPa) (Figure 5.2). This difference can be attributed to the increased resilience produced by the fact that the production yeast was in its 6th generation while the laboratory yeast was a 1st generation. Both production and laboratory yeasts were grown on brewers' wort.

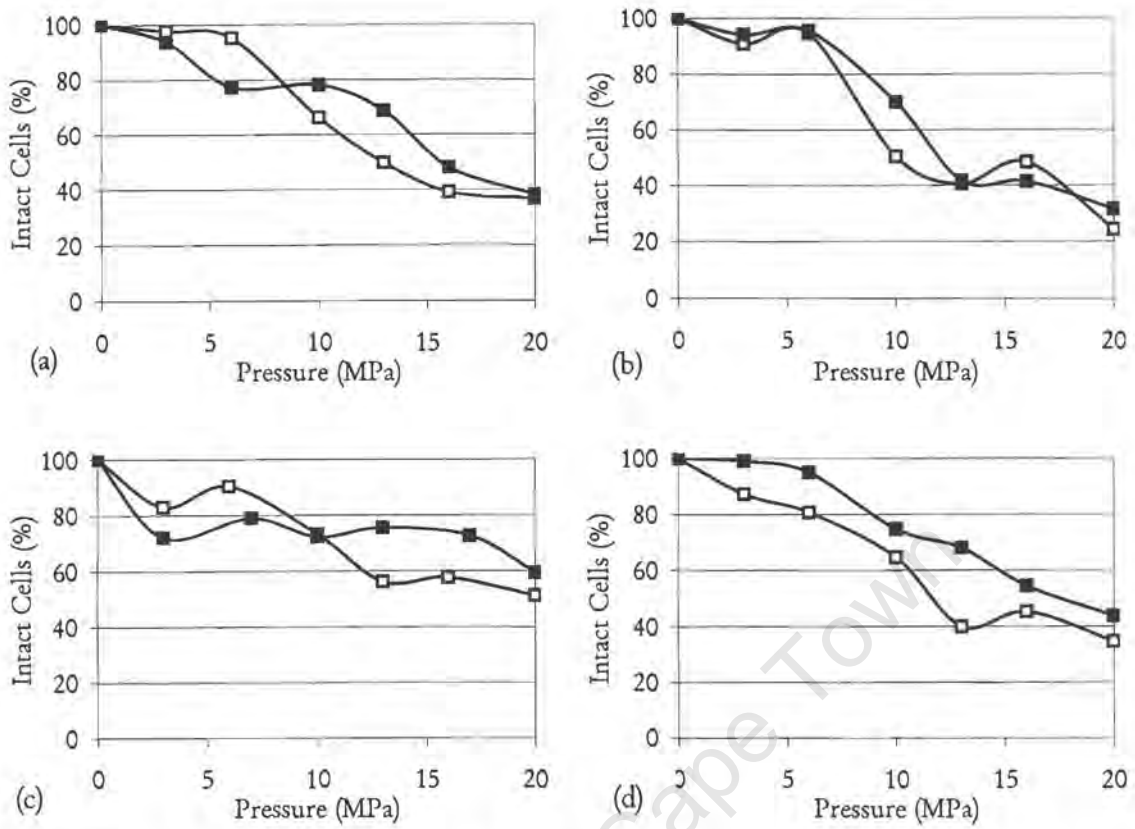

Figure 5.1. Disruption of laboratory propagated yeast following French Press treatment.
(■ aerobic, □ anaerobic, (a) SAB1, (b) SAB1/96, (c) SAB2, (d) SAB5)

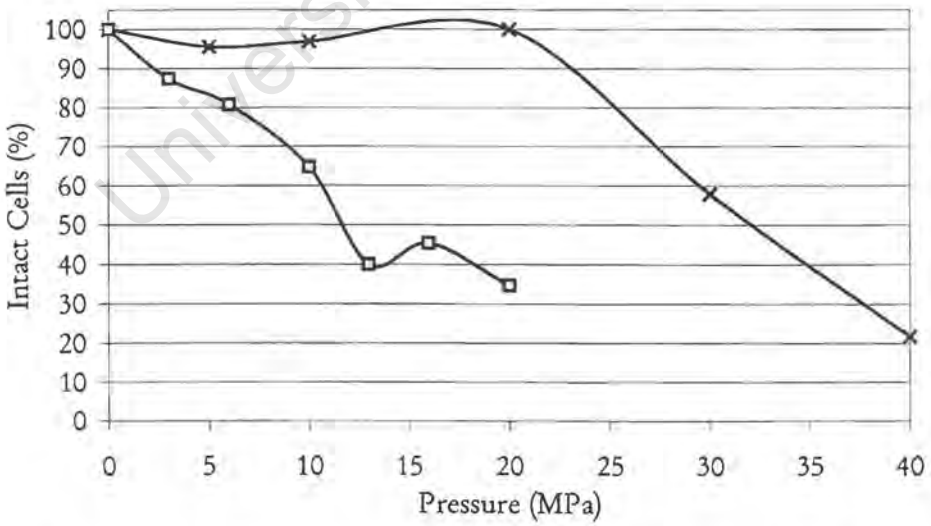

Figure 5.2. Comparison of disruption of 6th generation production yeast and laboratory grown SAB5 following French Press treatment.
(□ anaerobic laboratory SAB5, X 6th generation production yeast SAB5)

The critical pressure required to cause cell disruption appears to be between 6 and 10 MPa for the laboratory propagated strains in this study which equates to a total volumetric energy dissipation of between 6.7 x 10^7 and 11.1 x 10^7 $J.m^{-3}$. The total turbulent energy dissipated, calculated by Dunlop *et al.* (1994), to achieve cell lysis of carrot cells was $3x10^5$ J/m^3 which is 2 – 3 orders of magnitude smaller although the carrot cells are not physically as strong as yeast cells. Illing and Harrison (1999) used a turbulent flow capillary to study aggregate break-up of bacteria. At average energy dissipation rates in the range 5 – 10 $x10^3$ $m^2.s^{-3}$ they observed the break-up of aggregates but no cell disruption of the bacteria (cell size of 0.7 μm by 1.4 μm). In this study energy dissipation rates of 2 x 10^8 – 7 x 10^8 $m^2.s^{-3}$ were found to cause only sub-lytic damage.

5.3.2 Membrane Integrity

Protease can be released through the cell membrane in response to nitrogen starvation conditions at the end of cell growth and during storage (Mochaba *et al.*, 1993; Ormrod *et al.*, 1991). However, protease release can also be indicative of an increased membrane permeability. For example, under conditions of high shear stress the cell membrane can become damaged with the release of large quantities of protease. Under the conditions of hydrodynamic stress experienced in the French Press or on extreme mechanical handling, the release of protease is expected. Also, the time scale is insufficient to induce nitrogen starvation since these experiments were conducted within 6 hours following the start of stationary phase, hence the majority of the observed protease release can be attributed to a permeabilised cell membrane. The control sample, passed through the French Press at atmospheric pressure and exposed to all the pre, intermediate and post French Press steps was used to account for the natural protease release due to the nitrogen limitation conditions. The protease assay was performed with an 18 hour incubation period.

The results of the protease release assay on the four strains (aerobic and anaerobic propagations) following French Press treatment are provided in Figure 5.3. Below operating pressures of 6 MPa little extracellular protease activity is observed for the four laboratory propagated strains under both aeration conditions. At 10 MPa protease is first released and the amount of protease activity increases with further increases in operating pressure. At the higher pressures (10 – 20 MPa) more protease is generally released from the yeast which was propagated aerobically. SAB5 and SAB1 show this trend most clearly.

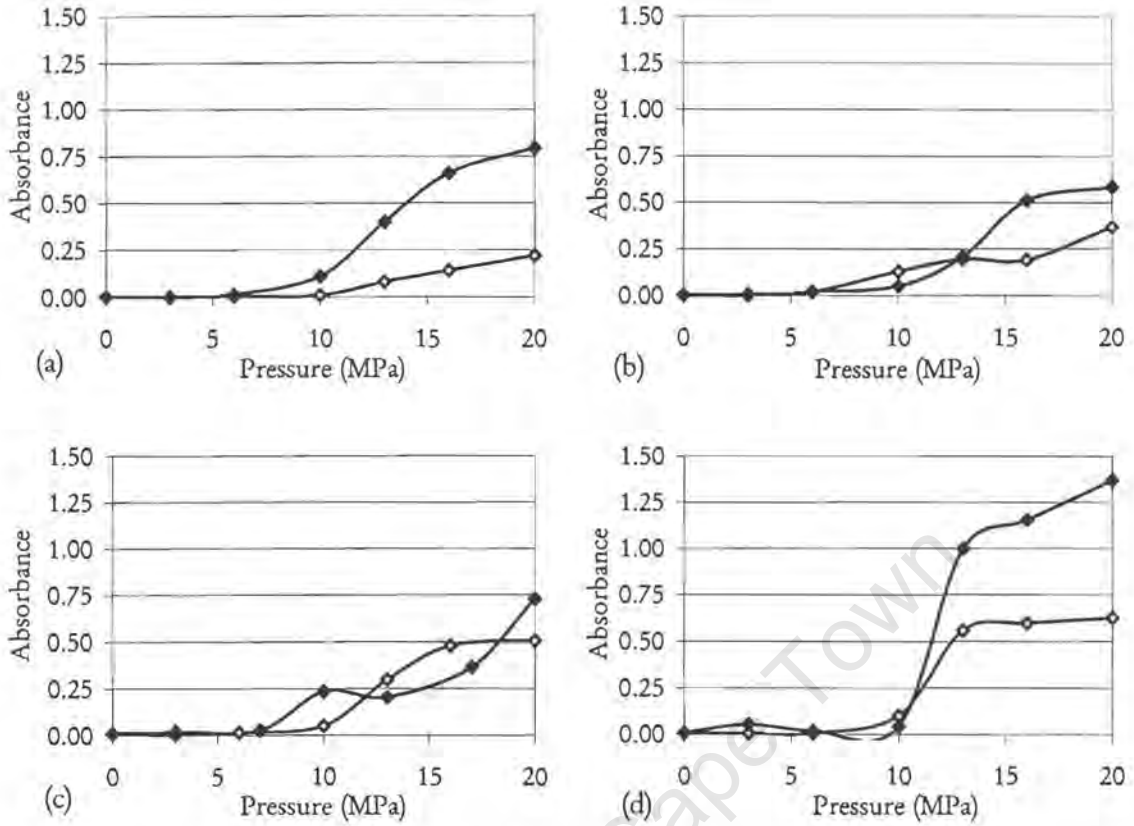

Figure 5.3. Protease release following French Press treatment of laboratory propagated yeast.

(♦ aerobic, ◊ anaerobic, (a) SAB1, (b) SAB1/96, (c) SAB2, (d) SAB5)

Figure 5.4 illustrates the protease release for the 6th generation production yeast (diluted in water) on exposure to the French Press. Although protease release was observed under less extreme conditions, the magnitude of protease release is significantly reduced compared to the laboratory propagated strains.

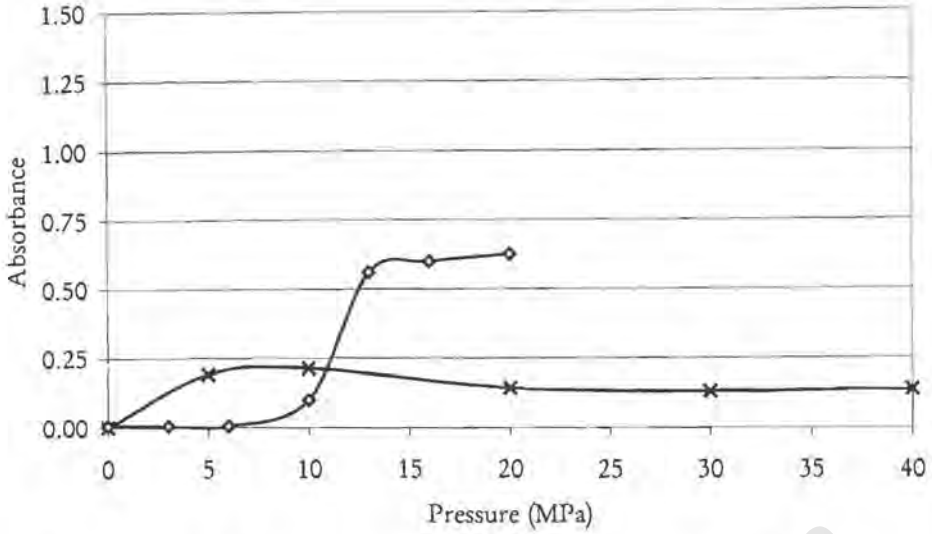

Figure 5.4. Comparison of protease release of 6th generation production yeast and laboratory grown SAB5 following French Press treatment.

(◊ anaerobic laboratory SAB5, X 6th generation production yeast SAB5)

The specific protease release was calculated by dividing the protease assay absorbance at the highest operating pressure by the concentration of disrupted cells. The results are presented in Table 5.3. From these results the specific protease content of aerobic yeast is seen to be much higher than for anaerobically propagated yeast by a factor of between 2.2 and 6.1. The specific protease release from the SAB5 production yeast (0.004) is 8 times lower than the anaerobically grown laboratory equivalent, indicating the observation of lower protease release from the brewery grown strain when exposed to high pressure disruption in the French Press.

Table 5.3. Specific protease release from laboratory propagated yeast.

Strain	Specific protease (Absorbance/10^6 disrupted cells/ml)		Ratio
	Aerobic	Anaerobic	(Aerobic/Anaerobic)
SAB1	0.0079	0.0013	6.1
SAB1/96	0.0041	0.0024	1.7
SAB2	0.0031	0.0019	1.6
SAB5	0.0071	0.0032	2.2

5.3.3 Cell Viability

Yeast viability was measured with the modified methylene blue staining technique detailed in section 3.2.1. The three flocculent strains (SAB1, SAB1/96, SAB5) and the non-flocculent strain (SAB2) were exposed to varying disruption pressures and the viability of the intact cells measured. The results are presented in Figure 5.5 for the strains propagated in the laboratory under aerobic and anaerobic conditions. Figure 5.6 compares the viability of 6th generation SAB5 production yeast to the first generation SAB5 laboratory propagated yeast. The viability of the intact yeast cells, measured in terms of the ability of the cells to exclude methylene blue through its membrane, remains high despite the high shear and rapid pressure drop to which they are exposed. Significant cell disruption (40 – 60%) was measured at operating pressures in the higher end of the range tested (Section 5.2.1). This indicates that while the shear applied is able to disrupt the cells, the viability of cells withstanding disruption remained high. The viability of the aerobic yeast remains greater than that of the anaerobic yeast across the range of pressures, indicating the greater resilience of the aerobic yeast under conditions of hydrodynamic stress.

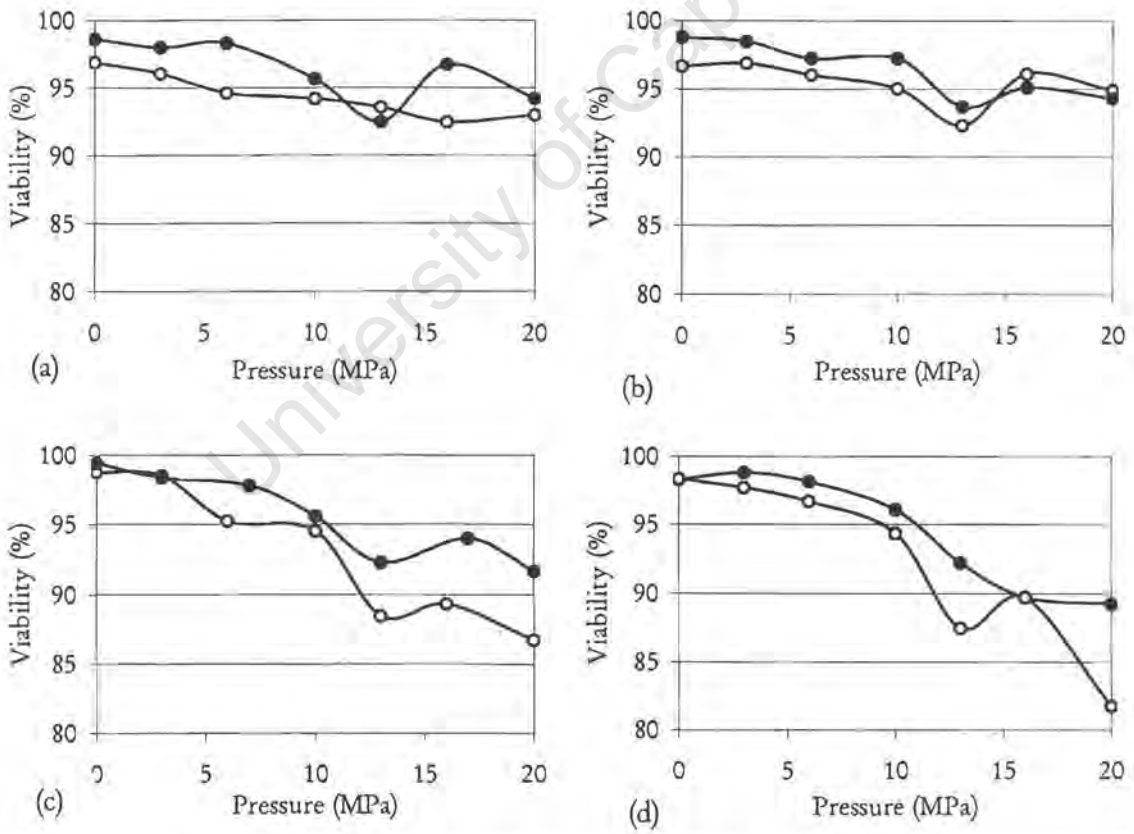

Figure 5.5. Intact cell viability of laboratory propagated yeast following exposure to the French Press.

(• aerobic, ○ anaerobic, (a) SAB1, (b) SAB1/96, (c) SAB2, (d) SAB5)

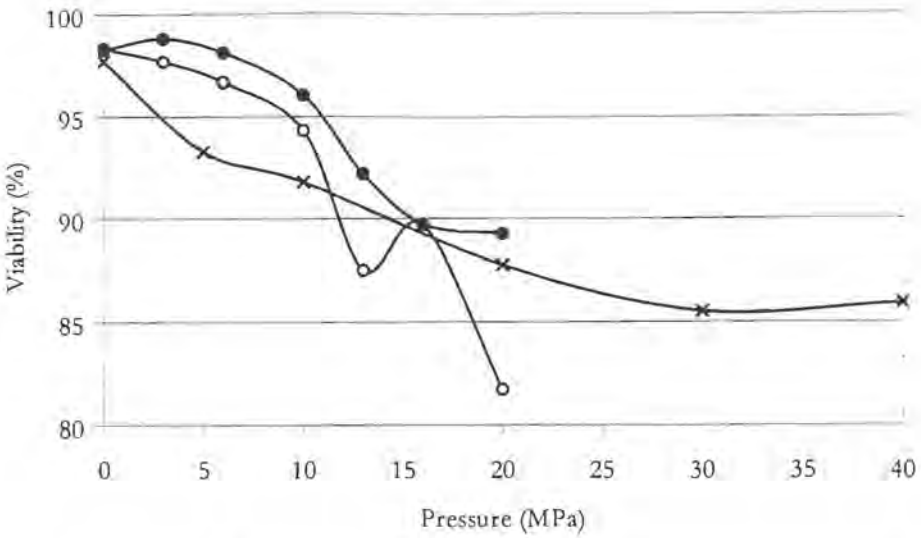

Figure 5.6. Comparison of viability of 6th generation production yeast and laboratory grown SAB5 following French Press treatment.

(● aerobic laboratory SAB5, ○ anaerobic laboratory SAB5, X 6th generation SAB5 production yeast)

When comparing the laboratory propagated yeast to the 6th generation production yeast, the aerobic laboratory propagated yeast retains a higher viability than either of the anaerobic yeasts. The anaerobic laboratory propagation remains more viable under mild pressures (0 - 20 MPa) than the 6th generation production yeast but approaches the same level of viability within the range between 83 and 87% at pressures greater than 20 MPa. The intermediate response of anaerobic laboratory propagated yeast may result from its more recent exposure to oxygen at the start of propagation compared to the 6th generations repeated exposure to low oxygen availability at the start of fermentation followed by long periods of exposure to a complete anaerobic environment.

5.4 Effect of Sub-Lytic Pressures on Yeast Surface

Considering the results of cell disruption presented in Section 5.3.1 as well as the release of intracellular protease (Section 5.3.2), both of which show negligible effect on cell wall and membrane integrity at low operating pressures in the French Press, a 'critical' pressure is required to achieve significant cell disruption. Disruption above this pressure may result from rapid pressure release, shear forces or cavitation. The shear forces below the critical pressure may cause rearrangement of the outer cell wall surface. Hence the effect of exposure to the French Press at sub-lytic pressures on cell surface properties and composition were studied. For laboratory propagated yeasts, the critical pressure for disruption is 6 – 10 MPa while that for the 6th generation production yeast the critical pressure was found to be 20 MPa.

5.4.1 Hydrophobicity

Changes in the hydrophobicity of laboratory propagated yeast following French Press treatment were investigated using strain SAB5 (Figure 5.7) and the 6th generation SAB5 production yeast (Figure 5.8). No change in hydrophobicity was observed on exposure of the laboratory propagated or production yeast to the French Press. Of note is the similarity in hydrophobicity index between the laboratory propagated anaerobic yeast and the 6th generation production yeast which has been exposed to repeated short aerobic/long anaerobic environments. The extent of hydrophobicity which develops in the anaerobic environment of the laboratory propagation system therefore appears to be the maximum extent of hydrophobicity which the yeast strain can develop.

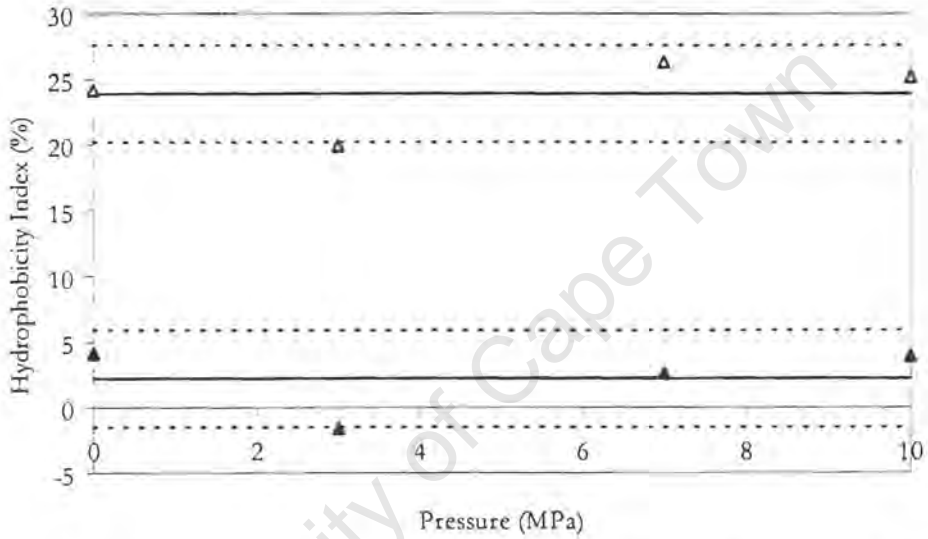

Figure 5.7. Hydrophobicity of laboratory propagated SAB5 following French Press treatment.

(▲ aerobic, Δ anaerobic, — average, - - - - standard deviation of assay)

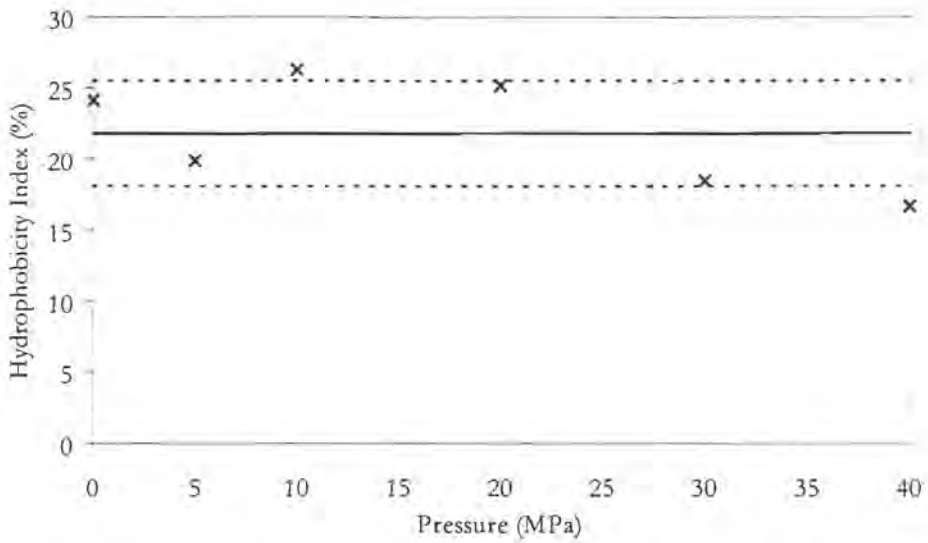

Figure 5.8. Hydrophobicity of 6th generation production yeast following French Press treatment.

(X 6th generation production yeast, — average, - - - - standard deviation of assay)

5.4.2 Surface Charge

5.4.2.1 Zeta Potential

The zeta potential of the four strains grown under the two oxygen availabilities in the laboratory and the 6th generation production yeast were measured across a pH range between 2.1 and 6.9 after being subjected to French Press treatment. Pressures of 0, 3, 6 and 10 MPa for the laboratory yeasts and 0, 5, 10 and 20 MPa for the production yeast were used to achieve sub-lytic conditions in the French Press. These results are plotted as zeta potential – pH profiles, illustrated in Figures 5.9 – 5.13, yielding sigmoidal profiles.

An anomaly was noted in the zeta potential measurements of the anaerobic propagations of strains SAB5 and SAB1 at the pH 2.1. A decrease in zeta potential is observed on decrease of pH from pH 3 to pH 2.1. This is attributed partly to the instability of the measurements taken at this low pH and partly to the higher ionic strength associated with this pH. Using a background electrolyte/buffer solution made up to a sodium acetate concentration of 20 mM, the drop in pH from 6.6 to 2.1 resulted in a change in ionic strength of 20 % from 0.04 molar to 0.048 molar. The effect of a higher ionic strength is to lower the measured zeta potential. At pH 3.0 error induced by increased ionic strength is 2.5 %. This error is insignificant at the higher pH values. The individual ionic strengths at specific pH values are taken into account when calculating the surface charge composition information, hence no error is propagated beyond this point in the analysis.

The general trend observed is that there is little or no change to the profiles of the aerobic propagations while an increase in the slope of the anaerobic profiles is observed. This is the result of the surface becoming more chargeable after the French Press treatment. This postulation is investigated further in the charge group composition analysis Section 5.4.2.2.

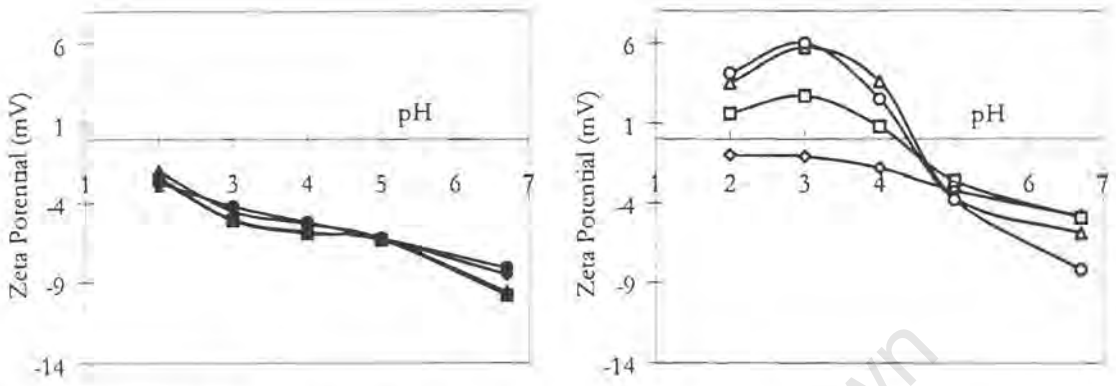

Figure 5.9. Zeta potential – pH profiles of laboratory propagated SAB1 following French Press exposure.

(♦ aerobic 0 MPa, ■ aerobic 3 MPa, ▲ aerobic 6 MPa, ● aerobic 10 MPa, ◊ anaerobic 0 MPa, □ anaerobic 3 MPa, Δ anaerobic 6 MPa, ○ anaerobic 10 MPa (a) aerobic, (b) anaerobic)

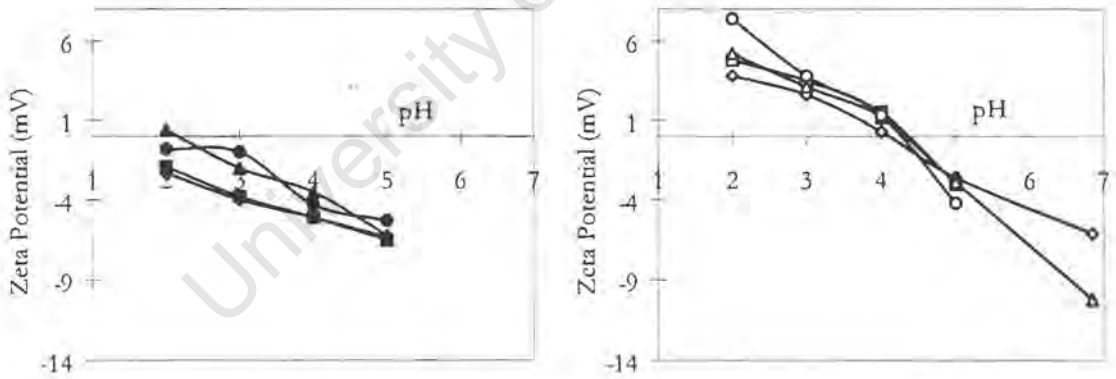

Figure 5.10. Zeta potential – pH profiles of laboratory propagated SAB1/96 following French Press exposure.

(♦ aerobic 0 MPa, ■ aerobic 3 MPa, ▲ aerobic 6 MPa, ● aerobic 10 MPa, ◊ anaerobic 0 MPa, □ anaerobic 3 MPa, Δ anaerobic 6 MPa, ○ anaerobic 10 MPa (a) aerobic, (b) anaerobic)

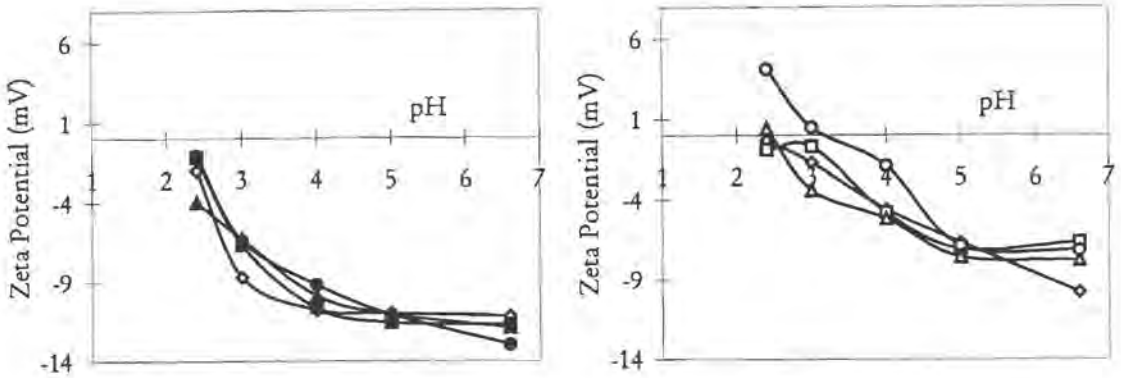

Figure 5.11. Zeta potential - pH profiles of laboratory propagated SAB2 following French Press exposure.

(♦ aerobic 0 MPa, ■ aerobic 3 MPa, ▲ aerobic 6 MPa, ● aerobic 10 MPa, ◊ anaerobic 0 MPa, □ anaerobic 3 MPa, Δ anaerobic 6 MPa, ○ anaerobic 10 MPa (a) aerobic, (b) anaerobic)

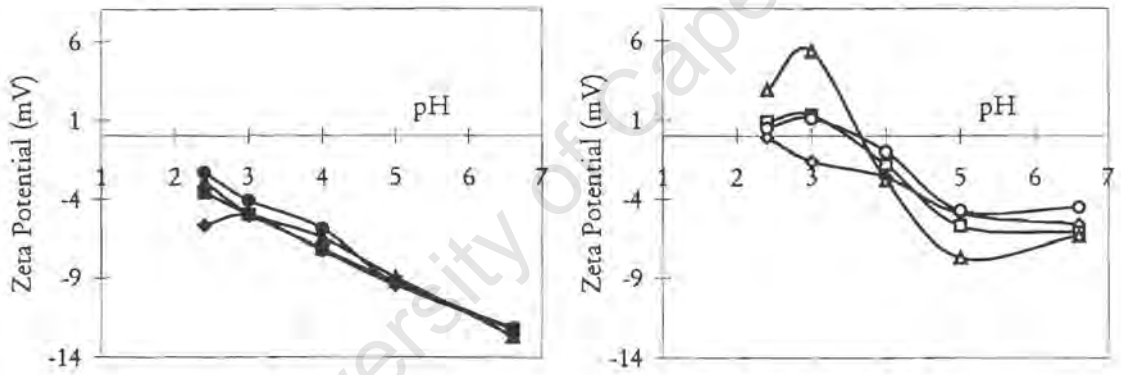

Figure 5.12. Zeta potential - pH profiles of laboratory propagated SAB5 following French Press exposure.

(♦ aerobic 0 MPa, ■ aerobic 3 MPa, ▲ aerobic 6 MPa, ● aerobic 10 MPa, ◊ anaerobic 0 MPa, □ anaerobic 3 MPa, Δ anaerobic 6 MPa, ○ anaerobic 10 MPa (a) aerobic, (b) anaerobic)

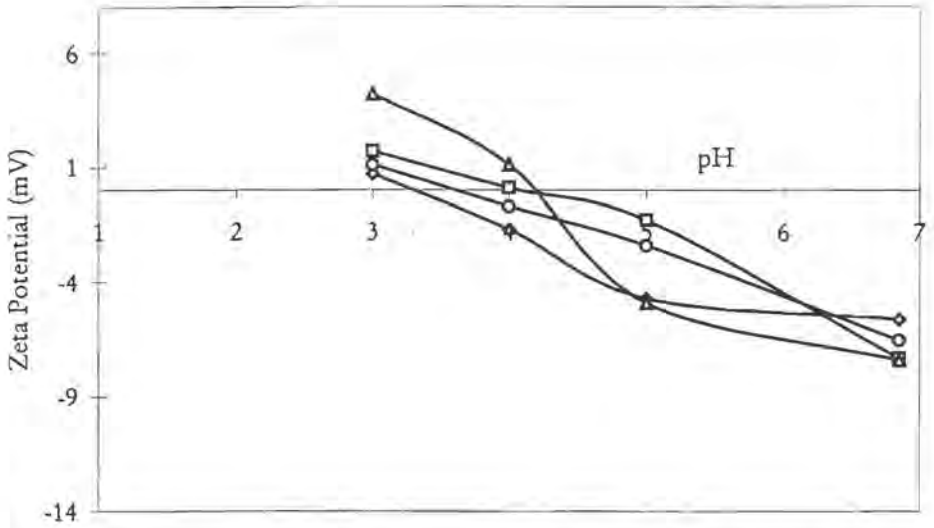

Figure 5.13. Zeta potential – pH profiles of 6'th generation SAB5 production yeast following French Press exposure.

(◊ 0 MPa, □ 5 MPa, Δ 10 MPa, ○ 20 MPa)

5.4.2.2 Charge Group Composition

The surface charge group composition of the yeasts were calculated from the zeta potential – pH profiles provided in Section 5.4.1.1. The total number of chargeable groups (N_s) and ratio of phosphate to carboxyl groups (q) for the 8 laboratory propagated and the 6th generation production yeast following French Press treatment are presented in Figures 5.14 – 5.18.

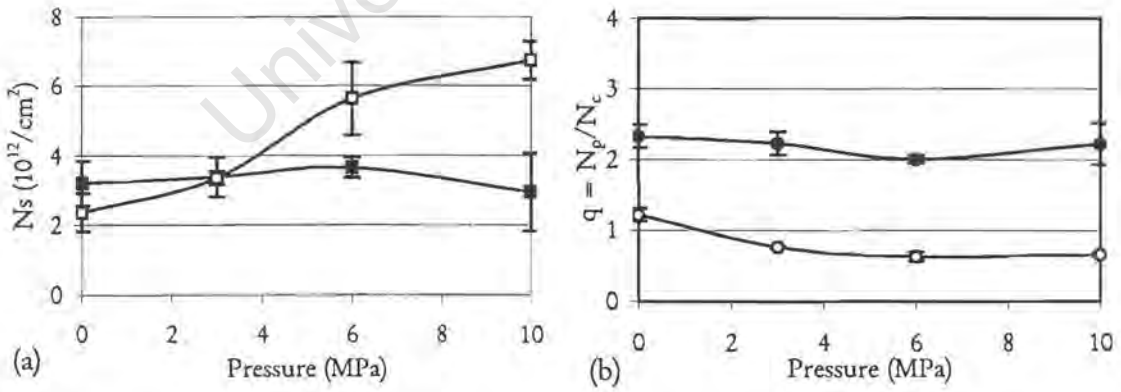

Figure 5.14. Charge group composition of laboratory propagated SAB1 following French Press exposure.

(■ aerobic N_s, ● aerobic q, □ anaerobic N_s, ○ anaerobic q)

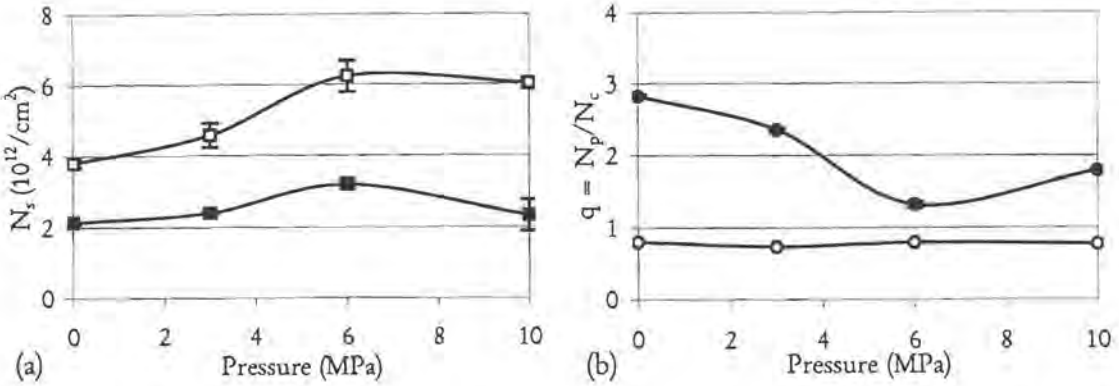

Figure 5.15. Charge group composition of laboratory propagated SAB1/96 following French Press exposure.

(■ aerobic N_s, ● aerobic q, □ anaerobic N_s, ○ anaerobic q)

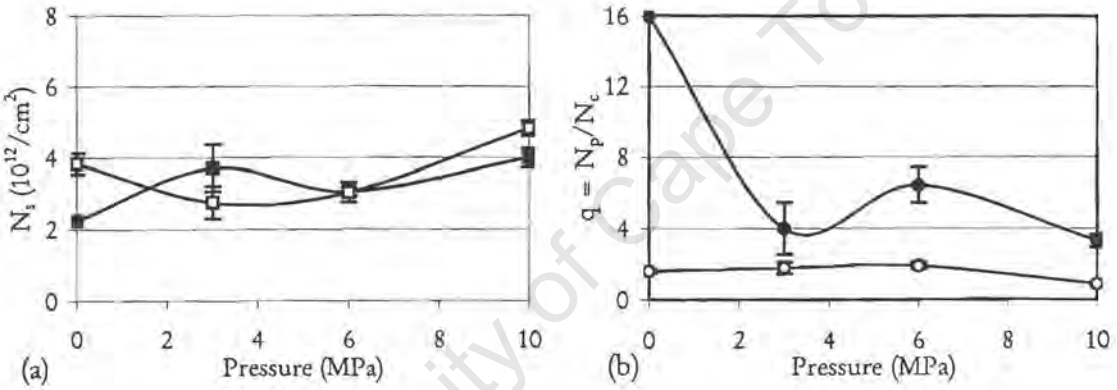

Figure 5.16. Charge group composition of laboratory propagated SAB2 following French Press exposure.

(■ aerobic N_s, ● aerobic q, □ anaerobic N_s, ○ anaerobic q)

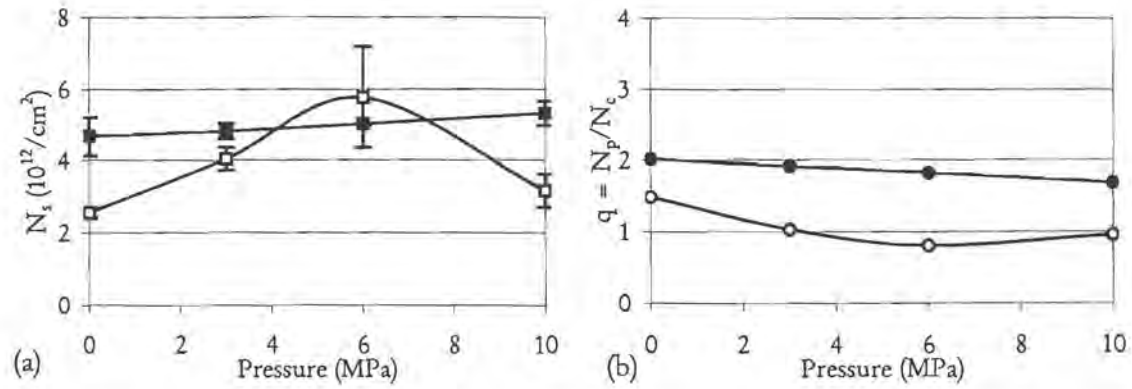

Figure 5.17. Charge group composition of laboratory propagated SAB5 following French Press exposure.

(■ aerobic N_s, □ anaerobic N_s, ● aerobic q, , ○ anaerobic q)

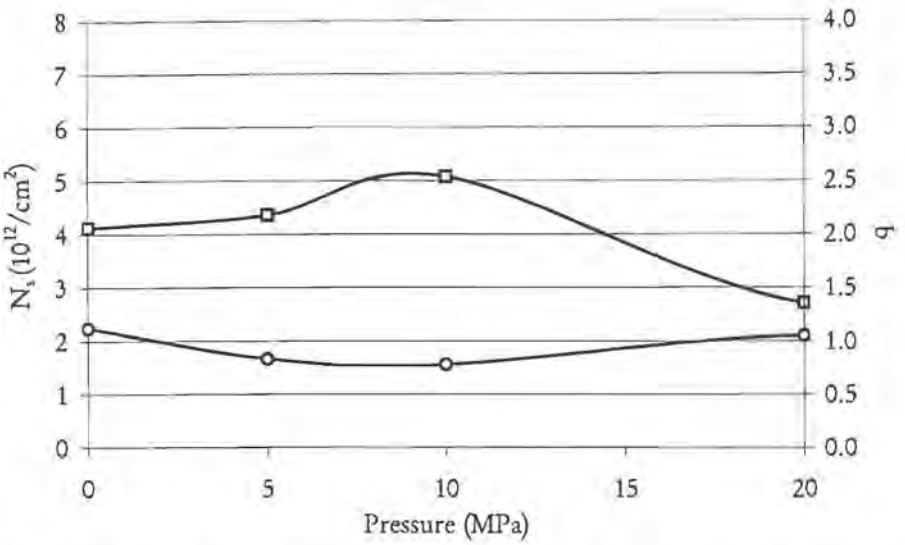

Figure 5.18. Charge group composition of 6th generation production yeast following French Press exposure.
(□ N_s, ○ q)

From the results presented, it is seen that the response of the aerobic and anaerobic laboratory propagated yeasts to French Press treatment differs. The total number of chargeable groups (N_s) among the aerobic yeasts appears to be unchanged by the shearing action of sub-lytic French Press treatment. Three of the anaerobic yeasts (SAB5, SAB1 and SAB1/96) show an increase in N_s values with increasing pressure in the sub-lytic region after which the total number of chargeable groups decreases. In a similar trend the 6th generation production yeast showed an increase in the total number of chargeable groups with increasing pressures in the French Press until 10 MPa. Thereafter, N_s decreased to a value below that of the original unsheared yeast obtained from the brewery.

The ratio of phosphate to carboxyl groups (q) for all the yeasts was either unchanged or showed a decrease with increasing shear intensity. Strains SAB1 and SAB5 had decreasing q-values (in the range 1.5 – 0.6) for the anaerobic yeasts after French Press action while the q-value of the aerobic yeasts of these strains remained the same, unaffected by the mechanical handling. The aerobic yeasts of strains SAB1/96 and SAB2 showed decreased q-values while the anaerobic yeasts were not affected. The aerobic variant of the non-flocculent strain of SAB2 showed the most dramatic change in q-value (a decrease from 16 to 4 over a pressure range 0 to 3 MPa). This strain developed an abnormally high q-value towards the end of its propagation. (q value of 16 compared to q values of 2.8 – 9.0 at the end of propagation of other strains).

In summary, the aerobic yeasts generally became more chargeable following exposure to the shearing action produced in the French Press. Since shear forces alone can not produce new charge groups, it

must be concluded that the shear forces caused the removal of groups from the surface which were not chargeable (e.g. mannan), thereby exposing chargeable groups. The constancy or slight decrease in q-value indicates that the ratio of phosphate to carboxyl groups remains approximately constant or a small loss of phosphate groups occurs.

The interesting situation of SAB2 which showed the dramatic decrease in q-value for the aerobic yeast requires further discussion. This strain is designated non-flocculent, showing less than 5 % flocculation according to the flocculation assay used in this study. As discussed in Section 2.4.3, proteinaceous lectins and 2 – 3 chain mannose residues forming part of the phosphomannan outer layer are required for flocculation of flocculent yeasts. Stratford (1992a) used *mnn* mutants with truncated side branches of phosphomannan to investigate the effect of these short side chains on flocculation. Of particular note was strain *mnn2* which was void of all side branch mannan and phosphate and was not able to be co-flocculated by other flocculent strains or aggregated by concanavalin A, a lectin with similar specificity to yeast flocculins. Natural phosphomannan has a 'feathery' structure with its many short side chains and few phosphate groups. A strain with few or no side chains would have a proportionally higher phosphate content from the lipids in the cell wall and hence a higher q value because it would not be shielded by the mass of non-chargeable mannan residues. Such a strain would also appear non-flocculent because of the lack of short chain mannose residues.

From the differences in the response of the four strains of yeast to French Press treatment in terms of their hydrophobicity and surface charge, one can conclude that these surface properties are produced by distinctly different surface components. The hydrophobicity of yeast from both aerobic and anaerobic laboratory propagations being unaffected by shear while the surface charge showed an increase in the concentration of chargeable groups and slight decrease in ratio of phosphate to carboxyl groups.

5.4.3 Flocculation

The flocculation process may be attributed to the interaction of genetically encoded flocculins and carbohydrate receptor sites (dominant among flocculent strains) and to attractive forces governed by hydrophobicity and surface charge (dominant in non-flocculent strains). Changes in the surface charge of yeast have been observed on mechanical handling in the French Press, while shear forces generated may remove or disrupt the structure of surface located flocculins and receptor sites. Hence it may be postulated that the extent of flocculation of yeast may be affected by French Press treatment. The extent of flocculation of the laboratory propagated yeast and 6th generation production yeast following French Press treatment is presented in Figures 5.19 and 5.20 respectively.

The aerobically propagated SAB5 is more flocculent than the anaerobic equivalent (0 MPa values in Figure 5.19). On subjection to French Press treatment, however, the aerobic yeast loses its flocculence more rapidly than the anaerobic yeast. This can be seen from the data at 3 MPa where the anaerobic yeast is four times as flocculent as the aerobic yeast. This is supported by data generated at higher pressures. The aerobic yeast has been rendered non-flocculent (< 10%) in the pressure range 3 - 10 MPa. The anaerobic yeast is more than 40 % flocculent at 3 MPa but this flocculence is gradually eroded at higher pressures to approximately 12 % at 10 MPa.

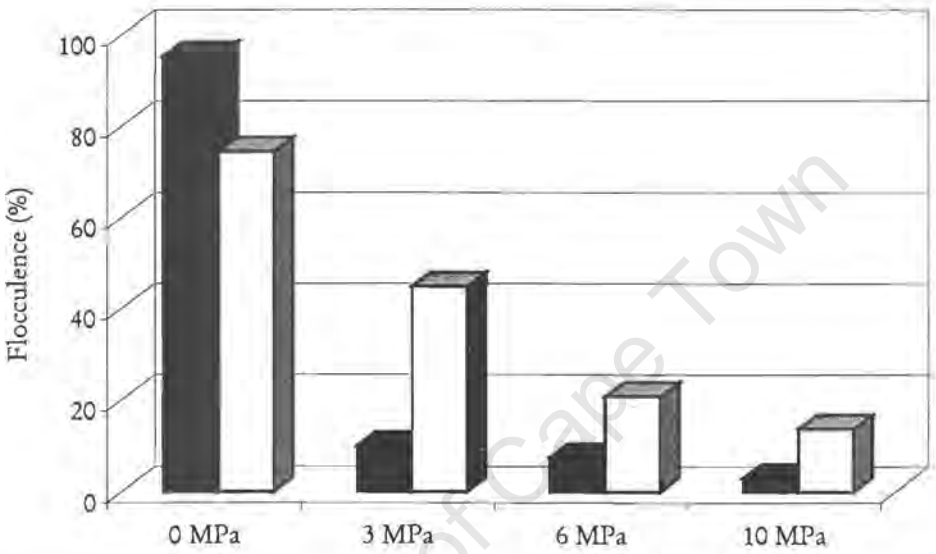

Figure 5.19. Flocculation of laboratory propagated SAB5 following French Press treatment. (■ aerobic propagation□ anaerobic propagation)

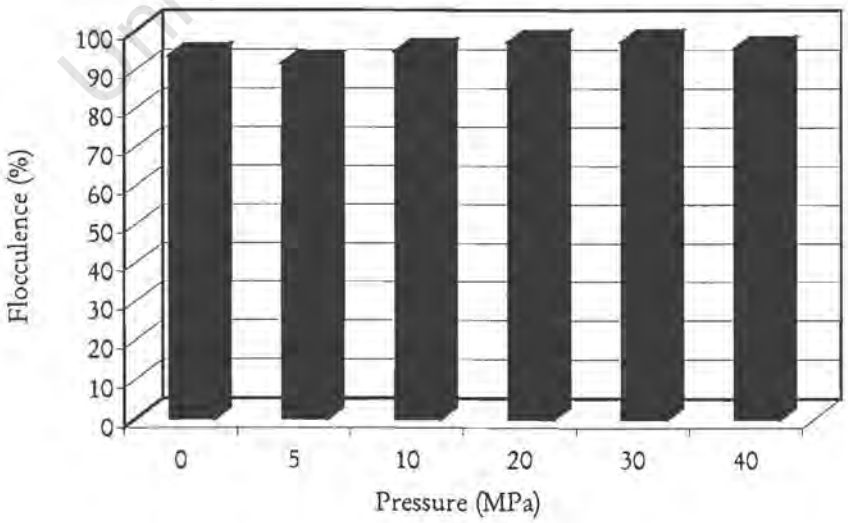

Figure 5.20. Flocculation of 6th generation production SAB5 following French Press treatment.

The 6th generation production yeast SAB5 is more flocculent than the anaerobically propagated laboratory yeast. Its flocculence is similar to that of the aerobic yeast, despite being subjected to anaerobic conditions. This difference may result from serial selection for more flocculent yeast through the cropping of settled yeast in the previous six transfers. The production yeast did not illustrate shear sensitivity with respect to flocculence, remaining highly flocculent (> 80 %) across the range of pressures investigated (5 – 40 MPa). The extent of flocculation of the 6th generation production yeast is higher (greater than 90 %) than the first generation yeast produced in the small scale fermenters (40 %). Several factors account for the difference in flocculation behaviour. The flocculence of the production yeast is that of the settled yeast whereas the laboratory yeast is the average of settled and suspended cells. The 6th generation yeast is the product of a flocculation concentration effect resulting from the cropping of settled flocculated yeast over successive generations with the less flocculent cells staying in suspension at the end of each fermentation. The time the yeast remains within the laboratory fermentations (10 days) is also longer than the typical time in the production fermenters (4 – 5 days) which would also exaggerate the selection of highly flocculent yeast in the production fermenters. Furthermore the geometry and scale of the fermenter may influence the yeasts' flocculation potential.

5.4.4 Fermentation Performance of Laboratory Propagated SAB5 Following Exposure to the French Press

The fermentation performance of the yeast exposed to the French Press was analysed with the aim of determining if hydrodynamic shear damage to yeast cells can alter the fermentation capacity of the yeast. This was achieved by determining the rate of fermentation (decrease in wort density). The beer quality indicators of SO_2, pH and diacetyl were not considered in this study.

5.4.4.1 Fermentation rate

The rate of decrease in density was used as the primary indicator for rate of fermentation to provide a measure of sugar utilisation. A rate constant was determined, based on the logistic expression (Equation 3.10). Fermentations were performed in replicate with 3, 2, 2 and 1 fermentations being performed for the 0, 3, 6 and 10 MPa experiments respectively. The fermentations were inoculated to give an initial viable cell concentration of 7.5 x 10^6 cells/ ml. The data are presented in Figure 5.21. The aerobic variant of the freshly propagated yeast had a higher initial fermentation rate than the anaerobically propagated yeast. This advantage which the aerobic propagation method has over anaerobic yeast is, however, lost upon French Press exposure. Variation in the fermentation performance following aerobic and anaerobic growth is insignificant following exposure to the French Press.

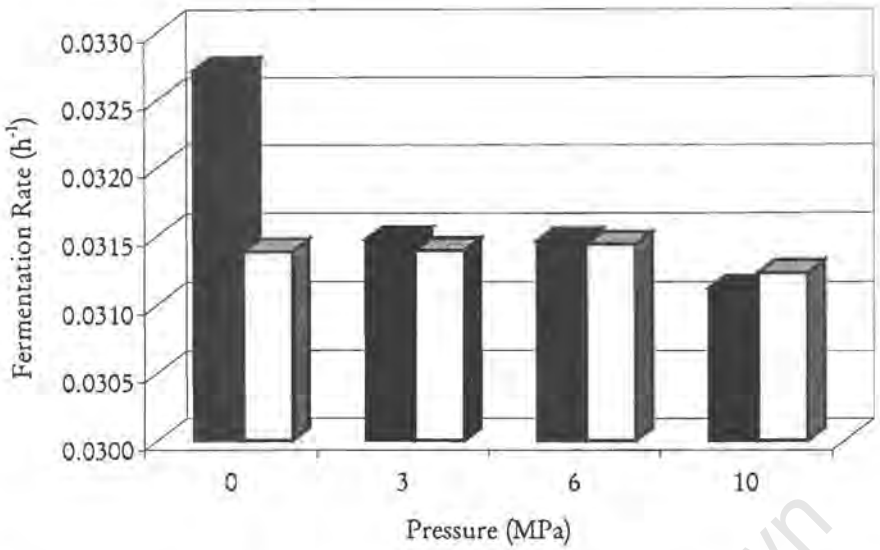

Figure 5.21. Comparison of fermentation rate of SAB5 following exposure to the French Press at increasing pressure.

(■ aerobic propagation□ anaerobic propagation)

5.4.4.2 Recovery of flocculation potential

The flocculation potential of the yeast is the parameter which determines the clarity of the beer following primary fermentation. Since a loss of flocculence was reported as a result of shear damage to the yeast in the French Press, it is important that the yeast is able to recover its flocculence during a subsequent fermentation. At the end of fermentation (day 10), the yeast was collected by removing the complete wort/yeast mixture. The yeast was then concentrated by centrifugation and prepared for the flocculation assay. The flocculence determined before and after fermentation for the aerobically and anaerobically propagated yeasts are given in Figure 5.22. Yeast which was not passed through the French Press under pressure was more flocculent before fermentation than on day 10 of the laboratory fermentation. The 0 MPa data points indicate that flocculence of the aerobic and anaerobically propagated yeasts fell to approximately 40% on day 10 of fermentation from pre-fermentation values of 90 and 70 % respectively. Flocculence of yeast damaged in the French Press was recovered during fermentation, resulting in approximately 40% flocculence following fermentation (compared to less than 10% pre-fermentation). The aerobically propagated yeast exposed to the French Press at 10 MPa remained an exception, recovering only 28% flocculence. The lower flocculence of the aerobic 10 MPa experiment may result from the low flocculence (< 5%) at the beginning of fermentation.

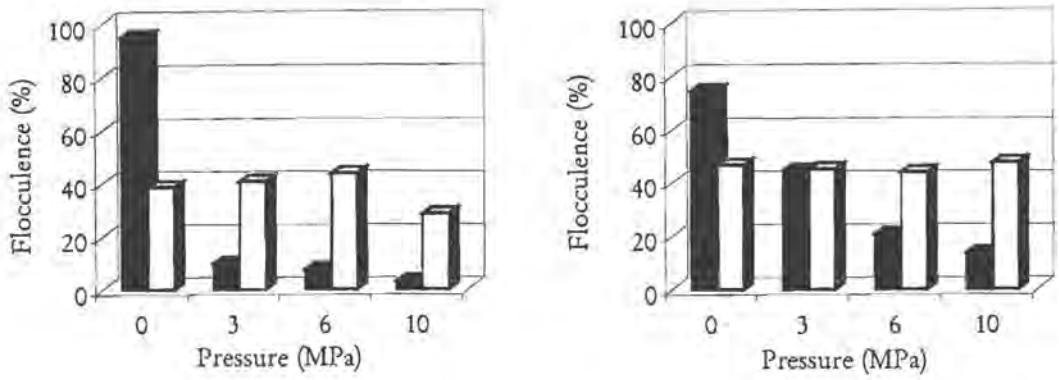

Figure 5.22. Flocculence of laboratory propagated yeast directly after French Press exposure and after a subsequent fermentation.

(■start of fermentation, □ end of fermentation, (a) aerobically propagated yeast, (b) anaerobically propagated yeast)

5.4.5 Surface Chemical Composition

The surface elemental and bond concentrations were determined (according to Section 3.4.2) for laboratory propagated yeast strain SAB5, following damage in the French Press. The results are tabulated in Table 5.4 for the aerobic yeasts and Table 5.5 for the anaerobic yeasts. For the aerobic yeasts the only significant (> 95% significance) difference in chemical composition is the increase in nitrogen content from 2.15 to 2.5 %. The oxygen and carbon concentrations and the various bond concentrations of these elements of the yeast exposed to the French Press are not significantly different from the undamaged yeast.

Table 5.4. Elemental and bond composition of the surface of aerobic laboratory propagated SAB5 yeast following exposure to the French Press.

Element	Bond	0 MPa	3 MPa	6 MPa
Carbon		69.7	68.2	69.9
	C-(C,H)	35.3	32.1	40.6
	C-(O,N)	27.9	29.8	23.6
	C=O	6.5	6.3	5.7
Oxygen		28.1	29.4	27.6
	O-(C,H)	24.6	26.8	23.7
	O=C	3.5	2.6	3.9
Nitrogen		2.15	2.49	2.51

Table 5.5. Elemental and bond composition of the surface of anaerobically propagated SAB5 yeast following exposure to the French Press.

Element	Bond	0 MPa	3 MPa	6 MPa
Carbon		72.7	72.8	70.6
	C-(C,H)	40.8	43.7	39.5
	C-(O,N)	24.2	24.2	24.9
	C=O	7.6	4.9	6.2
Oxygen		24.2	24.5	26.5
	O-(C,H)	19.8	21.6	24.2
	O=C	4.6	2.8	2.3
Nitrogen		2.92	2.72	2.92

For anaerobically propagated yeast, the carbon double bonded to oxygen (C=O) concentration appears to have decreased following shear damage as can be seen by the decreased concentration of this bond, from 7.6 to 4.9 and 6.2 for the 3 and 6 MPa data points respectively. Clear differences can not be made using the remaining two carbon bond compositions of C-(C,H) and C-(O,N). The amount of oxygen at the surface is increased from 24.2 for the fresh yeast to 26.5 % for the 10 MPa data point. The ratio of oxygen which is singly bonded to carbon to that doubly bonded changed from 4.5 at 0 MPa to 7.5 at 3 MPa and finally to 10.5 at 6 MPa. The greater number of changes to elemental composition of the anaerobic yeast is in keeping with the changes in surface properties and flocculation already observed. To more fully understand the observed changes, the molecular composition of the aerobic and anaerobic yeasts were calculated and these are presented in Figure 5.23 and 5.24 respectively. The only appreciable trend observed in the aerobically propagated yeast is the increased protein concentration which changed from 13 % to 15 % following hydrodynamic shear in the French Press. A decreased lipid and increased mannan concentration was observed in the anaerobically propagated yeast following exposure to the French Press.

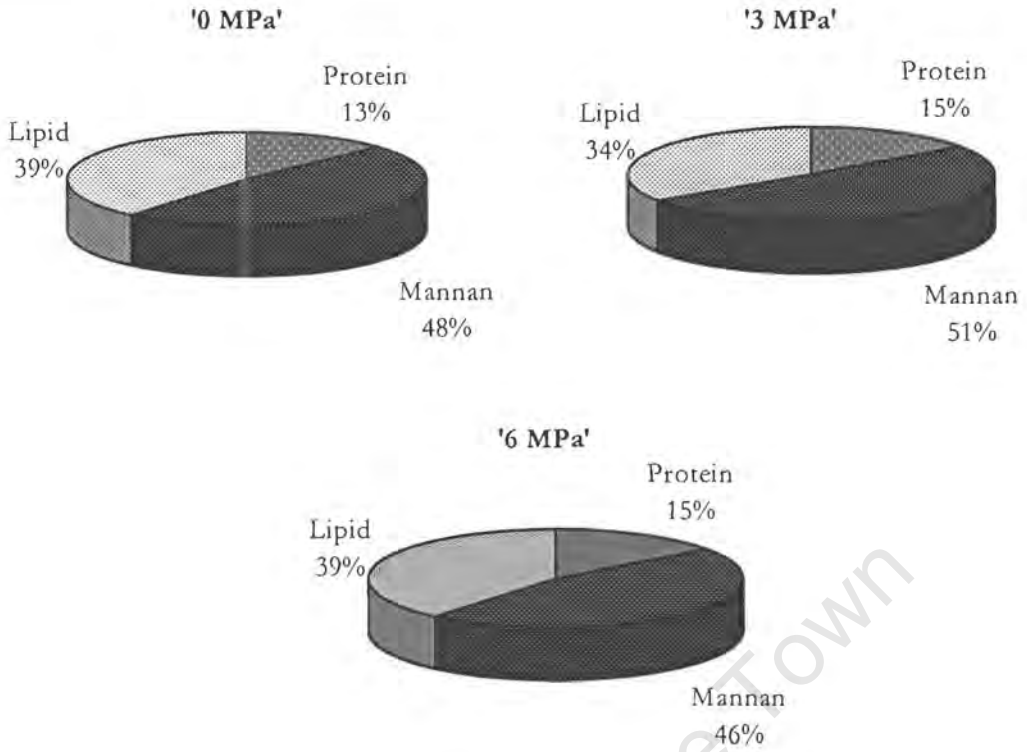

Figure 5.23. Molecular composition of aerobically propagated laboratory yeast of strain SAB5 following exposure to the French Press.

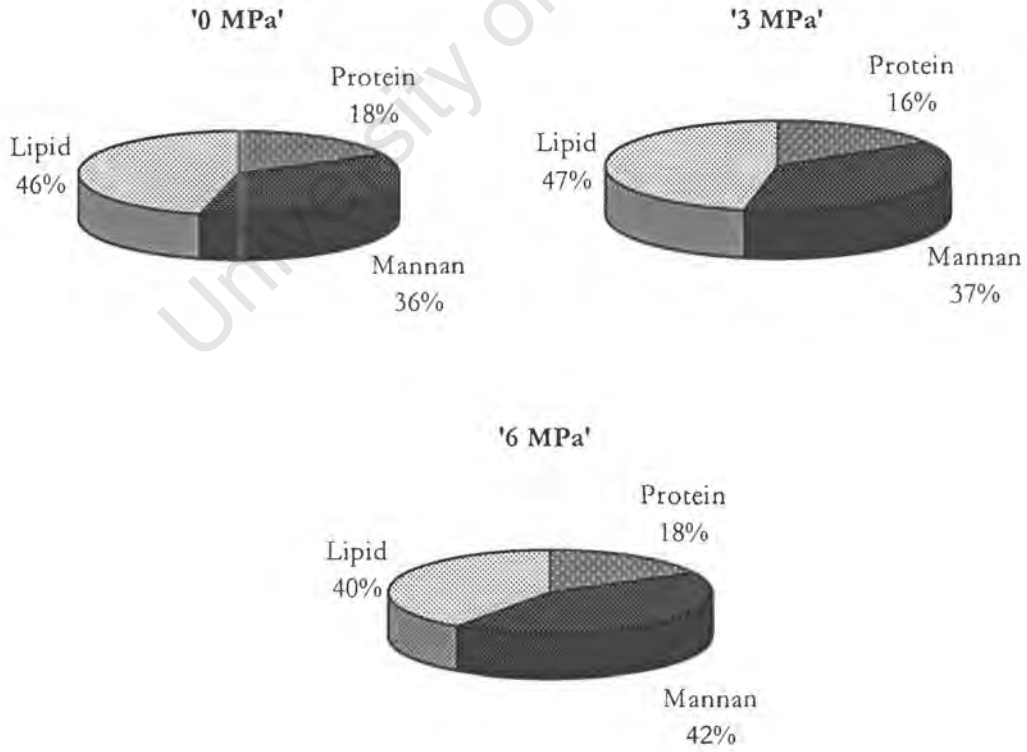

Figure 5.24. Molecular composition of anaerobically propagated laboratory yeast of strain SAB5 following exposure to the French Press.

The loss of flocculence observed when yeast was exposed to shear in the French Press would have been brought about by a loss of either flocculin proteins, mannan receptor sites or a loss of functionality of these groups. An alternative postulation for the reduction in flocculation potential resulting from the loss of ligand/receptor site functionality could be the generation of free radicals during cavitation altering the structure of these molecules. The loss of these molecules may have been correlated to changes in the protein, mannan or their ratio but was not observed. The possibility therefore exists that the ligand and receptor sites might become deactivated by the shearing action of the French Press or that the changes are too small to be detected by total protein and mannan concentrations. Likewise, changes in surface chargeability do not correlate to any changes in molecular composition. The surface analysis is therefore not sufficiently detailed to detect the changes detected by altered surface charge, hydrophobicity and flocculence.

5.5 Summary

The French Press was successfully used as a device capable of generating energy dissipation rates in excess of 10^8 $m^2.s^{-3}$ although the total energy dissipation was relatively small (0.25 J) due to the short exposure times (~ 10^{-5} s). This resulted in Kolmogorov eddies of size smaller than 0.3 μm travelling at velocities of more than 4 $m.s^{-1}$. The turbulence thus generated can accurately be described as isotropic and since the smallest eddy size is smaller than the mean cell size (6.65 μm), the energy dissipation is able to be transferred to the cells. The efficiency with which the French Press converted total pressure release into Reynolds stress that acts on the cell surface was high at 94.5 %.

Within the French Press, a range of pressures was identified which did not cause cell disruption. Within the range from 3 to 6 MPa, the laboratory propagated yeast could be studied to investigate the effect of sub-lytic shear conditions on the cell. For a 6th generation production yeast, the critical disruption pressure was higher than for laboratory propagated yeast at 20 MPa. Membrane permeabilisation was found to occur at lower operating pressures, although to a lesser extent at sub-lytic pressures. The laboratory grown cultures released protease at 6 MPa with the aerobically grown yeast having between 1.6 and 6.1 fold higher specific protease content than the anaerobic yeasts. The production yeast had the lowest specific protease content, 8 times lower than the anaerobic laboratory yeast of the same strain. The intact cell viability of aerobic cultures was more resilient than anaerobic cultures although there was a general high viability (> 80 %) even though between 40 and 60 % of the cells were disrupted. The production yeast was more susceptible to a loss of viability than the laboratory yeasts at the lower pressures (< 10 MPa) where the production yeast did not suffer from any appreciable disruption.

The sub-lytic pressures were used to investigate changes in surface properties as a result of shear stress. No change to hydrophobicity was observed in aerobic, anaerobic and production yeasts studied on exposure to French Press treatment. Surface charge was found to be affected when the yeast was grown anaerobically with the production yeast behaving similarly to the anaerobically grown yeast. These showed a broadening of the zeta potential – pH profile across the range from 2.2 to 6.8. This trend was backed-up by an increase in the total number of chargeable groups at the surface, N_s. The ratio of phosphate to carboxyl groups (q value) of these yeasts also showed changes with a general decrease being observed. The flocculence of the yeast was found to be decreased by the exposure to the French Press, with the aerobic yeast being more susceptible to a loss of flocculence than the anaerobically grown yeast. The production yeast did not show any effect of shear damage on flocculence in the French Press.

The fermentation performance of the yeast exposed to shear in the French Press was found to be limited to a reduction in fermentation rate for the aerobic yeast. The rate of fermentation of all anaerobically grown samples at the different operating pressures as well as the aerobically propagated yeast at 3, 6 and 10 MPa all had the same value which was lower than the undamaged aerobic culture.

Chapter 6: Centrifugation

6.1 Introduction

In the brewing industry at large, centrifuges are used for three main purposes. Firstly, beer can be recovered from spent yeast in a high biomass concentration separation. Secondly, trace yeast can be removed from beer prior to storage and/or filtration and bottling, this being a low biomass concentration process. In both of these situations it is the beer quality which should remain high. A third situation can arise where yeast does not agglomerate during fermentation, either through the use of non-flocculent strains or where fermentation is arrested early by the yeasts' removal, for the production of low and non-alcoholic beers. In this case too, a pure and unchanged clarified beer stream is to be produced by the centrifuge as well as an undamaged yeast concentrate stream for re-use in further fermentations.

Centrifuges have been introduced at a number of the breweries operated by South African Breweries to aid the partial removal of suspended yeast at the end of primary fermentation before lagering begins. For this operation the centrifuge reduces the free yeast cell concentration at the end of fermentation from 5-8 x 10^6 to 1-2 x 10^6 cells/ml. The biomass recovered in this process is discarded and the partially clarified beer is pumped to the storage cellars where secondary fermentation (lagering) takes place. Since the yeast separated to the concentrate stream is not the valuable product, it's 'quality' is not a major concern, however, damage to the remaining yeast in the clarified stream is to be avoided. Additionally, damage of the concentrate yeast could be potentially harmful to the beer. As seen from the French Press treatment of yeast in Section 5.3, damage can manifest itself as cell disruption with a subsequent release of intracellular products such as proteins, proteases and complex carbohydrates. These substances may negatively impact on foam stability and can cause carbohydrate/protein complexes which results in beer haze. More subtle forms of damage

are caused by abrasion of the cells resulting in the outer layers of the cell wall breaking away, forming fine particles not easily removed from the beer in either the centrifuge or subsequent sedimentation and filtering processes. Such damage to the outer surface of the yeast also alters the flocculation properties as well as surface charge and hydrophobicity of the cells.

In this chapter, the hydrodynamic flow patterns in the centrifuge are first described with the aim of identifying different regions within the centrifuge which can cause shear stress and damage the yeast cells. Thereafter the separation efficiency of the disc stack centrifuges is presented and compared to literature values. Evidence for the damaging effect of centrifugation on yeast is provided in terms of the possible shear regions within the centrifuge and compared with other reports of damage to biological particles upon centrifugation.

6.2 Disc Stack Centrifuges

The use of disc stack centrifuges have been widely reported for solid-liquid separation in the biotechnological field. The applications include *E. coli* (Wong *et al.*, 1997), mammalian hybridoma cells (Kempken *et al.*, 1995), yeast homogenate (Mosqueira *et al.*, 1981), inclusion bodies (Jin *et al.*, 1994) and whole yeast cells (Siebert *et al.*, 1987). Despite the widespread use of centrifugation for the separation of biological particles, few reports analyse the potential for biological cell damage in the centrifuge. To interpret loss of yeast quality, in the centrifuges, the flow pattern needs to be understood and analysed in terms of the operating parameters.

6.2.1 Description of Flow Patterns in Disc Stack Centrifuges

High separation efficiencies within centrifuges are best achieved by minimisation of the thickness of the liquid layer through which the particles settle. In general, this principle leads to the increased length of the centrifuge to accommodate high feed flow rates. By contrast, the disc stack centrifuges make use of the shallow liquid layer principle by the introduction of a number of closely packed conical discs into the bowl. This effectively reduces the sedimentation path of the solids and reduces the size and speed of the machine required for a given separation duty. The slurry is introduced through the central shaft to a distributor plate below the discs where it is deflected up through riser holes cut into the discs. The solids are concentrated on the undersides of these discs, moving radially outward to the collection zone against the outermost wall of the spinning bowl. Once the quantity of solids builds up to fill the solids hold-up space, the feed pump is stopped and nozzles open at the periphery of the bowl through which the solids are ejected due to the centrifugal pressure. The clarified liquid travels radially inward and collects against the outside of the feed pipe from where it is directed to the top of the centrifuge and removed by a centripetal pump. The operation is shown

diagrammatically in Figure 6.1 for the Westphalia SA 1 centrifuge which was set up to separate two immiscible liquids with different densities as well as remove solid particles.

The solids discharge system of these centrifuges can be operated in one of two ways. The frequency of discharge can be regulated by setting the solids residence time manually or electronically by the detection of solids in the clarified stream. By setting a desludge time interval shorter than that taken to fill the hold-up volume, the complete clarity of the clarified stream can be maintained. This form of operation, however, has the disadvantage of a prior knowledge requirement to set appropriate desludge intervals and limits flexibility of feed rate and concentrations. When the solids are discharged, the feed is shut off and the entire bowl contents (solids in the hold-up space as well as the liquid in the discs) are discharged through the nozzles. The mean outlet concentration will therefore vary depending on the feed rate, feed concentration and discharge frequency.

In the second mode of operation, the solids will fill the hold-up space and build up into the disc stack region until the solids front reaches the riser holes at which point they will 'breakthrough' into the clarified stream and trigger the desludge mechanism. In this mode, the mean outlet concentration will remain constant, irrespective of feed flow rate and feed solids concentration.

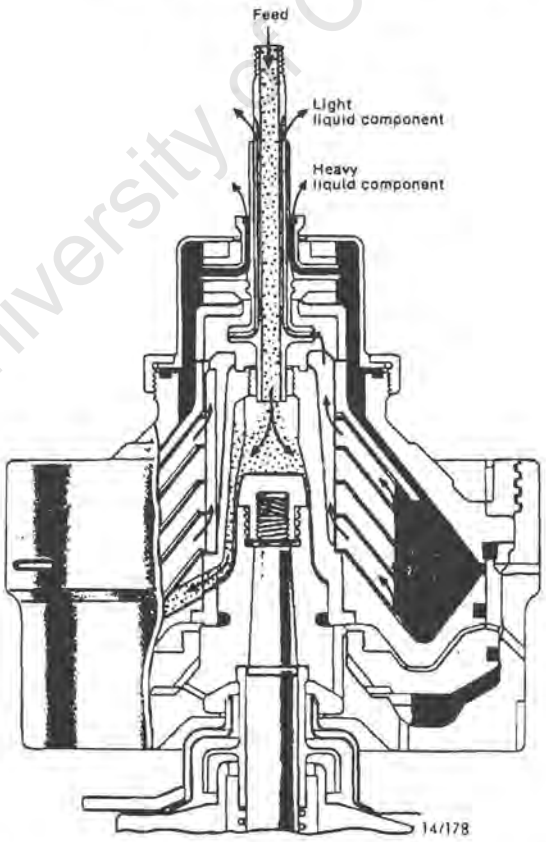

Figure 6.1 **Operating principle of the Westphalia SA 1 disc stack centrifuge.** (Westphalia SA 1 Instruction Manual)

6.2.2 Identification of Shear Zones

A closer inspection of the regions within the centrifuge reveals two distinct sub-processes in which solids are exposed to shear (Figure 6.2). The first is within the disc stack itself where solids are separated from the slurry by the high speed spinning discs. The second is the intermittent discharge of the collected solids through nozzles at the periphery of the bowl. In each of these regions the mechanism by which the cells are exposed to shear differs. By varying the operating parameters, the effect of shear in each of these regions is separable. During centrifuge operation, the parameters which determine the separation efficiency and shear characteristics are: feed solids concentration (C_{in}), feed flow rate (Q), solids discharge interval (τ) and centrifuge speed (N).

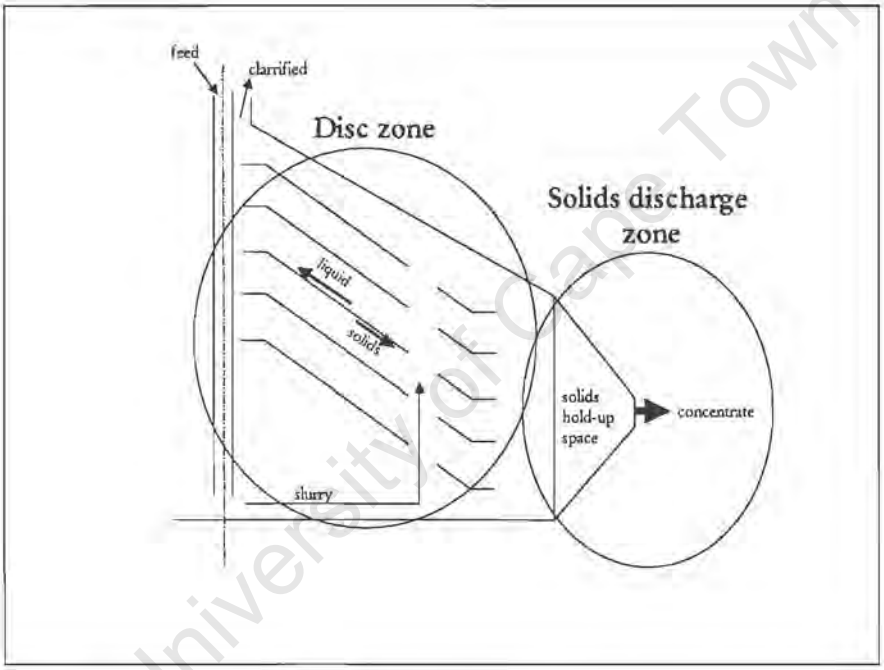

Figure 6.2 Flow pattern within a disc stack centrifuge.

Firstly within the disc zone, the parameters which influence shear are the rotational speed of the discs as well as the time spent by a cell in this zone. The inlet solids concentration affects the viscosity of the slurry. This influences both the shear and residence time of the cells in the disc zone. The feed flow rate will also impact on this disc zone residence time since higher flow rates result in the solid being transported closer to the centreline of the rotating disc bowl. The solids then have further to travel along the disc surface to reach the solids hold-up space. The parameters important for describing the disc zone shear are therefore N, C_{in} and Q.

In the desludge zone, the factors affecting shear are the mean concentration of the ejected concentrate stream (affecting the viscosity) and the force with which it is ejected. The solids

concentration is determined by the feed flow rate and concentration as well as the solids discharge interval while the rotational speed impacts on the ejection force. The shear characteristics of the solids desludge zone are therefore determined by N, C_{in}, Q and τ.

The solids discharge interval is the unique parameter which can be used to differentiate between the shear effects in the two zones. The effect of the solids discharge zone can therefore be studied by varying the desludge interval while maintaining constant feed concentration, feed flow rate and centrifuge speed. Trends observed on such plots would indicate a relationship between the biological response observed and the shear in the desludge zone.

Depending on the existence of cell damage in the solids discharge zone being established, there are two ways of studying the response in the disc stack zone. If cell damage in the solids discharge zone exists then one of either C_{in} or Q can be varied while maintaining the outlet solids concentration constant. Trends on such plots would indicate the existence of a shear effect in the disc zone. If no effect of solids discharge frequency on yeast quality is observed (thus indicating no effect of shear in the discharge zone) then variation of either C_{in} or Q while averaging the solids discharge intervals for the remaining two parameters will establish the existence of a disc stack zone effect.

When interpreting the various damage indicators, the above scheme is used to separate the shear effect of the two zones. Should the correlations described above not be observed then the existence of other zones of shear stress would be indicated.

In this study two types of Westphalia disc stack centrifuge, models SA 1-02-175 and OSC 4-91-006, were used, both supplied by GEA Process Technology SA (Pty) Ltd. The technical specifications of the centrifuges are summarised in Table 6.1 while the experimental equipment layout and conditions used in the trials are described in Section 3.3.3. The equivalent surface area of a centrifuge (Σ), defined as the surface area required by a gravity settler to achieve the same separation, is used as an indicator of separation capacity. For a disc stack centrifuge, Σ is calculated using Equation 6.1 (Perry *et al.*, 1984).

$$\Sigma = \frac{2\pi(n-1)(r_o^3 - r_i^3)\omega^2}{3g\tan\theta} \qquad (6.1)$$

where: n = number of discs

r_o = disc outer radius (m)

r_i = disc inner radius (m)

ω = angular velocity (rad.s^{-1})

θ = half included angle (°)

Table 6.1. Technical specifications of the Westphalia disc stack centrifuges.

Details	SA 1-02-175 (SA 1)	OSC 4-91-006 (OSC 4)
Bowl volume (l)	0.9	1.5
Solids hold-up volume (l)	0.25	0.9
Rotational speed (rpm)	4 000, 6875 & 9 800	9 000
Number of discs (n)	23	69
Disc inner radius (m)	0.0374	0.06
Disc outer radius (m)	0.0861	0.124
Disc spacing (mm)	0.5	0.5
Half included disc angle [θ]	38 °	38 °
Σ (m^2)	618, 1 826 & 3 862	28 315

The major difference between the two centrifuge models lies with the design of the solids discharge nozzles. The newer of the two models (OSC 4) has larger diameter openings with tapered inlets to the nozzles. Both centrifuges have nozzles directed backward from the direction of rotation to aid the discharge of solids. The design differences with the nozzles indicate that the OSC 4 model centrifuge would have less hydrodynamic shear associated with the solids discharge operation.

6.3 Separation Efficiency

Model SA 1 was operated at yeast slurry concentrations in the range 2.2 – 29.6 vol% and a feed flow rate of 7.2 – 32.4 $l.hr^{-1}$. The desludge frequency was set to obtain a constant mean outlet concentration. Model OSC 4 was operated with dilute slurries (0.6 – 4.8 vol%) at high flow rates (570 – 1470 $l.hr^{-1}$). The solids ejection frequency was varied to achieve a discharge concentration in the range 5.6 – 59.6 vol %. The 'breakthrough' of yeast into the clarified stream was avoided in both centrifuges as under these experimental conditions, no yeast cells were detected in the clarified stream by microscopic examination, i.e. less than 50 $cells.ml^{-1}$. The minimum feed concentration of 0.6 % (by volume) equates to a cell concentration of approximately 7.7×10^{10} $cells.ml^{-1}$. Hence the separation efficiency exceeds 99.9 % of cells. The normalised feed rate of a centrifuge, defined as the volumetric feed rate divided by the equivalent surface area of the centrifuge, is most often used as the benchmark for comparison of separation efficiencies. The normalised feed rates (Q/Σ) used in this study range from 1.5×10^{-5} to 5.2×10^{-7} $m.s^{-1}$ for the model SA 1 and from 1.4×10^{-5} to 5.6×10^{-6} $m.s^{-1}$ for the model OSC 4. Separation efficiencies can also be compared in terms of liquid residence time. The liquid residence times in this study were in the range from 1.7 to 7.5 minutes (SA 1) and 3.7 to 8.0 seconds (OSC 4).

In previous studies, the separation of *E. coli* homogenate (average cell size 1.4 μm) with efficiencies greater than 95 % was achieved with a normalised centrifuge feed rate (Q/Σ) of 4×10^{-9} $m.s^{-1}$ (Wong *et al.*, 1997) in a Veronesi KLE-160 disc stack centrifuge. Kempken *et al.* (1995) achieved a maximum recovery of 98 % of mammalian hybridoma cells (10 – 20 μm diameter) with residence times of 0.72 to 1.8 minutes in a Westphalia CSA-1 disc stack centrifuge. Whole yeast in a brewery was shown to be highly recoverable using industrial disc stack centrifuges by Siebert *et al.* (1987). Using a nozzle centrifuge (Alfa-Laval model FEUX) and an intermittently desludging type similar to the models used in this study (Westphalia SA 80) they found that the cell concentration in feed could be reduced from $4\,300 \times 10^3$ cells/ml to less than 1×10^3cells/ml and 15×10^3cells/ml in the clarified stream of the two centrifuges respectively, corresponding to a recovery of over 99.6 % of cells.

6.4 The Effect of Shear in a Disc Stack Centrifuge

The shear generated within disc stack centrifuges may cause shear sensitive particles to be damaged and rupture. Maybury *et al.* (2000) investigated centrifuge performance in industrial centrifuges used for the separation of shear sensitive materials. They observed the break-up of shear sensitive protein aggregates in the disc stack centrifuge and postulated this break-up to occur in the feed zone where the slurry is accelerated to the disc speed. Kempken *et al.* (1995) observed up to 20% disruption of hybridoma cells in the disc stack centrifuge at a centrifugal force of 5000g. Further energy dissipation in the centrifuge results in an increase in temperature of the clarified and concentrate streams relative to the feed stream. Kempken *et al.* (1995) observed temperature increases of up to 20 °C in the concentrate and 5 to 12 °C in the clarified stream depending on the feed flow rate.

Based on the structure of the cell wall given in the literature review, shear damage may occur at the cell surface. These changes could result in the release of small particulate matter from the wall, forming a beer haze, detrimental to beer quality because of increased costs of clarifying the beer. The cell membrane could also suffer a loss of integrity which would result in the release of intracellular compounds of which protease is a good indicator. Since viability is also associated with an intact membrane, shear damage may lead to the loss of cell viability. Changes to the surface properties viz. hydrophobicity and charge are possible indicators of alterations to the cell surface as a result of hydrodynamic shear in the centrifuge. Since flocculation of yeast occurs by the lectin mechanism, the loss of flocculation ability of the cell could result as lectins and receptor sites are susceptible to shear damage. Changes in flocculation is therefore another important indicator of cell surface damage. More extreme cell damage would be detected by altered fermentation performance. Shear damage in the centrifuge is investigated in terms of these assays and are presented in the following sections. Evidence for the existence of hydrodynamic shear is first presented as this action would result in increased temperatures of streams exiting the centrifuge.

6.4.1 Increase in Stream Temperature

Shear in the centrifuge would cause an increase in the temperature of the outlet streams as a result of friction. In this study, an increase in temperature was observed which was a function of feed flow rate. The SA 1 model disc stack was used at a rotational speed of 10 000 rpm to produce the increased temperature response indicated in Table 6.2. The results indicate a 2 – 3 °C temperature increase for the clarified stream and a 4 – 6 °C increase in the concentrate stream. Due to the mechanical design of the OSC 4 centrifuge, direct temperature measurement of the streams was not possible. At the flow rates used (570 – 1470 $l.hr^{-1}$), however, the temperature increase is expected to have been even smaller.

Table 6.2. Effect of feed flow rate on temperature increase in the SA 1 disc stack centrifuge.

Feed flow rate	Temperature (°C)		
($l.hr^{-1}$)	Feed	Clarified	Concentrate
7	15	18	21
27	15	17	20
28	16	18	21
67	14	16	18

Kempken *et al.* (1995) found a temperature increase in both concentrate and clarified streams which increased with increasing rotational speed and decreasing feed flow rate. The concentrate stream temperature increased by a maximum of 20 °C while the clarified stream temperature increased by between 5 and 12 °C depending on the feed flow rate. The greater increase in the concentrate stream temperature of this study is in agreement with the findings of Kempken *et al.* (1995) although the magnitude of the increase is smaller. At the higher flow rate (67 $l.hr^{-1}$) the temperature increase was less significant than at the lower flow rates which implies that the shorter liquid residence time in the centrifuge at high flow rates allows for better temperature dissipation to the streams. These small temperature increases observed are not expected to have a significant effect on yeast or beer quality. This finding is, however, proof of hydrodynamic shear and energy dissipation in the disc stack centrifuge.

6.4.2 Haze Formation

Particle size analysis in the range 0.05 to 850 µm by laser light scattering (Malvern Mastersizer) was used to quantify the fine particulate matter in the clarified stream exiting the centrifuge. Under all operating conditions used across both centrifuge models, the concentration of solids in the clarified stream was below the detection limit of 0.2 %.

The release of cell haze material from centrifuged yeast, demonstrated by Siebert *et al.* (1987) was one of the first reported cases of centrifuges causing damage and break-up of biological particles. Mannan was the major compound present in the fine particulate matter (0.5 - 1.0 μm) released into the clarified stream indicating that the yeast cell wall was the source of the haze. Fine haze formation increased with increasing centrifugal force and increasing residence time. The mechanism of cell damage was postulated to be the shearing action of the discs on the yeast cells. The size distribution of the fine haze material (sub 1 micron range) in the feed and clarified streams are presented in Figure 6.3 (Siebert *et al.*, 1987). Lim *et al.* (1992) monitored particle size distributions of a beer stream before centrifugation and the clarified stream after centrifugation and 2 days of storage. The centrifuged stream was found to contain large quantities of fine particulate matter less than 3 μm in size. In their study the feed stream at 7 x 10^4 l.hr^{-1} was fed to a Westphalia separator operated at 3300 rpm producing a relative centrifugal force of 5000 g. Since no particulate matter was observed in this study it would appear that the extent to which fine particulate matter was produced in the centrifuge was negligible or that the fine particles were recovered into the concentrate stream.

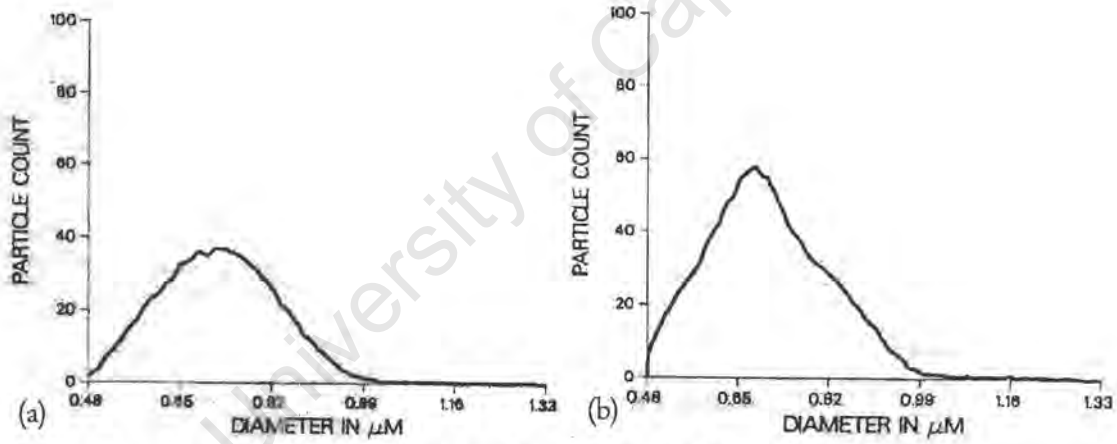

Figure 6.3. Particle size distribution of haze material (Siebert *et al.*, 1987).
((a) feed stream (b) concentrate stream)

To verify the absence of particulate haze released from the cell wall, sugar analysis was conducted. Samples of the feed, concentrate and clarified streams were collected following centrifugation under conditions expected to cause a high level of yeast damage. Centrifuge model SA 1 was operated at a feed rate of 67 l.hr^{-1}, a speed of 10 000 rpm, a desludge interval of 2 minutes 15 seconds and a feed concentration of 8.4 vol%. The samples were first centrifuged at 200 g for 3 minutes to remove the bulk of the yeast cells before being filtered through a 0.45 μm filter to ensure no cells were present when the sugar analysis was conducted. The analysis is presented in Table 6.3. No mannan was detected in any of the three streams.

Table 6.3. **Haze composition analysis of centrifuged sample.**

	Feed	Concentrate	Clarified	Error (%)
Total volume (l)	4.2	0.9	3.9	-
Solids conc. (wt %)	8.4	37.3	0.0	-
Solids mass (kg)	0.35	0.34	0.00	4.9
Solids volume (l)	0.30	0.28	0.00	4.9
Liquid volume (l)	3.9	0.6	3.3	0.4
Mannose conc. ($g.l^{-1}$)	0.00	0.00	0.00	-
Glucose conc. ($g.l^{-1}$)	0.01	0.08	0.00	-
Glucan conc. ($g.l^{-1}$)	0.13	0.33	0.09	-
Glucose - free (g)	0.04	0.05	0.01	64.8
Glucose – glucan (g)	0.52	0.20	0.30	3.3

The error introduced in the inaccuracies of determining the solids concentration result in less than 5% error on the liquid and solid mass balance across the centrifuge. The error associated with the sugar concentration determination was 0.02 $g.l^{-1}$. While the free glucose concentration was very low, further glucose was liberated by acid digestion of the cell free supernatant of the three streams. The glucose liberated is derived from glucan present as a residue of the wort production process or glucan released from the yeast cell wall. The mass balance on glucan present in the free supernatant of each stream yields a low error of 3.3 %. This is within the error of mass balance in the streams. Hence no glucan was released from the cell walls during centrifugation. The glucan present in the clarified and concentrate streams was already present in the feed. This glucan originated during wort production from the malt husks or was released from the cell wall before centrifugation. The former is hypothesised owing to large amounts of glucan present in malt husks. Furthermore, glucan in the cell wall lies below a layer of mannan. If the glucan was cell wall derived, a mannan fraction would also have been detected. From the sugar analysis it is evident that no carbohydrate haze coming from the cell wall was produced in the centrifuge under these operating conditions. It is therefore concluded that no haze was formed since there was no fine particulate phase present in the clarified stream and no carbohydrate haze originating at the cell wall was detected in either the clarified or concentrate streams.

6.4.3 Cell Viability

Viability was measured with the modified methylene blue staining assay. Since biomass is only present in the feed and concentrate streams, the effect of centrifugation on viability is easily illustrated using a parity chart to compare viability in the feed and concentrate streams. The parity diagram given in Figure 6.4 includes viability data for all centrifugation tests performed. A loss of

viability on centrifugation is clearly seen. Some 60 % of the data lies outside the 95% confidence limit shown in Figure 6.4.

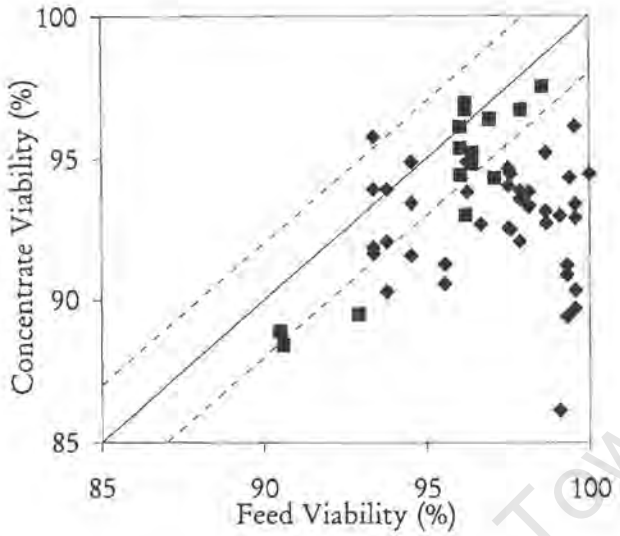

Figure 6.4. Parity diagram of centrifuged yeast cell viability.
(■ Centrifuge model SA 1 with strain SAB1, ♦ Centrifuge model OSC 4 with strain SAB5, - - - lines of 95% confidence)

The data collected from the OSC 4 model can be used to separate the effect of shear damage in the two zones (discs and nozzles) as described in Section 6.2.2. All trials on the OSC 4 centrifuge were conducted at the maximum centrifuge speed of 10 000 rpm using strain SAB5 across a range of generation numbers. Cell damage at the nozzle in the solids discharge zone is investigated by observing change in viability as a function of solids desludge interval (τ) at a constant feed flow rate (Q), feed concentration (C_{in}) and rotational speed (N). This analysis is illustrated in Figure 6.5 for each of the generation numbers of yeast tested. No constant trend in viability loss can be seen as a function of solids desludge interval, indicating that the solids discharge zone is not the primary region responsible for the loss of cell viability.

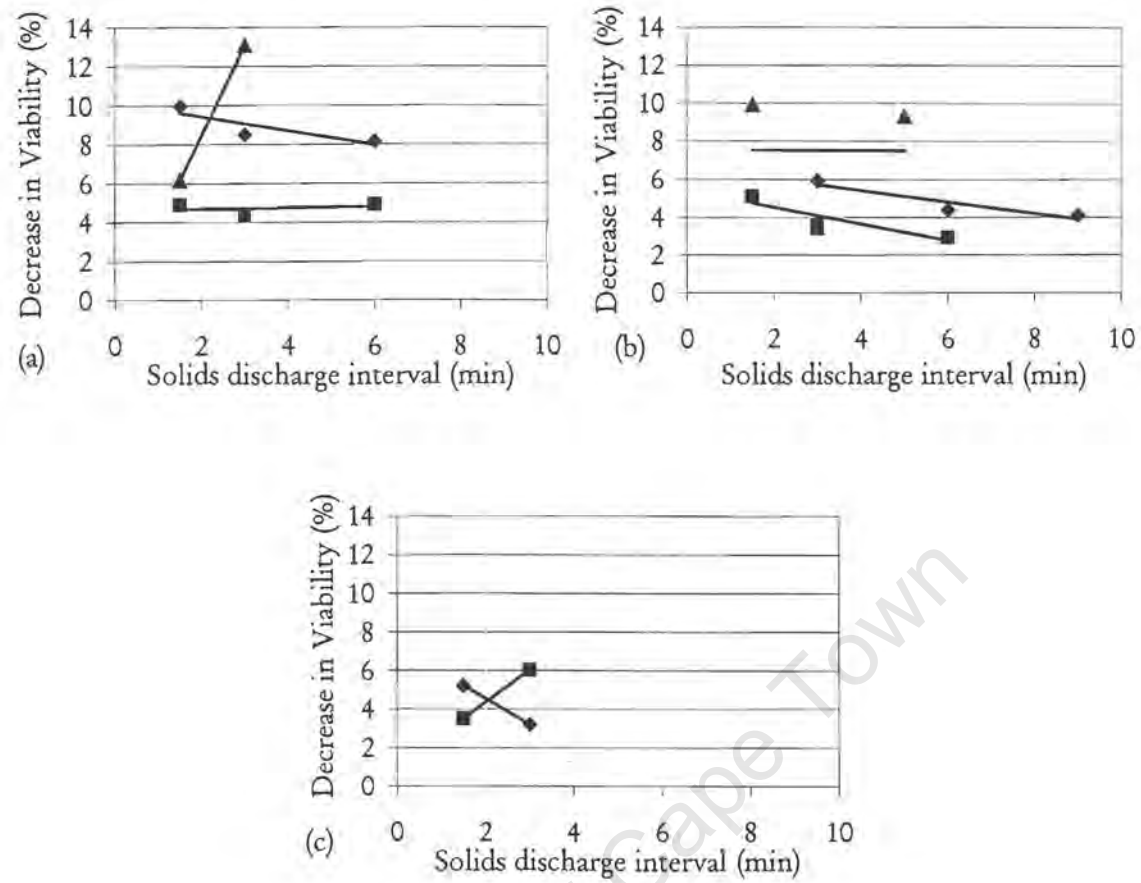

Figure 6.5. Viability loss as a function of solids discharge interval as a test for nozzle zone effect.

(Strain SAB5 with centrifuge OSC 4 at 10 000 rpm)

((a) Gen. No. 5, Q = 570 l.hr^{-1}, ■ C_{in} = 0.95%, ♦ C_{in} = 1.60%, ▲ C_{in} = 2.19%)

((b) Gen. No. 7, Q = 970 l.hr^{-1}, ■ C_{in} = 0.61%, ♦ C_{in} = 0.81%, ▲ C_{in} = 1.70%)

((c) Gen. No. 5, Q = 1470 l.hr^{-1}, ■ C_{in} = 0.52%, ♦ C_{in} = 0.81%)

Cell damage in the disc zone can be examined by observing viability loss as a function of feed concentration at fixed feed flow rates. This data is presented in Figure 6.6 for three generation numbers (1, 5 and 7) using viability data averaged across different solids discharge intervals. A positive correlation is observed between viability loss and feed concentration indicating that a shear effect in the disc stack zone causes the loss of viability in the centrifuge. It is seen that the first generation yeast was more resilient to viability loss while the 5th and 7th generations responded similarly to feed concentration.

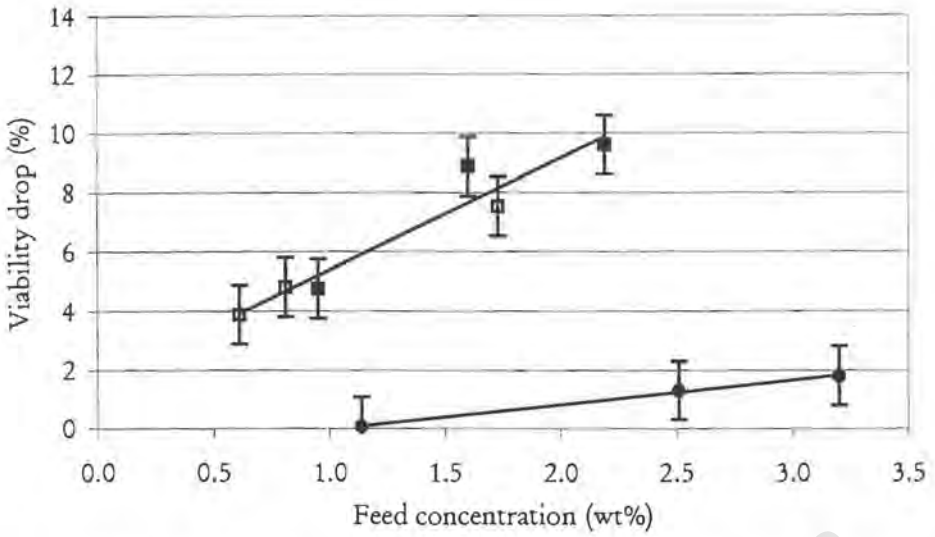

Figure 6.6. Viability loss as a function of feed concentration as test for disc zone effect. (Strain SAB5 with centrifuge OSC 4 at 10 000 rpm, ■ Gen. No. 5, Q = 570 l.hr^{-1}, □ Gen. No. 7, Q = 950 l.hr^{-1}, ● Gen. No. 1, Q = 570 l.hr^{-1})

Cell damage in the disc stack zone can be further confirmed by observing viability loss as a function of feed flow rate at constant feed concentrations (Figure 6.7). Data from the 5th and 7th generation yeast was grouped according to feed concentration into three concentration categories (0 – 1 , 1 – 2 and 2 – 3 wt%) at the different feed flow rates. No trend is observed suggesting that feed flow rate does not have a specific effect on the loss of cell viability in the centrifuge.

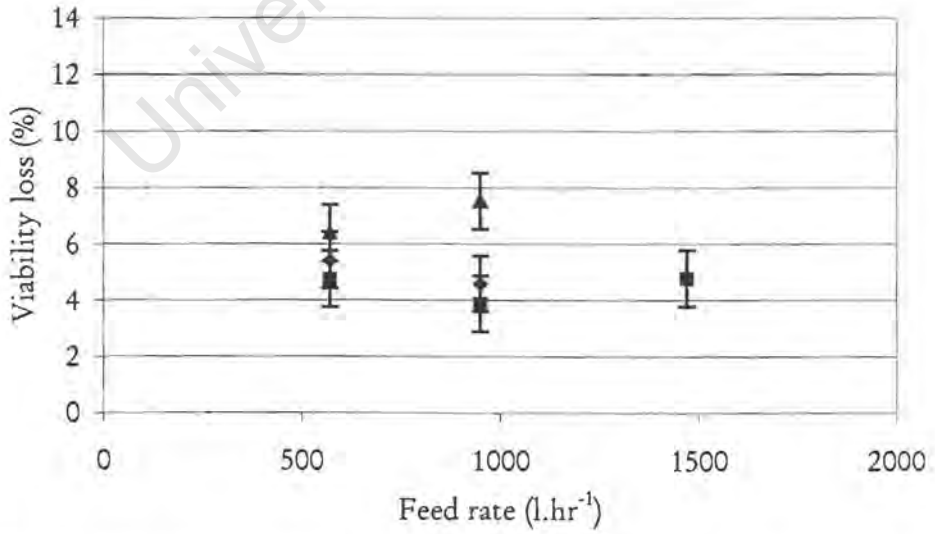

Figure 6.7. Viability loss as a function of feed flow rate as test for disc zone effect. (Strain SAB5 5th and 7th Generation with centrifuge OSC 4 at 10 000 rpm, ■ C_{in} = 0 – 1 %, ♦ C_{in} = 1 – 2 %, ▲ C_{in} = 2 – 3 %)

6.4.4 Protease Release

The release of protease into the supernatant is an indication of loss of membrane integrity. The protease activity in the clarified stream was consistently similar to that of the feed stream (Figure 6.8). Where protease release occurred, protease activity was detected in the concentrate stream. On investigating the effect of centrifuge speed on protease release (Figure 6.8), it was found that below a threshold rotational speed slight protease increase in the concentrate stream occurred. Above this speed (between 4 000 and 6 875 rpm), the membrane was permeabilised and protease released predominantly into the concentrate stream.

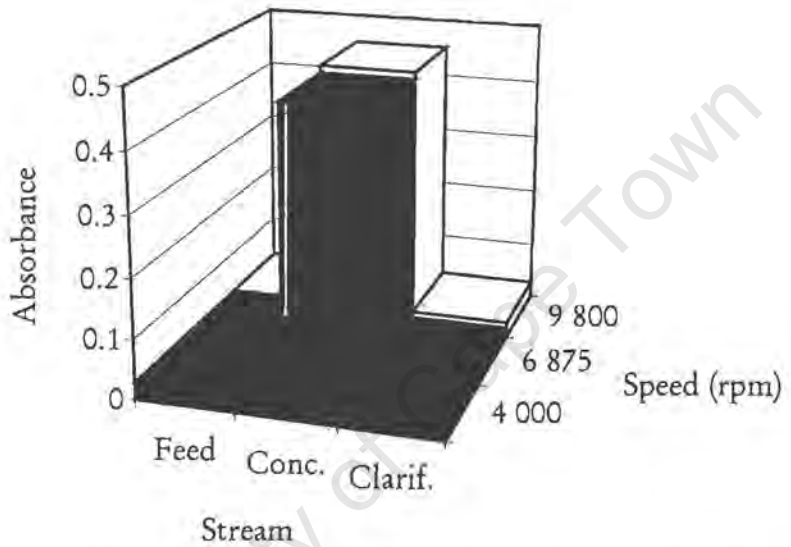

Figure 6.8. Release of protease on centrifugation as a function of centrifuge speed and stream.

(Yeast: Strain SAB1, 1st generation, Centrifuge: Westphalia SA 1, Operating conditions: Q = 27 $l.hr^{-1}$, rotational speed of 10 000 rpm, C_{in} = 19.1 wt%)

To investigate the shear effects in the solids discharge zone on membrane permeabilisation causing protease release, specific protease activity (protease absorbance / C_{out}) was plotted as a function of solids retention time within the OSC 4 centrifuge (Figure 6.9). The specific protease release is found to be constant and independent of solids retention time. This indicates that protease release is not a result of shear damage to the membrane in the solids discharge zone.

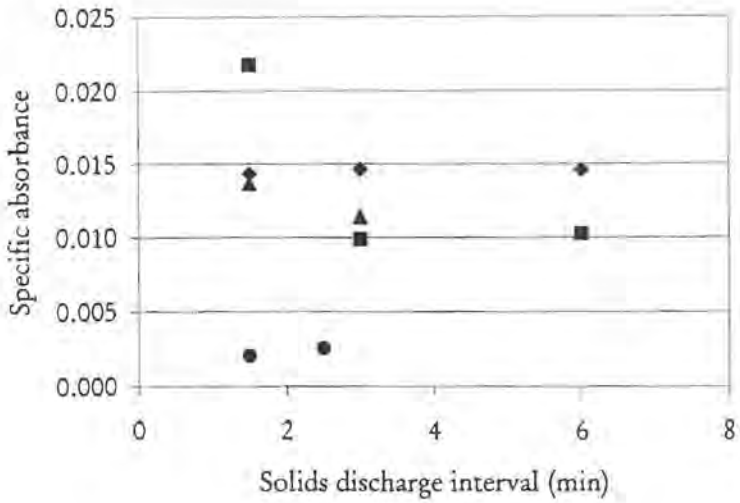

Figure 6.9. Specific protease release as a function of solids discharge interval as test for nozzle zone effect.

(Centrifuge: model OSC 4, Rotational speed: 10 000 rpm, Yeast: Strain SAB5, Q = 570 l.hr^{-1} , ■ C_{in} = 0.95%, ♦ C_{in} = 1.60%, ▲ C_{in} = 2.19%, ● C_{in} = 4.81%)

To investigate cell damage caused by shear generated in the disc zone the trends observed in specific protease release as a function of feed concentration are presented in Figure 6.10. Two trends are observed in model SA 1, the first being an increasing release of protease with increasing feed concentration. This trend is observed with 3rd and 4th generation yeast at a flow rate of 27 l.hr^{-1}. At a lower feed flow rate, with first generation yeast, the protease release appears to decrease with increasing feed concentrations. These opposing trends are likely to be a result of yeast generation number which have different resilience to shear. It was shown in Section 6.4.3 that the viability of first generation was less affected than the higher generation yeasts which corresponds to the greater susceptibility of the older yeast to membrane damage. In model OSC 4, the specific protease release is lower and no clear trends can be observed.

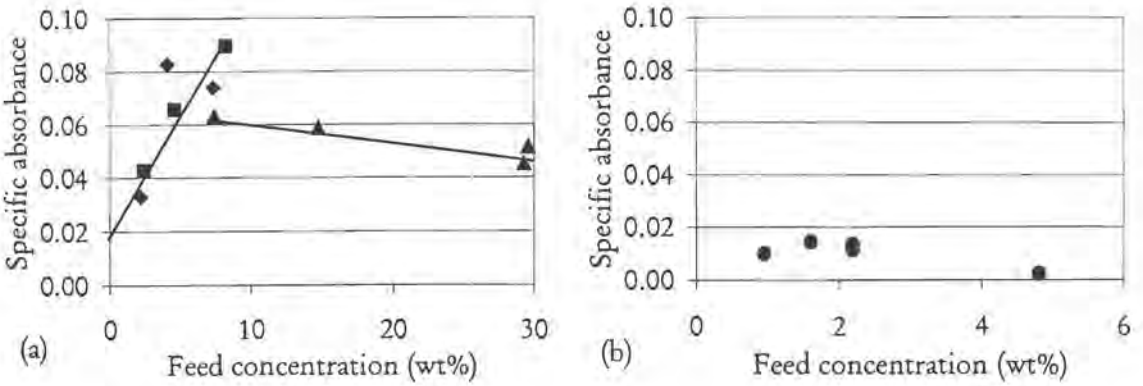

Figure 6.10. Specific protease release as a function of feed concentration as a test for disc zone effect.

((a) Yeast: Strain SAB1, Centrifuge: model SA 1 @ 9 800 rpm, ■ Q = 27 l.hr^{-1} Gen. No. 3, ♦ Q = 27 l.hr^{-1} Gen. No. 4, ▲ Q = 81.hr^{-1} Gen. No. 1, (b) Yeast: Strain SAB5, Centrifuge: model OSC 4 @ 10 000 rpm, ● Q = 570 l.hr^{-1} Gen. No. 5)

The higher specific protease release observed in the SA 1 model over that in the OSC 4 model may be as a result of a higher maximum protease content of strain SAB1 over strain SAB5 or the result could be due to the different centrifuge design causing harsher shear conditions in SA 1. The specific protease content of strains calculated in Section 3.2 indicates that SAB1 has 0.0013 absorbance units per 10^6 cells per ml, while SAB5 is twice as high at 0.0032. Hence model OSC 4 has a design which causes less shear damage to the suspended yeast cells than the model SA 1 centrifuge.

A broken cell membrane causes the leakage of the cells' contents into the supernatant. Protease is a readily detectable group of enzymes which is used as an indicator of membrane integrity. Since viability is also associated with membrane integrity, a correlation between loss of viability and protease release may be expected. It was postulated in Section 6.4.3 that viability was lost as a result of shear forces acting on the cells in the disc zone and not as a result of solids ejection in the discharge zone. Hence membrane damage in the disc zone would result in protease leaking out of the cells and increasing the protease activity in the clarified stream. The major increase in protease activity was, however, found in the concentrate and not in the clarified stream. This may be as a result of the slow release of protease from the damaged membrane and the short contact time between the cells and liquid before reporting to the clarified stream. The damaged yeast collected into the concentrate stream was assayed for protease activity approximately 4 hours after the centrifuge test, thus allowing sufficient time for the release of protease. The test for shear damage causing protease release showed a positive correlation between specific protease release and feed concentration. This result together with the viability results indicates that the loss of membrane integrity is caused by shear occurring in the disc stack zone and not in the solids discharge zone.

6.4.5 Hydrophobicity

The hydrophobicity of yeast in the feed and concentrate streams were measured and the results are presented in Tables 6.4 and 6.5 for the model SA 1 and OSC 4 centrifuge respectively. The average feed and concentrate indices of the different yeast generations are plotted in Figure 6.11 and it is observed that the hydrophobicity is greater for older generation yeast. The region within the centrifuge where this loss of hydrophobicity occurs is not identifiable from the available data.

Table 6.4. Loss of hydrophobicity of 4th generation SAB1 upon centrifugation in SA 1 at 9 800 rpm.

C_{in} (%)	Q ($l.hr^{-1}$)	HI_{feed} (%)	$HI_{concentrate}$ (%)
8.4	67	6.1	2.6
4.6	67	7.2	1.4

Table 6.5. Loss of hydrophobicity of SAB5 upon centrifugation in OSC 4 at 10 000 rpm.

Gen. No.	Q ($l.hr^{-1}$)	C_{in} (%)	τ (min)	HI_{feed} (%)	$HI_{concentrate}$ (%)
1	570	1.14	1.5	1.8	0.3
			3.0		3.5
			6.0		2.7
			12.0		2.3
		2.51	1.5	1.8	1.6
			6.0		1.4
		3.20	5.0	1.8	3.5
7	950	0.61	1.5	10.5	2.0
			6.0		5.1
		0.81	3.0	10.5	3.0
			9.0		5.8

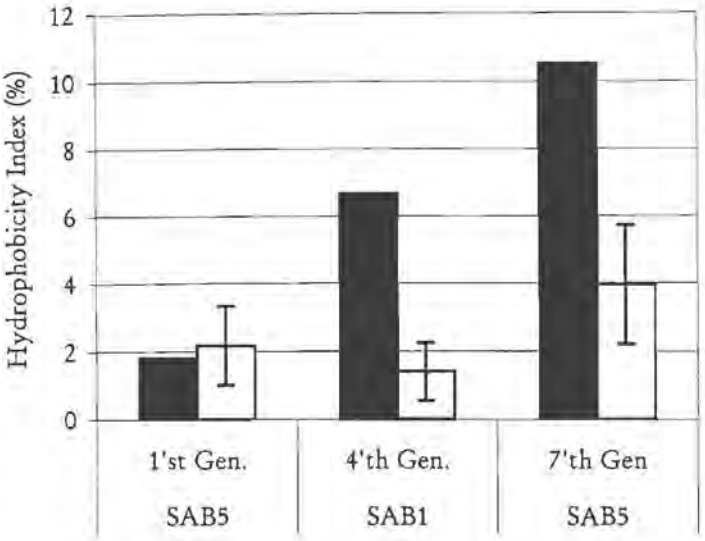

Figure 6.11. Loss of hydrophobicity as a function of yeast generation number following centrifugation of SAB5 in the OSC4 disc stack centrifuge.
(■ Feed,□ Concentrate, Error bars indicate one standard deviation in the concentrate stream values)

6.4.6 Surface Charge

The zeta potential profiles for 5th generation SAB5 yeast used in trials with the OSC 4 model disc stack centrifuge as a function of pH for different solids discharge intervals at fixed feed flow rates are presented in Figures 6.12 – 6.14. Two identical trials were conducted on the same batch of yeast with the second trial taking place 22 hours after the first. This allows for the effect of storage time on yeast surface charge and resilience to shear to be determined.

The distinguishing characteristics of all of the zeta potential profiles illustrated in Figures 6.12 – 6.14 is the broadening of the span of surface charge across the pH range tested for all the centrifuged yeast samples. In particular the potential at the pH extremes show this broadening with the zeta potential of centrifuged yeast at pH 3 being more positive and at pH 7 being more negative than for the feed samples. The iso-electric point (pI) also shows a shift of between 0.5 and 1.0 pH units from approximately 3.5 for feed samples to 4.0 for centrifuged samples. This trend is evident for all the centrifuged samples irrespective of operating conditions of solids discharge interval.

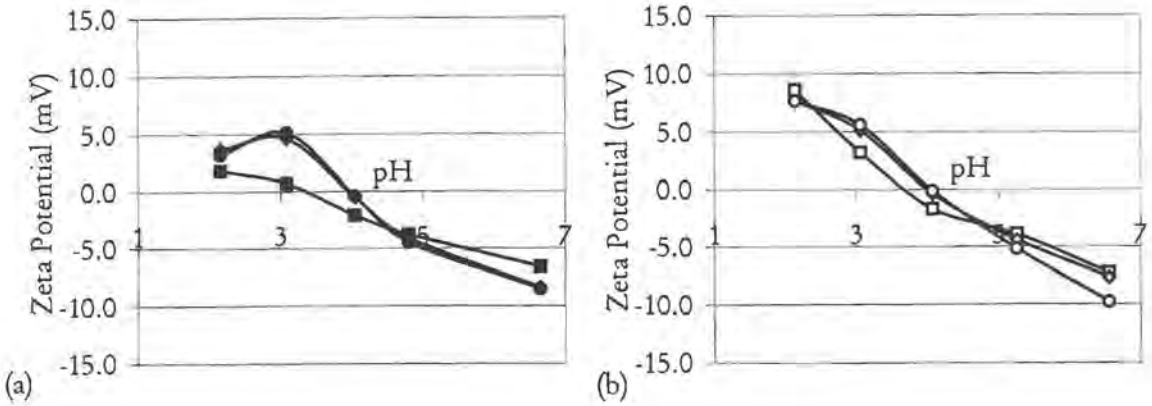

Figure 6.12. Effect of solids discharge interval on zeta potential profiles of 5th generation SAB5 with a feed rate of 570 l.hr^{-1}.

((a) 4 hour storage, ■ feed, ♦ 1.5 min, ● 3 min, (b) 26 hour storage, □ feed, ◊ 1.5 min ○ 3 min)

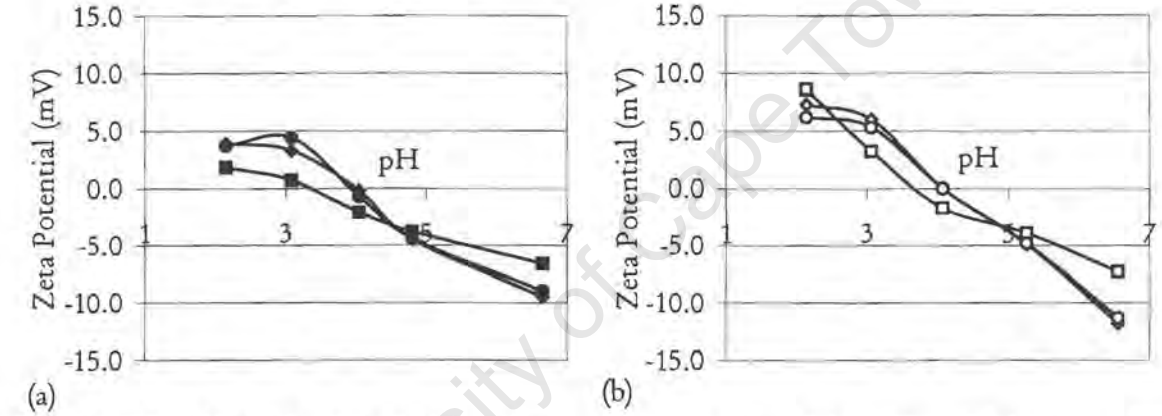

Figure 6.13. Effect of solids discharge interval on zeta potential profiles of 5th generation SAB5 with a feed rate of 950 l.hr^{-1}.

((a) 4 hour storage, ■ feed, ♦ 1.5 min, ● 3 min, (b) 26 hour storage, □ feed, ◊ 1.5 min ○ 3 min)

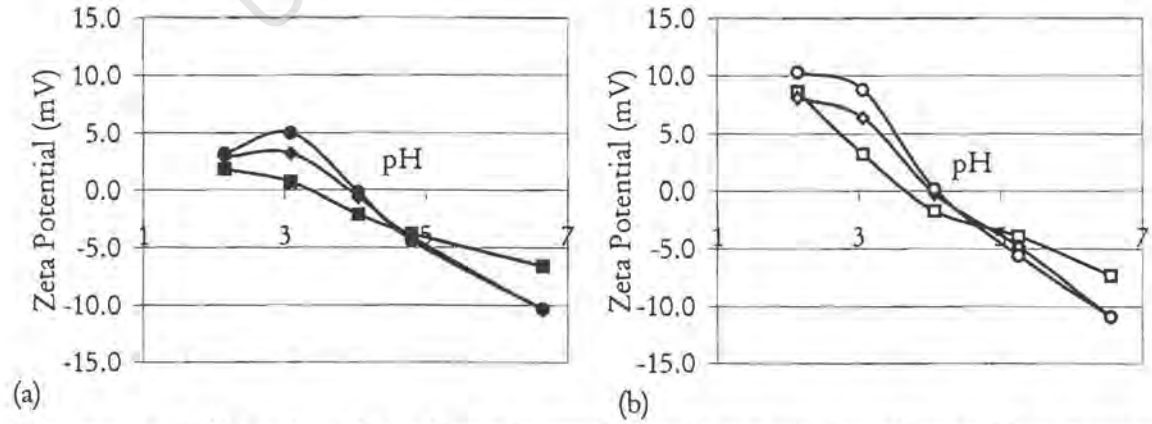

Figure 6.14. Effect of solids discharge interval on zeta potential profiles of 5th generation SAB5 with a feed rate of 1470 l.hr^{-1}.

((a) 4 hour storage, ■ feed, ♦ 1.5 min, ● 3 min, (b) 26 hour storage, □ feed, ◊ 1.5 min ○ 3 min)

These zeta potential profiles are used to calculate the surface charge composition of the feed and concentrate yeast streams, presented in Table 6.6 and Figure 6.15. The action of centrifugation on yeast is to increase the number of chargeable groups (N_s) and lower the phosphate to carboxyl ratio (q). However, no clear trend for the total number of chargeable groups (N_s) or ratio of phosphate to carboxyl groups (q) is seen as a function of solids discharge time at any of the feed flow rates or yeast storage times used. This lack of correlation between Ns and q with solids retention time indicates that the changes that are observed in surface charge group concentration are not caused in the solids discharge zone.

Table 6.6. Effect of storage time on surface charge group composition following centrifugation of 5th generation SAB5.

		Ns (x 10^{12} cm^{-2})		q (= N_P/N_C)	
Flow rate ($l.hr^{-1}$)	τ (min)	(4 hour)	(26 hour)	(4 hour)	(26 hour)
Feed	-	3.3	4.1	1.21	0.78
570	1.5	5.6	4.8	0.79	0.77
570	3	5.8	6.2	0.90	0.76
950	1.5	7.5	6.1	0.88	0.69
950	3	5.5	5.4	0.99	0.75
1470	1.5	7.1	5.0	0.91	0.80
1470	3	6.5	7.4	0.89	0.74

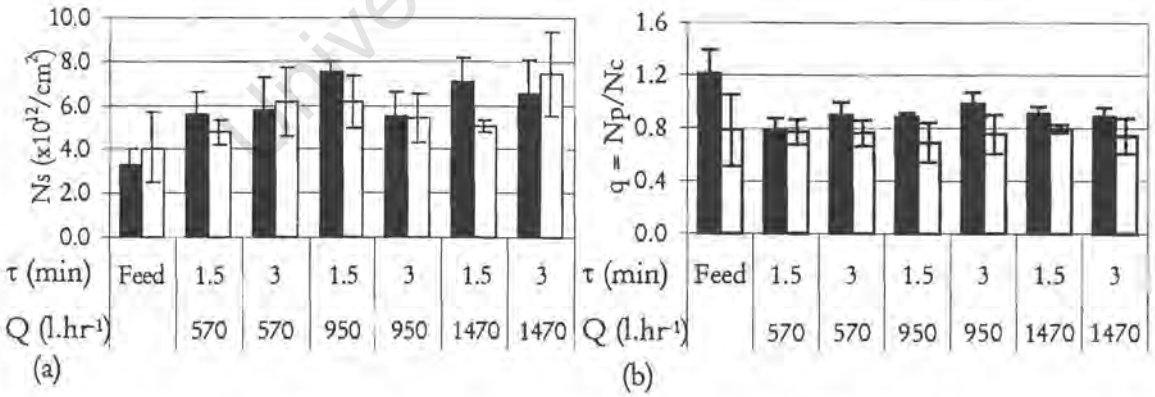

Figure 6.15. Surface charge group composition of yeast stored for 4 and 26 hours before centrifugation.

(Solids discharge interval and feed flow rate indicated on x axis with error bars indicating one standard deviation, (a) Ns (b) q, ■ 4 hour storage □ 26 hour storage)

To investigate changes in surface charge occurring as a result of shear in the disc stack zone, zeta potential as a function of pH and feed concentration are constructed and presented in Figure 6.16. This was done for a 5th generation SAB5 yeast fed at a rate of 950 l.hr^{-1} through the OSC 4 model centrifuge. No clear trend can be observed between changes in the profiles and the solids discharge interval at each of the feed concentrations. The broadening of the profile as well as the shift of pI from 3.5 to 4.0 are, however, still observed for the centrifuged yeast.

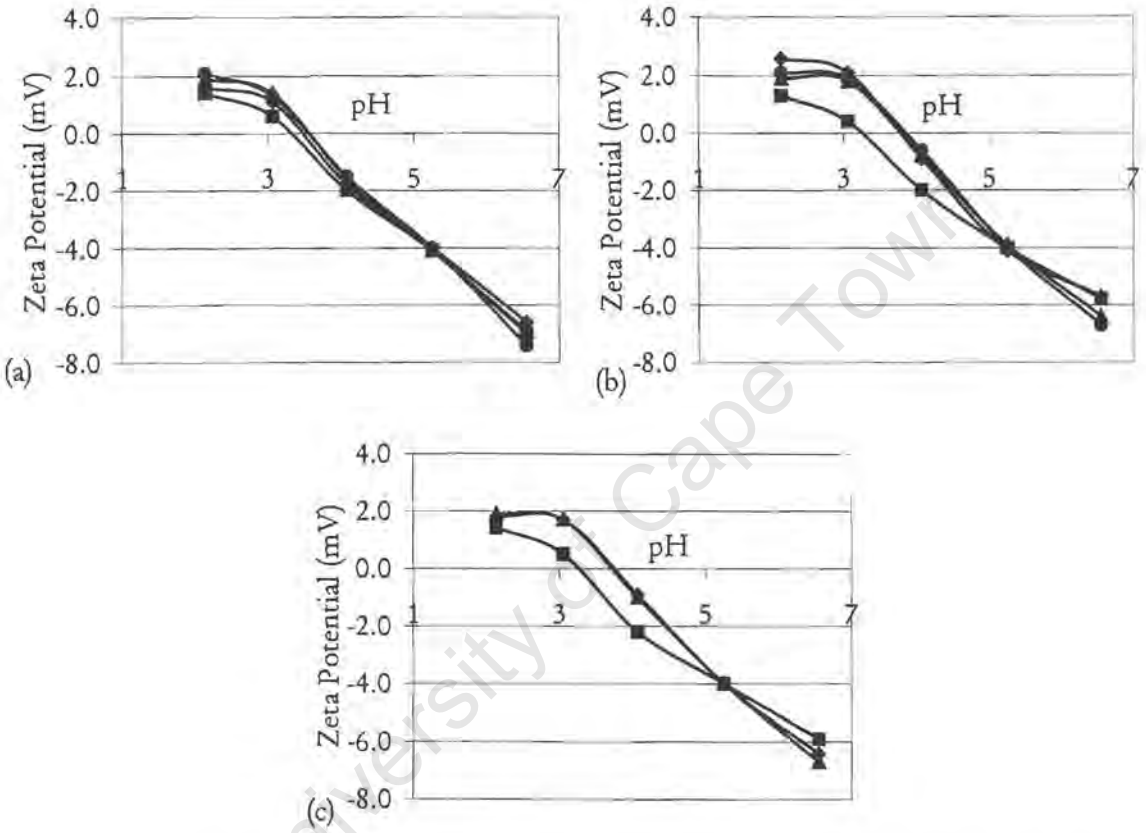

Figure 6.16. Zeta potential profiles as a function of feed concentration as test for disc zone effect.

(5th generation SAB5 pumped at 570 l.hr^{-1} through the OSC 4 model centrifuge operated at 10 000 rpm, ■ feed, ♦ 1.5 min solids discharge interval, ▲ 3 min solids discharge interval, ● 6 min solids discharge interval: (a) C_{in} = 0.95 wt %, (b) C_{in} = 1.60 wt %, (c) C_{in} = 2.16 wt %)

The surface charge composition was calculated and the results presented in Table 6.7 and Figure 6.17. The changes in both N_s and q are small but the common feature is the increased total charge group composition (N_s) of yeast in the concentrate stream relative to that of the feed. The ratio of phosphate to carboxyl groups (q) is also consistently lower for yeast in the concentrate than that in the feed stream. No trend can be identified between surface charge group composition with feed

flow rate in the centrifuge, hence it can not be established whether shear in the disc stack zone is responsible for changes in surface charge composition.

Table 6.7. Effect of feed solids concentration on surface charge group composition following centrifugation of 5th Generation SAB5 at Q = 570 l.hr^{-1}.

	N_s (x 10^{12} cm^{-2})			q (= N_P/N_C)		
τ (min)	0.95 wt %	1.60 wt %	2.19 wt %	0.95 wt %	1.60 wt %	2.19 wt %
Feed	3.5	2.6	2.6	0.94	1.14	1.21
1.5	3.0	3.9	3.7	1.03	0.75	0.84
3.0	3.7	3.5	3.5	0.84	0.81	0.84
6.0	3.8	3.4	-	0.83	0.87	-

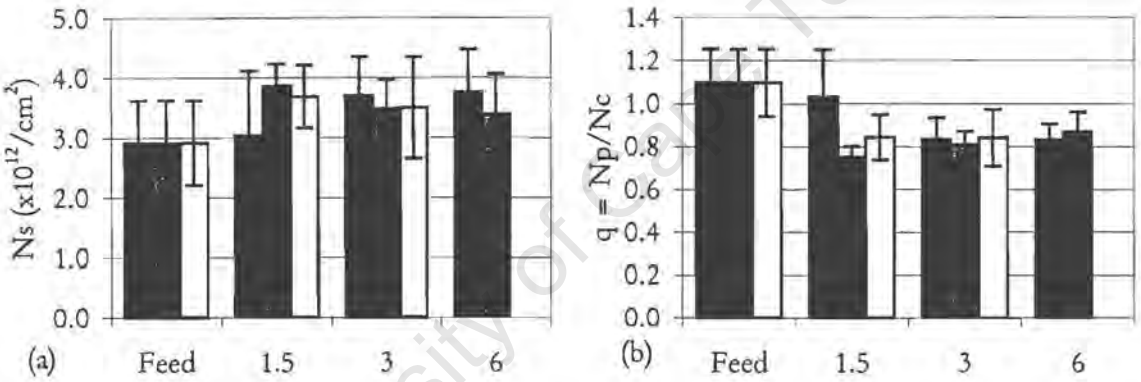

Figure 6.17. Comparison of surface charge composition for varied feed concentration at constant solids discharge intervals.

(5th generation SAB5 with Q = 570 l.hr^{-1} through OSC 4 with error bars indicating one standard deviation of the values. ■ C_{in} = 0.95 wt %, ▩ C_{in} = 1.60 wt % and □ C_{in} = 2.19 wt %, (a) N_s, (b) q,)

The common effect of centrifugation on surface charge composition is the increase in total charge group concentration, N_s, and a lowering of the ratio of phosphate to carboxyl groups, q. The average feed and concentrate N_s and q values and standard deviations are summarised in Table 6.8 together with the level of significance that there is a difference between the feed and concentrate streams. All of the trials show that the N_s value of yeast in the concentrate stream is greater than it is in the feed to greater than 99 % significance. The q value of the yeast which was stored for shorter periods of time before being centrifuged also shows significant differences at greater than 99.9 % confidence. Storage has the effect of increasing N_s as shown by the feed values of the 4 hour and 26 hour trials. There is greater than a 90 % probability that the 26 hour stored feed sample has a higher

N_s than that of the 4 hour feed sample while the certainty that q of the sample stored for 26 hours is also lower than the 4 hour sample is greater than 99 %.

Table 6.8. Significant differences in surface charge group concentrations between feed and concentrate yeast.

Details	N_s x 10^{12} (cm^{-2}) Feed	Conc.	Significance	q ($=N_p/N_c$) Feed	Conc.	Significance
Gen. 5						
Q (570-1470 $l.hr^{-1}$)	3.29 ±	6.35 ±		1.210 ±	0.893 ±	
C_{in} (0.52-1.63wt%)	0.321	0.462	99.99	0.077	0.029	> 99.99
τ (1.5-3)	(n = 2)	(n = 6)		(n = 2)	(n = 6)	
4 hr stored						
Gen. 5						
Q (570-1470 $l.hr^{-1}$)	4.08 ±	5.81 ±		0.784 ±	0.753 ±	
C_{in} (0.52-1.63wt%)	0.688	0.467	99.7	0.114	0.046	71.65
τ (1.5-3)	(n=2)	(n=6)		(n=2)	(n=6)	
26 hr stored						
Gen. 5						
Q (570 $l.hr^{-1}$)	2.91 ±	3.55 ±		1.097 ±	0.851 ±	
C_{in} (0.95-2.19wt%)	0.299	0.282	99.54	0.067	0.044	> 99.99
τ (1.5-6)	(n = 3)	(n = 8)		(n = 3)	(n = 8)	
not stored						

The region within the centrifuge where shear damage causes changes to the cell surface could not be identified due to the lack of sensitivity of both the zeta potential assay and method of determining surface charge group compositions. The changes in total charge group concentration (N_s) and ratio of phosphate to carboxyl groups (q) upon centrifugation can be interpreted in terms of shear damage to the surface of the yeast cells. The shearing action of the centrifuge can cause the loss of charged groups thereby reducing N_s. The loss of neutral groups on the other hand would cause the surface concentration of chargeable groups to increase. As was the case with exposure of yeast to the French Press, N_s increased thereby indicating the loss of more neutral than charged groups upon centrifugation. The most probable neutral molecules that would be removed from the surface of the yeast would be the carbohydrate mannan.

Since the q value (ratio of phosphate to carboxyl groups) is also found to decrease upon shear caused by the centrifuge the loss of phosphate groups are greater than the loss of carboxyl groups. From the structure of the cell wall surface, the phosphate groups are associated with mannan in the form of

phosphomannan while the carboxyl groups are part of the protein fraction. The loss of mannan and phosphomannan in particular would have the result of increasing N_s and lowering q. The loss of wall phosphomannan due to the shearing action of the disk stack centrifuge on the yeast cells is therefore postulated to be responsible for the changes observed in the surface potential of the cells.

6.4.7 Flocculation

The flocculence of yeast in the concentrate stream from the model OSC 4 centrifuge was monitored as a function of solids discharge interval at constant feed flow rate and feed solids concentration. The results of this study are presented in Figure 6.18 for 5th generation SAB5 yeast, Figure 6.19 for 7th generation SAB5 yeast and Figure 6.20 for 1st generation SAB5 yeast. These indicate a common trend of reduced flocculence potential of yeast in the concentrate stream with increasing solids desludge interval. This is indicated most clearly by the 5th generation (Figure 6.18) and 7th generation (Figure 6.20) SAB5 yeast while the 1st generation yeast (Figure 6.19) shows an immediate loss of flocculence at the shortest solids discharge interval. Since the flocculence of yeast is identified to be a function of solids discharge frequency it appears that the loss of flocculence is caused by shear effects in the solids discharge zone.

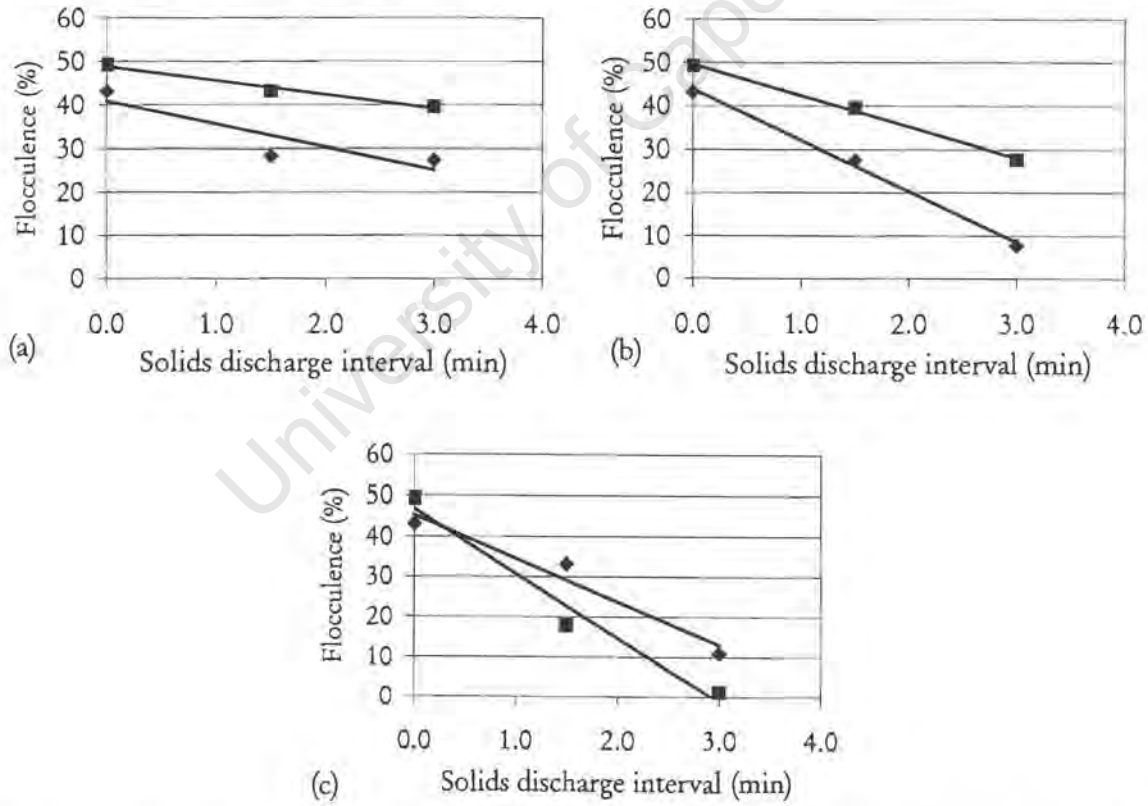

Figure 6.18. Influence of solids discharge interval on flocculence of 5th generation yeast at different feed flow rates.
(5th generation SAB5 fed to OSC 4 at 10 000 rpm with feed flocculence indicated as solids discharge interval = 0 min; (a) Q = 570 l.hr^{-1}, ■ C_{in} = 1.63 %, ♦ C_{in} = 2.53 %, (b) Q = 950 l.hr^{-1}, ■ C_{in} = 1.13 %, ♦ C_{in} = 1.76 % (c) Q = 1470 l.hr^{-1}, ■ C_{in} = 0.52 %, ♦ C_{in} = 0.82 %)

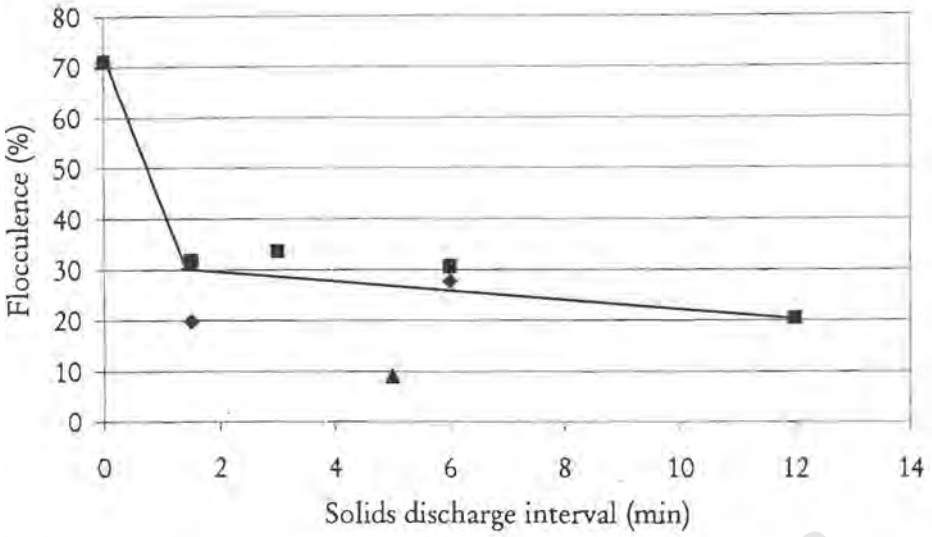

Figure 6.19. Influence of solids discharge interval on flocculence of 1st generation yeast. (OSC 4 at 10 000 rpm with feed flocculence indicated as solids discharge interval = 0 min; Yeast: SAB5, Q = 570 l.hr^{-1}, ■ C_{in} = 1.14 %, ♦ C_{in} = 2.513 %, ▲ C_{in} = 3.20)

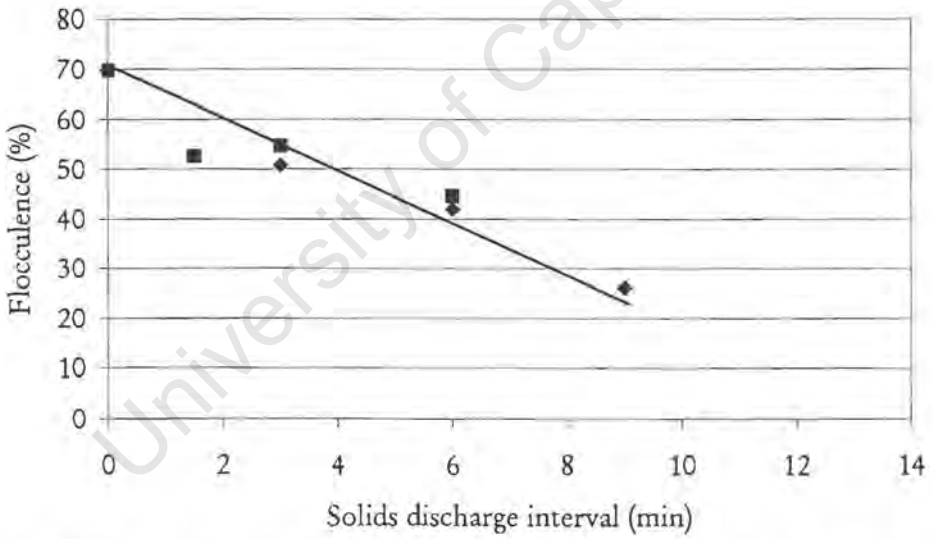

Figure 6.20. Influence of solids discharge interval on flocculence of 7th generation yeast. (OSC 4 at 10 000 rpm with feed flocculence indicated as solids discharge interval = 0 min; Yeast: SAB5, Q = 950 l.hr^{-1}, ■ C_{in} = 0.61 %, ♦ C_{in} = 0.81 %)

The apparent susceptibility of first generation yeast relative to higher generation yeast (5th and 7th) to a loss of flocculation as a result of shear stress is evident from the average flocculence before and after centrifugation under conditions of solids discharge interval (1.5 – 9 min), feed flow rate (570 and 950 l.hr^{-1}) and feed concentration (0.61 – 2.53 wt%) presented in Figure 6.21. The loss of flocculence of first generation yeast is the greatest at 65% while that of fifth generation yeast is 45% and only 26% loss is incurred for the seventh generation.

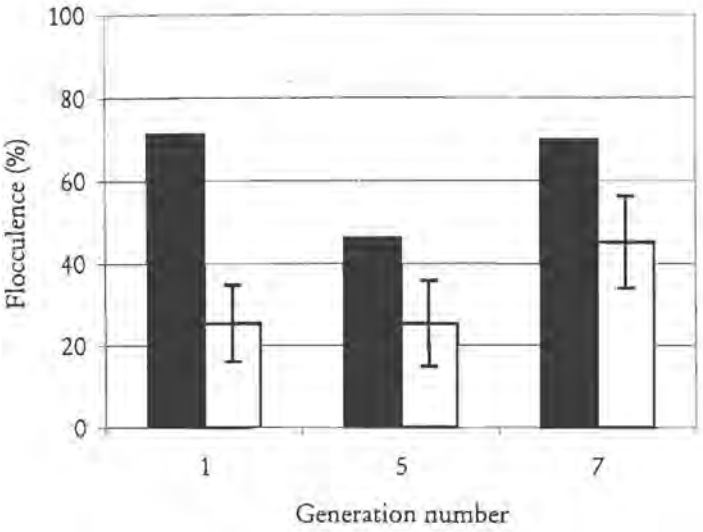

Figure 6.21. Effect of generation number on loss of yeast flocculence following centrifugation of SAB5 in the OSC4 disc stack centrifuge.
(■Feed, □Concentrate, Centrifuge model OSC 4 operated at 10 000 rpm with strain SAB5)

To investigate the loss of flocculence as a result of shear generated in the disc stack zone, the influence of feed concentration at constant feed flow rate and outlet concentration as well as the influence of feed flow rate at constant feed concentration and outlet concentration were investigated. Due to the requirement of maintaining both outlet concentration and either feed flow rate or feed concentration constant only three sets of data where this was achieved could be used. Two sets were at a constant feed flow rate of 570 $l.hr^{-1}$ and the outlet concentration achieved was between 13.5 and 14.9 % in the first and between 19.4 and 15.0 % in the second. This resulted in an error in the assumption of a constant outlet concentration of 9.2 % and 22.4 % in the two sets of data. Despite this error in the assumption the flocculence of the yeast can be seen to be lowered by increased feed concentration as indicated in Table 6.9. The third set of data had feed concentrations which were approximately equal (error of 7.3 %) and equal outlet concentrations (error of 10.0 %) which was used as a test for the effect of feed flow rate on loss of flocculation in the disc zone. It was found that the higher feed flow rate resulted in a lowering of the flocculation potential as seen in Table 6.10. These three sets of data do indicate that the loss of yeast flocculation is partly due to the effect of shear in the disc stack region.

Table 6.9. Effect of feed solids concentration on flocculence of centrifuged SAB5 yeast as test for disc zone effect.

Gen. No.	Q (l.hr^{-1})	C_{out} (wt%)	C_{in} (wt%)	Flocculence (%)
1	570	13.5	1.14	33.6
	570	14.9	2.51	19.8
		(error = 9.2 %)		
5	570	19.4	1.63	39.6
	570	15.0	2.53	28.4
		(error = 22.4 %)		

Table 6.10. Effect of feed flow rate on flocculence of centrifuged SAB5 yeast as test for disc zone effect.

Gen. No.	C_{in} (wt%)	C_{out} (wt%)	Q (l.hr^{-1})	Flocculence (%)
5	1.63	19.4	570	39.6
	1.76	17.4	950	27.6
	(error = 7.3 %)	(error = 10.0 %)		

6.4.8 Fermentation Performance

The possibility exists that a non-flocculent yeast could be used for fermentation thereby requiring the reuse of yeast collected in the concentrate stream of a centrifuge. For this reason the effect of centrifugation on the fermentation performance of yeast was investigated. This investigation studied the effect of feed concentration of SAB1 in its stationary phase in a flocculent form as well as in a deflocculated form (being achieved by the addition of EDTA). Yeast in the active growth phase was also used as feed to the centrifuge (model SA 1) to investigate the resilience of yeast in the early budding stage (26 hours after inoculation) and also in the late exponential phase (41 hour after inoculation). In this study the centrifuge was operated to achieve the maximum concentration effect by varying the discharge interval. The primary parameter used to evaluate the fermentation performance of yeast is the rate of decrease of gravity (rate of fermentation) while final beer quality was used to provide additional indicators. The procedure used to calculate the fermentation rate constant, based on the logistic equation, is presented in Section 3.4.3. Figure 6.22 represents the comparison of fermentation rate of the feed and concentrate as a parity chart. Also shown are the lines of standard deviation for the assay. The results indicate that the higher flow rates through the centrifuge (21.6 - 26.9 l.hr^{-1}) do not show any detrimental effect while the lower feed rate (7.2 l.hr^{-1}) does show a decreased fermentation rate for the centrifuged yeast. The deflocculated yeast did not

perform differently to the flocculated yeast following centrifugation at a high feed rate while the budding and late exponential phase yeast showed increased fermentation rates after centrifugation. By varying the feed concentration it was found that the fermentation rate was adversely affected at lower feed concentration (Figure 6.23) while at higher feed concentrations the relative fermentation rate was unaffected. Since the centrifuge was operated such that the outlet concentration was maintained, both the low feed concentration and slow feed flow rate would have the effect of increasing the length of time that the yeast spent in the centrifuge. It is this length of time spent by the cells in the centrifuge which may be responsible for the decreased rate of fermentation observed under low feed flow rate and inlet concentrations.

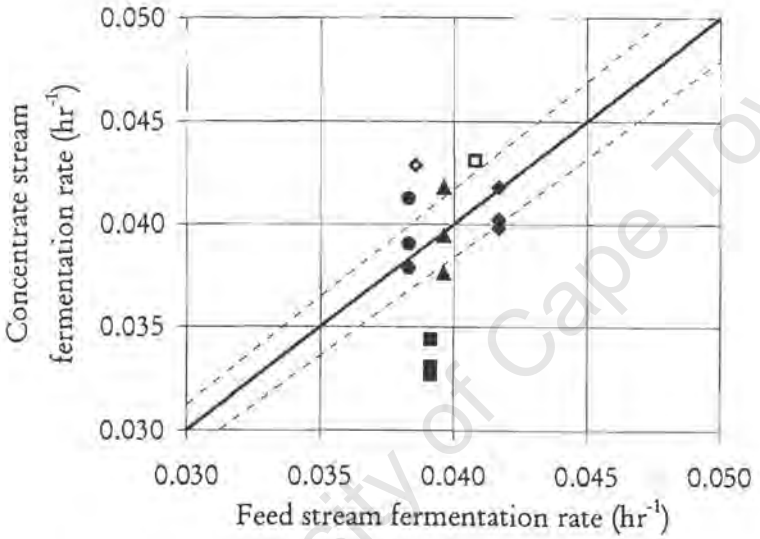

Figure 6.22. Parity chart of fermentation rate of SAB1 in feed and concentrate streams of centrifuge model SA 1 operated at 9 800 rpm.

(■ flocculated SAB1, Q = 7 l.hr^{-1}, ♦ flocculated SAB1, Q = 22 l.hr^{-1}, ▲ flocculated SAB1, Q = 27 l.hr^{-1}, ● deflocculated SAB1, Q = 28 l.hr^{-1}, □ budding SAB1, Q = 24 l.hr^{-1}, ◊ late exponential SAB1, Q = 32 l.hr^{-1})

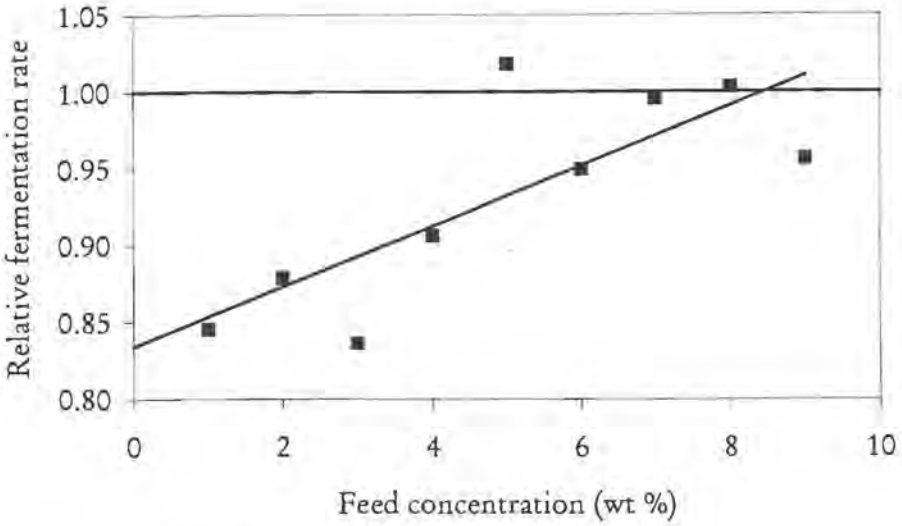

Figure 6.23. Dependence of relative fermentation rate of centrifuge concentrate stream as a function of feed concentration.
(4th and 5th generation SAB1 in flocculated state fed to SA 1 at 9 800 rpm)

The effect of centrifuge speed on fermentation performance (Figure 6.24) was studied using a feed concentration of 19.1 wt % and feed flow rate of 21.6 $l.hr^{-1}$. This shows that the lower centrifuge speed is more detrimental to the fermentation rate of yeast in the concentrate stream.

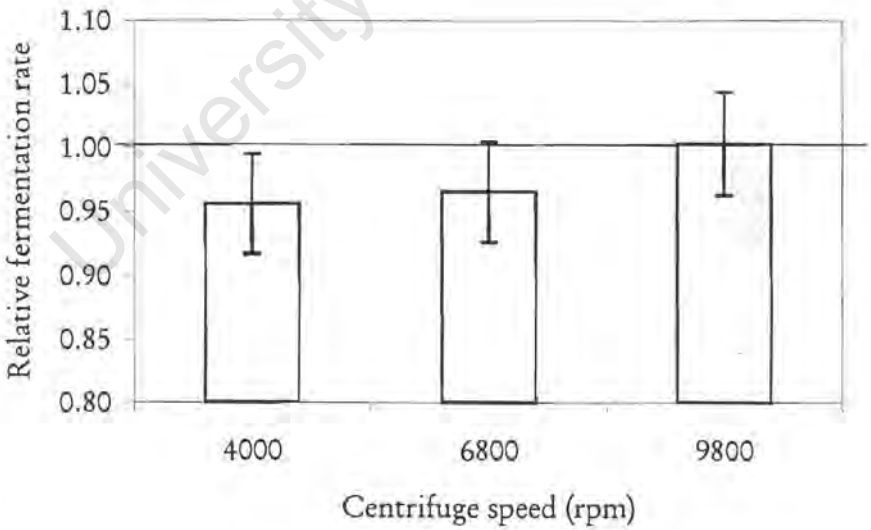

Figure 6.24. Effect of centrifuge speed (model SA 1) on fermentation performance of SAB1.
(Flocculated SAB1, Q = 28 $l.hr^{-1}$, C_{in} = 4.6 wt%)

The second indicator of fermentation performance is the beer quality of the fermented product. In terms of beer quality, the final pH as well as the concentrations of SO_2 and diacetyl at the end of fermentation were monitored. Due to slightly different wort and yeast inoculation procedures used

in the individual trials, the fermentation rate and beer quality are best studied as values relative to the fermentation characteristics of the feed yeast. The beer quality results on termination of fermentation (day 10) are summarised in Table 6.11. The growth parameter indicated in the table is the relative final biomass concentrations and indicates the growth potential of the yeast during fermentation. The beer quality indicators (SO_2 and diacetyl) have large variability with coefficients of variance for both compounds of 15.2 % (Appendix B.8). The variability of pH and biomass growth potential are smaller. The relative beer quality from the fermentations of yeast in the concentrate stream which differ by more than one standard deviation from the feed yeast fermentations have been highlighted. The predominant parameters which are shown to be different are the sulphur dioxide and diacetyl concentrations with fewer differences in pH and biomass growth ability. When deviations from the feed yeast beer quality did occur then SO_2 showed the greatest average deviation (32 %) followed by diacetyl (19 %) and pH (6 %).

Table 6.11. Beer quality results on day 10 of fermentation following centrifugation of SAB1.

Experiment	Feed rate ($l.hr^{-1}$)	Feed conc. (wt %)	SO_2 (relative to concentrations from feed yeast)	Diacetyl	pH	Growth
Flocculated	7.2	29.6	90.8	100.8	102.0	96.4
SAB1 yeast	7.2	29.3	100.9	**135.5**	**96.1**	**86.7**
with high	7.2	14.7	**71.9**	**115.3**	**104.1**	95.0
C_{in}	7.2	7.4	**71.7**	**125.6**	101.5	93.3
Flocculated	26.9	7.1	**224.4**	**116.8**	102.0	100.0
SAB1 yeast	26.9	4.1	**123.3**	**136.8**	98.0	96.7
with low C_{in}	26.9	2.2	**67.1**	100.0	103.0	110.7
Deflocculat	28.2	6.7	**130.2**	133.9	**95.1**	95.9
ed SAB1	28.2	8.2	96.7	93.5	103.0	99.2
yeast	28.2	4.6	99.2	97.2	102.0	102.7
	28.2	2.4	100.0	101.0	101.0	92.7
4000 rpm	21.6	19.1	**117.2**	114.4	100.5	98.9
6800 rpm	21.6	19.1	**116.2**	98.1	**104.1**	101.0
9800 rpm	21.6	19.1	106.1	95.9	**106.2**	103.3
Budding	24.0	2.0	**233.9**	**172.5**	**81.5**	102.2
Late exp.	32.4	2.2	**46.5**	**57.5**	**129.7**	104.8

The beer quality of the flocculated yeast fermentations appears to be adversely affected by centrifugation when considering the SO_2 and diacetyl levels which were generally higher. Both the high and low feed solids concentration experiments as well as those at slower centrifuge speed using flocculated yeast indicate higher compound concentrations. The fermentation rates of the

flocculated yeast fermentations, however, were not found to be different from the feed sample fermentations. Since the change in beer quality observed were not associated with slower fermentation rates this represents an inherent change in beer quality fermentation performance.

The quality of beer and fermentation rates from the deflocculated yeast experiments was found not to be affected by centrifugation.

For cells centrifuged while they were in the budding phase (26 hours after inoculation) the concentrations of both SO_2 and diacetyl were significantly higher at 234 % and 173 % respectively. This is more than 8 and 4 times the standard deviations of the two compounds respectively and since the values represented in Table 6.11 are the average for duplicate fermentations, this translates to a decrease in beer quality to a significance level of greater than 95 % for both compounds. The fermentation rate of these were significantly better (6 % faster) after centrifugation. The poorer beer quality observed could be related to the quicker fermentation as is occasionally observed during routine brewery production (Hulse, 2000).

The cells which were allowed to ferment for a longer time (41 hours) and so reach the maximum suspended cell concentration before being recovered by centrifugation also had altered levels of fermented beer quality. The concentrations of SO_2 and diacetyl were decreased by 47 and 58 % while the fermentation rate of this yeast was 11 % faster. Since the fermentation rate of centrifuged yeast following both 26 hour and 41 hour growth are faster, their different beer quality indicators shows the susceptibility of the cells metabolism at different times within the cell cycle to hydrodynamic shear. The difference between the two growth states (26 hours vs. 41 hours) is that while the budding yeast was at the start of the active reproduction phase, the cells at the maximum free cell concentration had stopped reproducing and were in their stationary phase. Stationary phase yeast is reported to be physically tougher (Fish and Lilly, 1984) and more resilient to shear damage than the growing cells. Cropped yeast usually used in these centrifuge trials, although also in the stationary phase may be less resilient due to the longer period of exposure to adverse environment of high ethanol concentration and nutrient depletion.

6.5 Summary

Separation efficiency of both centrifuge models, SA 1-02-175 & OSC 4-91-006, was greater than 99.9% under the operating conditions indicating complete separation of yeast cells from the feed stream.

The centrifuge can be divided into two physical regions where the mechanical forces acting on the cells can cause hydrodynamic damage. The first region is within the disc stack itself where the incoming yeast slurry is accelerated to the disc velocity and fed through riser holes in the discs. As the feed flows through these riser channels and enters the narrow spaces between the discs, it experiences shear forces. Damage occurring in this region would be detectable as a trend in biological response as a function of feed flow rate at constant feed solids concentration. Alternatively, the biological response trend as a function of inlet concentration would be observed at constant feed flow rate. The second region in the centrifuge where shear damage can occur is in the solids ejection zone. When the solids are released from the periphery of the spinning disc bowl, they pass through nozzles which cause shear. Damage to the yeast in this region can be separated from damage occurring in the disc region by observing a trend in biological response as a function of solids discharge interval at constant feed flow rate and feed concentration. Using these tests, the extent of damage to yeast is attributed proportionally to each of the two regions within the disc stack centrifuge.

This approach was successfully applied to determine the region of action where cell viability was lost and protease release occurred. The loss of viability occurs in the disc stack region with higher inlet concentrations being more detrimental to cell viability. Protease release from cells is also attributable to the disc stack zone although the increased levels of protease are only observed in the concentrate stream due to its slow release. The release was reduced at low centrifuge speeds with an apparent threshold speed, above which protease release occurs.

The analysis procedure of deconvoluting the data to determine the hydrodynamic region within the centrifuge where damage occurs was not successful for changes to the surface properties of charge and hydrophobicity. This is due to the insensitivity of the assays to detect subtle changes in the hydrophobicity as well as the loss of information in the case of zeta potential when the charge group composition is calculated. Fermentation performance could also not be used to determine the zone of action in which the yeasts' fermentation performance is affected. For these biological effects only general observations and simple trends could be identified. The zeta potential of centrifuged yeast was found to be affected by centrifugation, with a general increase of the zeta potential span across the pH range. This has the effect of shifting the iso-electric point from approximately 3.5 to 4.0. The surface charge composition parameters, N_s and q, were also affected. The total number of chargeable groups (N_s) of centrifuge concentrate samples were higher than the feed samples. The ratio of phosphate to carboxyl groups (q) decreased upon passage of the yeast through the centrifuge. These findings imply the net loss of uncharged material from the yeast surface as well as a loss of phosphate groups. Since phosphomannan molecules are relatively large mannose polymers with only single phosphate groups, the loss of phosphomannan without the loss of protein could

account for the observed changes in charge group concentration. The reduction of hydrophobicity index as a result of centrifugation was shown. Since a positive link between hydrophobicity and surface lipid content was established in Chapter 4, the reduced hydrophobicity could be a result of lipid loss. The loss of lipid, which is uncharged, could also be partly responsible for the increase in N_s mentioned above.

Flocculation potential of yeast decreased as a result of centrifugation and this loss of flocculation was proportional to the discharge interval of the solids. The loss of flocculation is therefore indicated to occur in the solids discharge zone. In addition, increased feed concentrations also lead to a greater loss of flocculence. This indicates that there is also a loss of flocculence in the disc stack region. The loss of flocculation is therefore identified to take place in both the disc stack and solids discharge zones.

The fermentation rate of flocculated yeast was generally increased by centrifugation with the greatest increase being found for yeast in its growth phase or early stationary phase as well as for late stationary phase yeast in a non-flocculated form. The beer quality produced by centrifuged yeast was generally poorer for yeast in a flocculated form. This manifests itself as elevated sulphur dioxide and diacetyl concentrations. Like fermentation rate, beer quality was more dependent on physiological status of the yeast fed to the centrifuge. Cells in the early growth phase (start of cell budding) produced significantly poorer beer quality while cells in late exponential to stationary phase produced improved beer quality. This implies that the rapid reuse of cropped yeast with minimal storage time would favour faster fermentation rates and improved beer quality.

Centrifugation therefore affects yeast at the level of surface properties (charge and hydrophobicity), flocculence, viability, protease release and fermentation performance as well as causing a slight increase in temperature of both clarified and concentrate streams. Three recommendations for centrifuge operation are:

1. To operate with the highest allowable feed flow rate that will achieve yeast separation within the disc stack as this will minimise the increase in temperature in the clarified stream.
2. By operating at a low inlet solids concentration the cell viability will remain high, thus minimising the potential of protease release into the clarified stream. If the centrifuge is used for cropping then the concentrate yeast will also maintain a higher fermentation rate.
3. Despite the increased loss of flocculation potential associated with longer solids discharge intervals, the interval should be set to the maximum which still achieves the required separation so that excess beer losses can be avoided.

Chapter 7: Brewery Yeast Handling Systems

7.1 Introduction

In the brewery, yeast is pumped from the base of a fermentation cone with a positive displacement pump through 65 mm diameter piping for distances of up to 150 meters to a plate and frame chiller where it is cooled from 14 to 2 °C before passing into a storage vessel. This process is termed cropping and occurs at the end of each primary fermentation. Once the yeast is in the storage vessel, agitation is started and the yeast concentration (consistency) and viability are measured to determine the quantity to be used to inoculate (pitch) the next series of fermentations. The pitching rate is calculated based upon a standard 14 kg of yeast with a 60% consistency and 100% viability per hectolitre (Equation 3.1). Since the quantity of yeast increases threefold during fermentation, each yeast crop can be reused to pitch up to three new fermenters. The required quantity of yeast is pumped from the storage vessel to a separate agitated pitching vessel where it is stored until needed for fermentation (generally not longer than 8 hours). For strain SAB1, the yeast is acid washed 30 minutes before pitching by the addition of an equal volume of food grade phosphoric acid. This reduces both the slurry viscosity and yeast flocculence as well as reducing bacterial contamination since few common brewery contaminants are able to withstand the low pH (2.2 - 2.4) usually obtained after acid washing of yeast slurries. After acid washing, the yeast slurry is pumped into the main wort line with the media feed to the next fermenter. For strain SAB5, no acid washing occurs.

The yeast is exposed to the shear generated due to the pumping, flow through pipes and constrictions, and the changing flow patterns in the plate and frame heat exchanger (chiller). In this chapter the results of brewery scale flow trials on yeast quality and fermentation performance are presented and discussed. In the preceding chapters the effect of shear on yeast quality, surface properties and fermentation performance were discussed with respect to the shear forces generated

in a laboratory French Press and pilot scale disc stack centrifuges. The trials presented in this chapter were conducted using brewery equipment and production yeast at SAB – Newlands brewery. The experimental conditions of flow rate, yeast generation, pump type and sampling positions used are first discussed for each of the four pump trials and two online trials. The shear stress and energy dissipation rates are calculated and used as a basis for comparing the biological responses observed in the individual trials. The effect of these flow conditions on yeast quality are then presented in terms of viability, protease release, surface properties and flocculation potential. The yeast quality was also studied by its fermentative ability which is analysed in terms of fermentation rate as well as the resultant beer quality.

7.2 Experimental Fluid Flow Conditions

Four 'offline' flow trials were conducted on spent yeast (yeast to be pumped to the spent yeast storage vessels and not further used in the brewery). Spent yeast was used to allow the pump type and flow rates to be extended beyond those accepted in operating practice in the brewery without risk of contamination or cell damage interrupting standard brewery operation. These trials were conducted using strain SAB1. In the first of these trials the flow rate was extended from the standard brewery cropping rate for SAB1 (60 – 70 kg.min^{-1}) to approach 190 kg.min^{-1}. This trial was performed to investigate the effect of high shear stress and turbulent flow on yeast quality. Thereafter the effect of repeated exposure of yeast to a pump and pipe-work section was studied. Two such trials were conducted, one lasting 2 hours and the other 6 hours, to determine the effect of total energy dissipation on yeast quality. The final 'scrapping' trial monitored the condition of yeast as a function of time during cropping or scrapping. From this a suitable time range during which yeast properties of the crop (flocculated yeast harvest) remained approximately constant could be identified. The identified times of constant yeast quality were used for sampling during the 'online' trials.

The 'online' cropping trials were conducted on yeast under the standard harvesting (cropping) conditions used for strains SAB1 and SAB5. Because of the uninterrupted pumping and physical location of the sampling points in these trials, the samples were not taken from a single 'plug' of yeast but rather covered a range of yeast quantity pumped out of the fermentation vessel. The online trial with SAB5 investigated flow through the pump, pipeline, switching panel and heat exchanger, i.e. that section of the yeast handling circuit between fermenter and storage vessel. The trial with SAB1 extended this to include the effect of storage and the acid washing procedure on yeast quality.

A schematic representation of the yeast handling rig used to study the scrapping of spent yeast, high flow rate and recirculation is presented in Figure 7.1. The rig consisted of three parts: a holding tank

(A), a pump trolley (B) and a holding tube section (C). There were three sampling points: before the pump (1), between the pump and holding tubes (2) and after the holding tubes (3). Yeast could either enter the pump section directly from the fermenter or the holding tank could be filled and used as the feed reservoir for the recirculation trials. The yeast could leave the test rig either before or after the holding tubes. The holding tubes had a physical length of 13.5 m and contained eighteen 90° long-radius bends. The holding tubes could be interchanged to provide piping with diameters of 25, 50 or 65 mm. Because pipe fittings, bends and joints cause the flow patterns to deviate from those found in linear pipe sections, they contribute more than the equivalent length of straight pipe to the pressure drop. Typical friction losses for these fittings are given in Table 7.1, reproduced from Coulson and Richardson (1990). The equivalent length added by each 90° long-radius bend used in this study is 20 and results in an additional pipe length of 9 m for the 25 mm, 18 m for the 50 mm and 23.4 m for the 65 mm diameter holding tubes. These equivalent lengths were determined to account for the increased pressure drop associated with them and for the purpose of this study it is assumed that the same equivalent lengths can be used to account for the anticipated increased shear damage.

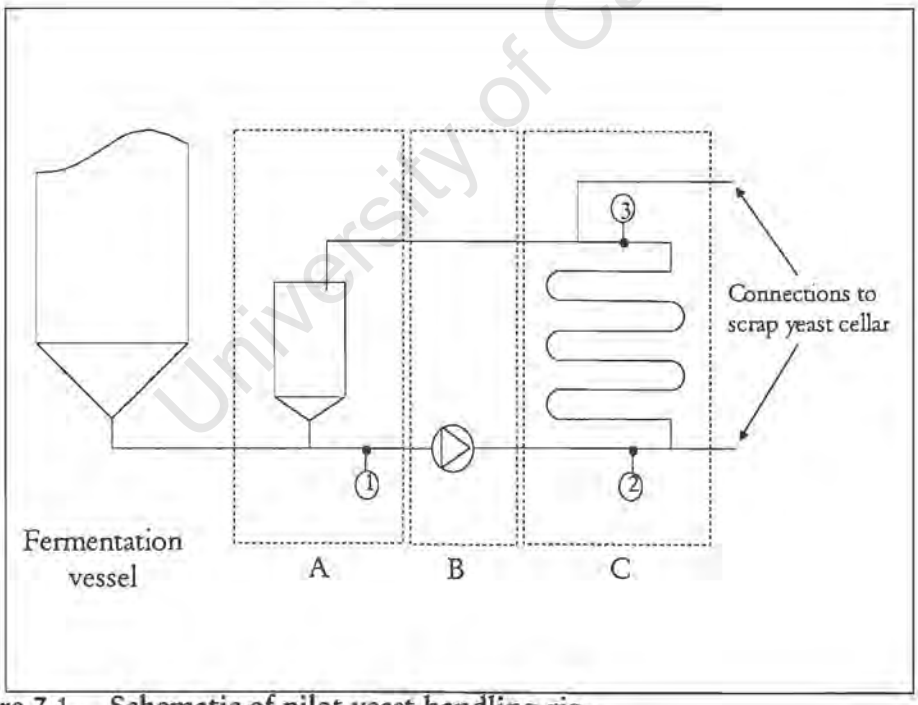

Figure 7.1. Schematic of pilot yeast handling rig.

Table 7.1. **Friction losses in pipe fittings (Coulson and Richardson, 1990).**

Fitting Type	Number of pipe diameters
45° elbows	15
90° elbows (short)	30 – 40
90° elbows (square)	60
Gate valves: Fully open	7
Three quarter open	40
Half open	200
Quarter open	800

7.2.1 Laminar vs. Turbulent Flow Trials

As discussed in Section 2.5 of the literature review, the calculated Reynolds number of flow is a measure of intensity of energy dissipation and an indicator of the flow type i.e. laminar or turbulent. The effect of high flow rates, with the associated high Reynolds numbers, and shear stress on yeast quality was investigated using the test rig described above, configured in the following way. The Scandi Brew gear pump was selected because of its high pumping capacity and low pulsation fluid delivery. The 25 mm diameter holding tubes were used to provide higher linear velocities and shear stresses. Fifth generation yeast was used. Yeast samples were taken at positions 2 (after pump) and 3 (after holding tubes), indicated on Figure 7.1 with the flow set to one pass through the holding tubes. The flow conditions of the trial are summarised in Table 7.2. The high solids concentration of yeast slurries results in the slurry displaying non-Newtonian behaviour with viscosity being inversely proportional to fluid shear rate. This trial used higher flow rates (67 – 187 $kg.min^{-1}$) than typical in the brewery (53 $kg.min^{-1}$) corresponding to greater fluid shear rate and lower apparent viscosity. From the experimentally measured pressure drop across the holding tubes for each flow rate, the Reynolds number of the three trials were calculated. This was done using the friction factor contribution of long-radius 90° bends of 20 times the pipe diameter for the 18 bends, adding 9 metres of length to the physical 13.5 m of 0.025 m diameter pipe (for the pressure drop calculations). Due to the height difference of 1.55 m between the entrance and exit of the holding tube section, the head loss of 16.2 kPa was subtracted in the calculation of pressure drop per unit length. From the definition of head loss (Equation 7.1) the friction factor can be related to the pressure drop (Equation 7.2). For laminar flow the Reynolds number is related to the friction factor through Equation 7.3 while for turbulent flow the friction factor and Reynolds numbers are related through the additional parameter of relative surface roughness as illustrated in Figure 7.2. Using these equations and correlations as well as a relative surface roughness (e/D) for 25 mm diameter stainless steel tubing of 0.0004 the friction factors and Reynolds numbers were calculated (Table 7.3). The

Reynolds numbers indicate a laminar flow pattern for the trial at a flow rate of 67 kg.min^{-1} while the higher flow rate trials showed a turbulent flow pattern in accordance with the transition from laminar to turbulent flow across the range 2100 – 3000 (Coulson and Richardson, 1990).

$$h_L = 2f_f \frac{L}{D} \frac{v_{avg}^2}{g} \tag{7.1}$$

$$f_f = \frac{\Delta P}{L} \frac{D}{2\rho v_{avg}^2} \tag{7.2}$$

$$f_f = \frac{16}{Re} \tag{7.3}$$

where: L = pipe length (m)

D = pipe diameter (m)

f_f = friction factor

h_L = head loss (m)

g = gravitational acceleration (m.s^{-2})

v_{avg} = average velocity (m.s^{-1})

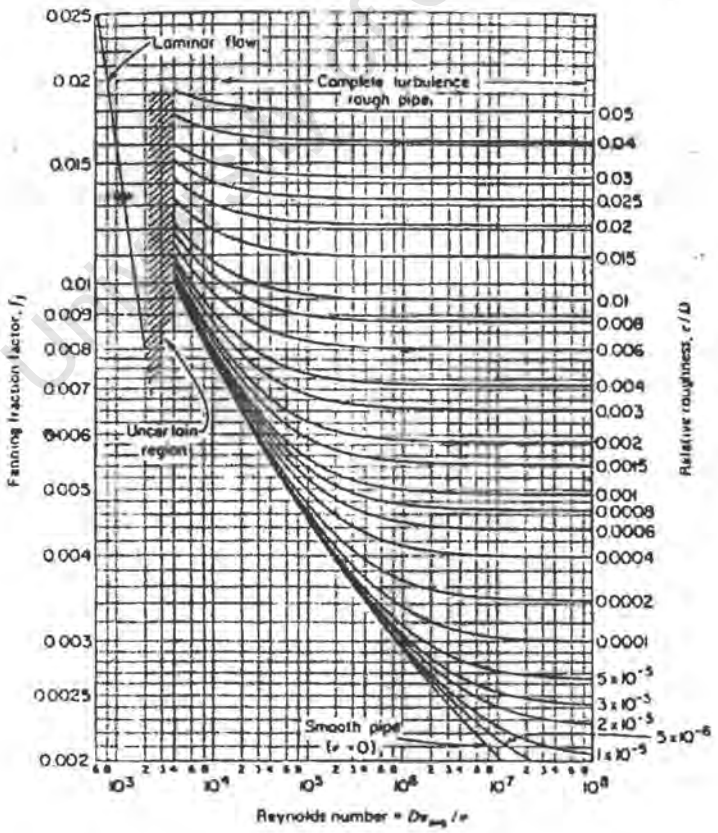

Figure 7.2. Friction factor as a function of Reynolds number and relative roughness. (Welty *et al.*, 1984: Figure 14.1)

Table 7.2. Experimental conditions of the flow rate trials.

Sample (position)	Flow rate ($kg.min^{-1}$)	Pressure (kPa)
A (2)	187.1	790
B (3)	187.1	440
C (2)	178.1	760
D (3)	178.1	460
E (2)	67.5	500
F (3)	67.5	380

Table 7.3. Experimentally determined pressure drop, friction factor and Reynolds numbers.

Flow rate (kg/min)	Pressure drop (kPa)	$\Delta P/L$ (kPa/m)	f_f	Re
187.1	334	14.8	0.0049	120 000
178.1	284	12.6	0.0046	200 000
67.5	104	4.6	0.0117	1371

Both laminar and turbulent flow result in the yeast cell being exposed to shear stress. The total shear stress profiles for both the laminar and the turbulent flow regimes were calculated according to Equation 2.6 and are illustrated in Figure 7.3. The ratio of viscous to turbulent shear stress, calculated from Equation 2.12, was used to determine the viscous and turbulent components for the flow trial with the highest Reynolds number and the results are graphically illustrated in Figure 7.3. The velocity profiles (Figure 7.4) of the laminar and turbulent trials were calculated using Equations 2.3, 2.4 and 2.5. The results indicate that turbulent flow has a higher shear stress and a relatively flatter velocity profile compared to the smaller shear stress and parabolic velocity profile of laminar flow. Also evident from the results is that the two components (Reynolds and viscous stresses) of the total stress in turbulent flow dominate in different parts of the pipe. Viscous stresses dominate in the region close to the wall while Reynolds stress dominate in the core of the pipe.

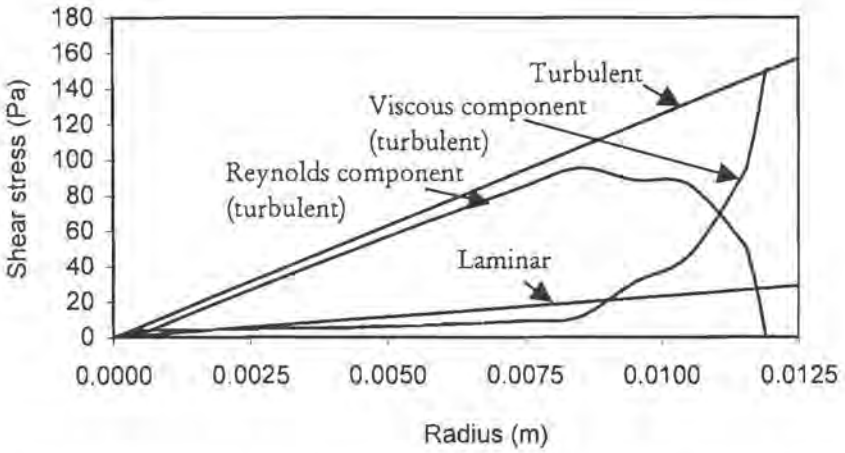

Figure 7.3. Shear stress profiles of the laminar and turbulent flow trials.

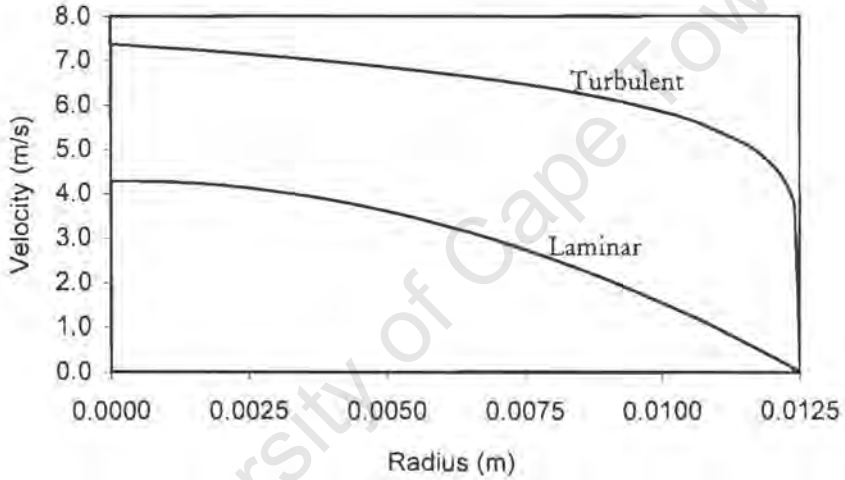

Figure 7.4. Velocity distributions of the laminar and turbulent flow trials.

From the velocity distributions the expected residence time distributions as a function of radial position were calculated and are presented in Figure 7.5. At the pipe wall the velocity is specified to be zero, thus making the residence time infinite. To provide a measure of the range of residence times present in the flow the values at the pipe centreline and at 95 % of the radius (the radial position of the laminar boundary layer in the turbulent trial) are chosen. Due to the flat velocity profile of the turbulent flow, the residence time distribution is between 2 and 3 seconds while that of the laminar flow lies between 3 and 34 seconds. It is to be expected that the extent of cell damage is influenced by both the magnitude of the shear stress as well as the duration of exposure. The turbulent flow situation exposes the cells to a higher shear stress for a shorter period of time. The difference in residence time between laminar and turbulent flow is more significant closer to the pipe wall where the shear rates are also the greatest.

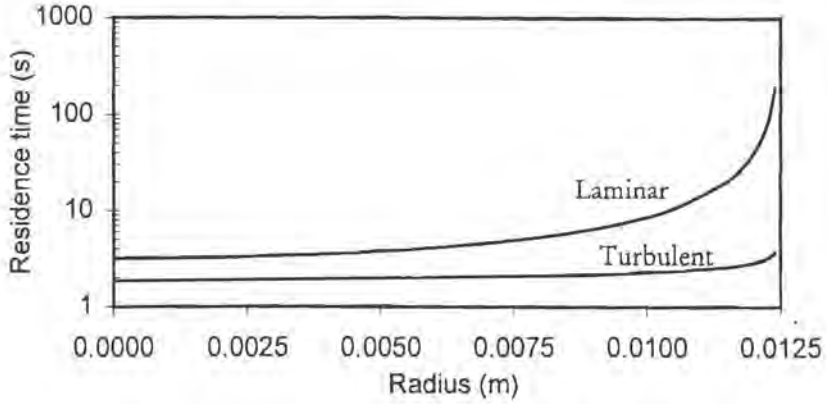

Figure 7.5. Residence time distribution of laminar and turbulent flow in a pipe.

The energy dissipation rate (E_T) (Equation 2.13) together with the total energy dissipated during flow (TE) (Equation 2.14) can be used to correlate damage effects under various flow situations. The specific energy dissipation rates (ε), average Reynolds and viscous shear stresses (τ^R and τ^V respectively) were calculated for the three trials using Equations 2.15, 2.24 and 2.25 and are presented in Table 7.4. There is good agreement between the average shear stress calculated from pressure drop per unit length (Equation 2.8) and the sum of the Reynolds and viscous shear stresses calculated from the energy dissipation rate. The Kolmogorov microscale length (l_c) calculated from the specific energy dissipation rate (ε) (Equation 2.22) indicates that the smallest eddies are approximately 20 times larger than the average yeast cell size. Eddies dissipate their energy and become smaller in size until the Kolmogorov size is reached and their remaining energy is dissipated by viscous action. Particles smaller than this size, therefore, are not exposed to the turbulent shear stress and only the viscous shear component of the total stress has an effect on the particles.

Table 7.4. Shear stress, energy dissipation rate and total energy dissipated during flow rate trials.

Q ($kg.min^{-1}$)	ΔP (kPa)	τ_{avg} (Pa)	τ_{wall} (Pa)	ε ($J.kg^{-1}.s^{-1}$)	E_T ($J.s^{-1}$)	TE (J)	τ^R (Pa)	τ^V (Pa)	l_c (μm)
187.1	334	61.9	157.3	139.2	980	2213	0.054	61.5	160
178.1	284	52.6	140.4	112.7	793	1880	0.048	52.4	156
67.5	104	19.3	28.9	15.6	110	688	-	-	-

7.2.2 Recirculation

Two recirculation trials were conducted lasting 2 and 6 hours, respectively. The holding tank was filled with yeast slurry from the bottom of a fermentation vessel which was then circulated through the 25 mm holding tubes at a flow rate of 70 $l.min^{-1}$ using a NDE lobe pump. Samples were taken at

position 2 (after the pump), indicated on Figure 7.1. The measured pressure drop, calculated viscosity and Reynolds number in the holding tubes for both trials are summarised in Table 7.5. Since the Reynolds number in both trials were less than 2100, the flow in the holding tubes was laminar. The wall and average shear stress (Equations 2.7 and 2.9), specific energy dissipation rate (Equation 2.15) and total energy dissipated (Equation 2.14) were calculated and are also presented in Table 7.5. After the six hour recirculation, one of the butterfly valves was throttled to the 45° position and recirculation continued for another 30 minutes. This additional recirculation time resulted in an additional exposure of 5 passes through the throttled valve.

In the first trial (2 hours), 500 litres of a second generation yeast was recirculated while 400 litres of a seventh generation yeast was used in the second trial lasting 6 hours. The sampling times and the corresponding mean number of passes through the pump and holding tube cycle (N_h) as well as the cumulative energy dissipation is presented in Table 7.6.

Table 7.5. Experimental conditions of the recirculation trials.

Parameter	2 Hour Trial	6 Hour Trial
Yeast Gen. No.	2	7
Flow Rate ($kg.min^{-1}$)	74.4	74.3
μ (Pa.s)	0.069	0.053
ρ ($kg.m^{-3}$)	1062.5	1061.9
Re	910	1191
Consistency (%)	61.0	56.7
Pressure drop (kPa)	190	135
τ_{avg} (Pa)	35.2	25.0
τ_{wall} (Pa)	52.8	37.5
ε ($J.kg^{-1}.s^{-1}$)	31.5	22.4
E_T per cycle ($J.s^{-1}$)	221.7	157.5
TE per cycle (J)	1259.1	960.9

Table 7.6. Sampling time and mean pump exposure number for the recirculation trials.

2 Hour Trial	Time (min)	15	45	75	90	110	130
	N_h	2	6	11	13	15	18
	TE (kJ)	2.64	7.93	13.22	15.86	19.39	22.92
6 Hour Trial	Time (min)	0	50	110	170	230	330
	N_h	0	9	19	30	40	58
	TE (kJ)	0	8.41	18.50	28.59	38.68	55.49

7.2.3 Removal of Spent Yeast from Fermentation - 'Scrapping'

The aim of this trial was to determine the variability of yeast quality in the fermentation cone. This information was used to identify suitable sampling times for the online trials. Although the yeast was expected to be a good quality 4th generation SAB1 yeast (and confirmed so by the samples taken during the trial), the yeast was removed from fermentation duty because of the surplus in the brewery. The Bredal SP/40 peristaltic pump was operated at a flow rate of 60 $kg.min^{-1}$ resulting in a Reynolds number for flow through the 65 mm diameter piping of 109 (assuming a viscosity of 0.088 Pa.s). The measured density of the slurry was 1063 $kg.m^{-3}$ and solids concentration varied between 57.9 and 60.0 %. Samples were taken every hour at sampling point 2 (after the pump) for the six hours that it took to scrap the entire yeast batch.

7.2.4 Brewery Online Trials

The online sampling trials were conducted at SAB – Newlands brewery during the normal cropping procedures on yeast batches destined for reuse. The first online trial was performed on 4th generation SAB1 yeast. The yeast was cropped through a lobe pump operated at 65 $kg.min^{-1}$ and sampling commenced one hour after the start of cropping and lasted 45 minutes. During the time of sampling a total of 2950 kg of yeast was cropped. The starting time of sampling commenced after a mass of 3900 kg had been cropped and sampling continued until 6850 kg had been cropped. This timing was chosen based on the results of the yeast scrapping trial. Figure 7.6 illustrates the yeast handling circuit at the brewery and the possible sampling points. During this online trial, sequential samples were taken at points 1 (before the pump), 3 (before the chiller, approximately 90 m after the pump), 4 (after the chiller), 5 (a mixed sample from the yeast cropping vessel, 30 minutes after the end of cropping 10790 kg), 6 (from the yeast pitching vessel, 19 hours after the end of cropping and before acid washing) and 6 (30 minutes after the start of acid washing).

The second online trial was conducted on an 8th generation SAB5 yeast at a cropping rate of 26 $kg.min^{-1}$ using a lobe pump. Three sets of samples were collected at the sampling points along the pipe length following 800 – 1200 kg, 3500 – 3900 kg and 4000 – 4400 kg yeast to test the variability of yeast collected in the cone of the fermenter as well as to test the response of yeast with different quality to the online flow conditions. The results presented in this work are those of the second set of samples. The total amount cropped was 4650 kg and the remainder from the fermentation vessel was scrapped. The sampling points used were 1 (before the pump), 3 (before the chiller) and 4 (after

the chiller). Two samples were taken from the yeast storage vessel, the first 30 minutes after the end of cropping and the second 90 minutes later. No acid washing was performed on this yeast.

The flow rate, shear stress and energy parameters of the two online trials are summarised in Table 7.7. The standard viscosity of 0.088 Pa.s was assumed for both trials which together with an average 90 metre distance between the fermenting vessel and the chiller leads to a total energy dissipation in this section of 5499 and 2204 J for the two trials. Due to the narrowing of the flow channels at the chiller, a much higher energy dissipation rate would occur and this could result in more substantial shear damage to the cells. Once within the cropping vessel, an overhead paddle stirrer is used to mix the slurry and this dissipates energy at a low shear rate to the cells which could also cause damage. As a result of the cumulative effect of the shear on the cells, the yeast quality can be negatively affected.

Table 7.7. Fluid flow, shear stress and energy dissipation parameters for flow of yeast slurry during the online trials.

Parameter	Online Trial SAB1	Online trial SAB5
Gen. No.	4	8
Flow rate ($kg.min^{-1}$)	65	26
Consistency (%)	58.0	65.0
Density ($kg.m^{-3}$)	1062.5	1063.2
Re	241	97
$\Delta P/L$ (Pa/m)	204.6	82.0
τ_{avg} (Pa)	2.2	0.9
τ_0 (Pa)	6.6	2.7
Residence time, pipe centre (s)	147	366
Residence time, 95% radius (s)	1229	3066

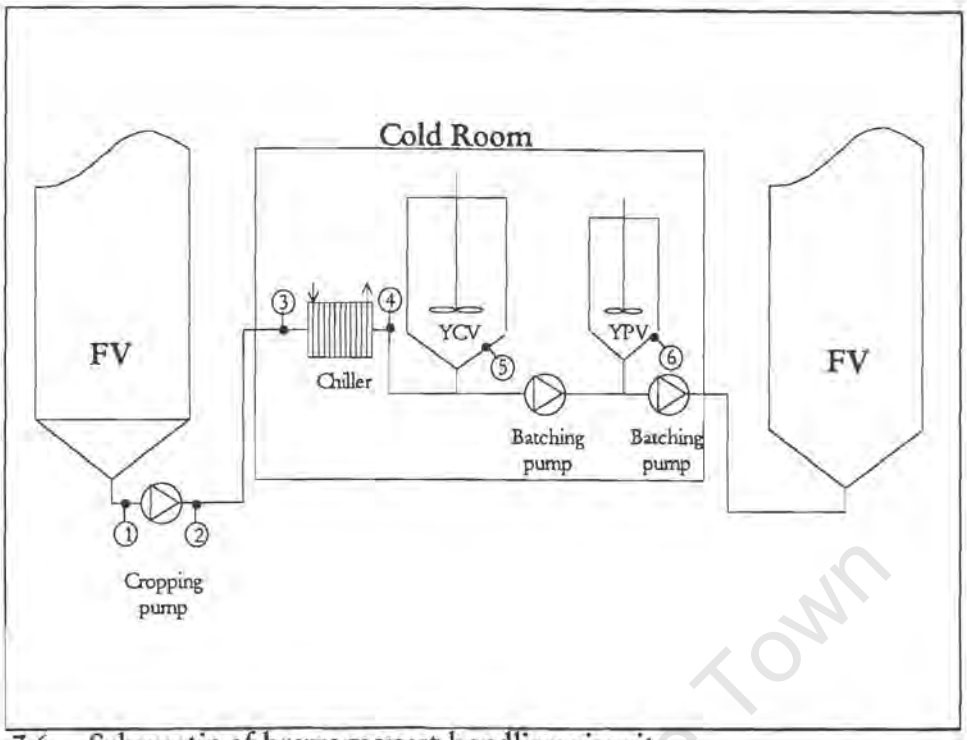

Figure 7.6. Schematic of brewery yeast handling circuit.

7.3 Effect of Fluid Flow Systems on Yeast Quality and Fermentation Performance

The four types of flow systems described above were used to investigate the effect of shear in the brewing environment on yeast quality and fermentative ability. The results of these trials are presented in this section, starting with the 'offline' trials (flow rate, recirculation and scrapping) and ending with the two online trials.

7.3.1 Laminar vs. Turbulent Flow Trials

The trials were classified as being either laminar or turbulent according to the calculated Reynolds number during the flow experiments. Using this system the trials at 178.1 and 187.1 kg.min^{-1} were grouped as turbulent while the 67.5 kg.min^{-1} trial was found to be in the laminar regime. The results of the two turbulent flow trials were averaged due to the similarities between their flow rates, shear stress and energy dissipation rates quoted in Table 7.4. The yeast quality indicators are summarised in Table 7.8 while Table 7.9 contains the results of the fermentation performance and beer quality at the end of fermentations in 2 l EBC tubes (day 12). Also indicated in Table 7.8 and 7.9 are the standard deviations of the turbulent trial data which implies a meaningful difference between the

yeast quality indicators of the laminar and turbulent trials. All fermentations were conducted in duplicate with the average values being reported.

Table 7.8. Yeast quality indicators of the flow rate trials using the Scandi Brew pump and 25 mm holding tubes with standard deviations quoted in brackets.

	Viability (%)	Protease Absorbance	%Damaged Cells (from protease)
Laminar – inlet	95.0	0.097	4.24
Laminar – outlet	96.1	0.170	7.47
Turbulent – inlet	95.7 (±0.9)	0.101 (±0.009)	4.44
Turbulent – outlet	94.1 (±0.1)	0.106 (±0.013)	4.66

Table 7.9. Fermentation performance and beer quality on day 12 of fermentation following the flow rate trials with standard deviations quoted in brackets.

	Fermentation Performance				Beer Quality	
	Rate (hr^{-1})	Final (°P)	Biomass Growth	pH	SO_2 (ppm)	Diacetyl (ppb)
Laminar – inlet	0.0451	1.9	2.9	4.3	14.4	155
Laminar – outlet	0.0380	1.8	2.9	4.3	11.6	119
Turbulent – inlet	0.0402	1.9	3.1	4.3	15.4	169
	(±0.0002)	(±0.0)	(±0.08)	(±0.0)	(±1.0)	(±4.4)
Turbulent – outlet	0.0405	1.8	2.9	4.3	14.6	147
	(±0.0017)	(±0.1)	(±0.07)	(±0.1)	(±3.8)	(±63.7)

The viability of all the yeast samples were identical to within the 2% limit of experimental accuracy and showed that the viability assay is insensitive to this level of damage to the cell membrane. Protease was, however, found to be released across the length of the holding tubes under laminar flow conditions. The increase in protease across the holding tubes under turbulent flow conditions was marginal. This indicates that there was cell damage in the laminar trial and only slight damage to the cellular membranes in the turbulent trials. The fermentation rate of the laminar flow trial showed a 16% decrease at the outlet compared to the laminar inlet sample while the turbulent inlet and outlet sample fermentation rates were similar to each other. The slower rate of fermentation indicates cell damage supported by the membrane damage identified by protease release in the laminar trial. To investigate the reason for the cell damage occurring under laminar flow conditions and not under turbulent conditions, the relative shear stresses and time period of exposure of the yeast to these shear stresses needs to be considered. Although the total shear stress is larger in the turbulent flow

situation, Reynolds stresses dominate in a large portion of the flow in the pipe as seen in Figure 7.2. The smallest eddies that exist in the flow (the Kolmogorov microscale length of 156 μm) were calculated to be approximately 24 times larger than the average yeast cell size (6.5 μm), indicating that the energy associated with the turbulent eddies is unable to be dissipated on the yeast cells. Therefore it is appropriate to only consider the viscous contribution to the shear under turbulent conditions and compare that to the laminar shear in the laminar flow situation. From Figure 7.2 it can be seen that the laminar and viscous shear stresses are equal at a distance of 4 mm from the wall (68% of the pipe radius). At distances closer to the pipe wall there is more viscous shear in the turbulent flow than laminar shear stress in the laminar trial. The quantity of flow associated with this outer region of the pipe equals 28.8 % of the total laminar flow and 48.3 % of the total in the turbulent flow trial. This indicates that if the shear stress is the only parameter of importance then the turbulent flow would have resulted in significantly more cell damage than the laminar trial. It therefore appears that there is also a minimum exposure time required to cause cell damage since these in the turbulent trial are shorter than in the laminar trial.

To determine the extent of cell damage it is assumed for this study that the release of cellular protease from a damaged cell is complete and that sufficient time has elapsed for the protease to leak out through the damaged membrane, i.e. either there is complete release of protease from a damaged cell or no release from an undamaged cell. Additionally, it is assumed that all cells have an equal likelihood of being damaged when exposed to the same forces for the same period of time, i.e. all cells have identical resilience to stress. Using these assumptions, the quantity of yeast which is damaged in both the laminar and turbulent trials can be determined. The specific protease content of cells of strain SAB1 calculated in Chapter 4 was 0.0013 absorbance units/10^6 cells/ml and the cellular concentration of a slurry of 57.7 % consistency was 1750 * 10^6 cells/ml. Based on this, the fraction of damaged cells (Table 7.8) at the inlet and outlet of the holding tubes in both trials was calculated. This indicates that 3.35 % of the undamaged cells entering the holding tubes were damaged in the holding tubes in the laminar flow trial while only 0.23 % were damaged in the turbulent trial. Assuming that all these damaged cells were in the region closest to the wall where the shear stresses and residence times are the greatest then this equates to the outermost 1.2 mm of pipe from the wall, based on the volumetric flow through this portion for the laminar flow trial. At this radius the laminar shear stress is 26.1 Pa and the residence time is 16.8 seconds. This marks the position of the pair of critical shear stress and exposure time, above which cell damage will occur. There is no radial position in the turbulent flow where the residence time exceeds 16.8 seconds, hence despite the viscous shear stress exceeding the critical shear stress of 26.1 Pa at radial distances between 0.0083 m from the pipe centre line and the pipe wall (r = 0.0125), little damage to the cells occurred.

From the analysis of Zhang *et al.* (1993), cells would preferentially distribute themselves out of the laminar boundary layer adjacent to the pipe wall during turbulent flow. In this turbulent flow situation, the laminar boundary layer is 0.6 mm thick and the volumetric flow rate through this circular annulus is 6.2 % of the total. With no cells in this layer, the maximum viscous shear stress to which the yeast was exposed decreased from 157 Pa to 150 Pa. This would appear an insignificant decrease since shear stresses in the laminar flow trial of between 28.9 and 26.1 Pa appeared to be sufficient to cause cell damage.

The fermentation performance of the yeast samples (Table 7.9) indicate that the fermentation rate and beer quality were impacted upon by the flow pattern. Cell damage occurring in the laminar flow trial appears to lower the fermentation rate of the yeast while turbulent flow results in the yeast maintaining its fermentative ability. This decrease in fermentation rate is the result of damaged yeast being used to inoculate the fermenters. The resultant smaller inoculum of healthy cells displayed a corresponding slower fermentation rate. The changes in the final gravity of fermentation (0.1°P) are within the limits of experimental reproducibility of the fermentation assay and as such indicate that although the rate of fermentation is decreased by the laminar flow action, the end point of fermentation is not affected. The amount of biomass growth is also unaffected. Beer quality of the samples taken from the turbulent flow trials were similar at the entrance and exit to the holding tubes but the laminar flow trials showed an improvement at the exit with lower SO_2 levels (19%) as well as lower diacetyl levels (23%). The turbulent flow yeast samples had similar beer quality to the inlet laminar flow trial sample.

The results indicate that laminar flow caused cellular damage as indicated by the higher protease release and decreased rate of fermentation compared to the turbulent flow conditions. The slower fermentation observed for the laminar flow trial, however, did not affect the end point of the fermentation and resulted in the major beer quality indicators showing an improvement of approximately 20%. The improvement in beer quality indicators found for the slower fermentation is in line with industrial experience where fast fermentations are often associated with poor beer quality (Hulse, 2000).

7.3.2 Recirculation

The recirculation of a yeast slurry through a pump and 25 mm diameter holding tubes has the effect of repeatedly exposing the yeast cells to a shear environment. Laminar flow was chosen since it was seen in the flow rate studies that laminar flow showed the most cell damage. The shear action results in energy dissipation which may cause damage to the cells. The damage to animal cells on exposure to shear stress has been postulated to result from fatigue owing to repeated exposure (McQueen *et*

al., 1987). Each time the yeast is recirculated, the total energy dissipated to the yeast is increased. In the 2 hour recirculation trial 1259.1 J was dissipated per cycle at an average shear stress of 35.2 Pa while 960.9 J was dissipated during each cycle in the 6 hour trial at an average shear stress of 25.0 Pa. The difference in energy dissipation is brought about by the difference in viscosity of the two yeast slurries in the trials, 0.069 and 0.053 Pa.s respectively. By plotting the biological response as a function of the cumulative energy dissipation one can observe changes in yeast quality as a result of yeast handling which may not be evident in a single pass as was investigated in the flow rate trials.

Figure 7.7 indicates the changes in yeast quality as a function of total energy dissipation in the two trials. The viability of the cells does not appear to change during recirculation with all values falling within the 2% accuracy of the assay. The oxygen utilisation rate, an indicator of yeast vitality, also does not appear to be affected in either of the two recirculation trials. Increased permeability of the cell membrane was illustrated by protease release during the 6 hour trial. There was no significant increase in protease activity during the 2 hour trial although the trial started with a yeast slurry containing a higher concentration of protease. This indicates that the yeast in the two hour trial was already in a poor condition and further energy dissipation that occurred during the trial did not cause any further deterioration in cell quality.

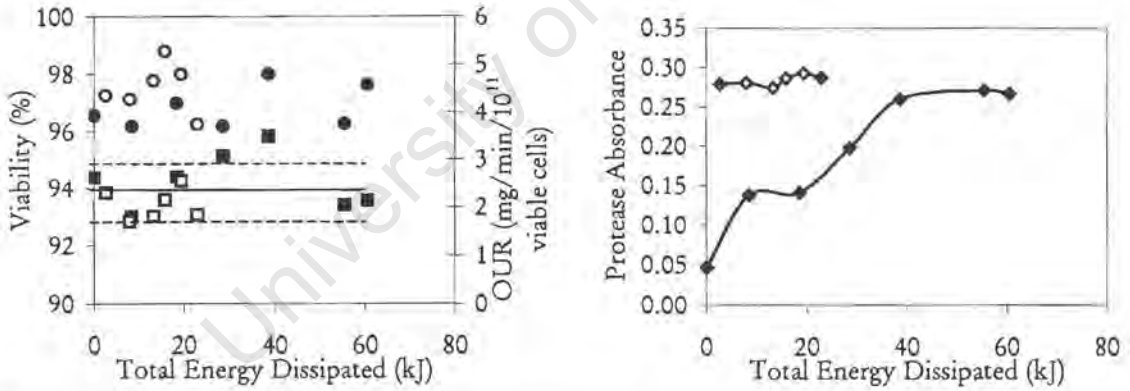

Figure 7.7. Yeast quality during recirculation through pump and pipe test network.
(■ 6 hr trial viability, □ 2 hr trial viability, ● 6 hr trial OUR, o 2 hr trial OUR, ♦6 hr protease, ◊ 2 hr protease with average and standard error lines indicated for viability)

The fermentation performance of the yeast samples was determined with increasing number of passes. The average fermentation rate of the duplicate fermentations is illustrated as a function of cumulative energy dissipation in Figure 7.8. Although there is some scatter among the individual data points, the majority fall within the standard deviation of the assay. This holds for both the 2 hour and 6 hour recirculation trials. The final beer quality values (day 12) of the fermentation are summarised in Tables 7.10 and 7.11. Although the values differ between the two trials, there is no significant difference within the individual trials. The exception is the slight decrease in SO_2 with

increasing recirculation in both trials. The final SO_2 concentration of the fermentations inoculated with yeast from the commencement of recirculation was higher than the remaining fermentations by 17 % in the 2 hour trial and more than 50% higher than those of the 6 hour trial. This is in agreement with the reduced levels of SO_2 produced in the laminar flow trial fermentations in Section 7.3.1.

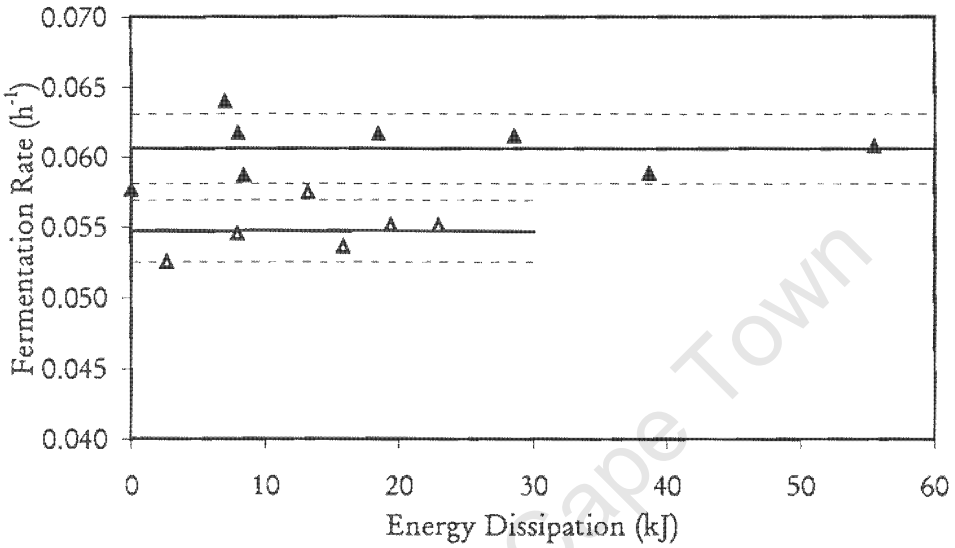

Figure 7.8. Fermentation rate of yeast sampled during the recirculation trials.
(▲6 hr trial, Δ 2 hr, — mean value, - - - standard error in assay)

Table 7.10. Beer quality on day 12 of fermentation following 2 hour recirculation trial.

Recirculation Time	pH	SO_2 (ppm)	Diacetyl (ppb)	Acetaldehyde (ppm)
0:15	4.41	7.8	134	35.4
0:30	4.40	6.5	142	39.4
0:45	4.45	7.2	135	28.8
1:00	4.41	6.0	136	41.2
1:30	4.43	7.3	134	35.2
2:10	4.42	6.3	122	26.1

Table 7.11. Beer quality on day 12 of fermentation following 6 hour recirculation trial.

Recirculation Time	pH	SO_2 (ppm)	Diacetyl (ppb)
0:00	4.38	18.4	118
0:50	4.38	12.4	120
1:50	4.37	12.2	118
2:50	4.38	11.5	120
3:50	4.40	13.1	136
5:30	4.38	11.9	123
5:35T	4.36	10.8	115
6:00T	4.37	12.0	126

T – indicates samples collected while pumping through a partially throttled valve.

7.3.3 Removal of Spent Yeast from Fermentation – 'Scrapping'

Variations in yeast quality can occur within a batch of yeast in a fermentation vessel, which is typically between 9 and 12 tons. The rapidly flocculating yeast which settled first is compacted at the bottom on the vessel by subsequent yeast flocculation. The initial yeast is held under non-optimal conditions where nutrient starvation may occur for longer and may be of a poorer quality, in terms of viability and vitality, than that which settled later. The yeast settling at the top may also have inappropriate qualities for the brewing environment in terms of poor flocculation ability or reduced vitality and viability. The yeast in a fermentation vessel can therefore be divided into three types: the early, middle and late flocculent, each with varying quality. By sequentially sampling the yeast from the bottom of a fermentation vessel during cropping or scrapping, the variations in yeast quality and fermentation performance were investigated. This was studied using a 4th generation SAB1 yeast.

The results of the yeast quality assays are summarised in Table 7.12 and indicate that the cell viability and protease concentrations do not vary significantly as a function of time during the crop and hence with position in the cone and time of flocculation in the fermenter. The oxygen utilisation rate (OUR) of the yeast, indicating its metabolic activity, varied by up to 67% during the trial. The results indicate that the initial 4 tons of yeast were the least active with activity increasing through the middle of the crop, peaking at 8 tons and then decreasing slightly. The low activity of the yeast at the bottom of the cone is consistent with early flocculation and prolonged nutrient limitation. The position of the peak of highest cell activity in the middle of the crop is consistent with the flocculation of active yeast responsible for the bulk of fermentation. The less active yeast still in suspension flocculated later settling at the top of the yeast cone and resulting in the tailing off of activity towards the end of the crop.

Table 7.12. Yeast quality indicators during yeast scrapping trial.

Yeast Mass Cropped (kg)	Viability (%)	Oxygen Utilisation Rate (mg/l/min/10^9 viable cells)	Protease Absorbance
2 000	93.2	0.06	0.24
4 000	93.7	0.06	0.26
6 000	92.0	0.07	0.25
8 000	92.1	0.10	0.25
10 000	94.1	0.09	0.22
12 000	92.9	0.08	0.26

The beer quality indicators (day 10) and fermentation performance of duplicate fermentations performed at the 500 ml scale are summarised in Table 7.13. The fermentation rate and final fermentation density did not vary. The yeast towards the end of the crop did show better biomass growth ability than the yeast which settled earlier as indicated by the increase in biomass growth factor from 2.9 to 3.2/3.3 times the initial mass of yeast inoculated with the standard deviation being 0.1. The beer quality indicators are similar and within the experimental error associated with replicate fermentations. Although the initial yeast activity measured by its oxygen utilisation rate was lower for the yeast at the bottom of the cone, the yeast may have had sufficient recovery time during the fermentation for any changes to be observed during fermentation. Along with fermentation rate and extent, the beer quality of the different fermentations was not a function of the position of the yeast in the cone.

Table 7.13. Fermentation performance indicators and beer quality on day 10 of fermentation following yeast scrapping trial.

Scrapped mass (kg)	Fermentation Performance			pH	Beer Quality		
	Rate (h^{-1})	Final (°P)	Yeast Growth		SO_2 (ppm)	Diacetyl (ppb)	Acetaldehyde (ppm)
2 000	0.0455	2.24	2.9	4.6	17	328	27
4 000	0.0455	2.25	3.1	4.6	16	339	27
6 000	0.0423	2.28	3.1	4.6	21	329	22
8 000	0.0445	2.23	3.0	4.6	20	320	21
10 000	0.0454	2.24	3.3	4.6	21	320	31
12 000	0.0463	2.23	3.2	4.5	18	321	29

7.3.4 Online Trials

Figure 7.9 represents the cell viabilities at each point in the yeast handling circuit for both online trials. Also indicated are the 2% error bars which show that viability is not affected through the handling circuit. The intactness of the cell membrane showed a decrease with progression along the yeast handling circuit, indicated in Figure 7.10 by increasing extracellular protease concentration. The online trial conducted with SAB1 yeast was characterised by a faster rate of pumping than the trial with SAB5 yeast and showed the expected pronounced relative increase in protease activity. The specific protease activity of the two strains of yeast used in the different trials are 0.0013 absorbance units/10^6cells/ml for SAB1 and 0.0032 absorbance units/10^6cells/ml for SAB5 yeast. Hence the trial with SAB1 yeast, which had a lower specific protease content, showed an even greater loss of membrane integrity. The lower shear stress and energy dissipation rates of the SAB5 trial therefore had a positive effect on lowering the shear damage to the cells.

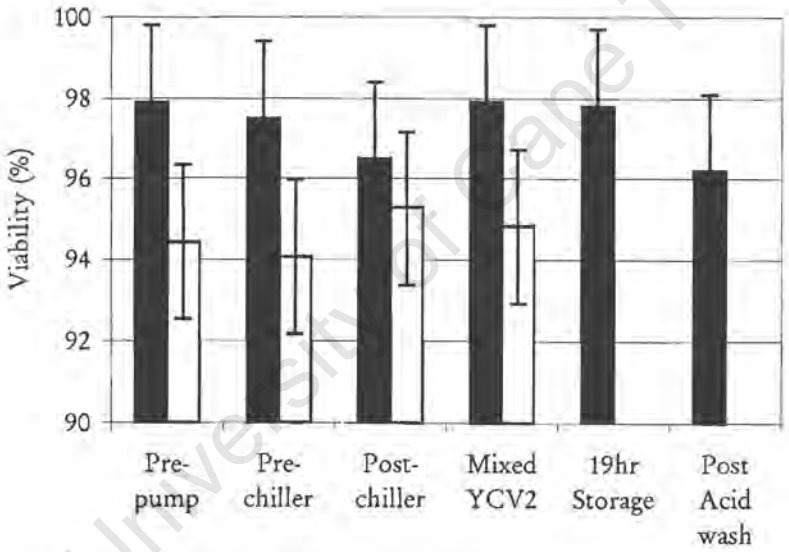

Figure 7.9. Viability during online cropping trials.
(■ SAB1, □ SAB5)

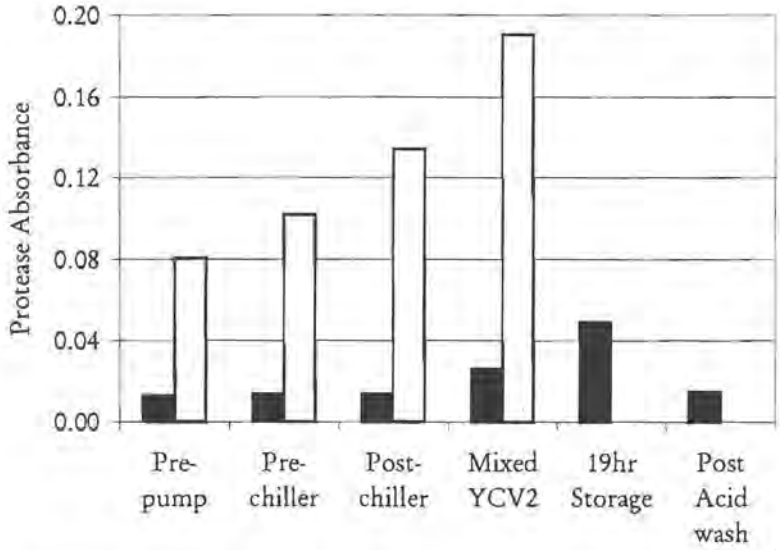

Figure 7.10. Protease release during online cropping trials.
(■ SAB1, □ SAB5)

The surface properties of hydrophobicity, charge and flocculence can also be altered by the cumulative shear effect in yeast handling. These properties have been shown to be affected by shear damage in the French Press and centrifuge trials. During online cropping where shear stress was relatively low in comparison to the French Press and centrifuge trials, changes in hydrophobicity were not observed except at the position after the chiller which showed a 35% decrease in hydrophobicity index for strain SAB1 and 5% decrease for SAB5 (Figure 7.11) The error associated with the hydrophobicity assay was 3.9 %. Since cooling such as that occurring in the heat exchanger is known to alter the structure and physical properties of lipid bilayer membranes (Alonso *et al.*, 1997), a similar mechanism may alter lipid structure and hydrophobic properties in the cell wall of yeast. The hydrophobicity of the mixed YCV sample is higher than at the position after the chiller which may have resulted from it being a mixed sample, averaged across the entire quantity of yeast cropped, unlike the samples in the pipe work which were taken sequentially and represent a point in time during cropping. During storage of the yeast in the vessel, hydrophobicity was found to decrease by nearly 30% (SAB1). The acid washing restored the yeasts' hydrophobicity to its initial value. Wilcocks and Smart (1995) monitored the effect of acid washing on cell hydrophobicity and found a strain specific response. The hydrophobic coupling capacity of the lager strain (KS1) was unaffected while that of the ale yeast (NCYC 1119) showed an initial decrease during the first 3 hours of acid washing followed by a dramatic increase. During the SAB5 trial, the cropped yeast was reused without first being stored, hence the effect of storage was not determined.

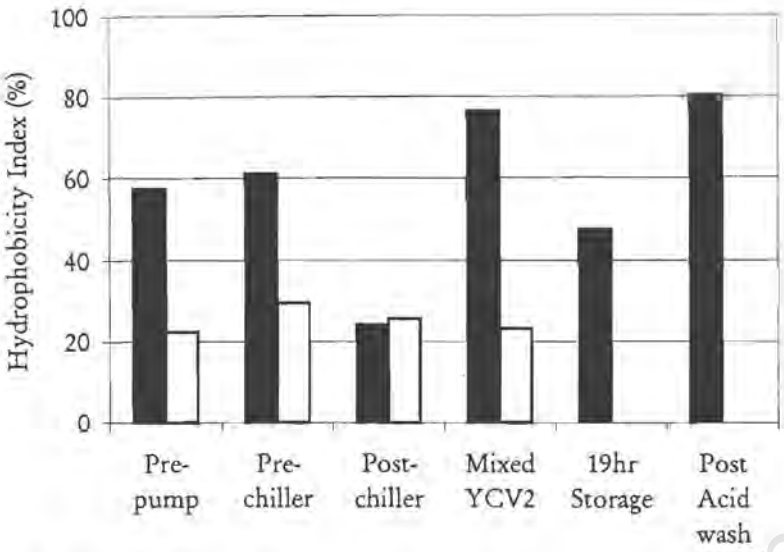

Figure 7.11. Hydrophobicity changes during online cropping trials.
(■ SAB1□ SAB5)

The cell surface charge of the yeast cell samples taken during the SAB1 trial was determined by the alcian blue dye retention technique. These results, presented in Figure 7.12, show that there is little or no effect of cropping on surface charge. Alcian blue dye retention was used by Wilcocks and Smart (1995) to study the effect of acid washing on cell surface charge. They showed no change in surface charge with acid washing over times less than 2 hours with longer exposure resulting in a decrease in dye retention by lager yeast, and an increase with ale yeast. This difference in response of the ale and lager yeasts could be related to their flocculation behaviour where ale yeast floats to the surface and lager yeast settles. The technique of dye adsorption is, however, less descriptive of the charge on the cell surface because was only conducted at a single pH, hence the SAB5 trial was analysed using the zeta potential measurement to determine the charge across a wide range of pH. The results of this study were used to calculate the total number of chargeable groups (N_S) and ratio of phosphate to carboxyl groups (q) on the cell surface. The zeta potential profiles (Figure 7.13) are not substantially different across the pH range used, all showing a pI of 3.5 ± 0.05. Figure 7.14, depicting the N_S and q values with the 95% confidence error bars, shows that the surface charge group composition is not significantly affected by the cropping procedure.

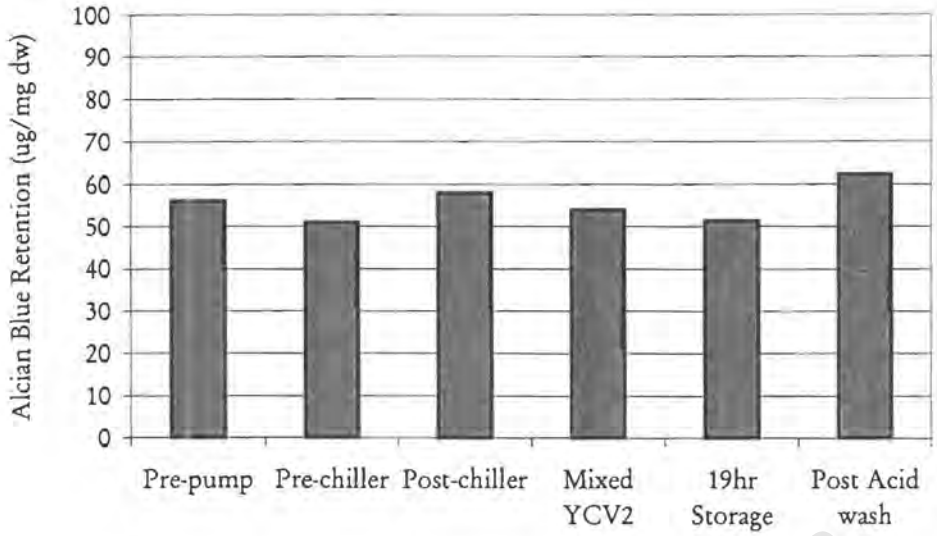

Figure 7.12. Changes in Alcian Blue dye retention during the online trial with SAB1 yeast.

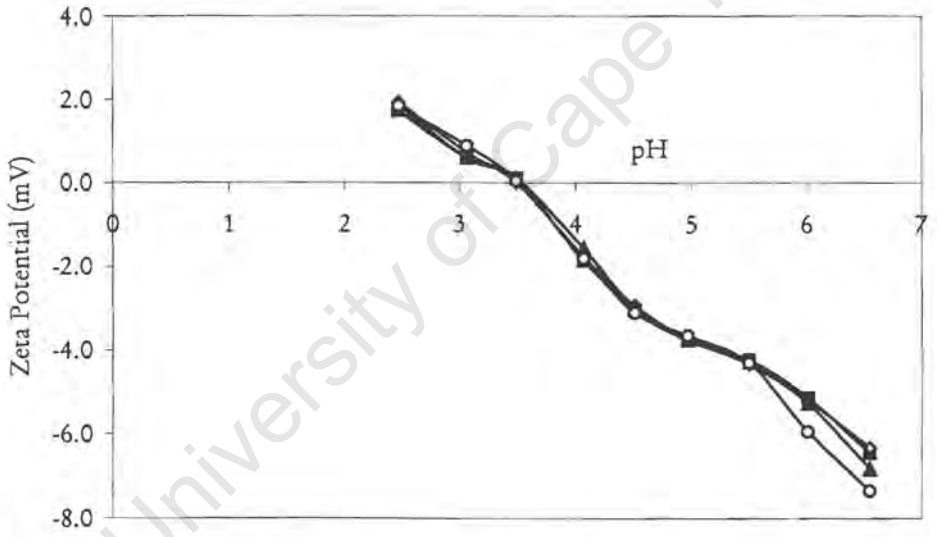

Figure 7.13. Zeta potential profiles of yeast during the online trial with SAB5 yeast.
(■ pre pump, ◊ chiller inlet, ▲ chiller outlet, ○ yeast cropping vessel)

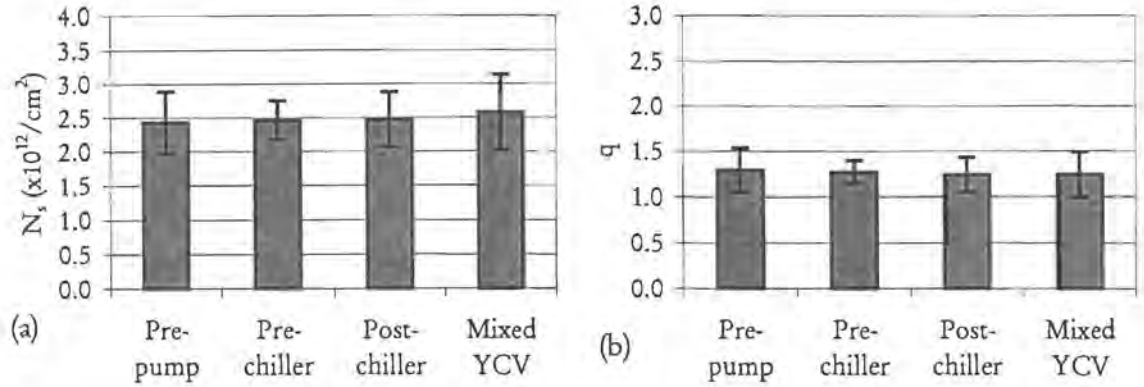

Figure 7.14. Changes to surface charge group composition during the online SAB5 trial.
((a) total number of chargeable groups, (b) ratio of phosphate to carboxyl groups)

The yeast samples taken during the online trial with SAB5 yeast indicated no loss of flocculence across the portion of the handling circuit (Figure 7.15). The shear stresses observed in the online trial are lower than those present in the French Press and centrifuge trials in which decreases in yeast flocculation was seen (Section 5.4.3. and 6.4.7). It therefore appears that the loss of flocculence requires higher shear forces than those typically observed during brewery cropping procedures.

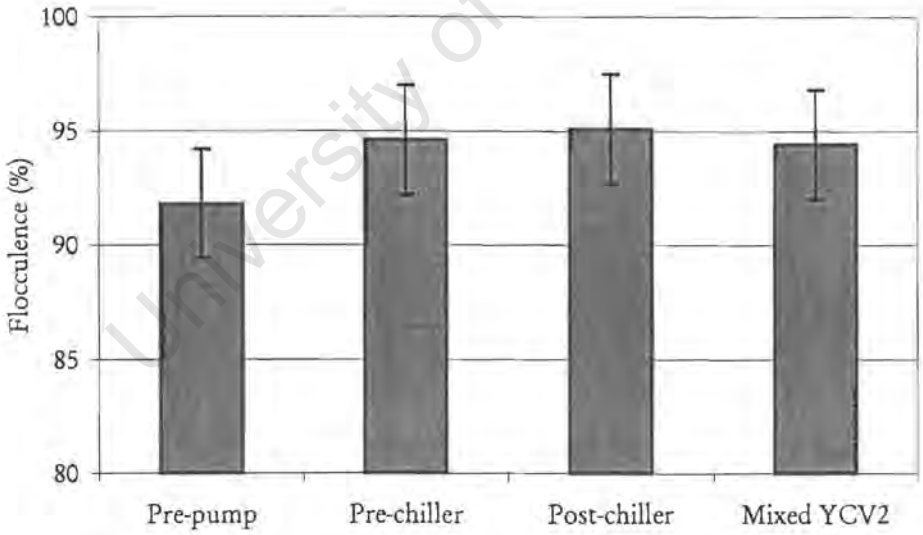

Figure 7.15. Yeast flocculence during yeast cropping trial with SAB5 yeast.

The effect of shear stress on fermentation performance of the yeast during the online trials were determined in terms of the rate and extent of fermentation as well as the final quality of beer produced in the 2 litre small scale fermentations. These fermentations were inoculated at 1/7th the standard rate which accounts for the higher biomass growth of between 4.7 and 6.0 achieved in these fermentations. Figure 7.16 depicts the rate and extent of fermentation. The rates show an increase through the yeast handling circuit which is greater than the standard error of 4.1 % for replicate

fermentation rates. The extent of fermentation did not show any variation, indicating that the slight increase in fermentation rate did not impact on the final density of fermentation.

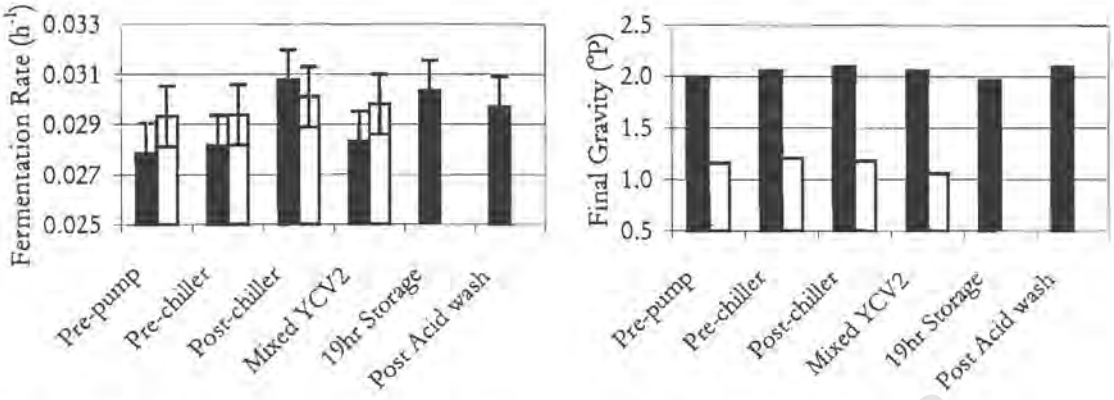

Figure 7.16. Fermentation rate and extent from online trial fermentations.
(■ SAB1,□ SAB5)

The beer quality indicators of the SAB1 and SAB5 online trials are summarised in Table 7.14 and Table 7.15 respectively. The first trial shows that the level of diacetyl, acetaldehyde and pH are not affected along the handling circuit while there is a slight increase in the yeasts' biomass growth factor along the handling circuit. The concentration of SO_2 appears to decrease along the cropping route particularly during storage and acid washing. This change in beer quality (exceeding the standard deviation of replicate samples) was also noted for the laminar flow and recirculation trials and indicates a real change in beer quality. The beer quality assays of the second trial did not include SO_2 levels since this assay was removed from the standard operating assays required for SAB5. This trial, however, did not show any of the beer quality indicators (diacetyl and ethanol) to be different at any point along the yeast handling circuit.

Table 7.14. Final beer quality indicators (day 10) for online trial with SAB1 yeast.

Sample	Biomass Growth	pH	SO_2 (ppm)	Diacetyl (ppb)	Acetaldehyde (ppm)
Pre-pump	4.7	4.2	14.6	286	22
Chiller-inlet	4.9	4.1	16.0	268	22
Chiller-outlet	4.9	4.1	15.3	253	22
YCV	5.1	4.1	13.1	286	19
Stored-19hr	5.2	4.1	12.2	255	22
Post-acid wash	5.1	4.1	10.8	255	21

Table 7.15. **Final beer quality indicators (day 10) for online trial with SAB5 yeast.**

Sample	Biomass Growth	pH	Diacetyl (ppb)	Ethanol (g/l)
Pre-pump	6.0	4.1	113	7.4
Chiller-inlet	5.9	4.1	123	7.3
Chiller-outlet	5.8	4.1	96	7.1
YCV	6.0	4.1	112	7.2

7.4 Summary

The shear stress, energy dissipation rate, total energy dissipated and residence times within the holding tubes and pipe section of the online trial are summarised in Table 7.16 while the various biological responses to shear stress in each of the brewery system trials are presented and summarised in Table 7.17. Protease activity showed an increase in all but the 2 hour recirculation and turbulent flow trials. The two hour recirculation trial, however, used yeast with a high protease initial concentration indicating the loss of some cell membrane integrity before the start of recirculation. Small changes were recorded in the fermentation rate of hydrodynamically stressed cells in individual trials. The laminar trial showed a reduction in fermentation rate of 16% while the two online trials, conducted at significantly lower shear rates, showed slight increases in fermentation rate (3 – 11%). The beer quality indicator, SO_2 concentration, was found to be reduced by shear action in the flow trials and was not always accompanied by slower fermentation rates.

While the greatest total shear stress and energy dissipation rates were found in the turbulent flow trial, the least effect on yeast quality and fermentation indicators resulted. The remainder of the trials were conducted under laminar conditions and showed varying degrees of damage to the yeast and its fermentation ability. This indicates that less cell damage occurs in turbulent flow which is explained by the protective aspect of the turbulent eddies with the smallest eddies of sizes equal to the Kolmogorov micoscale length being too large to interact with the cell, to cause cell damage resulting in the yeast cells merely being transported within these eddies. The viscous shear stress is therefore the only portion of the total shear stress which can cause cell damage. Despite the higher viscous shear stress present in a large portion of flow in the pipe during the turbulent flow trial compared to the laminar trial, the shorter residence time to which the cells are exposed to the shear results in little actual damage to the cells. It is therefore important to consider in combination the magnitude of shear stress and its exposure time when assessing cell damage.

To prevent cell damage due to hydrodynamic shear stress in pipe flow around the brewery it is recommended that the yeast is either pumped sufficiently slowly such that the maximum shear stress

is below the critical stress required to cause damage as illustrated in the online trial with SAB5 where the wall shear stress was 2.7 Pa. Alternatively it should be possible to pump the slurry sufficiently fast to ensure turbulent flow in which Kolmogorov microscale lengths larger than the cell size are ensured to avoid cell damage by Reynolds shear stress and cell damage by viscous shear stress is minimised by reducing the residence time to which the cells are exposed to the stress.

Table 7.16. Summary of shear stress, energy dissipation and residence time values of the brewery handling trials.

	ε ($J.kg^{-1}.s^{-1}$)	E_T ($J.s^{-1}$)	TE (J)	τ_0 (Pa)	$t_{95\%}$ (s)	τ_{avg} (Pa)	t_{avg} (s)
Turbulent	126.0	887	2047	148.9	3	57.3	2
Laminar	15.6	110	688	28.9	34	19.3	6
Recirculation 2 hr	31.5	221.7*	1259*	52.8	30*	35.2	6*
Recirculation 6hr	22.4	157.5*	960*	37.5	33*	25.0	6*
Online SAB1	0.059	19	5499	6.6	1229	2.2	298
Online SAB5	0.0095	3	2204	2.7	3066	0.9	733

* - per pass through holding tubes

Table 7.17. Summary of biological responses during brewery system trials.

Treatment	Yeast Quality			Yeast Surface Properties			Fermentation Performance				Beer Quality			
Trial	Viab.	OUR	Prot.	Flocc.	Charge	Hydro.	Ferm. Rate	Extent of Ferm.	Biomass Growth	pH	SO_2	Diac.	Acet.	EtOH
Laminar flow	×	/	↑ (75%)	/	/	/	↓ (15%)	×	×	×	↓ (19%)	↓ (23%)	/	/
Turbulent flow	×	/	×	/	/	/	×	×	×	×	×	×	/	/
Recirculation (2 hour)	×	×	×	/	/	/	×	×	×	×	↓ (17%)	×	×	/
Recirculation (6 hour)	×	×	↑ (500%)	/	/	/	×	×	×	×	↓ (50%)	×	×	/
Online SAB1	×	/	↑ (277%)	/	×	↓ (61%)	↑ (11%)	×	↑ (10%)	×	↓ (32%)	×	×	/
Online SAB5	×	/	↑ (141%)	×	×	/	↑ (3%)	×	×	×	/	×	/	×

↑ (%) – increased response/concentration with increased hydrodynamic shear

↓ (%) – decreased response/concentration with increased hydrodynamic shear

× – no biological response

/ – not measured

It is possible to postulate the existence of a critical shear stress, below which no cell damage can occur despite an infinite exposure time to the stress. This is supported by the lack of cell damage in the two online trials along the section of pipe leading to the heat exchanger where the wall shear stress was low (6.6 and 2.7 Pa) while the exposure times were long (in excess of 1229 and 3066s in the region close to the pipe). As the shear stress is increased beyond the critical value (overstress), the time required to cause cell damage would be reduced. This could be seen in the recirculation trial where a wall shear stress of 38 Pa and associated exposure time in excess of 33 seconds per cycle was able to cause more than 5 times the protease release in just 9 exposures (or a total exposure time of 297 seconds) than in the pipe section of the online trials. A shorter exposure time of 3 seconds in the turbulent trial was seen to be too short to cause cell damage despite the higher wall shear stress of 149 Pa. The hypothesis that is therefore proposed is that a critical stress is required to cause cell damage and that the rate of cell damage occurring is proportional to the overstress and the exposure time.

Chapter 8: Conclusions

In this study, a scheme whereby the hydrodynamic stress could affect the yeast by four possible routes depending on the severity of the stress is hypothesised. Firstly, the loss or rearrangement of molecules from the outermost layers of the cell wall may occur under mild hydrodynamic shear conditions. Such alterations at the cell surface may be detected by changes to the surface charge, hydrophobicity and flocculation potential of the yeast. Secondly, integrity of the cell membrane or permeabilisation of the cell membrane can also occur at higher shear stress. This damage may be detected by the loss of viability or release of protease enzymes. More severe stress may cause damage to the cytoskeleton of the cell altering the yeasts fermentation performance with cell disruption occurring at extreme stresses. By use of appropriate analysis of the fluid shear forces with which the cells are in contact as well the time of exposure, the biological response of the cells may be predicted.

Changes to the outer cell surface were detected by changes to the hydrophobicity, surface charge and flocculation potential of the cell. The zeta potential profiles of the cell surface across a range of pH between 2.2 and 7.5 allowed for the calculation of the relative quantities of the carboxyl and phosphate groups at the surface as well as the total number of surface charge groups. The surface elemental composition and molecular composition were also measured and provided an indication of the quantity of the major compounds present at the surface. The loss of membrane integrity was determined by a methylene blue viability stain as well as by the extracellular detection of elevated levels of protease. Overall yeast quality and cytoskeletal function were monitored by fermentations to quantify fermentation rate and the quality of the produced beer. Cell disruption was monitored by microscopic cell counts and particle size analysis was used for the detection of cell fragments and fine haze material.

Both aerobically and anaerobically produced yeast are subjected to mechanical handling in the brewery: the former during the stages of propagation and the latter on cropping between fermentations. Hence it is important to investigate the relative resilience of each type of culture to hydrodynamic shear damage. For this purpose, three flocculent strains (SAB1, SAB1/96, SAB5) and one non-flocculent strain (SAB2) were grown in 1.5l bioreactors under both aerobic and near anaerobic conditions. The growth of cells was found to be described by the logistic equation which showed that aerobic propagation resulted in a 15 – 25 % increase in the logistic growth rate constant, k. Aerobic propagation also produced a 2 to 3 fold higher final biomass concentration. The ratio of the aerobic to anaerobic yield coefficients ($Y_{X/(S+E)}$) of the three flocculent strains were similar to the ratio of final biomass concentrations ($1/\beta$). This indicated the consistency of the split of carbon flux between biomass and ethanol under the two growth conditions. This supports the existence of the Crabtree effect under conditions of high sugar concentration as found in brewing wort. The Crabtree effect is also evident in the non-flocculent strain but the effect is less pronounced than compared to the flocculent strains. This was observed from the higher yield ratio and lower ratio of maximum biomass concentration ($1/\beta$) which implied the strains preferred production of biomass to ethanol under aerobic conditions.

During the aerobic and anaerobic propagations, it was found that the surface properties, including hydrophobicity, charge and composition, approached constant values toward the late exponential to early stationary phase. This finding allowed cell surface changes observed following hydrodynamic shear stress to be attributed to cell damage and not merely a sensitivity to the growth phase.

The surface properties of the stationary phase yeast was found to be dependent on the oxygen availability during growth. The increased availability of oxygen during cell growth resulted in the yeast having a higher total surface charge group concentration (N_S), as much as 70% more than the anaerobic cultures. This increase in total charge group concentration at the surface was found to be a result of the increased concentration of mannan and protein at the cell surface. The ratio of phosphate to carboxyl groups at the surface (q) was increased some 4.7 fold for aerobic growth which corresponded to a higher mannan to protein ratio at the cell surface. The hydrophobicity of yeast grown anaerobically was found to be greater than that grown aerobically. This was supported by the increased lipid content of the anaerobic cultures over aerobic cultures. The aerobically produced flocculent yeast was found to be more flocculent than the anaerobic cultures. This increased flocculation occurred despite the increased surface charge and reduced hydrophobicity, refuting the role of the DLVO theory of flocculation. This provides additional evidence to that already in literature that flocculation among "flocculent" strains of brewing yeast occurs by specific antigen/antibody interactions between lectins and receptor sites on adjacent cells. Hence, exposure to hydrodynamic shear stress has potential to cause the loss of flocculation potential due to the loss

or damage of either the lectins or receptor sites. The non-flocculent strain of yeast showed a slight increase in flocculation under anaerobic growth conditions than under aerobic conditions. The difference in surface charge and hydrophobicity of these cells was consistent with increased flocculation in accordance with DLVO theory.

The French Press was used to generate a high degree of turbulence with Kolmogorov sized eddies smaller than the size of the yeast cells. This resulted in a high efficiency with which the pressure drop was converted to Reynolds shear stress acting on the cell surface (94.5%). A pressure differential in the French Press of less than 6-10 MPa caused sub-lytic damage to the cells propagated under laboratory conditions while for production yeast this critical pressure was 20 MPa. At pressures greater than this critical pressure cell disruption occurred but the cell viability of the intact cells remained appreciable. This indicated that cell disruption at extreme hydrodynamic stresses occurred as a single discrete event rather than as a result of gradual attrition and loss of cell wall strength due to fatigue.

The resilience of the yeast as a function of the oxygen availability was investigated using the French Press apparatus. Across the range of pressures used there was no significant difference between aerobically and anaerobically propagated yeast with regard to the extent of cell disruption. However, the production strain SAB5 yeast showed a greater resilience to cell disruption than the laboratory propagated yeast of the same strain. Under super-lytic operating pressures the specific protease content of aerobically propagated yeast was found to be the highest while that of the production yeast was the lowest with the anaerobically propagated yeast having an intermediate specific protease content.

Sub-lytic pressures were then used to investigate the effect of non disruptive shear stress on the surface properties of the yeast cells. No change to hydrophobicity was observed in aerobic, anaerobic and production yeasts studied. Surface charge was found to be affected when the yeast was grown anaerobically at either production yeast or laboratory scale. Change in surface charge was characterised by a broadening of the zeta-potential – pH profile across the range from 2.2 to 6.8 with increased hydrodynamic stress. This trend was supported by an increase in the total number of charge groups at the surface, N_s. The ratio of phosphate to carboxyl groups (q) of these yeasts also showed changes with a general decrease being observed. The flocculence of the yeast was found to be decreased by the exposure to the French Press, with the aerobic yeast being more susceptible to a loss of flocculence than the anaerobically grown yeast. The flocculation potential was, however, found to be recoverable in subsequent fermentation. The production yeast did not show any effect of shear damage on cell flocculence in the French Press.

Centrifuges are increasingly being used in the brewery and as such their effect on the yeast quality was investigated. A hypothesis was proposed to attribute the shear stress damage that occurred in the disc stack centrifuge to two separate zones within the centrifuge. The disc zone was identified as the first high stress region with which the cells come into contact. In this zone the feed is accelerated to the velocity of the rotating discs and is distributed by upward flow through riser holes in the discs. The cells sediment out of suspension in this zone and pass along the underside of the discs to the solids-holdup space. Here they accumulate until their removal from the centrifuge through a set of nozzles. The intermittent discharging of the cells through these nozzles at the periphery of the holdup space was identified as the second zone of high shear. Biological response of yeast cells as a result of centrifugation in the disc stack machine included a loss of cell viability and the release of protease into the concentrate stream of the centrifuge. These effects were attributed to shear in the disc zone. Changes occurring at the cell surface included the loss of hydrophobicity, the increase in total cell surface charge (N_s), the reduction in the ratio of phosphate to carboxyl groups (q) and the loss of flocculation potential. Neither the loss of hydrophobicity not the changes in charge group composition could be attributed to specific zones within the centrifuge. The loss of flocculation ability was, however, attributed to shear in both the disc and solids discharge zones. Although variable fermentation performance of centrifuged yeast was observed, the fermentation rate was generally slightly increased. This increase in fermentation rate was accompanied by a decrease in beer quality (increased diacetyl and SO_2 concentrations) produced by fermentation. Cells at early stationary phase on removal from fermentation by centrifugation were found to result in faster subsequent fermentation rates as well as improved beer quality. This has the implication that yeast reuse should commence as soon as possible after reaching its stationary phase with storage times being reduced to a minimum to achieve improved fermentation performance.

The effect of hydrodynamic shear, caused by the flow of yeast slurries through a pipe on yeast quality and fermentation performance was investigated. The results indicated that laminar flow with high viscous shear stresses along a fixed pipe length resulted in more cell damage than turbulent flow, as observed by increased protease release and decreased fermentation performance. When examining the shear stresses in turbulent flow, the contribution from the Reynolds shear stress could be negated as the Kolmogorov microscale length was approximately 24 times larger than the average cell size and therefore the energy in the turbulent spectrum was unable to be transmitted to the individual cells. The viscous shear stress in the turbulent flow dominates near the pipe wall and was higher than the laminar shear stress encountered at the wall in the laminar flow trial. Thus, besides the magnitude of the shear stress, the time of exposure is also significant when predicting cell damage due to shear stress. Although fermentation rate decreased for the laminar flow regime this did not adversely affect the beer quality but rather lower SO_2 levels (19%) and diacetyl concentration (23%) was observed.

The repeated exposure to laminar shear stress was examined in the recirculation trials operated under laminar flow conditions. The only yeast quality indicator affected was the protease for the 6 hour trial as seen by its increased release with total energy dissipated. The fermentation rates were unchanged although again improved beer quality was observed by decreased SO_2 and diacetyl concentrations (17 % for the 2 hour trial and 50 % for the 6 hour trial).

The yeast quality and fermentation performance did not vary significantly with position in the cone of the fermentation vessel although the oxygen utilisation rate of the yeast was found to be highest in the middle portion of the crop. Hence the most appropriate sampling times set for the online trials were either during the middle or at the end of the crop where the yeast was most active. During the online trials, cell viability was not affected along the cropping route. An increase in protease release along the route indicated an increase in membrane permeability. Of the surface properties (hydrophobicity, charge, flocculation ability), only hydrophobicity was affected through the plate and frame heat exchanger (35% decrease for SAB1 and 5 % decrease for SAB5). Fermentation rates of yeast sampled along the cropping route was found to either unaffected or increased slightly while the extent of fermentation did not increase. The only change to beer quality was a slight decrease in SO_2 concentration.

From the data collected in this study it has been possible to postulate the existence of a critical shear stress, below which no cell damage occurs despite an infinite exposure time to the stress. This is supported by the lack of cell damage in the two online trials along the section of pipe leading to the heat exchanger where the wall shear stress was low (6.6 and 2.7 Pa) while the exposure times were long (in excess of 1229 and 3066s in the region close to the pipe). As the shear stress is increased beyond the critical value (overstress), the time required to cause cell damage would be reduced. This is seen in the recirculation trial where a wall shear stress of 38 Pa and associated exposure time in excess of 33 seconds per cycle was able to cause more than 5 times the protease release in just 9 exposures (or a total exposure time of 297 seconds) than in the pipe section of the online trials. A shorter exposure time of 3 seconds in the turbulent trial was seen to be too short to cause cell damage despite the higher wall shear stress of 149 Pa. The extreme case of intense shear stresses of between 2.8×10^6 and 9.5×10^6 Pa for an instantaneously short exposure time of $10^{-4} - 10^{-5}$ seconds in the French Press was seen to be sufficient to cause a range of cell damage from mild surface changes to complete cell disruption. The hypothesis has therefore been supported that a critical stress is required to cause cell damage and that the rate of cell damage occurring is proportional to both the magnitude of the overstress and the exposure time.

Chapter 9: References

Agerkvist I and Enfors S-O (1990). Characterisation of *E. coli* cell disintegrates from a bead mill and high pressure homogenizers. *Biotechnology and Bioengineering*, **36**:1083-1089.

Aiba S, Shoda M and Nagatani M (1968). Kinetics of product inhibition in alcohol fermentation. *Biotechnology and Bioengineering*, **10**:845-864.

Alonso A, Queiroz CS and Magalhaes AC (1997). Chilling stress leads to increased membrane rigidity in roots of coffee (*Coffea arabica* L.) seedlings. *Biochemica et Biophysica Acta* **1323**:75-84.

Amory DE and Rouxhet PG (1988). Surface properties of *Saccharomyces cerevisiae* and *Saccharomyces carlsbergensis*: chemical composition, electrostatic charge and hydrophobicity. *Biochimica et Biophysica Acta*, **938**:61-70.

Amory DE, Mozes N, Hermesse MP, Leonard AJ and Rouxhet PG (1988). Chemical analysis of the surface of microorganisms by X-ray photoelectron spectroscopy. *FEMS Microbiology Letters*, **49**:107-110.

Amri MA, Bonaly R, Duteurte B and Moll M (1982). Yeast Flocculation: Influence of nutritional factors on cell wall composition. *Journal of General Microbiology*, **128**:2001-2009.

Arnold WN (1981). Yeast Cell Envelopes; Biochemistry, Biophysics and Ultrastructure Vol. 1, CRC Press, Boca Raton.

Bacon JSD, Davidson ED, Jones D and Taylor IF (1966). The location of chitin in the yeast cell wall. *Biochemical Journal*, **101**:36c-38c.

Bailey JE and Ollis DF (1986). Biochemical Engineering Fundamentals. 2nd Edition. McGraw-Hill, Singapore.

Baker DA and Kirsop BH (1972). Flocculation in *Saccharomyces cerevisiae* as influenced by wort composition and actidione. *Journal of the Institute of Brewing*, **78**:454-463.

Ball A (1994). Brewery Yeast Routing Principles. *The Brewer*, **Feb**:53-56.

Ballou CE and Raschke WC (1974). Polymorphism of the Somatic Antigen of Yeast. *Science*, **184**:127-134.

Ballou L, Cohen E and Ballou CE (1980). *Saccharomyces cerevisiae* mutants that make mannoproteins with a truncated carbohydrate outer chain. *Journal of Biological Chemistry*, **255**:5986-5991.

Barker MG and Smart KA (1996). Morphological changes associated with the cellular ageing of a brewing yeast strain. *Journal of the American Society of Brewing Chemists*, **54**(2):121-126.

Basson L (1996). Mechanical handling of yeast: An investigation of cropping. *MSc Thesis. University of Cape Town*, South Africa

Basson L, Robinson A, Godfrey TA, O'Connor-Cox E, Axcell B and Harrison STL (1997). Mechanical handling of brewer's yeast during cropping and its effect on yeast quality. *Proceedings of the Institute of Brewing Convention (Central & Southern African sections)*, **6**:55-60

Beavan MJ, Belk DM, Stewart GG and Rose AH (1979). Changes in electrophoretic mobility and lytic enzyme activity association with development of flocculating ability. *Canadian Journal of Microbiology*, **25**:888-895.

Bentham AC, Bonnerjea CB, Orsborn CB, Ward PN and Hoare M (1990). The separation of affinity flocculated yeast cell debris using a pilot plant scroll decanter centrifuge. *Biotechnology and Bioengineering*, **36**:397-401.

Bidard F, Bony M, Blondin B, Denquin S and Barre P (1995). The *Saccharomyces cerevisiae* FLO1 Flocculation Gene Encodes for a Cell Surface Protein. *Yeast*, 11:809-822.

Bird RB, Stewart WE and Lightfoot EN (1960). Transport Phenomena. Wiley International Edition, John Wiley and Sons New York.

Bony M, Thines-Sempoux D, Barre P and Blondin B (1997). Localization and cell surface anchoring of the *Saccharomyces cerevisiae* flocculation protein Flo1p. *Journal of Bacteriology*, **179**:4929-4936.

Bony M, Barre P and Blondin B (1998). Distribution of the flocculation protein, Flop, at the cell surface during yeast growth: the availability of Flop determines flocculation level. *Yeast*, 14:25-35.

Boughton RA (1983). Are You Getting the 'Best' out of your Yeast?. *The Brewer*, **69**:260-264.

Boughton RA (1987). Practically Managing Yeast. *MBAA Technical Quarterly*, **24**:133-136.

Bowen WR and Cooke RJ (1989). Studies of *Saccharomyces cerevisiae* during fermentation - an in vivo electrokinetic investigation. *Biotechnology and Bioengineering*, **33**:706-715.

Bowen WR, Sabuni AM and Ventham TJ (1992). Studies of the cell wall properties of *Saccharomyces cerevisiae* during fermentation. *Biotechnology and Bioengineering*, **40**:1309-1318.

Bowen WR and Ventham TJ (1994). Aspects of yeast flocculation. Size distribution and zeta-potential. *Journal of the Institute of Brewing*, **100**:167-172.

Bratby J (1980). Coagulation and Flocculation. Uplands Press Ltd. Croydon

Brookman JSG (1975). Further studies on the mechanism of cell disruption by extreme pressure extrusion. *Biotechnology and Bioengineering*, **17**:465-476.

Büchs J, Mozes N, Wanderey C and Rouxhet PG (1988). Cell adsorption control by culture conditions. *Applied Microbiology and Biotechnology*, **29**:119-128.

Calleja GB (1987). Cell aggregation. In: A.H. Rose and J.S.Harrison (eds.). The Yeasts. Vol.2. 2nd edition. Academic Press, London.

Carstens E, Lambrechts MG and Pretorius IS (1998). Flocculation, pseudohyphal development and invasive growth in commercial wine yeast strains. *South African Journal of Enology and Viticulture*, **19**:52-61.

Charpentier C, Nguyen Van Long T, Bonaly R and Feuillat M (1986). Alteration of cell wall structure in *Saccharomyces cerevisiae* and *Saccharomyces bayanus* during autolysis. *Applied Microbiology and Biotechnology*, **24**:405-413.

Cherry RS and Papoutsakis ET (1988). Physical mechanisms of cell damage in microcarrier cell culture bioreactors. *Biotechnology and Bioengineering*, **32**:1001-1014.

Cherry RS and Kwon K-Y (1990). Transient shear stresses on a suspension cell in turbulence. *Biotechnology and Bioengineering*, **36**:563-571.

Coulson JM and Richardson JF (1990). Chemical Engineering. Vol 1. 4th Edition pp 60. Pergamon Press, Oxford.

Croughan MS, Hamel J-F and Wang DIC (1987). Hydrodynamic effects on animal cells grown in microcarrier cultures. *Biotechnology and Bioengineering*, **29**:130-141.

Dabee S-K (1997). Maximising oxygen transfer and minimising shear damage in the microbial production of GLA by *Mucor rouxii*. *MSc* thesis. *University of Cape Town*, South Africa.

Day AW, Poon NH and Stewart GG (1975). Fungal fimbriae. III. The effect on flocculation in *Saccharomyces cerevisiae*. *Canadian Journal of Microbiology*, **21**:558-564.

De Nobel JG, Dijkers C, Hooiberg E and Klis FM (1989). Increased cell wall porosity in *Saccharomyces cerevisiae* after treatment with dithiolthreitol or EDTA. *Journal of General Microbiology*, **135**:2077-2084.

Dengis PB, Gerin PA and Rouxhet PG (1995a). X-ray photoelectron spectroscopy analysis of biosurfaces: examination of performances with yeast cells and related compounds. *Colloids and Surfaces B: Biointerfaces*, 4:199-211.

Dengis PB, Nélissen LR and Rouxhet PG (1995b). Mechanisms of yeast flocculation: comparison of top- and bottom-fermenting strains. *Applied and Environmental Microbiology*, **61**:718-728.

Dengis PB and Rouxhet PG (1996). Preparation of yeast cells for surface analysis by XPS. *Journal of Microbiological Methods*, **26**:171-183.

Denk V (1995). How to avoid 'mincing' your trub. *Brewers Digest International*, **Nov**: 20-21.

Doulah MS, Hammond TH and Brookman JSG (1975). A hydrodynamic mechanism for the disintegration of *Saccharomyces cerevisiae* in an industrial homogenizer. *Biotechnology and Bioengineering*, **17**:845-858.

Dufrêne YF and Rouxhet PG (1996). Surface composition, surface properties, and adhesiveness of *Azospirillum brasilense* - variation during growth. *Canadian Journal of Microbiology*, **42**:548-556.

Dunlop EH, Namdev PK and Rosenberg MZ (1994). Effect of fluid shear forces on plant cell suspensions. *Chemical Engineering Science.*, **49**:2263-2276.

Ebbing DD and Wrighton MS (1990). General Chemistry. Houghton Mifflin, Boston.

ECB Analytica Microbiologica (1977). *Journal of the Institute of Brewing*, **83**:109-118.

Eddy AA and Rudin AD (1958). Comparison of the respective electrophoretic and flocculation characteristics of different strains of *Saccharomyces*. *Journal of the Institute of Brewing*, **64**:139-142.

Einspahr H, Parks EH, Phillips SR and Suddath FL (1988). Crystal structure studies of legume lectins. In Bøg-Hansen, TC and Freed DLJ (Eds.), Lectins-Biology, biochemistry, clinical biochemistry. Vol. 6, Sigma Chemical Company, USA.

Engler CR (1979). Disruption of microorganisms in high pressure flow devices. *PhD Thesis. University of Waterloo*, Canada.

Engler CR and Robinson CW (1981). Disruption of *Candida utilis* cells in high pressure flow devices. *Biotechnology and Bioengineering*, **23**:765-780.

Engler CR (1985). Chapter 20: Disruption of microbial cells. In: Moo-Young M. (ed.). Comprehensive Biotechnology. Vol 2. Pergamon Press, Oxford.

Farkas V, Svoboda A and Bauer S (1970). Secretion of cell wall glycoproteins by yeast protoplasts. Effect of 2-deoxy-D-glucose and cycloheximide. *Biochemical Journal*, **118**:755-758.

Feizi T (1985). Demonstration by monoclonal antibodies that carbohydrate structures of glycoproteins and glycolipids are onco-developmental antigens. *Nature*, **314**:53-57.

Felix H (1982). Permeabilised cells. *Analytical Biochemistry*, **120**:211-234.

Fish NM and Lilly MD (1984). The interactions between fermentation and protein recovery. Bio/Technology, 623-627.

Fleet GH and Manners DJ (1975). Isolation and composition of an alkali-soluble glucan from the cell walls of *Saccharomyces cerevisiae*. *Journal of General Microbiology*, **94**:180-186.

Fleet GH (1984). In: C Nombela (ed.). Microbial Cell Wall Synthesis and Autolysis. Elsevier, Amsterdam.

Fleet GH (1991). In: AH Rose and JS Harrison (eds.). The Yeasts. Vol. 4. Academic Press, London.

Gasent-Ramirez JM, Castrejon E, Querol A, Ramon D and Benitez T (1999). Genomic stability of *Saccharomyces cerevisiae* baker's yeast. *Systematic and Applied Microbiology*, **22**(3):329-340.

Gerhardt P and Judge JA (1964). Porosity of isolated cell walls of *Saccharomyces cerevisiae* and *Bacillus megaterium*. *Journal of Bacteriology*, **87**:945-951.

Gerson DF (1980a). Cell surface energy, contact angles and phase partitioning. I. Lymphocytic cell lines in biphasic aqueous mixtures. *Biochimica et Biophysica Acta*, **602**:269-280.

Gerson DF and Akit J (1980b). Cell surface energy, contact angles and phase partitioning. II. Bacterial cells in biphasic aqueous mixtures. *Biochimica et Biophysica Acta*, **602**:281-284.

Gerson DF and Scheer D (1980c). Cell surface energy, contact angles and phase partitioning. III. Adhesion of bacterial cells to hydrophobic surfaces. *Biochimica et Biophysica Acta*, **602**:506-510.

Gilliland RB (1951). The flocculation characteristics of brewing yeasts during fermentation. *Proceedings of the European Brewing Convention Congress*, Brighton, 35-58.

Golovina IG, Saveleva ND, Loginova LG and Zararzin GA (1973). Lysis of *Hydrogenomonas eutropha* Z-1 cells by enzymes of *Micromonospora vulgaris* PA II-4. *Mikrobiologiya*, **42**(5):899-903

Hallsworth JE (1998). Review: Ethanol-induced water stress in yeast. *Journal of Fermentation and Bioengineering*, **85**:125-137.

Hammond JRM (1986). Brewers' Yeast. p8-56. In: Rose AH and Harrison JS (ed.). The Yeasts. Vol 5. Academic Press, London.

Harrison STL, Chase HA and Dennis JS (1991). The disruption of *Alcaligenes eutrophus* by high pressure homogenisation: Key factors involved in the process. Bioseparation, **2**: 155-166.

Hazen K C and Hazen B W (1987). A polystyrene microsphere assay for detecting surface hydrophobicity variations within *Candida albicans* populations. *Journal of Microbiological Methods*, **6**:289-299.

Herrera VE and Axcell BC (1991a). Induction of premature yeast flocculation by a polysaccharide fraction isolated from malt husk. *Journal of the Institute of Brewing*, **97**:359-366.

Herrera VE and Axcell BC (1991b). Studies on the binding between yeast and a malt polysaccharide that induces heavy yeast flocculation. *Journal of the Institute of Brewing*, **97**:367-373.

Hodgson JA, Berry DR and Johnston JR (1985). Discrimination by heat and proteinase treatments between flocculent phenotypes conferred on *Saccharomyces cerevisiae* by the genes FLO1 and FLO5. *Journal of General Microbiology*, **131**:3219-3227.

Hough JS (1985). The biochemistry of malting and brewing. Cambridge University Press, Cambridge.

Hottiger T, Boller T and Wiemken A (1987). Rapid changes of heat and desiccation tolerance correlated with changes of trehalose content in *Saccharomyces cerevisiae* cells subjected to temperature shifts. *FEBS Letters*, **220**:113-115.

Huheey JE (1983). Inorganic chemistry: principles of structure and reactivity. p256–285. 3rd edition. Harper and Row, New York.

Hull AS and Middelberg PJ (1993). Evidence that septated *E. coli* disrupt preferentially during high-pressure homogenization. *Transactions of the Institution of Chemical Engineers*, **71C**:264-266.

Hulse (2000). Personal Communication.

Hussain T, Salhi O, Lematre J, Charpentier C and Bonaly R (1986). Comparative studies of flocculation and deflocculation of *Saccharomyces uvarum* and *Kluyveromyces bulgaricus*. *Applied Microbiology and Biotechnology*, **23**:269-273.

Illing S and Harrison STL (1999). The kinetics and mechanism of *Corynebacterium glutamicum* aggregate breakup in bioreactors. *Chemical Engineering Science*, **54**:441-454.

Jansen HE and Mendlik F (1951). A study on yeast flocculation. *Proceedings of the European Brewing Convention Congress*, Brighton, 59-83.

Jayatissa M and Rose AH (1976). Role of wall phosphomannan in flocculation of *Saccharomyces cerevisiae*. *Journal of General Microbiology*, **96**:165-174.

Jin Y-L and Speers RA (1998). Flocculation of *Saccharomyces cerevisiae*. *Food Research International*, **31**:421-440.

Jin K, Thomas ORT and Dunnill P (1994). Monitoring recombinant inclusion body recovery in an industrial disc stack centrifuge. *Biotechnology and Bioengineering*, **43**:455-460.

Johnson JR and Reader HP (1982). Genes conferring and suppressing flocculation in brewing and laboratory strains of *Saccharomyces*. *Proc. 11'th Int. Conf. On Yeast Genetics and Molecular Biology*. Pontpellier, 124.

Johnson BF, Sowden LC, Walker T, Yoo BY and Calleja GB (1989). Use of electron microscopy to characterise the surfaces of flocculent and non-flocculent yeast cells. *Canadian Journal of Microbiology*, **35**:1081-1086.

Kabat EA (1978). Dimensions and specificities of recognition sites on lectins and antibodies. *Journal of Supramolecular Structure*, **8**:79-88.

Kamada K and Murata M (1984). On the mechanism of brewer's yeast flocculation. *Agricultural and Biological Chemistry*, **48**:2423-2433.

Kempken R, Preissmann A and Berthold W (1995). Assessment of a disc stack centrifuge for use in mammalian cell separation. *Biotechnology and Bioengineering*, **46**:132-138

Kihn JC, Masy CL and Mestdagh MM (1988a). Yeast flocculation: competition between nonspecific repulsion and specific bonding in cell adhesion. *Canadian Journal of Microbiology*, **34**:773-778.

Kihn JC, Masy CL, Mestdagh MM and Rouxhet PG (1988b). Yeast flocculation: factors affecting the measurement of flocculence. *Canadian Journal of Microbiology*, **34**:779-781.

King LM, Schisler DO and Ruocco JJ (1981). Epifluorescent method for detection of nonviable yeast. *Journal of the American Society of Brewing Chemists*, **39**:52-54.

Klis FM (1994). Review: Cell Wall Assembly in Yeast, *Yeast*, **10**:851-869.

Kolmogorov AN (1941a). Compt. Rend. Acad. Sci. URSS, **30**: 301.

Kolmogorov AN (1941b). Compt. Rend. Acad. Sci. URSS, **32**: 16.

Koopal LK (1978). Inference of polymer adsorption from electrical double layer measurements. H Veenman & B V Zonen, Wageningen.

Kruger L, Ryder DS, Alcock C and Murray JP (1982). Malt quality: Prediction of malt fermentability. Part 1. *MBAA Techanical Quarterly*, **19**:45-51.

Krzystek L and Ledakowicz S (1998). Yield and maintenance coefficients in *S. cerevisiae* cultures. *Journal of Chemical Technology and Biotechnology*, **71**:197-208.

Kuriyama H, Umeda I and Kobayashi H (1990). Role of cations in the flocculation of *Saccharomyces cerevisiae* and discrimination of the corresponding proteins. *Canadian Journal of Microbiology*, **37**:397-403.

Lampen JO (1968). External enzymes of yeasts: their nature and formation. *Antonie van Leeuwenhoek*, **34**:1-18.

Lee SS, Robinson FM and Wang HY (1981). Rapid determination of yeasts viability. *Biotechnology and Bioengineering Symposium*, **11**:641-649.

Lewis MJ and Poerwantaro WM (1991). Release of haze material from the cell walls of agitated yeast. *Journal of the American Society of Brewing Chemists*, **49**:43-46.

Lewis JG, Learmouth RP and Watson K (1995). Induction of heat, freezing and salt tolerance by heat and salt shock in *Saccharomyces cerevisiae*. *Microbiology-UK*, **141**:687-694.

Lim YH, Pecar M, Sudarmana D, Peel R, Freeman M and Hawthorne D (1992). Effect of Storage Conditions on the Filterability of Beer. *MBAA Technical Quarterly*, **29**:37-41.

Lillie RD (1997). H.J. Conn's biological stains: A handbook on the nature and uses of the dyes employed in the biological laboratory. 9th edition. Williams and Wilkins, Baltimore.

Lo WS and Dranginis AM (1996). FLO11, a gene related to the STA genes, encodes a novel cell surface flocculin. *Journal of Bacteriology*, **178**:7144-4151.

Lu CF, Kurjan J and Lipke PN (1994). A pathway for cell wall anchorage of *Saccharomyces cerevisiae* α-agglutinin. *Molecular and Cellular Biology*, **14**:4825-4833.

Lyons TP and Hough JS (1970). Flocculation of brewer's yeast. *Journal of the Institute of Brewing*, 76:564-571.

Lyons TP and Hough JS (1971). Further evidence for the cross-bridging hypothesis for flocculation of brewer's yeast. *Journal of the Institute of Brewing*, 77:300-305.

Malvern Training Manual. Training Manual for Malvern PCS Systems Issue 1.3, Malvern Instruments.

Manners DJ, Masson AJ and Patterson JC (1973a). The structure of a β-(1-3)-D-glucan from yeast cell walls. *Biochemical Journal*, **135**:19-30.

Manners DJ, Masson AJ, Patterson JC, Björndal H and Lindberg B (1973b). The structure of a β-(1-6)-D-glucan from yeast cell walls. *Biochemical Journal*, **135**:31-36.

Masschelein CA (1986). The biochemistry of maturation. *Journal of the Institute of Brewing*, 92:213-219.

Masy CL, Henquinet A and Mestdagh MM (1991). Fluorescence study of lectinlike receptors involved in the flocculation of the yeast *Saccharomyces cerevisiae*. *Canadian Journal of Microbiology*, **38**:405-409.

Masy CL, Henquinet A and Mestdagh MM (1992). Flocculation of *Saccharomyces cerevisiae*: inhibition by sugars. *Canadian Journal of Microbiology*, **38**:1298-1306.

Matile PH, Moor H and Robinow CF (1969). Chapter 6: Yeast Cytology, In: Rose AH and Harrison JS (eds.). The Yeasts. Vol 1. Academic Press, London.

Maybury JP, Hoare M and Dunnill P (2000). The use of laboratory centrifugation studies to predict performance of industrial machines: Studies of shear insensitive and shear sensitive materials. *Biotechnology and Bioengineering*, **67**:265-273.

McCaig R and Bendiak DS (1985). Yeast handling studies II: Temperature of storage of pitching yeast. *Journal of the American Society of Brewing Chemists*, **43**:119-122.

McMurrough I and Rose AH (1967). Effect of growth rate and substrate limitation on the composition and structure of the cell wall of *Saccharomyces cerevisiae*. *Biochemical Journal*, **105**:189-203.

McQueen A, Meilhoc E and Bailey JE (1987). Flow effects on the viability and lysis of suspended mammalian cells. *Biotechnology Letters*, 9:831-836.

Middelberg APJ, O'Neill BK, Bogle DL and Snoswell MA (1991). A novel technique for the measurement of disruption in high pressure homogenizers: Studies on *E. coli* containing recombinant inclusion bodies. *Biotechnology and Bioengineering*, **38**:363-370.

Middelberg APJ, O'Neill BK and Bogle DL (1992a). A new model for the disruption of *Escherichia coli* by high-pressure homogenization part I. Model development and verification. *Transactions of the Institution of Chemical Engineers*, 70C:205-212.

Middelberg APJ, O'Neill BK Bogle DL, Gully NJ, Rogers AH and Thomas CJ (1992b). A new model for the disruption of *Escherichia coli* by high-pressure homogenization Part II. A correlation for the effective cell strength. *Transactions of the Institution of Chemical Engineers*, 70C:213-218.

Middelberg APJ (1993). Extension of the wall-strength model for high-pressure homogenization to multiple passes. *Transactions of the Institution of Chemical Engineers*, 71C:215-219.

Miki BLA, Poon NH, James AP and Seligy VL (1982a). Possible mechanism for flocculation interactions governed by gene FLO1 in *Saccharomyces cerevisiae*. *Journal of Bacteriology*, 150:878-889.

Miki BLA, Poon NH and Seligy VL (1982b). Repression and induction of flocculation interactions in *Saccharomyces cerevisiae*. *Journal of Bacteriology*, 150:890-899.

Milburn PT and Dunnill P (1994). The release of virus-like particles from recombinant *Saccharomyces cerevisiae*: Effect of freezeing and thawing on homogenization and bead milling. *Biotechnology and Bioengineering*, 44:736-744.

Mill PJ (1966). Phosphomannans and other components of flocculent and non-flocculent walls of *Saccharomyces cerevisiae*. *Journal of General Microbiology*, 44:329-341.

Mochaba F, Turine PA and Axcell B (1993). Resorufin labelled casein as a substrate for protease activity in beer. *EBC Congress* 533-541.

Mosqueira FG, Higgins JJ Dunnill P and Lilly MD (1981). Characteristics of mechanically disrupted bakers' yeast in relation to its separation in industrial centrifuges. *Biotechnology and Bioengineering*, 23:335-343.

Mozes N, Leonard AJ and Rouxhet PG (1988). On the relations between elemental surface composition of yeasts and bacteria and their charge and hydrophobicity. *Biochimica et Biophysica Acta*, 945:324-334.

Murray CR, Barich T and Taylor D (1984). The effect of yeast storage conditions on subsequent fermentations. *MBAA Technical Quarterly*, 21:189-194.

O'Connor-Cox ESC (1994). Handling AJL 2036: Current Impressions. South African Breweries (Beer Division), Johannesburg.

O'Connor-Cox ESC (1995), Yeast vitality measurements: Progress report, recommendations and future directions. South African Breweries (Beer Division), Johannesburg.

Ormrod IHL, Labor EF and Sharpe FR (1991). The release of proteolytic enzymes into beer. *Journal of the Institute of Brewing*, 97:441-443.

Papoutsakis ET (1991). Fluid-mechanical damage of animal cells in bioreactors. *Trends in Biotechnology*, 9:427-437.

Parkkinen E, Oura E and Suomalainen H (1976). Comparison of methods for the determination of cell viability in stored baker's yeast. *Journal of the Institute of Brewing*, 82:283-285.

Perry RH, Green DW and Maloney JO (1984). Perry's chemical engineerings' handbook. 6th edition. McGraw-Hill, Singapore.

Pham HTB, Larsson G and Enfors S (1998). Growth and energy metabolism in aerobic fed-batch cultures of *Saccharomyces cerevisiae*: Simulation and model verification. *Biotechnology and Bioengineering*, 60:474-482.

Pickerell ATW, Hwang A and Axcell BC (1991). Impact of Yeast Handling Procedures on Beer Flavour Development During Fermentation. *Journal of the American Society of Brewing Chemists*, 49:87-92.

Piper PW (1995). The heat shock and ethanol stress response of yeast exhibit extensive similarity and functional overlap. *Microbiol.-UK*, 134:121-127.

Poon NH and Day AW (1975). Fungal fimbriae. I. Structure, origin and synthesis. *Canadian Journal of Microbiology*, 21:537-546.

Prokop A and Bajpai RK (1992). The sensitivity of biocatalysts to hydrodynamic shear stress. *Advances in Applied Microbiology*, 37:165-232.

Quain DE (1991). Stress and the yeast cell. *Ferment*, 4:155-156.

Quain DE, Thurston PA and Tubb RS (1981). The structural and storage carbohydrates of *Saccharomyces cerevisiae*: Changes during fermentation of wort and a role for glycogen catabolism in lipid biosynthesis. *Journal of the Institute of Brewing*, 87:108-111.

Ramsay AM and Douglas LJ (1979). Effects of phosphate limitation of growth on the cell wall and lipid composition of *Saccharomyces cerevisiae*. *Journal of General Microbiology*, 110:185-191.

Raschke WC and Ballou CE (1971). Immunochemistry of the phosphomannan of the yeast *Kloeckera brevis*. *Biochemistry*, 10:4130-4135.

Reynders MB, Rawlings DE and Harrison STL (1996). Studies on the growth, modelling and pigment production by the yeast *Phaffia rhodozyma* during fed-batch cultivation. *Biotechnology Letters*, **18**:649-654.

Rhymes MR and Smart KA (1996). Effect of starvation on the flocculation of ale and lager brewing yeasts. *Journal of the American Society of Brewing Chemists*, **54**:50-56.

Rose AH (1977). History and scientific basis of alcoholic beverage production. In: Rose AH (ed.). Economic microbiology, Vol 1: Alcoholic beverages. p1-41. Academic Press, London.

Rosenberg M, Gutnick D and Rosenberg E (1980). Adherence of bacteria to hydrocarbons: a simple method for measuring cell surface hydrophobicity. *FEMS Microbiology Letters*, **9**:29-33.

Rouxhet PG and Genet MT (1991). Chapter 8: Chemical Composition of the Microbial Cell Surface by XPS. In: Mozes N, Handley PS, Busscher HJ and Rouxhet PG (eds.). Microbial Cell Surface Analysis: Structural and physico-chemical methods. VCH, New York.

Rouxhet PG, Mozes N, Dengis PB, Dufrêne YF, Gerin PA and Genet MJ (1994). Application of x-ray photoelectron spectroscopy to microorganisms. *Colloids and Surfaces B: Biointerfaces*, **2**:347-369.

SAB Analytical Methods Manual (1995). Plato Tables.

Sales K, Brandt WF, Rumbak E. and Lindsey GG (2000). The LEA-like protein HSP 12 in *Saccharomyces cerevisiae* has a plasma membrane location and protects membranes against desiccation and ethanol induced stress. *Biochimica et Biophysica Acta*. **1463**:267-278.

Save SS, Pandit AB and Joshi JB (1994). Microbial cell disruption: role of cavitation. *Chemical Engineering Journal*, **55**:B67-72.

Save SS, Pandit AB and Joshi JB (1997). Use of hydrodynamic cavitation for large scale microbial cell disruption. *Transactions of the Institution of Chemical Engineers*, **75C**:41-49.

Schatzmann H (1975). Anaerobes Wachstum von *Saccharomyces cerevisiae*. In: AH Rose and JG Morris (ed.). Advances in Microbial Physiology, Vol. 22 : p141. Academic Press, London.

Sharon N and Lis H (1972). Lectins: Cell-agglutinating and sugar-specific proteins. *Science*, 177:272-275.

Shankar CS and Umesh-Kumar S (1994). A surface lectin associated with flocculation in brewing strains of *Saccharomyces cerevisiae*. *Microbiology*, 140, 1097-1101.

Shaw DJ (1980). Introduction to colloid and surface chemistry. 3rd edition. Butterworth-Heinemann, Oxford.

Shirgaonkar IZ, Lothe RR and Pandit AB (1998). Comments on the mechanism of microbial cell disruption in high pressure and high speed devices. *Biotechnology Progress*, **14**:657-660.

Siebert KJ, Stenroos LE and Reid DS (1981). Characterisation of amorphous particle haze. *Journal of the American Society of Brewing Chemists*, **39**:1-11.

Siebert KJ, Stenroos LE, Reid DS and Grabowski D (1987). Filtration difficulties resulting from damage to yeast during centrifugation. *MBAA Technical Quarterly*, **24**:1-8.

Slaughter JC and Nomura T (1992). Activity of the vacuolar proteases of yeast and the significance of the cytosolic protease inhibitors during the post fermentation decline phase. *Journal of the Institute of Brewing*, **98**:335-338.

Smart KA, Boulton CA, Hinchliffe E and Molzahn S (1995). Effect of physiological stress on the surface properties of brewing yeasts. *Journal of the American Society of Brewing Chemists*, **53**:33-38.

Smart KA and Whisker S (1996). Effect of serial repitching on the fermentation properties and condition of brewing yeast. *Journal of the American Society of Brewing Chemists*, **54**:41-44.

Smart KA, Chambers KM, Lambert I, Jenkins C and Smart CA (1999). Use of methylene violet staining procedures to determine yeast viability and vitality. *Journal of the American Society of Brewing Chemists*, **57**:18-23.

Smit G, Straver MH, Lugtenberg BJJ and Kijne JW (1992). Flocculation of *Saccharomyces cerevisiae* cells is induced by nutrient limitation, with cell surface hydrophobicity as a major determinant. *Applied and Environmental Microbiology*, **58**:3709-3714.

Soares EV, Teixeira JA and Mota M (1994). Effect of cultural and nutritional conditions on the control of flocculation expression in *Saccharomyces cerevisiae*. *Canadian Journal of Microbiology*, **40**:851-857.

Soares EV and Mota M (1996). Flocculation onset, growth phase, and genealogical age in *Saccharomyces cerevisiae*. *Canadian Journal of Microbiology*, **42**:539-547.

Speers A, Durance TD, Tung MA and Tou J (1993). Colloidal properties of flocculent and nonflocculent brewing yeast suspensions. *Biotechnology Progress*, **9**:267-272

Stathopoulos NA and Hellums JD (1985). Shear stress effects on human embryonic kidney cells *In Vitro*. *Biotechnology and Bioengineering*, **27**:1021-1026.

Stanley GA and Pamment NB (1993). Transport and intracellular accumulation of acetaldehyde in *Saccharomyces cerevisiae*. *Biotechnology and Bioengineering*, **42**:24-29.

Stewart GC, Russell I and Garrison IF (1973). Further studies and co-flocculation in brewer's yeast strains. *Proceedings of the American Society Brewing Chemists* 100-106.

Stewart GC and Russell I (1977). The identification, characteristics and mapping of a gene for flocculation in *Saccharomyces sp. Canadian Journal of Microbiology*, **23**:441-447.

Stratford M (1989a). Yeast flocculation: Calcium specificity. *Yeast*, **5**:487-496.

Stratford M (1989b). Evidence for two mechanisms of flocculation in *Saccharomyces cerevisiae*. *Yeast*, **5**:S441-445.

Stratford M and Brundish HM (1990). Yeast flocculation: Cationic inhibition. *Yeast*, **6**:77-86.

Stratford M and Assinder S (1991). Yeast flocculation: Flo1 and NewFlo phenotypes and receptor structure. *Yeast.*, **7**:559-574.

Stratford M (1992a). Yeast flocculation: Receptor definition by mnn mutants and Concanavalin A. *Yeast*, **8**: 635-645.

Stratford M (1992b). Yeast flocculation: A new perspective. *Advances in Microbial Physiology*, **33**:1-71.

Stratford M (1992c). Yeast flocculation: Reconciliation of physiological and genetic viewpoints. *Yeast*, **8**:25-38.

Stratford M (1993). Yeast flocculation: Flocculation onset and receptor availability. *Yeast* , **9**:85-94.

Stratford M and Carter AT (1993). Yeast flocculation: Lectin synthesis and activation. *Yeast*, **9**:371-378.

Stratford M (1996). Induction of flocculation in brewing yeasts by change in pH value. *FEMS Microbiology Letters*, **136**:13-18.

Straver MH, van der Aar PC, Smit G and Kijne JW (1993). Determinants of flocculence of brewer's yeast during fermentation in wort. *Yeast* , **9**:527-532.

Straver MH, Smit G and Kijne JW (1994). Purification and partial characterization of a flocculin from brewer's yeast. *Applied and Environmental Microbiology*, **60**:2754-2758.

Stryer L (1988). Biochemistry. Freeman, New York.

Suzuki S (1981). In: WN Arnold (ed.), Yeast Cell wall Envelopes; Biochemistry, Biophysics and Ultrastructure. Vol. 1. CRC Press, Boca Raton.

Teunissen AWRH, van den Berg JA and Steensma HY (1995). Localization of the dominant flocculation genes FLO5 and FLO8 of *Saccharomyces cerevisiae*. *Yeast*, 11:735-745.

Trinh K, Garcia-Briones M, Hink F and Chalmers JJ (1994). Quantification and damage to suspended insect cells as a result of bubble rupture. *Biotechnology and Bioengineering*, **43**:37-45.

Vandanjon L, Rossignol N, Paouen P, Robert JM and Quemeneur F (1999). Effects of shear on two microalgae species. Contribution of pumps and valves in tangential flow filtration systems. *Biotechnology and Bioengineering*, **63**:1-9.

van Hamersveld EH, van Loosdrecht MCM and Luyben KchAM (1994). How important is the physicochemical interaction in the flocculation of yeast cells? *Colloids and Surfaces B: Biointerfaces*, 2:165-171.

van Loosdrecht MCM, Lyklema J, Norde W, Schraa G and Zehnder AJB (1987a). The role of bacterial cell wall hydrophobicity in adhesion. *Applied and Environmental Microbiology.*, **53**(3):1893-1897.

van Loosdrecht MCM, Lyklema J, Norde W, Schraa G and Zehnder AJB (1987b). Electrophoretic mobility and hydrophobicity as a measure to predict the initial steps of bacterial adhesion. *Applied and Environmental Microbiology.*, **53**(8):1898-1901.

Welty JR, Wicks CE and Wilson RE (1984). Fundamentals of momentum, heat, and mass transfer. 3rd edition. John Wiley and Sons, Singapore.

Wessels JGH and Sietsma JH (1981). Chapter 15: Fungal Cell Walls: A Survey, In Encyclopaedia of Plant Physiology, New Series, Volume 13B. Springer, Berlin.

Wilcocks KL and Smart KA (1995). The importance of surface charge and hydrophobicity for the flocculation of chain-forming brewing yeast strains and resistance of these parameters to acid washing. *FEMS Microbiology Letters*, **134**:293-297.

Wong HH, O'Neill BK and Middelberg APJ (1997). Centrifugal processing of cell debris and inclusion bodies from recombinant *Escherichia coli*. *Bioseparation*, **6**:361-372.

www.antigenics.com/tech/why.html (2000). Why heat shock proteins?.

Yamashita I and Fukui S (1984). *Agricultural and Biological Chemistry*, **48**:131

Zhang Z, Al-Rubeai M and Thomas CR (1993). Estimation of disruption of animal cells by turbulent capillary flow. *Biotechnology and Bioengineering*, 42:987-993.

Appendix A: Cell Propagation Data

A.1 Biomass Calibration Curves

Data for the four strains of *Saccharomyces cerevisiae* consisting of dry weights, cell counts (*10^6/ml) and absorbances at 660 nm are presented below. The cell dry weights were determined by oven drying the yeast pellet at 80 °C for 3 days while the cell count was performed by microscopic enumeration using a haemocytometer. Where only absorbance data was collected, these calibration curves were used to obtain corresponding cell count and dry biomass estimates. Values of absorbance were obtained by linear interpolation between the nearest points while dry weight was obtained by linear best fit of the points. The values are plotted in the Figure A.1 and A.2 and presented in Table A.1.

Table A.1. Dry weight, cell count and absorbance data for strains SAB1, SAB1/96, SAB2 and SAB5.

SAB1			SAB1/96		
Dry Weight ($g.l^{-1}$)	Cell Count ($10^6.ml^{-1}$)	Absorbance (@660nm)	Dry Weight ($g.l^{-1}$)	Cell Count ($10^6.ml^{-1}$)	Absorbance (@660nm)
5.0	1618.9	2.79	8.0	2648.3	2.86
2.6	854.9	2.41	4.2	1284.0	2.59
1.7	468.9	2.15	2.1	561.8	2.19
0.8	218.8	1.73	1.0	224.9	1.72
0.4	128.8	1.30	0.6	135.6	1.35
0.3	68.9	0.76	0.3	75.6	0.92
0.1	45.3	0.52	0.2	49.8	0.61
0.1	28.3	0.36	0.1	31.5	0.38
0.0	15.8	0.21	0.1	20.7	0.22

SAB5			SAB2		
Dry Weight ($g.l^{-1}$)	Cell Count ($10^6.ml^{-1}$)	Absorbance (@660nm)	Dry Weight ($g.l^{-1}$)	Cell Count ($10^6.ml^{-1}$)	Absorbance (@660nm)
7.7	2768.6	2.90	4.5	1445.0	2.66
3.8	1297.4	2.63	2.9	861.3	2.43
1.8	604.6	2.23	1.8	484.9	2.13
1.0	304.6	1.84	0.9	287.3	1.74
0.4	133.3	1.23	0.7	187.9	1.33
0.3	59.9	0.71	0.3	114.1	0.84
0.1	34.7	0.40	0.3	64.0	0.46
0.0	18.0	0.21	0.2	35.8	0.27

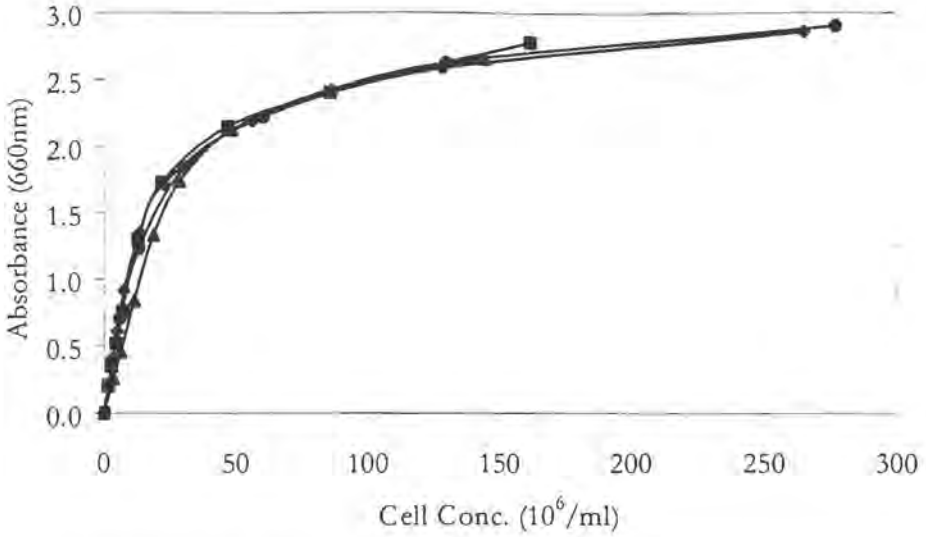

Figure A.1. **Absorbance vs. cell concentration curves for laboratory yeast strains.**
(■ SAB1, ♦ SAB1/96, ▲ SAB2, ● SAB5)

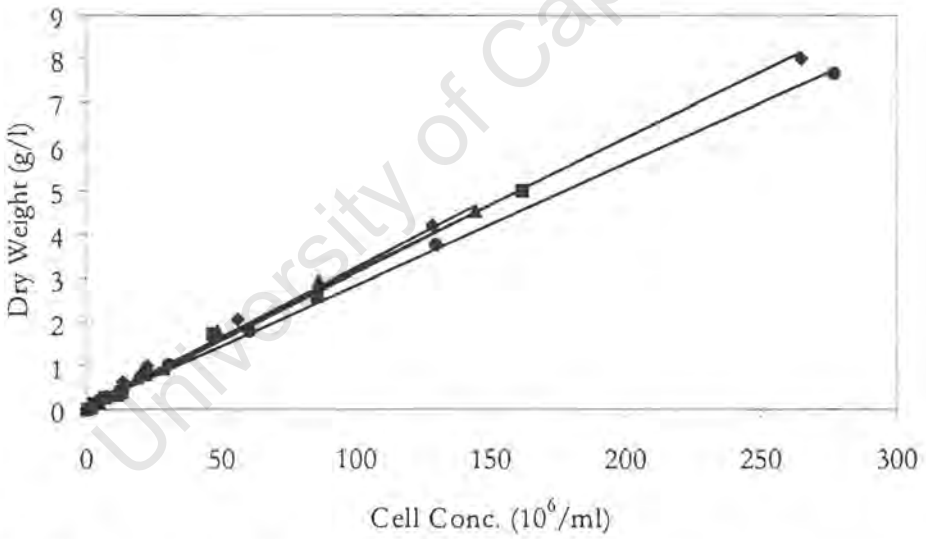

Figure A.2. **Dry weight vs. cell concentration curves for laboratory yeast strains.**
(■ SAB1, ♦ SAB1/96, ▲ SAB2, ● SAB5)

A.2 Yield Coefficients

Biomass yield coefficients were measured for each of the four strains of yeast, grown under both near anaerobic and full aerobic conditions. The constants, presented in Table A.2, were measured when the cells had reached the stationary phase i.e. overall biomass yield. Cell density determinations were performed by air drying pellets of cells which were centrifuged at 3000 g for 5 minutes and air dried for 12 hours before recording the wet weight of the cells. The pellets were then oven dried at 80 °C for 3 days to remove all water from within the cells and the density determined. From numerous dry and wet weight determinations, it was found that the water content of the centrifuged cell pellet was 91 %. The cells' average diameter and density for the four strains are also given in Table A.2.

Table A.2. Biomass yield coefficients

Strain	Dry Wt. ($g/10^6$cells)	Wet Weight Yield ($Y_{x/s}$) (g/0.01 °P)		Diameter (μm)	Density (kg/m^3)
		Aerobic	Anaerobic		
SAB1	3.08×10^{-5}	0.127	0.041	6.65	1053
SAB1/96	3.03×10^{-5}	0.099	0.031	6.89	1094
SAB2	3.17×10^{-5}	0.126	0.045	6.34	1250
SAB5	2.77×10^{-5}	0.091	0.021	6.17	1185

Appendix B: Assay Methods

B.1 Hydrophobicity

B.1.1 Latex Microbead Attachment Assay

Reagents

PUM Buffer (pH ±7.1)

8.47 g K_2HPO_4

3.63 g KH_2PO_4

0.90 g Urea

0.91 g $MgSO_4.7H_2O$

Made up to 500ml distilled water

0.02M Sodium Acetate Buffer (pH 4.0)

Add 1.2 g Acetic acid to 500 ml distilled water

Dissolve 1.64 g Sodium acetate in 500 ml distilled water

Add approx. 250ml of the sodium acetate solution to the acid solution to obtain a final pH of 4.0 then dilute to 1000 ml with distilled water.

Method (1)

1. Add 3µl 0.8µm diameter latex bead suspension (Sigma paramagnetic latex beads, 67% magnetite content, 10% solids) to 0.997 ml PUM buffer.
2. Cool on ice and store in sterile Eppendorf tube.
3. Wash yeast once with distilled water and resuspend in cold PUM buffer to a concentration of about 10^6 cells/ml.
4. Add 100µl yeast suspension to 10µl bead suspension and vortex for 30 seconds.
5. Count the number of cells with more than 3 beads attached ($N_{3\text{-bead-cells}}$) as well as the total number of cells (N_{total}) using brightfield microscopy.

Method (2)

1. As 1 above
2. As 2 above
3. Wash yeast with distilled water and resuspend in acetate buffer to 10^6 cells/ml.
4. Measure the absorbance of the suspension at 660 nm (A_1).
5. Mix 985µl yeast and 15µl bead suspensions and incubate at room temperature for 20 minutes.

6. Hold a magnet against the side of the cuvette to remove the beads and yeast cells with beads attached.
7. Decant and measure the new absorbance (A_2).

Analysis

$$\text{(Method 1):}\quad \text{Hydrophobicity Index} = \frac{N_{3\text{-}bead\text{-}cells}}{N_{total}} * 100\% \qquad \text{(B.1)}$$

$$\text{(Method 2):}\quad \text{Hydrophobicity Index} = \frac{A_1 - A_2}{A_1} * 100\%$$

B.1.2 Solvent Partitioning

Reagents

PUM Buffer (pH ±7.1)

Preparation: As for latex microbead attachment assay.

Method

1. Pipette 3ml yeast into a sealable test tube.
2. Centrifuge for 10 minutes at 500 g and decant.
3. Resuspend yeast in 5ml deionised distilled water and centrifuge.
4. Resuspend yeast in 5ml PUM buffer in the test tube.
5. Pipette 0.02 ml of the yeast suspension into 9.98 ml PUM buffer in a McCartney bottle to produce a suspension of approximately 10^6 cells/ml.
6. Measure the absorbance at 660 nm (A_1).
7. Pipette 2.4 ml of the yeast suspension prepared in (5) above into wide mouthed test tube and add 0.2 ml xylene.
8. Vortex and allow to stand for 15 minutes.
9. Remove the aqueous phase with a Pasteur pipette and measure its absorbance (A_2).

Analysis

$$\textit{Hydrophobicity Index} = \frac{A_1 - A_2}{A_1} * 100\% \qquad \text{(B.2)}$$

B.1.3 Reproducibility

The hydrophobicity of a sample of production yeast, strain SAB1, was tested using the methods described above and the results and reproducibility are compared in Table B.1. From these, it was decided that the solvent partitioning method would be used to quantify cell surface hydrophobicity, based on the lower coefficient of variance for the assay.

Table B.1. Hydrophobicity reproducibility data.

Sample No.	Latex Bead Method 1 (counting)	Latex Bead Method 2 (magnetic separation)	Solvent Partitioning
1	0.25	0.19	0.42
2	0.16	0.32	0.40
3	0.34	0.24	0.43
4	0.24	0.31	0.39
5	0.21	0.20	0.41
Average	0.24	0.25	0.41
Standard deviation	0.066	0.061	0.016
Coefficient of variance	27.5 %	24.2 %	3.9 %

B.2 Surface Charge

B.2.1 Dye Adsorption

Reagents

0.02M acetate buffer (pH 4.0)

0.02M acetate buffer (pH 4.0) containing 50µg/ml Alcian blue 8GX

Method

1. Pipette 3 ml yeast suspension into a sealable test tube.
2. Centrifuge for 10 minutes at 500 g and decant.
3. Resuspend in 10 ml acetate buffer then transfer 1 ml into another sealable test tube and centrifuge.
4. Remove the supernatant and stand the tube upside down to allow excess liquid to drain.
5. Add 10 ml acetate buffer containing the Alcian blue dye to the cells and resuspend.
6. Determine the cell concentration, it should be approximately 10^6 cell/ml.
7. Incubate for 30 minutes at 30 °C on an orbital shaker.
8. Centrifuge the tubes for 10 minutes at 500 g rpm and recover the supernatant.

9. Measure the absorbance of the supernatant (A_{sample}) and of the buffer containing Alcian Blue (A_{50}) at 607 nm.

Analysis

The dye retention per million cells is calculated as follows:

$$\text{Dye Retention (g/10}^6\text{ cells)} = \frac{\frac{A_{50} - A_{sample}}{A_{50}} * 50}{Cell\ Conc.} \qquad \text{(B.3)}$$

B.2.2 Surface Zeta Potential

Reagents

0.020 *M* sodium acetate/acetic acid buffer (pH 2.2 to 7.3)

Method

1. Centrifuge the yeast suspension for 10 minutes at 500 g and discard the supernatant.
2. Wash the cells with deionised water and centrifuge. Repeat three times.
3. Resuspend in buffer electrolyte to a concentration of 10^6 cells/ml.
4. Sonicate the suspension to disperse the flocs.
5. Inject the sample into the Zetasizer to determine the zeta potential of the yeast cells.
6. The voltage is applied intermittently to the sample to avoid heating which would alter the viscosity.
7. The electrophoretic mobility and zeta potential are calculated internally and the results displayed.

Analysis

The zeta potential of the samples is calculated by the Zetasizer by using the Henry equation:

$$U_E = \frac{\varepsilon z f(K_a)}{6 \pi \mu} \qquad \text{(B.4)}$$

where: U_E = electrophoretic mobility ($\mu m.s^{-1}.V^{-1}.cm^{-1}$)

z = zeta potential (V)

μ = viscosity (Pa.s)

ε = dielectric constant

$f(K_a)$ = factor including double electric layer thickness and particle diameter

For measurement of small particles < 0.2 micron in non-polar media, $f(K_a) = 1.0$, while for larger particles including yeast cells in polar media, $f(K_a) = 1.5$. The Henry equation then reduces to the Smoluchowski approximation:

$$U_E = \frac{\varepsilon z}{4\pi\mu} \tag{B.5}$$

which in an aqueous environment at the operating temperature of 25 °C reduces to:

$$z = 12.85 U_E \quad (mV) \tag{B.6}$$

B.2.3 Reproducibility

Five samples of production yeast, SAB1, were used to quantify the reproducibility of the dye retention technique of determining surface charge with the summary given in Table B.2. The error associated with the assay is small with a coefficient of variance of 7 %. It indicates that the method is applicable to be used as a routine assay for single pH surface charge determination. Zeta potential gives information on charge across a range of pH, thereby providing information on a range of types of charged groups. The reproducibility of the zeta potential method of determining surface charge was performed on 4 samples of yeast, measured at 9 pH values with each measurement being the average of 5 measurements on the Zetasizer. The results, average and standard deviation are provided in Table B.3. The standard deviation in zeta potential across the range of pH is between 0.1 and 0.3 mV.

Table B.2. Reproducibility of dye retention assay for surface charge.

Sample No.	Dye Retention ($\mu g/10^6$cells)
1	3.24
2	3.88
3	3.52
4	3.41
5	3.69
Average	3.55
Standard Deviation	0.248
Coefficient of Variance (%)	7.0

Table B.3. Reproducibility of zeta potential assay for surface charge.

	pH								
Sample No.	2.15	2.87	3.43	3.93	4.53	5.01	5.52	6.12	7.26
1	2.0	1.4	-0.6	-2.4	-3.6	-4.3	-5.4	-6.9	-8.1
2	1.4	1.2	-0.1	-2.0	-3.3	-4.1	-5.6	-6.9	-8.0
3	1.4	1.3	-0.3	-2.5	-3.5	-4.3	-5.5	-7.0	-8.0
4	1.9	0.9	-0.2	-2.0	-3.3	-4.2	-5.4	-6.6	-7.6
Average (mV)	1.7	1.2	-0.3	-2.2	-3.4	-4.1	-5.5	-6.9	-7.9
Standard Deviation (mV)	0.3	0.2	0.2	0.3	0.2	0.1	0.1	0.2	0.2

B.3 XPS Analysis

Sample Preparation

1. Samples of yeast slurry were pipetted into Eppendorf reaction vessels and washed 3 times with deionised water.
2. The tubes were immersed in liquid nitrogen and left for 10 minutes.
3. Tubes were then stored in a freezer at –80 °C until freeze drying.
4. When freeze drying, the microfuge tubes were opened and sealed with a piece of perforated parafilm and placed inside a glass freeze drying vessel at –80 °C.
5. The vessel was connected to a Labotec Dry-O-Vac to dry. The pressure reached < 0.15 torr in 5 minutes during which time the sample temperature gradually rose to room temperature. The triple point of water is 0.01 °C and 4.6 torr, so provided the pressure is reduced to below 4.6 torr before the temperature has risen to 0.01 °C, no melting of the ice can occur and the frozen water inside the cells sublimes as gaseous water.
6. After freeze drying at < 0.04 torr for 18 hours, the vessel was disconnected and the sample tubes resealed and placed inside a desiccator at room temperature.
7. All samples were analysed 3-4 days after freeze drying.
8. Each sample was carefully removed from the Eppendorf tube and placed in a platen and pressed flat with a clean spatula. Four samples were loaded into the machine at a time within 10 minutes, thus minimising any contamination effects from the atmosphere.

Equipment Used and Operating Method

A Physical Electronics, Quantum 2000 scanning ESCA Microscope was used to analyse the samples. The spectrometer uses a monochromatised Al K_α x-ray beam to irradiate the sample. Beam rastering

was used over an area of 500 x 500 μm to avoid the sample degradation sometimes associated with the beam spot mode of older machines. The aluminium anode was powered at 15 kV with a current of 0.62 mA producing a beam size of 50 μm with a power of 9.4 W. The analyser was placed at an angle of 45° to the sample normal. Sample stabilisation (to avoid sample charging effects caused by the continual loss of electrons from the surface) was achieved by a combination of low energy ions and electron neutralisation. The base vacuum in the analysis chamber was 8 x 10^{-9} Torr. All samples were analysed in the following sequence; first a wide scan from 600 to 0 eV using a constant pass energy of 117.4 eV followed by narrow scans on O_{1s}, N_{1s}, C_{1s}, P_{2s} and S_{2s} using a pass energy of 29.3 eV. Data from the wide scan was collected for 15 minutes while each of the five narrow scans was collected for 5 minutes. Sensitivity factors for the elements were taken from the Multipack data base for the Physical Electronics Quantum 2000. The binding energies of the peaks were determined by setting the C-(C,H) component of the C_{1s} peak at 284.7 eV and peak decomposition performed.

B.4 Flocculence

Reagents

2mM EDTA

Dissolve 0.83g of EDTA-tetra sodium salt in 1 litre of distilled water

Flocculation buffer: 20mM Na-Acetate - 0.1%$CaCl_2$ buffer (pH 4.5) [9 mM]

Add 3.0 g Acetic acid to 500 ml distilled water

Dissolve 4.1g Sodium acetate and 1g $CaCl_2$ in 500 ml distilled water

Add the acid solution to the Sodium acetate solution to obtain a final pH of 4.0

Dilute the resultant solution to 1000 ml with distilled water

Method

1. Wash yeast with distilled water and collect by centrifuging for 5 minutes at 500 g in a Beckman TJ-6 refrigerated centrifuge (4 °C).
2. Resuspend in 2mM EDTA and centrifuge once again.
3. Wash twice with distilled water and leave a small amount of water to resuspend the cells.
4. 22 ml of flocculation buffer was added to the glass U-tube inside the spectrometer and zeroed against buffer.
5. The air was opened and the flow rate adjusted to give a bubbling rate of 55 to 65 bubbles per minute.
6. 1 – 1.5 ml of washed concentrated cells are added to the U-tube to give an A_{660} of 2.2 - 2.5 without bubbling.
7. The bubbling provided the agitation necessary to initiate flocculation and an acclimatisation period of 10 minutes was allowed while agitation was maintained.

8. The air supply was stopped and absorbance logging started for 5 minutes using a signal averaging time of 0.1 seconds.
9. The initial and final absorbances were converted into cell concentrations using absorbance/cell concentration conversion curves provided in Appendix A.
10. The extent of flocculation was calculated as:

$$Flocculation\% = \frac{Cells_{(initial)} - Cells_{(final)}}{Cells_{(initial)}} * 100\% \qquad (B.7)$$

B.4.1 Reproducibility

The flocculence method was used to assay the flocculation potential of samples of production yeast, SAB5, to determine the reproducibility of the assay. The summary of the extent of flocculation measured is provided in Table B.4 which indicates that the coefficient of variance is 0.5 %.

Table B.4. Reproducibility of flocculation assay.

Sample No.	Iinitial cell conc. (10^6cells/ml)	Final cell conc. (10^6cells/ml)	Flocculence (%)
1	446.7	15.8	96.5
2	476.5	13.6	97.1
3	396.0	12.5	96.8
4	345.6	13.1	96.2
5	341.8	13.1	96.2
Average	-	-	96.6
Standard deviation	-	-	0.4
Coefficient of variance (%)	-	-	0.5

B.5 Haze Carbohydrate Analysis

Carbohydrate hydrolysis

1. Centrifuge the yeast suspension at 200 g and 4 °C for 3 minutes (Beckman TJ-6) to remove the bulk of yeast particles.
2. Filter the supernatant through a Whatman No. 1 filter to remove all traces of yeast.
3. Freeze the filtrate to aid the formation of soluble haze particles by lowering their solubility.
4. Centrifuge a thawed sample at 13 200 g and 4 °C for 40 minutes and resuspend the pellet in the supernatant such that a 10 fold concentration of haze is obtained. Similarly collect another

sample in distilled water, recentrifuge as above and collect in distilled water. These two samples of haze represent the total and water insoluble fractions.

5. Pipette 15 ml of each into boiling tubes and add H_2SO_4 to obtain a 6% acid solution, boil for 4 hours maintaining the liquid level by addition of deionised water.
6. Neutralise by adding $Ba(OH)_2$, recording the volume added.

Determination of sugars (glucose, fructose and mannose) (Using Boehringer Mannheim test kit No.139 106 and No.131 202)

The principle of the assay is that both glucose and fructose are phosphorylated by hexokinase (HK) and adenosine-5'triphosphate (ATP) to glucose-6-phosphate (G-6-P) and fructose-6-phosphate(F-6-P).

$$D-Glucose+ATP \xrightarrow{HK} G-6-P+ADP$$
$$D-Fructose+ATP \xrightarrow{HK} F-6-P+ADP$$
$$D-Mannose+ATP \xrightarrow{HK} M-6-P+ADP$$

The G-6-P is oxidised by nicotinamide-adenine dinucleotide phosphate (NADP) and glucose-6-phosphate dehydrogenase (G6P-DH) to gluconate-6-phosphate with the production of reduced nicotinamide-adenine dinucleotide phosphate (NADPH). The NADPH formed is measured by its light absorbance.

$$G-6-P+NADP^+ \xrightarrow{G6P-DH} D-gluconate-6-phosphate+NADPH+H^+$$

After completion of the above reaction, F-6-P is converted to G-6-P by phosphoglucose isomerase (PGI). The G-6-P formed reacts to produce more NADPH.

$$F-6-P \xleftrightarrow{PGI} G-6-P$$
$$G-6-P+NADP^+ \xrightarrow{G6P-DH} D-gluconate-6-phosphate+NADPH+H^+$$

Upon the addition of phosphomannose isomerase(PMI), M-6-P is converted to F-6-P which in turn is converted to G-6-P under the action of PGI and finally produces NADPH.

$$M-6-P \xrightarrow{PMI} F-6-P$$
$$F-6-P \xrightarrow{PGI} G-6-P$$
$$G-6-P+NADP^+ \xrightarrow{G6P-DH} D-gluconate-6-phosphate+NADPH+H^+$$

The concentration of the sugars can be calculated from the general formula:

$$C(g/l)=\frac{V*MW}{\varepsilon*d*v*1000}*\Delta A$$

where: V = total volume (ml)

v = sample volume (ml)

MW = molecular weight of substance (g/mol)

d = light path (cm)

ε = extinction coefficient of NADPH = 6.3 ($l.mmol^{-1}.cm^{-1}$) at 340 nm

	Blank	Sample
7. Pipette solutions into 3 ml quartz cuvettes and cover with parafilm, measuring absorbances at 340 nm.		
8. Add solution 1 [NADP, ATP, pH buffer]	1.000 ml	1.000 ml
9. Add sample (v ml)	-	0.1 to 2.0 ml
10. Add deionised water	2.000 ml	1.9 to 0.0 ml (V = 3ml)
11. Mix and read (A1) after 3 minutes.		
12. Add suspension 2 [HK, G6P-DH]	0.020 ml	0.020 ml
13. Mix and read (A2) after end of reaction (10 - 15 min).		
14. Add suspension 3 [PGI]	0.020 ml	0.020 ml
15. Mix and read (A3) after end of reaction (15 minutes).		
16. Add suspension 4 [PMI]	0.020 ml	0.020 ml
17. Mix and read (A4) between 30 and 60 minutes to get the maximum absorbance.		

Analysis

Determine absorbance differences:

$$\Delta A_{D\text{-glucose}} = (A_2\text{-}A_1)_{sample}\text{-}(A_2\text{-}A_1)_{blank}$$

$$\Delta A_{D\text{-fructose}} = (A_3\text{-}A_2)_{sample}\text{-}(A_3\text{-}A_2)_{blank}$$

$$\Delta A_{D\text{-mannose}} = (A_4\text{-}A_3)_{sample}\text{-}(A_4\text{-}A_3)_{blank}$$

$$Glucose(g/l) = \frac{3.02 * 180.16}{6.3 * \upsilon * 1000} * \Delta A_{D-glucose} \quad \text{(B.8)}$$

$$Fructose(g/l) = \frac{3.04 * 180.16}{6.3 * \upsilon * 1000} * \Delta A_{D-fructose} \quad \text{(B.9)}$$

$$Mannose(g/l) = \frac{3.06 * 180.16}{6.3 * \upsilon * 1000} * \Delta A_{D-mannose} \quad \text{(B.10)}$$

where: v is the volume of sample added (ml).

Multiply the calculated sugar concentration by the dilution factor obtained when hydrolysing, neutralising and concentrating the haze sample to obtain the true sugar concentrations in the original sample.

B.5.1 Reproducibility

Due to the variable sample volume required in the assay, the maximum total sugars and detection limit vary, with the upper and lower limits given in Table B.5. The reproducibility of the assay is variable too, as it is a function of the absorbance response of the spectrophotometer.

Table B.5. Sensitivity and limits applicable to the enzymatic sugar assay.

Sample volume (ml)	0.1	2.0
Detection limit (g/l sample)	0.005	0.0002
Max. Total sugars (g/l sample)	1.137	0.0570

B.6 Methylene Blue Viability

The methylene blue vitality staining method is that of Lee *et al.*, 1981 where the staining solution consists of methylene blue (0.25 g/l), NaCl (9 g/l), KCl (0.42 g/l), $CaCl_2.6H_2O$ (0.48 g/l), $NaHCO_3$ (0.2 g/l) and glucose (10 g/l) dissolved in distilled water giving a final methylene blue concentration of 0.025% (w/v). Dilute the yeast slurry with phosphate buffered saline(PBS) (pH 7.4) to give a concentration of 10^7 cells/ml. Add 0.1 ml of yeast suspension to 0.9 ml of methylene blue staining solution and swirl mix for 1 minute. Place a drop of this solution onto a haemocytometer and count the number of blue (N_{blue}) and total number of cells (N_{total}) under a brightfield microscopy at 400 X magnification. The viability is then expressed as the ratio of clear to total cells:

$$Viability = \frac{N_{total} - N_{blue}}{N_{total}} * 100\% \qquad \text{(B.11)}$$

B.6.1 Reproducibility

From the standard deviation of the viability measurements used in this study was calculated to be 0.95%.

B.7 Extracellular Protease

Reagents

Incubation Buffer: Tris-HCl Buffer
(0.2 mol/l Tris-HCl, pH 7.8, 0.02 mol/m $CaCl_2$)

Stop Reagent: Trichloroacetic acid
(5% w/v in deionised, distilled water)

Assay Buffer: Tris-HCl
(0.5 mol/l, pH 8.8)

Substrate Solution: 15mg Casein, resorufin-labelled (Boehringer Mannheim, Universal Protease substrate Cat. no 1080733)
preparation: add 3.75 ml deionised, distilled water to contents. Batch out 50 µl into Eppendorf tubes. Store in deep freeze.

Method

1. Centrifuge the yeast slurry in an Eppendorf microfuge at 10 000rpm for 5 min.
2. Decant supernatant.
3. Recentrifuge supernatant for 5 minutes and decant.
4. Pipette 50µl substrate into fresh Eppendorf tubes. (Pre-prepared)
5. Add 50µl Incubation buffer (0.2 mol/l Tris-HCl) to substrate
6. For sample : add 100µl supernatant

   For blank: add 100µl deionised, distilled water.
7. Mix by tapping gently on bench.
8. Incubate at 37°C for 60 minutes.
9. Add 480µl Stop reagent (Trichloroacetic acid) and mix.
10. Incubate at 37°C for 10 minutes.
11. Centrifuge for 5 minutes and decant.
12. Pipette 400µl supernatant into glass microcuvettes.
13. Add 600µl Assay buffer (0.5 mol/l Tris-HCl)
14. Mix by tapping gently on bench.
15. Immediately measure absorbance at 574 nm using UV / visible spectrophotometer.

Analysis

$$\text{Protease Absorbance} = A_{sample} - A_{blank} \qquad \text{(B.12)}$$

B.7.1 Reproducibility

The reproducibility of the protease assay was tested at the upper limit of the linear detection range (absorbance of ± 0.6). These results are presented in Table B.6.

Table B.6. Reproducibility of the protease assay.

Sample No.	Absorbance
1	0.593
2	0.534
3	0.556
4	0.541
5	0.556
Average	0.556
Standard deviation	0.023
Coefficient of variance (%)	4.1

B.8 Small Scale Fermentation Reproducibility

Five replicate fermentations were performed in the 500 ml fermentation system and the density, cell counts, beer quality and calculated rate of fermentation determined. The density and cell counts are provided in Table B.7 and B.8 while the calculated logistic rate, extent of fermentation (final density) and beer quality results are presented in Table B.9.

Table B.7. Density data of 5 replicate 500 ml fermentations (°P).

Time (hr)	1	2	3	4	5	Average	Standard Deviation	Coefficient of Variance
0	14.91	14.80	14.91	14.91	14.92	14.89	0.05	0.3
25	12.47	12.42	12.51	12.45	12.43	12.45	0.03	0.2
39	10.34	10.57	10.52	10.47	10.44	10.47	0.09	0.9
57	7.59	7.90	7.76	7.74	7.72	7.74	0.11	1.4
77	5.19	5.81	5.50	5.48	5.37	5.47	0.22	4.0
101	3.88	4.28	3.90	3.98	3.77	3.96	0.19	4.8
152	2.77	2.82	2.53	2.59	2.44	2.63	0.16	6.1
242	1.70	1.89	1.76	1.95	1.87	1.83	0.10	5.5

Table B.8. Cell concentration data of 5 replicate 500 ml fermentations (10^6 cells.ml^{-1}).

Time (hr)	1	2	3	4	5	Average	Standard Deviation	Coefficient of Variance
0	20.0	19.1	17.3	17.6	18.4	18.5	1.1	6.0
25	38.1	35.2	39.9	37.7	36.3	37.4	1.8	4.8
32	44.1	49.9	49.5	41.4	51.3	47.2	4.2	9.0
39	46.5	50.6	54.2	46.5	51.4	49.9	3.3	6.7
45	49.4	48.3	53.7	58.2	46.7	51.3	4.7	9.1
51	44.1	46.1	47.8	53.1	49.3	48.1	3.4	7.1
57	40.3	45.3	44.7	43.9	42.3	43.3	2.0	4.6
77	21.2	23.3	19.2	23.9	22.9	22.1	1.9	8.6
101	8.0	5.0	5.7	6.0	4.3	5.8	1.4	24.2

Table B.9. **Rate, extent and beer quality of 5 replicate 500 ml fermentations.**

Sample No.	Logistic rate (h^{-1})	Final Density (°P)	pH	SO_2 (ppm)	Diacetyl (ppb)
1	0.0469	1.70	4.17	4.73	102.6
2	0.0413	1.89	4.25	7.03	132.8
3	0.0429	1.76	4.19	5.26	105.4
4	0.0433	1.95	4.23	5.65	121.1
5	0.0433	1.87	4.17	5.40	89.7
Average	0.0435	1.83	4.20	5.63	110.3
Standard Deviation	0.0020	0.10	0.04	0.86	26.8
Coefficient of Variance (%)	4.7	5.5	0.9	15.2	15.2

Appendix C: Electrokinetic Analysis of the Yeast Cell Surface

C.1 Derivation of charge density from the diffuse layer

An electrical double layer is formed around all charged surfaces. It is composed of two layers of charge, that which forms part of the surface of the particle and a counter charge layer, with the same magnitude as that at the surface, in the solution. In this way the ions set up an electrical potential around the particle. In practice this potential charge layer in the solution takes the form of a diffuse layer which progressively neutralises the surface potential as the distance away from the surface increases. The decay of the potential layer can be described by the Boltzmann distribution. The ion concentration close to the surface can then be given by the equation:

$$\rho = \sum_i z_i e n_{i\infty} \exp\left(-z_i e\psi / k_B T\right) \qquad \text{(C.1)}$$

Where
$e = 1.6\times10^{-19}$ [C]
$k_B = 1.38\times10^{-23}$ [J.K^{-1}]
$n_{i\infty}$ = bulk ion concentration [ions.m^{-3}]
T = temperature [K]
z_I = charge on the ion
ψ = potential [V]

The decay of potential is depicted in Figure C-1 with the surface potential, Stern potential and zeta potential indicated.

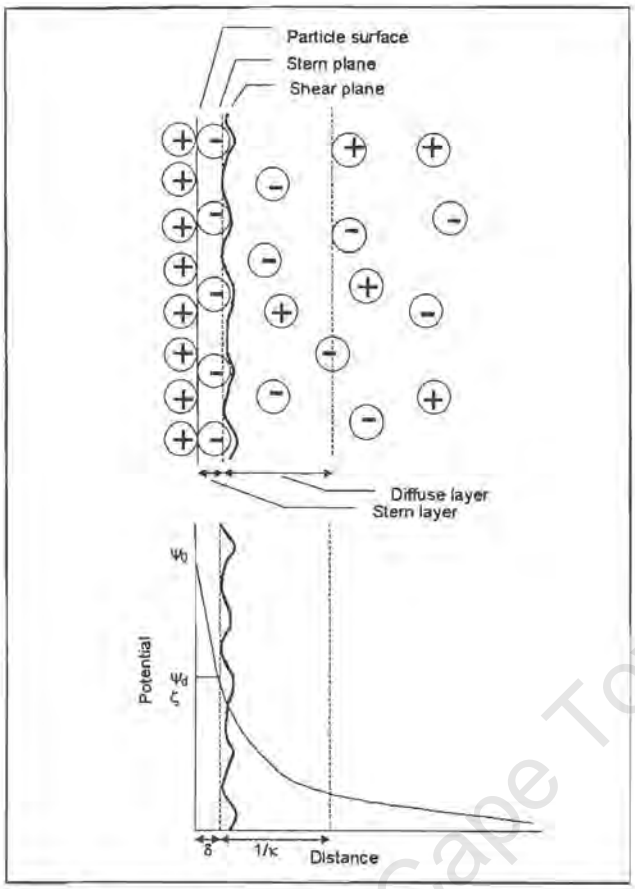

Figure C-1. Schematic representation of the structure of the electric double layer according to Stern's theory. (Shaw, 1980)

The first approximation to the manner in which the potential decreases with increasing distance away from the particle is given by the Debye-Huckel equations. This assumes that $ze\psi_0/2kT << 1$ which at a temperature of 25°C and a monovalent ion solution requires the surface potential (ψ_0) to be less than 25.7mV. For a planar surface this results in:

$$\psi = \psi_o \exp(-\kappa x) \tag{C.2}$$

where x = distance away from the particle surface [m]

κ = Debye-Huckel parameter [m^{-1}]

ψ_0 = surface potential [V]

while for a spherical particle the following equation is valid:

$$\psi = \psi_o \left(\frac{R_S}{r}\right) \exp\left(-\kappa\left(r - R_S\right)\right) \tag{C.3}$$

where r = distance from the centre of the particle [m]

R_S = radius of the particle [m]

and κ, the Debye-Huckel parameter is given by :

$$\kappa = \left[\left(1000 e^2 N_A / \varepsilon k_B T \right) \sum_i z_i^2 M_i \right]^{1/2} \qquad (C.4)$$

Where:

M_i = molar concentration of species i [moles.dm^{-3}]

$N_A = 6.02 \times 10^{23}$ [mol^{-1}]

ε = permitivity of solution [C^{2}J^{-1}m^{-1}]

The inverse of this parameter is sometimes called the electrical double layer thickness because of its units [m]. The dielectric constant (ratio of permitivity of the substance to the permitivity of a vacuum) for water at 25°C is 78.54 which results in a permitivity value for water of 6.95×10^{-10} C^{2}J^{-1}m^{-1}. For the case of an aqueous 1:1 electrolyte at 25°C this reduces to the following equation.

$$\kappa = 2.32 * 10^9 (2M_i)^{1/2} \qquad (C.5)$$

Unless stated elsewhere all zeta potential measurements were conducted at a sodium acetate concentration of 20 mM which provides a κ^{-1} value of 2.16×10^{-9} m. Since the radius of yeast cells are between 2.8 and 3.5 micrometer, the ratio of the double layer thickness to particle radius is less than 1:1300 and the cells can be considered to be flat plates for this and all further analysis.

Although the measured zeta potential at the shear plane is always below 25.7 mV for yeast with values less than 18 mV, the surface potential is larger and so might be close to the limit for the Debye-Hückel approximation to still be valid. A second approximation to the decrease in potential around a charged particle is given by the Gouy-Chapman theory. This does not have the restriction of low surface potentials and for planar surfaces the equation describing the potential decay is:

$$\gamma = \gamma_0 \exp(-\kappa x)$$

$$\textit{where}: \quad \gamma = \left[\exp\left(ze\psi / 2k_B T \right) - 1 \right] \Big/ \left[\exp\left(ze\psi / 2k_B T \right) + 1 \right] \qquad (C.6)$$

which for the planar situation can be converted into an equation for the surface charge density:

$$\sigma_0 = (8 n_0 \varepsilon k_B T) \sinh\left(ze\psi_0 / 2k_B T \right) \qquad (C.7)$$

For water at 25°C, T = 298 (K), n_0 = 6.02x10^{26}C (moles.m^{-3}), ε = 6.95x10^{-10} (C^{2}J^{-1}m^{-1}) and k_B = 1.38x10^{-23} (JK^{-1}) reduces to:

$$\sigma_0 = 0.117c^{1/2}\sinh(19.45\psi_o) \qquad (C.8)$$

Where the concentration of electrolyte, C, is given in units of moles/dm^3 and the surface potential in Volts. This equation is equally valid for the charge concentration at the Stern plane with σ_0 and ψ_0 being replaced with σ_d and ψ_d. As the background electrolyte does not contain any long chain polymers or ions which are surface active, the plane of shear is close to the Stern plane resulting in the measured zeta potential being numerically very close to the Stern potential. Provided that no specific ion adsorption occurs at the surface then the potential decal within the Stern layer is regarded as linear and thus the ratio of the surface charge to charge at the shear plane is constant. The thickness of the Stern layer being determined by the ionic species present. Figure C-2 represents the ratio of charge at the surface to the shear plane for particles with different surface charge.

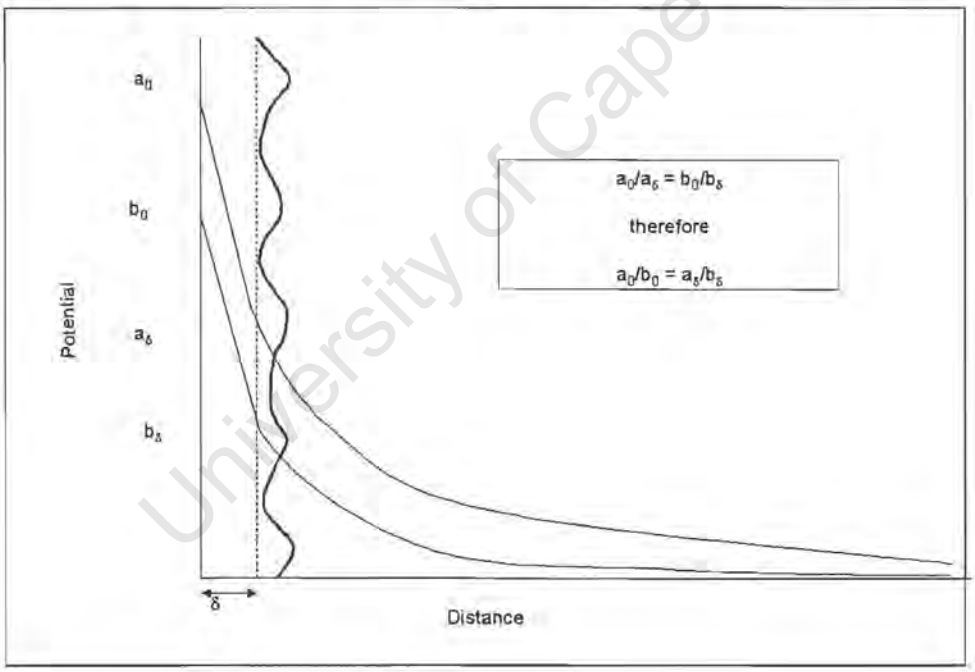

Figure C-2. Ratio of charge at the surface to charge at the shear plane.

C.2 Derivation of charge density from surface group concentrations.

The total charge density at the surface is equal to the sum of the concentrations of the charged groups multiplied by the electron charge. For the yeast surface containing phosphate, carboxyl and amine groups, the surface charge concentration can be calculated theoretically from:

$$-\sigma_0 = e[R_2PO_4^-] + e[RCOO^-] - e[RNH_3^+] \quad (C.9)$$

The equilibrium equations for the ionisation of phosphate and carboxyl groups are:

$$\begin{aligned} R_2HPO_4 &\xleftrightarrow{K_1} R_2PO_4^- + H^+ \\ RCOOH &\xleftrightarrow{K_2} RCOO^- + H^+ \end{aligned} \quad (C.10)$$

where

$$K_1 = \frac{[R_2PO_4^-][H_s^+]}{[R_2HPO_4]}$$

$$K_2 = \frac{[RCOO^-][H_s^+]}{[RCOOH]}$$

and the concentration of H^+ at the surface is altered due to the surface being charged, causing H_s^+ to be higher than the bulk when the surface is negative and lower when the surface is positive H_s^+ can be related to the surface potential according to:

$$[H_s^+] = [H_b^+]\exp\left(-\frac{e\psi_0}{kT}\right) \quad (C.11)$$

An expression for the charged carboxyl group concentration can now be determined by defining the ratios of phosphate to carboxyl and amine to carboxyl as follows:

$$q = N_P / N_C \qquad \text{and} \qquad r = N_N / N_C \quad (C.12)$$

the total number of carboxyl groups is the sum of the charged and uncharged groups;

$$N_C = [RCOOH] + [RCOO^-]$$

i.e.

$$[RCOOH] = N_C - [RCOO^-] \quad (C.13)$$

Substituting the above into the equilibrium constant expression and rearranging for the charged carboxyl group concentration results in:

$$[RCOO^-] = \frac{N_C}{1 + [H_S^+]/K_2} \quad (C.14)$$

Recalling the ratios of phosphate and amine to carboxyl and that the total number of sites is given by

$$N_S = N_C + N_P + N_N \tag{C.15}$$

the total number of carboxyl sites can be expressed as;

$$N_C = N_S \Big/ (1 + q + r) \tag{C.16}$$

The charged carboxyl concentration can now be expressed in terms of N_s, q and r:

$$\left[RCOO^-\right] = \frac{N_S}{1+q+r}\left(\frac{1}{1+\frac{\left[H_S^+\right]}{K_2}}\right) \tag{C.17}$$

Similarly the charged phosphate concentration can be expressed as:

$$\left[R_2PO_4^-\right] = \frac{N_S}{\left(1 + 1/q + r/q\right)}\frac{1}{\left(1+\left[H_S^+\right]/K_1\right)} \tag{C.18}$$

For amine groups found on protein, the pK_a is approximately 11 and since all the zeta potential data was collected at pH values below 7, all amine groups can be assumed to be positively charged. From this assumption the charged amine concentration can be expressed as:

$$\left[RNH_3^+\right] = N_S \frac{r}{(1+q+r)} \tag{C.19}$$

Substituting these expressions for the charged species concentrations into the theoretical expression for surface charge concentration (Equation C.9) results in:

$$-\sigma_S = eN_S\left[\left(\frac{1}{1+1/q+r/q}\right)\left(\frac{1}{1+\left[H_S^+\right]/K_1}\right)+\left(\frac{1}{1+q+r}\right)\left(\frac{1}{1+\left[H_S^+\right]/K_2}\right)-\left(\frac{r}{1+q+r}\right)\right] \tag{C.20}$$

C.3 Solution Method for Charge Group Analysis Using Statistica®

The theoretical expression for surface charge density can be equated to the experimentally determined values for surface charge and values for the two unknown parameters (N_S, and q) can be found. The ratio of carboxyl to amine groups was taken to be constant at 0.63, based upon the amino acid content of surface proteins of *Saccharomyces cerevisiae* cells (Amri *et al.*, 1982). The approximate values of pK_a for phosphate and carboxyl groups are 2 and 4 but due to slight differences in the local environments within the cell wall, these values can vary slightly between strains, growth conditions and experimental run. Because of these variations, estimates for K_1 and K_2 were found at the same time as those for N_S and q. The values for K_1 and K_2 were averaged for different strains within each experimental run and these were then used to determine the values of N_S and q. The best fit equation parameters were obtained using the non-linear estimation module of Statistica® '98 Edition for Windows.

The solution method for a sample data set is presented below:

1. Zeta potential vs. pH data with standard deviations for each value is entered into Statistica and estimates for the parameters pK_1 and pK_2 obtained with their associated standard errors (SE).

2. The values and standard errors obtained for pK_1 and pK_2 were used to calculate the average pK values for the experiment. The loss function used to calculate the mean pK being $1/\sigma^2 *(pK_{observed} - pK_{mean})\hat{}2$ where $\sigma^2 = (SE*SN^{0.5})^2$, SE is the standard error and SN is the sample number, (pH values used in the experiment). Typical weighted average pK values obtained for a data set of 11 zeta potential vs. pH scans is 2.740 and 4.668.

3. Using the average pK values calculated in step 2, the pH-ZP data is re-analysed using the surface charge equations with known values for pK_1 and pK_2 to give the two parameters N_S and q along with their standard errors. The R values indicating the goodness of fit between the modelling equation and the data are calculated.

4. The standard errors found for N_S and q can be converted into confidence limits by using the number of degrees of freedom (SN-1) and the t-value obtained from tables, taken as 95% in this experiment. The confidence limits are calculated as

$$\text{Interval} = SE * t\text{-value}_{(SN-1)}.$$

A 95% confidence limit was chosen to be significant in this study which results in a typical t-value(8) of 2.31.

5. With confidence intervals set, decisions about differences, trends and similarities can be made for the data.